CODATA recommended values of the fundamental physical constants: 2018*

Eite Tiesinga[†]

Joint Quantum Institute and Joint Center for Quantum Information and Computer Science, College Park, Maryland 20742, USA
and National Institute of Standards and Technology, Gaithersburg, Maryland 20899, USA

Peter J. Mohr,[‡] David B. Newell,[§] and Barry N. Taylor[‖]

National Institute of Standards and Technology, Gaithersburg, Maryland 20899, USA

(published 30 June 2021)

We report the 2018 self-consistent values of constants and conversion factors of physics and chemistry recommended by the Committee on Data of the International Science Council (CODATA). The recommended values can also be found at physics.nist.gov/constants. The values are based on a least-squares adjustment that takes into account all theoretical and experimental data available through 31 December 2018. A discussion of the major improvements as well as inconsistencies within the data is given. The former include a decrease in the uncertainty of the dimensionless fine-structure constant and a nearly two orders of magnitude improvement of particle masses expressed in units of kg due to the transition to the revised International System of Units (SI) with an exact value for the Planck constant. Further, because the elementary charge, Boltzmann constant, and Avogadro constant also have exact values in the revised SI, many other constants are either exact or have significantly reduced uncertainties. Inconsistencies remain for the gravitational constant and the muon magnetic-moment anomaly. The proton charge radius puzzle has been partially resolved by improved measurements of hydrogen energy levels.

DOI: 10.1103/RevModPhys.93.025010

CONTENTS

I. Introduction 2
II. Purpose of the Adjustment and Overview of Constants 3
III. Least-Squares Adjustments 3
IV. Overview of Notable Changes 4
A. Electrical units 4
B. Particle and relative atomic masses and the atomic mass constant 4
C. Proton charge radius and Rydberg constant or frequency 5
D. Fine-structure constant and electron magnetic-moment anomaly 6
E. Muon magnetic-moment anomaly 6
F. Newtonian constant of gravitation 6
V. Outline of Paper 6
VI. Relationships among the Rydberg Constant, Fine-Structure Constant, Electron Mass, and Atomic Mass Constant 7
VII. Atomic Hydrogen and Deuterium Transition Energies 8
A. Theory of hydrogen and deuterium energy levels 8
1. Dirac eigenvalue 8
2. Relativistic recoil 9
3. Self-energy 9
4. Vacuum polarization 10
5. Two-photon corrections 10
6. Three-photon corrections 12
7. Finite nuclear size and polarizability 12
8. Radiative-recoil corrections 13
9. Nucleus self-energy 13
B. Total theoretical energies and uncertainties 13

*This review is being published simultaneously by the Journal of Physical and Chemical Reference Data.

This report was prepared by the authors under the auspices of the CODATA Task Group on Fundamental Constants. The members of the task group are:

F. Bielsa, Bureau International des Poids et Mesures
K. Fujii, National Metrology Institute of Japan, Japan
S. G. Karshenboim, Pulkovo Observatory, Russian Federation and Max-Planck-Institut für Quantenoptik, Germany
H. Margolis, National Physical Laboratory, United Kingdom
P. J. Mohr, National Institute of Standards and Technology, United States of America
D. B. Newell, National Institute of Standards and Technology, United States of America
F. Nez, Laboratoire Kastler-Brossel, France
R. Pohl, Johannes Gutenberg-Universität Mainz, Germany
K. Pachucki, University of Warsaw, Poland
J. Qu, National Institute of Metrology of China, China
A. Surzhykov, Physikalisch-Technische Bundesanstalt, Germany
E. Tiesinga, National Institute of Standards and Technology, United States of America
M. Wang, Institute of Modern Physics, Chinese Academy of Sciences, China
B. M. Wood, National Research Council, Canada

[†]eite.tiesinga@nist.gov
[‡]mohr@nist.gov
[§]dnewell@nist.gov
[‖]barry.taylor@nist.gov

C. Experimentally determined transition energies in hydrogen and deuterium 14
1. Measurement of the hydrogen 2S − 4P transition 15
2. Measurement of the hydrogen two-photon 1S − 3S transition 16
3. Measurement of the hydrogen 2S − 2P Lamb shift 17
VIII. Electron Magnetic-Moment Anomaly 18
IX. Relative Atomic Masses 20
X. Atom-Recoil Measurements 22
XI. Atomic g-Factors in Hydrogenic ^{12}C and ^{28}Si ions 23
A. Theory of the bound-electron g-factor 23
B. Measurements of precession and cyclotron frequencies of $^{12}C^{5+}$ and $^{28}Si^{13+}$ 26
C. Observational equations for $^{12}C^{5+}$ and $^{28}Si^{13+}$ experiments 26
XII. Muonic Hydrogen and Deuterium Lamb Shift 27
A. Muonic hydrogen Lamb shift 27
B. Muonic deuterium Lamb shift 28
C. Deuteron-proton charge radius difference 29
XIII. Electron-Proton and Electron-Deuteron Scattering 29
A. Proton radius from e-p scattering 30
B. Deuteron radius from e-d scattering 30
XIV. Magnetic-Moment Ratios of Light Atoms and Molecules 30
A. Definitions of bound-state and free g-factors 30
B. Theoretical ratios of g-factors in H, D, ^{3}He, and muonium 31
C. Theoretical ratios of nuclear g-factors in HD and HT 32
D. Ratio measurements in atoms and molecules 32
XV. Proton Magnetic Moment in Nuclear Magnetons 32
XVI. Muon Magnetic-Moment Anomaly 34
A. Measurement of the muon anomaly 34
B. Theory of the muon anomaly 34
C. Analysis of experiment and theory for the muon anomaly 36
XVII. Electron-to-Muon Mass Ratio and Muon-to-Proton Magnetic-Moment Ratio 37
A. Theory of the muonium ground-state hyperfine splitting 37
B. Measurements of muonium transition energies 40
C. Analysis of the muonium hyperfine splitting and mass ratio m_μ/m_e 41
XVIII. Lattice Spacings of Silicon Crystals 41
XIX. Newtonian Constant of Gravitation 42
A. Corrected value of the 2010 measurement at JILA 43
B. Measurements from the Huazhong University of Science and Technology 43
XX. Electroweak Quantities 50
XXI. The 2018 CODATA Recommended Values 51
A. Tables of values 54
XXII. Summary and Conclusion 54
A. Comparison of 2014 and 2018 CODATA recommended values 54
B. Implications of the 2018 adjustment for metrology and physics 56
1. Electrical metrology 56
2. Electron magnetic-moment anomaly, fine-structure constant, and QED theory 56
3. Proton radius and Rydberg constant 56
4. Muon mass and magnetic moment 57
5. Newtonian constant of gravitation 57
6. Proton mass 57
7. Physics in general 57
List of Symbols and Abbreviations 58
Acknowledgments 60
References 60

I. INTRODUCTION

This report gives a detailed account of the 2018 least-squares adjustment of over 300 recommended values of basic fundamental constants in nature based on the latest relevant precision measurements and improvements of theoretical calculations. The work has been carried out under the auspices of the Task Group on Fundamental Constants (TGFC) of the Committee on Data of the International Science Council (CODATA). The cutoff date for accepted data was at the close of 31 December 2018, and the new set of values became available on World Metrology Day, 20 May 2019, at http://physics.nist.gov/constants, a website of the Fundamental Constants Data Center of the National Institute of Standards and Technology (NIST), Gaithersburg, Maryland, USA.

The compilation of values of fundamental constants arguably started with Birge (1929) and afterwards occurred at irregular intervals until 1998. Since that year, updated and improved adjustments have been published every four years (Mohr and Taylor, 2000, 2005; Mohr, Taylor, and Newell, 2008a, 2008b, 2012a, 2012b; Mohr, Newell, and Taylor, 2016a, 2016b). In 2017, a special adjustment was done to provide values for the redefinition of the International System of Units (SI) (Mohr *et al.*, 2018; Newell *et al.*, 2018). Specifically, recommended exact numerical values for the Planck constant h, elementary charge e, Boltzmann constant k, and Avogadro constant N_A were provided. See Mills *et al.* (2011) for a review of the proposals that led to the redefinitions. The revised SI units for time, length, mass, current, temperature, amount of substance, and luminous intensity based on these exact values together with the already exactly defined frequency of the ground-state cesium hyperfine splitting and speed of light in vacuum c officially became effective on World Metrology Day. Table I lists the values of the defining constants including that of the luminous efficacy, a measure of light intensity as observed by the human eye. The revision has played an important role in the 2018 least-squares adjustment.

The four newly fixed defining constants h, e, k, and N_A within the revised SI replace four constants that previously helped define the SI. These were the mass of the international prototype of the kilogram (IPK) $m(\mathcal{K})$, the permeability of vacuum (magnetic constant) μ_0, the temperature at the triple point of water T_{TPW}, and the molar mass of a carbon 12 atom at rest and in its ground state, $M(^{12}C)$. In the revised SI, these must now be determined experimentally and are no longer fundamental (Mohr *et al.*, 2018; Newell *et al.*, 2018). For example, the permeability of vacuum and the molar mass of carbon 12 are calculable from other (inexact) recommended values; specifically, these are the measurable fine-structure constant and the mass of a single carbon 12 atom, respectively. In this adjustment, we find $\mu_0 = 4\pi \times 10^{-7}[1 + 55(15) \times 10^{-11}]$ N A^{-2} and $M(^{12}C) = 0.012 \times [1 - 35(30) \times 10^{-11}]$ kg mol^{-1}.

The quantities T_{TPW} and $m(\mathcal{K})$ cannot be determined from other fundamental constants. Of course, the triple point of water can still be regarded "fundamental" in that this point has

TABLE I. Exact quantities and their mathematical symbols relevant for the revised SI.

Quantity	Symbol	Value	Unit
hyperf. transition freq. of ^{133}Cs	$\Delta\nu_{\mathrm{Cs}}$	9 192 631 770	Hz
speed of light in vacuum	c	299 792 458	$\mathrm{m\,s^{-1}}$
Planck constant[a]	h	$6.626\,070\,15 \times 10^{-34}$	$\mathrm{J\,Hz^{-1}}$
	$\hbar$	$1.054\,571\,817\ldots \times 10^{-34}$	J s
elementary charge	e	$1.602\,176\,634 \times 10^{-19}$	C
Boltzmann constant	k	$1.380\,649 \times 10^{-23}$	$\mathrm{J\,K^{-1}}$
Avogadro constant	N_{A}	$6.022\,140\,76 \times 10^{23}$	$\mathrm{mol^{-1}}$
luminous efficacy	K_{cd}	683	$\mathrm{lm\,W^{-1}}$

[a]The energy of a photon with frequency ν expressed in unit Hz is $E = h\nu$ in unit J. Unitary time evolution of the state of this photon is given by $\exp(-iEt/\hbar)|\varphi\rangle$, where $|\varphi\rangle$ is the photon state at time $t = 0$ and time is expressed in unit s. The ratio $Et/\hbar$ is a phase.

a well described definition that can be realized by any interested party. To date, however, no theoretical model can reach the accuracy of the best experimental determinations and, thus, T_{TPW} is no longer relevant for the adjustment. The prototype of the kilogram is also no longer relevant for the adjustment, but for a different reason. In this case, the prototype is no longer fundamental. That is, it is no longer unique among massive objects. For further information see the *Mise en pratique* for the definition of the kelvin and kilogram in the online version of the SI brochure found at https://www.bipm.org/en/publications/si-brochure.

The cornerstone of this 2018 CODATA adjustment, as in previous adjustments, is the validity of physical theory as understood today. Prominent in these theories are the concepts of energy and momentum. For example, the energy of a particle of mass m at rest is mc^2 from special relativity. The energy of a single photon with angular frequency ω is $\hbar\omega$ from quantum electrodynamics (QED). Here, $\hbar$ is the reduced Planck constant. From quantum mechanics we know about the particle-wave duality and that the momentum of a massive or massless object is $\mathbf{p} = \hbar\mathbf{k}$, where the wave vector $\mathbf{k}$ has a length $|\mathbf{k}| = 2\pi/\lambda$ and λ is the particle's wavelength. Of course, energy and momentum conservation then ensures, for example, that when an atom absorbs a photon (without ionizing) its momentum changes and its mass slightly increases. Finally, statistical mechanics and thermodynamics tell us that the mean kinetic energy of a three-dimensional classical gas of noninteracting atoms is $3kT/2$ per atom at temperature T.

It is worth noting that the possible time variation of the fine-structure constant α, proton-to-electron mass ratio, and other dimensionless constants or ratios (Safronova *et al.*, 2018) does not affect the 2018 adjustment. That is, our final uncertainty for these quantities is orders of magnitude larger than current upper bounds on their time variation.

II. PURPOSE OF THE ADJUSTMENT AND OVERVIEW OF CONSTANTS

Our periodic CODATA evaluations of the fundamental constants of physics and chemistry serve two purposes. First, they provide a self-consistent set of recommended values of the constants for all to use. Second, because they necessitate a summary and analysis of a wide range of experimental and theoretical data, they can identify possible inconsistencies among the data and suggest areas for future work.

A constant is only fundamental as a matter of convention. For our adjustment, obvious constants are those that appear in basic physical and chemical theory, such as h, c, e, and k as well as the Newtonian constant of gravitation G and the dimensionless fine-structure constant α. Products and ratios of these constants, like the Josephson constant $K_{\mathrm{J}} = 2e/h$, the molar gas constant $R = N_{\mathrm{A}}k$, and the Planck mass $(\hbar c/G)^{1/2}$, are natural extensions. Over the years, many such products and ratios have been given dedicated names as these combinations appear as natural units for measurement observables.

Masses and magnetic moments of the lightest charged leptons, i.e., the electron and muon, and of light nuclei also fall within the scope of our work as their precise evaluation often involves knowledge of the fine-structure and other constants. Our Task Group only publishes updated values for the neutron and nuclei with charge number $Z = 1$ or 2. We provide masses in the SI unit kg and as relative atomic masses in the atomic mass unit $1\ \mathrm{u} = m_{\mathrm{u}}$ (i.e., in units of one-twelfth of the mass of a neutral ^{12}C atom). An extensive listing of relative atomic masses for stable and unstable atoms in the periodic table can be found in the Atomic-Mass-Data-Center publications (Huang *et al.*, 2017; Wang *et al.*, 2017). Particle properties relevant for high-energy physics, such as the masses of the W, Z, and Higgs particles, the Fermi coupling constant, decay modes of mesons, and many other quantities are collected by the Particle Data Group (Tanabashi *et al.*, 2018).

We also maintain values for the lattice constant of natural silicon single crystals and the shielded magnetic moments of the proton in liquid-water and the helion in ^{3}He gas. For the adjustment, the former are relevant for the calibration of x-rays. Before the redefinition of the SI, the precise values of the Si lattice constants in natural and enriched silicon crystals were used to help measure the Avogadro and Planck constants. The shielding factors are relevant because often only shielded magnetic-moment ratios are available.

For conciseness, this review summarizes results from the four years before our 31 December 2018 closing date, as previous CODATA reports describe older data. Detailed discussions of theoretical calculations and experiments are omitted and only noteworthy features are mentioned.

Often a result is identified by an abbreviation for the institution at which it was obtained and the last two digits of the year in which the result was published in an archival journal. However, a result does not have to be published in such a journal to be considered as having met the 31 December 2018 closing date of the adjustment if it was available by this date in a detailed preprint. Any input datum with a 20 or earlier date after its institutional abbreviation has met this requirement. A comprehensive list of Symbols and Abbreviations is given near the end of this report.

III. LEAST-SQUARES ADJUSTMENTS

The least-squares procedure for the determination of the values of fundamental constants is based on the assumption of a

normal probability distribution for correlated input data and is described in detail in Appendix E of Mohr and Taylor (1999) and Mohr and Taylor (2000). Key points are as follows. Experiment as well as theory provide input data that are used to determine a set of independent quantities, the unknowns or variables of the adjustment. They will be called *adjusted constants*. The expression that relates an input datum to the adjusted constants is its *observational equation*, and the one-standard-deviation uncertainties of and covariances among the input data determine the weights of the data contributing to χ^2 (chi squared), which is minimized in the least-squares adjustment.

Observational equations are given by

$$X \doteq F(A_1, A_2, \ldots), \tag{1}$$

where X and $F(\cdots)$ are the input datum and its relationship to adjusted constants A_j with $j = 1, 2\ldots$, respectively. The symbol $\doteq$ implies that the quantities on either side are equal in principle but need only agree to within the constraints of the adjustment. In its simplest form, the observational equation is $X \doteq A$. We simplify to $X \doteq X$ when no confusion can arise. A good example of such a case is Newton's gravitational constant G, where experimentalists directly measure G.

One-standard-deviation uncertainties will also be called *standard uncertainties*. For quantity X they are presented as either an absolute standard uncertainty $u(X)$ with the same unit as X or a dimensionless relative standard uncertainty $u_r(X) = u(X)/|X|$. Throughout this article, covariances $u(X, Y)$ between quantities X and Y are specified in terms of correlation coefficients $r(X, Y) = u(X, Y)/[u(X)u(Y)]$ with values between -1 and 1.

Theoretical expressions, say for the g-factor of the electron, often have uncertainties due to inexact numerical calculations or uncalculated terms whose size cannot be ignored. They are dealt with by introducing an additive correction $\delta_{\rm th}$ to the relevant theoretical expression and including δ as an input datum with magnitude zero and an uncertainty equal to that of the theoretical expression. An observational equation $\delta \doteq \delta_{\rm th}$ is then added to χ^2. Corrections $\delta_{\rm th}$ are thus adjusted constants whose values and uncertainties are found in the least-squares procedure. Correlations, sometimes significant, among the δ due to common sources of uncertainty are taken into account in χ^2 where appropriate.

A measure of the consistency of our least-squares adjustment for the ith input datum X_i is its *normalized residual* $r_i = (X_i - \langle X_i \rangle)/u(X_i)$, where $\langle X_i \rangle$ is its fitted, or adjusted, value. An absolute value greater than two is problematic and is reduced to less than two by the application of a multiplicative expansion factor to the initially assigned uncertainties of the input datum in question as well as related input data. For data pair X_i and X_j, expansion factors are applied in such a way that their correlation coefficient $r(X_i, X_j)$ is unchanged. This procedure makes the effective data consistent. Several expansion factors have been used in this adjustment.

After the application of all expansion factors, we characterize the quality of an adjustment with N input data and M adjusted constants by the probability $p(\chi^2|\nu)$ of obtaining a value of χ^2 by chance that large or larger, where $\nu = N - M$ and the Birge ratio $R_{\rm B} = \sqrt{\chi^2/\nu}$.

For the 2018 adjustment, the input data and adjusted constants separate into three independent data sets, corresponding to input data related to the determination of the gravitational constant, input data related to natural-silicon lattice spacings, and, finally, all remaining input data and adjusted constants. Each data set is treated separately. The gravitational constant is determined from $N = 16$ measurements and an expansion factor of 3.9 is needed to decrease the residuals to below two. This modification leads to $\chi^2 = 12.9$, $p(\chi^2|\nu) = 0.61$, and $R_{\rm B} = 0.93$. For the natural-silicon lattice-spacing determination, there are $N = 21$ input data and $M = 12$ adjusted constants. No expansion factor is needed and $\chi^2 = 7.3$, $p(\chi^2|\nu) = 0.60$, and $R_{\rm B} = 0.90$. The third least-squares adjustment has $N = 105$ and $M = 62$ with $\chi^2 = 31.5$, $p(\chi^2|\nu) = 0.88$, $R_{\rm B} = 0.87$. Two expansion factors are included. A factor of 1.6 is applied to the 62 input data determining the Rydberg constant and proton and deuteron charge radii. A factor 1.7 is used for the two input data that determine the relative atomic mass of the proton.

The input data for the 2018 CODATA adjustment can be found in Tables VIII, X, XVIII, XXI, XXVII, and XXIX. Links to tables with correlation coefficients are given in the captions of these tables. The adjusted constants are given in Tables XI and XIX. Observational equations are found in Tables XXIII and XXVI.

IV. OVERVIEW OF NOTABLE CHANGES

A. Electrical units

The introduction of the revised SI has brought electrical metrology back into the SI. Between 1988 and 2018, on the recommendation of the Consultative Committee for Electricity (CCE) and adopted by the International Committee for Weights and Measures (CIPM) (Quinn, 1989; Taylor and Witt, 1989), the electrical units of current, voltage, resistance, etc. were the ampere-90, volt-90, ohm-90, etc. derived by fixing the Josephson and von Klitzing constants to the exact, conventional values $K_{\rm J-90} = 483\,597.9$ GHz/V and $R_{\rm K-90} = 25\,812.807\ \Omega$, respectively, instead of using $K_{\rm J} = 2e/h$ and $R_{\rm K} = h/e^2$ based on the most accurate values for h and e. Then, for example, a measurement of the resistance of a resistor would result in a number times $R_{\rm K-90}$, which is then expressed in the unit Ω_{90} (often the subscript 90 would be dropped) using the value of $R_{\rm K-90}$. Now these conventional 1990 electrical units are obsolete, because with exact values for h and e in SI units, the Josephson and von Klitzing constants are exact. This leads to fractional changes of two to twenty times 10^{-8} when reexpressing values of electrical quantities from conventional 1990 to the revised SI units. These changes, however, are generally much smaller than the relative uncertainties associated with most everyday measurements of electrical quantities and are only noticeable when comparing quantum electrical standards.

B. Particle and relative atomic masses and the atomic mass constant

Overnight, the revision of the SI has led to almost two orders of magnitude improvement in the uncertainties of the

electron, neutron, and nuclear and atomic masses in the SI unit kg when compared to those found in the 2014 CODATA adjustment. The atomic mass constant, one-twelfth of the mass of the ^{12}C atom in its ground state, has similarly become more accurate. These masses are now often known with relative uncertainties of a few times 10^{-10}.

By fixing h and e, the reduced uncertainty is achieved by combining the results of several distinct measurements with equally accurate theoretical calculations for these measurements. For example, in the revised SI the atomic mass constant is most accurately determined through

$$m_u = \frac{1}{12} m(^{12}\mathrm{C}) = \frac{1}{A_r(\mathrm{e})} m_e = \frac{2hR_\infty}{A_r(\mathrm{e})\alpha^2 c}, \tag{2}$$

where the adjusted constants are the Rydberg constant R_∞, the fine-structure constant α, and the relative atomic mass of the electron $A_r(\mathrm{e})$. Here, we use the Rydberg energy $hcR_\infty = \alpha^2 m_e c^2/2$, and m_e is the mass of the electron. The Rydberg constant is mainly constrained by measurements of the 1S-2S transition energy in hydrogen. (In practice, this transition energy is measured as a two-photon process.) The fine-structure constant is determined from a combination of calculations and measurements of the electron g-factor as well as atom-recoil measurements. Finally, the relative atomic mass of the electron (not m_e in kg) is found from spin-precession and cyclotron-frequency-ratio measurements on hydrogenic $^{12}C^{5+}$.

Of the three adjusted constants on the right-hand side of Eq. (2), the fine-structure constant α is by far the least well known with a still-impressive relative standard uncertainty of 1.5×10^{-10}. The relative uncertainty of $A_r(\mathrm{e})$ is 2.9×10^{-11}, while that for R_∞ is 1.9×10^{-12}. We find that the relative uncertainty for m_u is slightly less than twice that of α once the small covariances among the three adjusted constants are taken into account.

The mass for a neutral atom X is most accurately found from

$$m(X) = m_X = A_r(X) m_u, \tag{3}$$

where we rely on the 2016 Atomic-Mass-Data-Center (AMDC16) values of relative atomic masses for neutral atoms throughout the periodic table (Huang *et al.*, 2017; Wang *et al.*, 2017). These relative atomic masses often have a smaller relative uncertainty than m_u, even though the accuracy of m_u has improved significantly. The masses of nuclei can be found by accounting for the electron masses and electron removal energies where available.

In 2016, the Atomic Mass Data Center updated the relative atomic mass of hydrogen based on the then-available data. In 2017, Heiße *et al.* (2017) made an accurate measurement of the cyclotron frequency ratio of the proton and the $^{12}C^{6+}$ nucleus. The implied relative atomic masses of the proton and hydrogen atom from these two sources are inconsistent and require an expansion factor in our least-squares adjustment. The uncertainties added by accounting for the electron mass and binding energy are negligible.

C. Proton charge radius and Rydberg constant or frequency

The disagreement between the (root-mean-square) charge radius of the proton r_p obtained from Lamb-shift measurements in muonic hydrogen (a muon bound to a proton) and the value obtained from transition frequency measurements in hydrogen and electron-proton elastic scattering data, sometimes referred to as the "proton-radius puzzle," has been partly resolved. Therefore, for this 2018 CODATA adjustment, the TGFC decided that the muonic hydrogen data, some of which were already available in 2010, as well as related muonic deuterium data, should no longer be excluded.

The reduced disagreement in the determinations of the proton charge radius is mainly due to two new hydrogen spectroscopic measurements (Beyer *et al.*, 2017; Bezginov *et al.*, 2019), as they imply a smaller r_p closer to that found from muonic hydrogen data. Figure 1 illustrates the improved agreement for r_p as well as its strong correlation with the determination of the Rydberg constant R_∞. We observe that our 2018 value for r_p has a three-times improved uncertainty compared to that found in the 2014 CODATA evaluation. Moreover, the correlation coefficient between r_p and R_∞ has significantly decreased. The covariance error ellipse is more circular in the 2018 adjustment. Similar observations hold for the determination of the deuteron charge radius r_d. Our 2018 relative standard uncertainties for r_p, r_d, and R_∞ are 2.2×10^{-3}, 3.5×10^{-4}, and 1.9×10^{-12}, respectively.

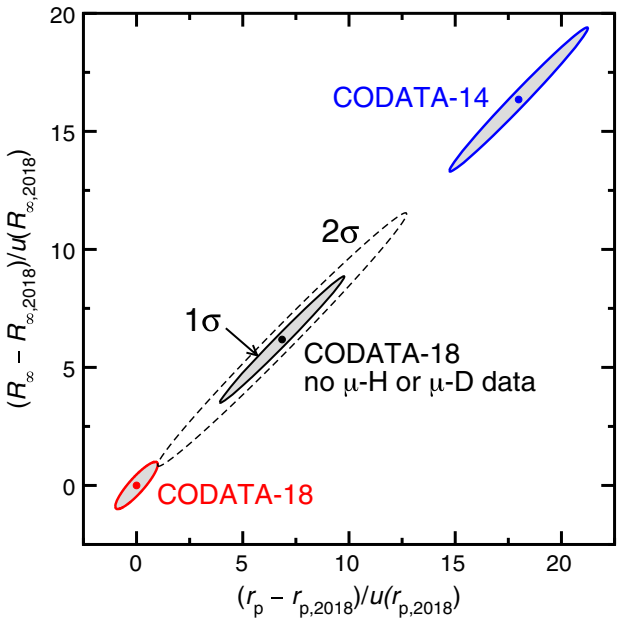


FIG. 1. Covariance error ellipses for the proton radius r_p and the Rydberg constant R_∞ from the 2014 (blue marker and curve) and the current 2018 (red marker and curve) CODATA adjustment. The black marker and ellipses correspond to a 2018 adjustment where the experimental data from muonic hydrogen and muonic deuterium have not been included. Solid and dashed curves correspond to the one- and two-standard-uncertainty ellipses, respectively. The x- and y-axis data are shifted and normalized by the 2018 recommended values and standard uncertainties of r_p and R_∞, respectively.

The tension between the two approaches determining r_p and r_d has not been fully resolved. In fact, to obtain consistency among the many input data that contribute to the determination of R_∞, r_p, and r_d, a multiplicative expansion factor of 1.6 is applied to their uncertainties. Further experiments are needed.

D. Fine-structure constant and electron magnetic-moment anomaly

The fine-structure constant, the dimensionless coupling constant in QED, is determined primarily by measuring either the electron magnetic-moment anomaly a_e or the recoil momentum of an atom from emitting or absorbing a resonant photon. To date, the two approaches lead to a roughly equal uncertainty for α. Figure 2 summarizes these data and the 2018 recommended value of α. The relative standard uncertainty of the 2018 recommended value of α is 1.5×10^{-10}, a value that has improved steadily over the past hundred years, since its definition by Sommerfeld (1916).

The uncertainty of the theoretical expression for the electron magnetic-moment anomaly a_e, mainly a function of α, has now been reduced to the point where it contributes negligibly to the determination of the fine-structure constant α obtained by equating the experimental value of a_e to the theoretical expression. For example, Laporta (2017) evaluated the four-virtual photon QED coefficient virtually exactly and hadronic corrections have been updated.

The most recent experimental value for a_e has a relative standard uncertainty of 2.4×10^{-10} (Hanneke, Fogwell, and Gabrielse, 2008). Its derived value for α is shown in Fig. 2 as Harvard-08.

An important new atom-recoil input datum is that by Parker *et al.* (2018) measured at the University of California at Berkeley, USA. Using atom interferometry with laser-cooled ^{133}Cs, the quotient $h/m(^{133}\mathrm{Cs})$ was measured

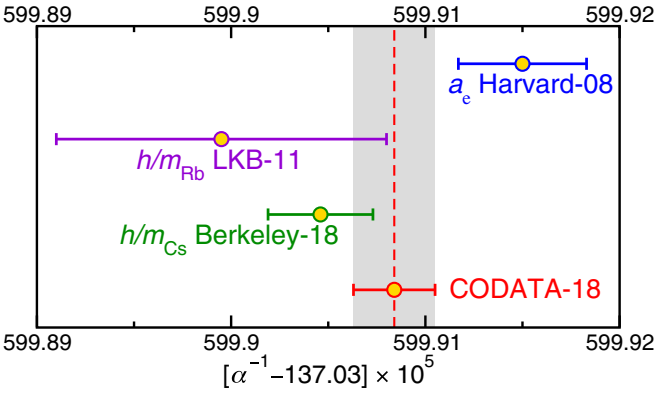


FIG. 2. Results of measurements relevant for determining the 2018 CODATA recommended value of the fine-structure constant α. Error bars correspond to one-standard-deviation uncertainties. Labels "Harvard-08," "LKB-11," and "Berkeley-18" denote the laboratories and the last two digits of the year in which the result was reported. The individual values for $(\alpha^{-1} - 137.03) \times 10^5$ are 599.9150(33), 599.8998(85), and 599.9048(28) for Harvard-08, LKB-11, and Berkeley-18, respectively. See discussion of this figure for references.

with $u_r = 4.0 \times 10^{-10}$. It provides a value of α with $u_r = 2.0 \times 10^{-10}$, which is the smallest uncertainty of all relevant measurements. It agrees with the less-accurate value of α from a ^{87}Rb atom-interferometry measurement (Bouchendira *et al.*, 2011) made at the Laboratoire Kastler-Brossel (LKB), France. Both data are shown in Fig. 2 and labeled by Berkeley-18 and LKB-11, respectively. We also observe that there exists tension between the a_e and $h/m(^{133}\mathrm{Cs})$ measurements; their inferred values of α differ by five times the uncertainty of the 2018 recommended value of α. Nevertheless, no expansion factor for the uncertainties of these three input data is required.

E. Muon magnetic-moment anomaly

The theoretical expression for the muon magnetic-moment anomaly a_μ is omitted from this CODATA adjustment as in the two previous adjustments. Although there has been progress in the theory in the past four years, there are still concerns about the hadronic and light-by-light vacuum-polarization contributions, and the 3σ to 4σ disagreement between theory and experiment remains. Currently, researchers at the Experiment E989 (Keshavarzi, 2019) of the Fermi National Accelerator Laboratory, USA and the muon $g-2$ J-PARC experiment (Abe *et al.*, 2018) of the High Energy Accelerator Research Organization (KEK), Japan hope to resolve this discrepancy.

F. Newtonian constant of gravitation

Inconsistencies among measurements of the Newtonian constant of gravitation G have long been a problem. This is no different in the 2018 adjustment. Sixteen measurements lead to a relative uncertainty $u_r = 2.2 \times 10^{-5}$, a factor of two reduction compared to our previous adjustment. An expansion factor of 3.9, however, is needed to reduce the absolute value of all residuals below two. Two recent results, both with relative standard uncertainties of 1.2×10^{-5} (Li *et al.*, 2018), have contributed to the improved recommended value. The two values differ by 2.7 times the root-mean square of their uncertainties.

V. OUTLINE OF PAPER

The remainder of the paper describes the input data in the 2018 CODATA adjustment, analyzes these data where appropriate, and explains the observational equations. Recommended values of the fundamental constants and conversion factors of energy equivalents are presented and discussed.

We begin by describing the relationship among four important adjusted constants in the CODATA adjustments. Section VI shows how the determination of the Rydberg constant, the Hartree energy, the fine-structure constant, the electron mass, and the atomic mass constant are interconnected.

The next five sections describe five types of experiments that determine the values of these five fundamental constants. Section VII explains the theory for and measurements of transition energies in hydrogen and deuterium relevant to the determination of the Rydberg constant or the Hartree energy.

Section VIII summarizes the theory for the magnetic-moment anomaly or g-factor of the electron. In addition, the sole direct measurement of the anomaly is discussed. This measurement is one of two ways to determine the fine-structure constant.

Section IX describes input data for the relative atomic masses of various nuclei and atoms, i.e., masses specified in units of the atomic mass constant or, equivalently, atomic mass units. Electron ionization and removal energies of H, ^{3}H, ^{3}He, ^{4}He, ^{12}C, and ^{28}Si are also specified. Section X describes atom-recoil experiments, which determine the mass of neutral ^{87}Rb and ^{133}Cs atoms in SI unit kg.

Section XI explains the theoretical calculations of the g-factor of the electron in hydrogenic $^{12}C^{5+}$ and $^{28}Si^{13+}$. In addition, the section describes measurements of the ratio of precession to cyclotron frequencies of these hydrogenic ions. Together, these theoretical g-factors and measurements, after accounting for electron removal energies, are the most accurate means to determine the electron mass in atomic mass units (or the atomic mass constant in units of the electron mass).

The next two sections describe input data that determine the proton and deuteron charge radii. Section XII summarizes theory for and spectroscopic measurements of the Lamb shift for muonic hydrogen and deuterium. Proton and deuteron charge radii from electron-proton and electron-deuteron elastic scattering data are described in Sec. XIII.

Sections XIV and XV describe the input data for magnetic-moment ratios of light nuclei. Both theoretical estimates and experimental data for these ratios are given.

The g-factor and mass of the muon are discussed in the next two sections. Section XVI describes both theoretical calculations and measurements of the magnetic-moment anomaly of the muon. Due to long-standing discrepancies between the theory and experiments, the Task Group has decided to only use the experimental data to determine the muon anomaly.

Section XVII describes the input data for the determination of the mass of the muon relative to that of the electron. Data rely on measurements and theoretical calculations of the hyperfine splitting of ground-state muonium, an electron bound to an antimuon. These data also fix the muon-to-proton magnetic-moment ratio.

Section XVIII summarizes the input data that determine the lattice spacing of natural silicon. Section XIX describes the input data for the determination of the Newtonian constant of gravitation. Section XX gives values for some electroweak quantities, i.e., the Fermi coupling constant and the weak mixing angle.

Section XXI lists the 2018 CODATA recommended Values. Tables of values and some calculational details are given. Section XXII gives a summary and conclusion based on a comparison of 2014 and 2018 CODATA recommended values. Changes in values are either due to the revision of the SI or due to newly available input data. We give implications of the 2018 adjustment for electrical metrology, the proton radius and Rydberg constant, the fine-structure constant, and Newton's gravitational constant. We also make suggestions for future work.

VI. RELATIONSHIPS AMONG THE RYDBERG CONSTANT, FINE-STRUCTURE CONSTANT, ELECTRON MASS, AND ATOMIC MASS CONSTANT

Several sections in this article describe, in detail, how the Rydberg constant R_∞, the Hartree energy E_h, fine-structure constant α, the atomic mass constant m_u, and the electron mass m_e are determined. Their determinations are interrelated in CODATA adjustments and involve five distinct measurements combined with state-of-the-art theoretical calculations within QED. A succinct, simplified flow diagram of the most important relationships and measurements is shown in Fig. 3. At the heart of the diagram are the relationships

$$E_h \equiv 2R_\infty hc = \alpha^2 m_e c^2, \tag{4}$$

where h and c are exact in the revised SI. The relationships, for example, imply that measuring two of E_h, α, or m_e in SI units determines the third. (Of course, the dimensionless fine-structure constant will have the same numerical value in any complete set of units.) Alternatively, measuring all three constants confirms the validity of the equation.

Spectroscopy on the hydrogen atom, discussed in Sec. VII, and, in particular, the measurement of the 1S-to-2S transition energy or frequency determines the Rydberg constant or, equivalently, the Hartree energy in SI units. In fact, R_∞ or E_h has a unique place in the adjustment. Its relative uncertainty is orders of magnitude smaller than that of our other adjusted constants.

The measurement of the ratio of spin-precession and cyclotron frequencies of a single, free electron in a magnetic flux density gives an accurate value for its g-factor. Combined with theoretical calculations of g as a function of α, this gives a competitive value for α. Details are given in Sec. VIII. Of the adjusted constants, the fine-structure constant has the second smallest relative uncertainty. Currently, the two types of measurements combined with Eq. (4) give the most accurate value for m_e in kg.

Measurements of the ratio of precession and cyclotron frequencies of hydrogenic $^{12}C^{5+}$ (and to a lesser extent $^{28}Si^{13+}$) are used to determine the relative atomic mass of the electron, $A_r(e) = m_e/m_u$. Here, theoretical calculations of the g-factor of the bound electron (as a function of α) are also essential. Details can be found in Sec. XI. From the measurement of $A_r(e)$ and the value for the electron mass, an accurate value for the atomic mass constant m_u is derived.

Finally, Fig. 3 shows how atom-recoil experiments that measure the mass of ^{87}Rb and ^{133}Cs in kg combined with measurements of their relative atomic masses as compiled by the Atomic Mass Data Center form a second pathway to determine m_e, but most importantly, a second competitive determination of the fine-structure constant. These experiments and data are discussed in Secs. IX and X, respectively.

The directions of the arrows in Fig. 3 indicate the paths traversed to find the most accurate values for our four constants. The figure, however, does not show all relationships. For example, atom-recoil experiments and the data from the Atomic Mass Data Center can be used to determine m_u as well. Its value, however, would be less accurate. The transition energies among the eigenstates in hydrogen also depend on α

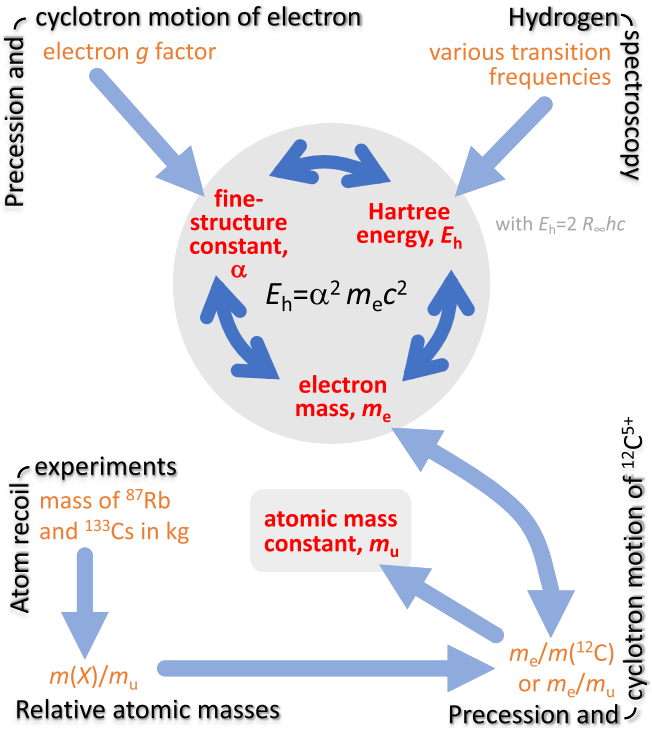


FIG. 3. Relationships in the determinations of E_h, α, m_e, and m_u (red text and symbols) as well as the theoretical and experimental means (black text with orange measured quantity) to determine their values. Blue directed arrows give the most commonly traversed connections between the constants and measured quantities.

and, thus, could constrain its value. Still, the measurement of the g-factor of the free-electron and atom-recoil experiments are currently the best means to determine α. Moreover, hydrogen spectroscopy is also used to constrain the proton radius.

VII. ATOMIC HYDROGEN AND DEUTERIUM TRANSITION ENERGIES

The comparison of theory and experiment for electronic transition energies in atomic hydrogen and deuterium is currently the most precise way to determine the Rydberg constant, or equivalently the Hartree energy, and to a lesser extent the charge radii of the proton and deuteron. Here, we summarize the theory of and the experimental input data on H and D energy levels in Secs. VII.A and VII.C, respectively.

The charge radii of the proton and deuteron are also constrained by data and theory on muonic hydrogen and muonic deuterium as well as by those from electron scattering. These data are discussed in Secs. XII and XIII, respectively.

The electronic eigenstates of H and D are conveniently labeled by $n\ell_j$, where $n = 1, 2, \ldots$ is the principal quantum number, $\ell = 0, 1, \ldots, n-1$ is the quantum number for the electron orbital angular momentum $\mathbf{L}$, and $j = \ell \pm 1/2$ is the quantum number of the total electronic angular momentum $\mathbf{J}$. Following the usual convention, we use S, P, D, … to denote $\ell = 0, 1, 2, \ldots$ states.

Theoretical values for the energy levels of H and D are determined by the Dirac eigenstate energies, QED effects such as self-energy and vacuum-polarization corrections, as well as proton size and nuclear recoil effects. The expression for energy levels quickly becomes complex. The energies, however, do satisfy

$$E = -\frac{E_h}{2n^2}(1+\mathcal{F}) = -\frac{R_\infty hc}{n^2}(1+\mathcal{F}), \tag{5}$$

where $E_h = \alpha^2 m_e c^2 = 2R_\infty hc$ is the Hartree energy, R_∞ is the Rydberg constant, and α is the fine-structure constant. The dimensionless $\mathcal{F}$, small compared to one, is determined by QED, recoil corrections, etc. Consequently, the measured H and D transition energies determine E_h and R_∞ as h and c are exact in the SI. The transition energy between states i and i' with energies E_i and $E_{i'}$ is given by

$$\Delta\mathcal{E}_{ii'} = E_{i'} - E_i. \tag{6}$$

Alternatively, we write $\Delta\mathcal{E}_{ii'} = \Delta\mathcal{E}(i - i')$.

A. Theory of hydrogen and deuterium energy levels

This section describes the theory of hydrogen and deuterium energy levels. References to the original literature are generally omitted; these may be found in the recent review by Yerokhin, Pachucki, and Patkóš (2019), on which we rely for recent developments, but also in earlier CODATA reports, Sapirstein and Yennie (1990) and Eides, Grotch, and Shelyuto (2001, 2007). Literature references to new developments are given where appropriate. Nine contributions to the energies with different physical origins have been isolated. Each is discussed in one of the following subsections. Moreover, each contribution has "correlated" and/or "uncorrelated" uncertainties due to limitations in the calculations. An important correlated uncertainty is where a contribution to the energy has the form C/n^3 with a coefficient C that is the same for states with the same ℓ and j. The uncertainty in C leads to correlations among energies of states with the same ℓ and j. Such uncertainties are denoted as uncertainty type u_0 in the text. Uncorrelated uncertainties, i.e., those independent of the quantum numbers, are denoted as type u_n. Other correlations are those between corrections for the same state in different isotopes, where the difference in the correction is only due to the difference in the masses of the isotopes. Calculations of the uncertainties of the energy levels and the corresponding correlation coefficients are further described in Sec. VII.B.

1. Dirac eigenvalue

The largest contribution to the energies is the Dirac eigenvalue for an electron bound to an infinitely heavy point nucleus or a stationary point nucleus. It is

$$E_D = f(n,\kappa)m_e c^2, \tag{7}$$

where

$$f(n,\kappa)=\left[1+\frac{(Z\alpha)^2}{(n-\delta)^2}\right]^{-1/2}, \tag{8}$$

with $\delta=|\kappa|-\sqrt{\kappa^2-(Z\alpha)^2}$ and κ is the angular momentum-parity quantum number ($\kappa=-1,1,-2,2,-3$ for $\ell_j=\mathrm{S}_{1/2}$, $\mathrm{P}_{1/2}$, $\mathrm{P}_{3/2}$, $\mathrm{D}_{3/2}$, and $\mathrm{D}_{5/2}$ states, respectively). States with the same n and $j=|\kappa|-1/2$ have degenerate eigenvalues. Finally, $\ell=|\kappa+1/2|-1/2$ and we retain the atomic number Z in the equations in order to classify the various contributions to the energies in this and other sections.

For a nucleus with a finite mass m_N, we have

$$E_M(\mathrm{H})=Mc^2+[f(n,\kappa)-1]m_\mathrm{r}c^2-[f(n,\kappa)-1]^2\frac{m_\mathrm{r}^2c^2}{2M}+\frac{1-\delta_{\ell 0}}{\kappa(2\ell+1)}\frac{(Z\alpha)^4m_\mathrm{r}^3c^2}{2n^3m_N^2}+\cdots \tag{9}$$

for hydrogen and

$$E_M(\mathrm{D})=Mc^2+[f(n,\kappa)-1]m_\mathrm{r}c^2-[f(n,\kappa)-1]^2\frac{m_\mathrm{r}^2c^2}{2M}+\frac{1}{\kappa(2\ell+1)}\frac{(Z\alpha)^4m_\mathrm{r}^3c^2}{2n^3m_N^2}+\cdots \tag{10}$$

for deuterium, where $\delta_{\ell\ell'}$ is the Kronecker delta, $M=m_\mathrm{e}+m_N$, and $m_\mathrm{r}=m_\mathrm{e}m_N/(m_\mathrm{e}+m_N)$ is the reduced mass. Note that in this equation the energy of $n\mathrm{S}_{1/2}$ states differs from that of $n\mathrm{P}_{1/2}$ states.

It is worth noting that in Eqs. (9) and (10) we follow a slightly different classification of terms when compared to that used by Yerokhin, Pachucki, and Patkóš (2019). Specifically, contributions of order $(m_\mathrm{e}/m_N)^2(Z\alpha)^4m_\mathrm{e}c^2$ in our equations are classified as relativistic-recoil corrections that are second order in the mass ratio by Yerokhin, Pachucki, and Patkóš (2019). The remaining difference between the CODATA expressions for the Dirac energy and those of Yerokhin, Pachucki, and Patkóš (2019) is of order $(m_\mathrm{e}/m_N)^2(Z\alpha)^6m_\mathrm{e}c^2$, negligible for our current purposes.

2. Relativistic recoil

The leading relativistic-recoil correction, to lowest order in $Z\alpha$ and all orders in m_e/m_N, is (Erickson, 1977; Sapirstein and Yennie, 1990)

$$E_\mathrm{S}=\frac{m_\mathrm{r}^3}{m_\mathrm{e}^2m_N}\frac{(Z\alpha)^5}{\pi n^3}m_\mathrm{e}c^2\times\left\{\frac{1}{3}\delta_{\ell 0}\ln(Z\alpha)^{-2}-\frac{8}{3}\ln k_0(n,\ell)-\frac{1}{9}\delta_{\ell 0}-\frac{7}{3}a_n-\frac{2}{m_N^2-m_\mathrm{e}^2}\delta_{\ell 0}\left[m_N^2\ln\left(\frac{m_\mathrm{e}}{m_\mathrm{r}}\right)-m_\mathrm{e}^2\ln\left(\frac{m_N}{m_\mathrm{r}}\right)\right]\right\}, \tag{11}$$

where $a_n=-2\ln(2/n)-2+1/n-2\sum_{i=1}^{n}(1/i)$ for $\ell=0$ and $a_n=1/[\ell(\ell+1)(2\ell+1)]$ otherwise. Values for the Bethe logarithms $\ln k_0(n,\ell)$ are given in Table II.

Additional contributions to lowest order in the mass ratio and of higher order in $Z\alpha$ are

TABLE II. Relevant values of the Bethe logarithms $\ln k_0(n,\ell)$. Missing entries are for states for which no experimental measurements are included.

n	S	P	D
1	2.984 128 556		
2	2.811 769 893	−0.030 016 709	
3	2.767 663 612		
4	2.749 811 840	−0.041 954 895	−0.006 740 939
6	2.735 664 207		−0.008 147 204
8	2.730 267 261		−0.008 785 043
12			−0.009 342 954

$$E_\mathrm{R}=\frac{m_\mathrm{e}}{m_N}\frac{(Z\alpha)^6}{n^3}m_\mathrm{e}c^2[D_{60}+Z\alpha G_\mathrm{REC}(Z\alpha)], \tag{12}$$

where $D_{60}=4\ln 2-7/2$ for $\ell=0$ and $D_{60}=2[3-\ell(\ell+1)/n^2]/[(2\ell-1)(2\ell+1)(2\ell+3)]$ otherwise. The function $G_\mathrm{REC}(x)$ is

$$G_\mathrm{REC}(x)=D_{72}\ln^2(x^{-2})+D_{71}\ln(x^{-2})+D_{70}+\cdots, \tag{13}$$

where $D_{72}=-11/(60\pi)\delta_{\ell 0}$. Other D_{7x} coefficients are not known analytically. Instead, we use the numerically computed $G_\mathrm{REC}(x)$ of Yerokhin and Shabaev (2015, 2016) for nS states with $n=1,\ldots,5$ as well as for the $2\mathrm{P}_{1/2}$ and $2\mathrm{P}_{3/2}$ states. For $x=\alpha$, these values and uncertainties (both multiplied by π) are reproduced in Table III. For nS states with $n=6,8$, we extrapolate $G_\mathrm{REC}(\alpha)$ using g_0+g_1/n, where coefficients g_0 and g_1 are found from fitting to the $n=4$ and 5 values of $G_\mathrm{REC}(\alpha)$. The values are 14.8(1) and 14.7(2) for $n=6$ and 8, with uncertainties based on comparison to values obtained by fitting $g_0+g_1/n+g_2/n^2$ to the $n=3,4$, and 5 values. For the other $\ell>0$ states, we use $G_\mathrm{REC}(x)=0$ and an uncertainty in the relativistic-recoil correction $E_\mathrm{S}+E_\mathrm{R}$ equal to $0.01E_\mathrm{R}$.

The covariances for $E_\mathrm{S}+E_\mathrm{R}$ between pairs of states with the same ℓ and j follow the dominant $1/n^3$ scaling of the uncertainty, i.e., are of type u_0.

3. Self-energy

The one-photon self-energy of an electron bound to a stationary point nucleus is

$$E_\mathrm{SE}^{(2)}=\frac{\alpha}{\pi}\frac{(Z\alpha)^4}{n^3}F(Z\alpha)m_\mathrm{e}c^2, \tag{14}$$

TABLE III. Values of the function $\pi\times G_\mathrm{REC}(x=\alpha)$ from Yerokhin and Shabaev (2015, 2016). Numbers in parentheses are the one-standard-deviation uncertainty in the last digit of the value. [The definitions of $G_\mathrm{REC}(x)$ in this adjustment and that of Yerokhin and Shabaev (2015, 2016) differ by a factor π.] Missing entries are states for which data are not available from these references.

n	S	$\mathrm{P}_{1/2}$	$\mathrm{P}_{3/2}$
1	9.720(3)		
2	14.899(3)	1.5097(2)	−2.1333(2)
3	15.242(3)		
4	15.115(3)		
5	14.941(3)		

TABLE IV. Values of the function $G_{\rm SE}(\alpha)$.

n	$S_{1/2}$	$P_{1/2}$	$P_{3/2}$	$D_{3/2}$	$D_{5/2}$
1	−30.290 240(20)				
2	−31.185 150(90)	−0.973 50(20)	−0.486 50(20)		
3	−31.047 70(90)				
4	−30.9120(40)	−1.1640(20)	−0.6090(20)		0.031 63(22)
6	−30.711(47)				0.034 17(26)
8	−30.606(47)			0.007 940(90)	0.034 84(22)
12				0.009 130(90)	0.035 12(22)

where the function $F(x)$ is

$$F(x) = A_{41}\ln(x^{-2}) + A_{40} + A_{50}x + A_{62}x^2\ln^2(x^{-2}) + A_{61}x^2\ln(x^{-2}) + G_{\rm SE}(x)x^2, \quad (15)$$

with $A_{41} = (4/3)\delta_{\ell 0}$, $A_{40} = -(4/3)\ln k_0(n,\ell) + 10/9$ for $\ell = 0$ and $A_{40} = -(4/3)\ln k_0(n,\ell) - 1/[2\kappa(2\ell+1)]$ otherwise. Next, $A_{50} = (139/32 - 2\ln 2)\pi\delta_{\ell 0}$, $A_{62} = -\delta_{\ell 0}$, and

$$A_{61} = \left[4\left(1 + \frac{1}{2} + \cdots + \frac{1}{n}\right) + \frac{28}{3}\ln 2 - 4\ln n - \frac{601}{180} - \frac{77}{45n^2}\right]\delta_{\ell 0} + \frac{n^2-1}{n^2}\left(\frac{2}{15} + \frac{1}{3}\delta_{j\frac{1}{2}}\right)\delta_{\ell 1} + \frac{[96n^2 - 32\ell(\ell+1)](1-\delta_{\ell 0})}{3n^2(2\ell-1)(2\ell)(2\ell+1)(2\ell+2)(2\ell+3)}.$$

Values for $G_{\rm SE}(\alpha)$ in Eq. (15) are listed in Table IV. The uncertainty of the self-energy contribution is due to the uncertainty of $G_{\rm SE}(\alpha)$ listed in the table and is taken to be type u_n. See Mohr, Taylor, and Newell (2012a) for details.

Following convention, $F(Z\alpha)$ is multiplied by the factor $(m_{\rm r}/m_{\rm e})^3$, except the magnetic-moment term $-1/[2\kappa(2\ell+1)]$ in A_{40}, which is instead multiplied by the factor $(m_{\rm r}/m_{\rm e})^2$, and the argument $(Z\alpha)^{-2}$ of the logarithms is replaced by $(m_{\rm e}/m_{\rm r})(Z\alpha)^{-2}$.

4. Vacuum polarization

The stationary point nucleus second-order vacuum-polarization level shift is

$$E^{(2)}_{\rm VP} = \frac{\alpha}{\pi}\frac{(Z\alpha)^4}{n^3}H(Z\alpha)m_{\rm e}c^2, \quad (16)$$

where $H(x) = H^{(1)}(x) + H^{(\rm R)}(x)$ with

$$H^{(1)}(x) = V_{40} + V_{50}x + V_{61}x^2\ln(x^{-2}) + G^{(1)}_{\rm VP}(x)x^2.$$

Here, $V_{40} = -(4/15)\delta_{\ell 0}$, $V_{50} = (5\pi/48)\delta_{\ell 0}$, and $V_{61} = -(2/15)\delta_{\ell 0}$. Values of $G^{(1)}_{\rm VP}(\alpha)$ are given in Table V. Moreover, $H^{(\rm R)}(x) = G^{(\rm R)}_{\rm VP}(x)x^2$ with

$$G^{(\rm R)}_{\rm VP}(x) = \frac{19}{45} - \frac{\pi^2}{27} + \left(\frac{1}{16} - \frac{31\pi^2}{2880}\right)\pi x + \cdots \quad (17)$$

for $\ell = 0$. Higher-order and higher-ℓ terms are negligible. We multiply Eq. (16) by $(m_{\rm r}/m_{\rm e})^3$ and include a factor of $(m_{\rm e}/m_{\rm r})$ in the argument of the logarithm of the term proportional to V_{61}.

Vacuum polarization from $\mu^+\mu^-$ pairs is

$$E^{(2)}_{\mu\rm VP} = \frac{\alpha}{\pi}\frac{(Z\alpha)^4}{n^3}\left[-\frac{4}{15}\delta_{\ell 0}\right]\left(\frac{m_{\rm e}}{m_\mu}\right)^2\left(\frac{m_{\rm r}}{m_{\rm e}}\right)^3 m_{\rm e}c^2, \quad (18)$$

while the hadronic vacuum polarization is given by

$$E^{(2)}_{\rm had\,VP} = 0.671(15)E^{(2)}_{\mu\rm VP}. \quad (19)$$

Uncertainties are of type u_0. The muonic and hadronic vacuum-polarization contributions are negligible for higher-ℓ states.

5. Two-photon corrections

The two-photon correction is

$$E^{(4)} = \left(\frac{\alpha}{\pi}\right)^2\frac{(Z\alpha)^4}{n^3}F^{(4)}(Z\alpha)m_{\rm e}c^2, \quad (20)$$

where

TABLE V. Values of the function $G^{(1)}_{\rm VP}(\alpha)$.

n	$S_{1/2}$	$P_{1/2}$	$P_{3/2}$	$D_{3/2}$	$D_{5/2}$
1	−0.618 724				
2	−0.808 872	−0.064 006	−0.014 132		
3	−0.814 530				
4	−0.806 579	−0.080 007	−0.017 666		−0.000 000
6	−0.791 450				−0.000 000
8	−0.781 197			−0.000 000	−0.000 000
12				−0.000 000	−0.000 000

$$F^{(4)}(x) = B_{40} + B_{50}x + B_{63}x^2\ln^3(x^{-2}) + B_{62}x^2\ln^2(x^{-2}) + B_{61}x^2\ln(x^{-2}) + B_{60}x^2 + B_{72}x^3\ln^2(x^{-2}) + B_{71}x^3\ln(x^{-2}) + \cdots \quad (21)$$

with

$$B_{40} = \left[\frac{3\pi^2}{2}\ln 2 - \frac{10\pi^2}{27} - \frac{2179}{648} - \frac{9}{4}\zeta(3)\right]\delta_{\ell 0} + \left[\frac{\pi^2\ln 2}{2} - \frac{\pi^2}{12} - \frac{197}{144} - \frac{3\zeta(3)}{4}\right]\frac{1-\delta_{\ell 0}}{\kappa(2\ell+1)},$$

$$B_{50} = -21.554\,47(13)\delta_{\ell 0},$$

$$B_{63} = -(8/27)\delta_{\ell 0},$$

$$B_{62} = \frac{16}{9}\left[\frac{71}{60} - \ln 2 + \psi(n) + \gamma - \ln n - \frac{1}{n} + \frac{1}{4n^2}\right]\delta_{\ell 0} + \frac{4}{27}\frac{n^2-1}{n^2}\delta_{\ell 1}.$$

Here, $\zeta(z)$, γ, and $\psi(z)$ are the Riemann zeta function, Euler's constant, and the psi function, respectively, and

$$B_{61} = \left\{\frac{413\,581}{64\,800} + \frac{4N(n\mathrm{S})}{3} + \frac{2027\pi^2}{864} - \frac{616\ln 2}{135} - \frac{2\pi^2\ln 2}{3} + \frac{40\ln^2 2}{9} + \zeta(3) + \left(\frac{304}{135} - \frac{32\ \ln\ 2}{9}\right)\left[\frac{3}{4} + \gamma + \psi(n) - \ln\ n - \frac{1}{n} + \frac{1}{4n^2}\right] - \frac{43}{36} + \frac{133\pi^2}{864}\right\}\delta_{\ell 0} + \left[\frac{4}{3}N(n\mathrm{P}) + \frac{n^2-1}{n^2}\left(\frac{31}{405} + \frac{1}{3}\delta_{j\frac{1}{2}} - \frac{8}{27}\ln 2\right)\right]\delta_{\ell 1},$$

where the relevant values and uncertainties for the function $N(n\ell)$ are given in Table VI. The last two terms contributing to B_{61} for S states are recently computed light-by-light corrections obtained by Czarnecki and Szafron (2016).

Before describing the next term in Eq. (21), i.e., B_{60}, it is useful to observe that Karshenboim and Ivanov (2018b) have derived that

$$B_{72} = \left(-\frac{139}{48} + \frac{4\ln 2}{3} - \frac{5}{72}\right)\pi\delta_{\ell 0}.$$

In addition, they find the difference

$$B_{71}(n\mathrm{S}) - B_{71}(1\mathrm{S}) = \pi\left(\frac{427}{36} - \frac{16}{3}\ln 2\right)\left[\frac{3}{4} - \frac{1}{n} + \frac{1}{4n^2} + \psi(n) + \gamma - \ln n\right] \quad (22)$$

for S states, but also that

$$B_{71}(n\mathrm{P}) = \pi\left(\frac{139}{144} - \frac{4\ln 2}{9} + \frac{5}{216}\right)\left(1 - \frac{1}{n^2}\right)$$

for P states, and $B_{71}(n\ell) = 0$ for states with $\ell > 1$.

We determine the coefficients $B_{60}(1\mathrm{S})$ and $B_{71}(1\mathrm{S})$ by combining the analytical expression for B_{72} and the values and uncertainties for the remainder

$$G_{\mathrm{QED2}}(x) = B_{60} + B_{72}x\ln^2(x^{-2}) + B_{71}x\ln(x^{-2}) + \cdots \quad (23)$$

for the 1S state extrapolated to $x \le 2\alpha$ by Yerokhin, Pachucki, and Patkóš (2019) from numerical calculations of $G_{\mathrm{QED2}}(x)$ as a function of x for $x = Z\alpha$ with $Z \ge 15$ given by Yerokhin, Indelicato, and Shabaev (2008) and Yerokhin (2009, 2018). Specifically, the remainder has three contributions. The largest by far has been evaluated at $x = 0$ and α. The remaining two are available for $x = \alpha$ and 2α. Fits to each of the three contributions give corresponding contributions to $B_{60}(1\mathrm{S})$ and $B_{71}(1\mathrm{S})$. We assign a type-u_0 state-independent standard uncertainty of 9.3 for $B_{60}(1\mathrm{S})$ and a 10% type-u_0 uncertainty to $B_{71}(1\mathrm{S})$. The difference $B_{60}(n\mathrm{S}) - B_{60}(1\mathrm{S})$, given by Jentschura, Czarnecki, and Pachucki (2005), is then used to obtain $B_{60}(n\mathrm{S})$ for $n > 1$ and adds an additional small state-dependent uncertainty. Similarly, the expression for $B_{71}(n\mathrm{S}) - B_{71}(1\mathrm{S})$ in Eq. (22) is used to determine $B_{71}(n\mathrm{S})$.

Values for B_{60} for nP and nD states with $n = 1, \ldots, 6$ are those published by Jentschura, Czarnecki, and Pachucki (2005) and Jentschura (2006), but using in place of the results in Eqs. (A3) and (A6) of the latter paper the corrected results given in Eqs. (24) and (25) by Yerokhin, Pachucki, and Patkóš (2019). For $n > 6$, we use $B_{60} = g_0 + g_1/n$ with g_0 and g_1 determined from the values and uncertainties of B_{60} at $n = 5$ and 6.

Relevant values and uncertainties for $B_{60}(n\ell)$ and $B_{71}(1\mathrm{S})$ are listed in Table VII. For the B_{60} of S states, the first number in parentheses is the state-dependent uncertainty of type u_n, while the second number in parentheses is the state-independent uncertainty of type u_0. Note that the extrapolation procedure for nS states is by no means unique. In fact, Yerokhin, Pachucki, and Patkóš (2019) used a different approach that leads to consistent and equally accurate values for $B_{60}(n\mathrm{S})$. For $B_{71}(1\mathrm{S})$ and $B_{60}(n\ell)$ with $\ell > 0$, the uncertainties are of type u_0.

As with the one-photon correction, the two-photon correction is multiplied by the reduced-mass factor $(m_r/m_e)^3$, except the magnetic-moment term proportional to $1/[\kappa(2\ell+1)]$ in B_{40} which is multiplied by the factor $(m_r/m_e)^2$, and the argument $(Z\alpha)^{-2}$ of the logarithms is replaced by $(m_e/m_r)(Z\alpha)^{-2}$.

TABLE VI. Values of $N(n\ell)$ used in the 2018 adjustment and from Jentschura (2003) and Jentschura, Czarnecki, and Pachucki (2005).

n	$N(n\mathrm{S})$	$N(n\mathrm{P})$
1	17.855 672 03(1)	
2	12.032 141 58(1)	0.003 300 635(1)
3	10.449 809(1)	
4	9.722 413(1)	−0.000 394 332(1)
6	9.031 832(1)	
8	8.697 639(1)	

TABLE VII. Values of B_{60} and $B_{71}(n\mathrm{S}_{1/2})$ used in the 2018 adjustment. The uncertainties of B_{60} are explained in the text.

n	$B_{60}(n\mathrm{S}_{1/2})$	$B_{60}(n\mathrm{P}_{1/2})$	$B_{60}(n\mathrm{P}_{3/2})$	$B_{60}(n\mathrm{D}_{3/2})$	$B_{60}(n\mathrm{D}_{5/2})$	$B_{71}(n\mathrm{S}_{1/2})$
1	−78.7(0.3)(9.3)					−116(12)
2	−63.6(0.3)(9.3)	−1.8(3)	−1.8(3)			−100(12)
3	−60.5(0.6)(9.3)					−94(12)
4	−58.9(0.8)(9.3)	−2.5(3)	−2.5(3)		0.178(2)	−91(12)
6	−56.9(0.8)(9.3)				0.207(4)	−88(12)
8	−55.9(2.0)(9.3)			0.245(5)	0.221(5)	−86(12)
12				0.259(7)	0.235(7)	

6. Three-photon corrections

The three-photon contribution in powers of $Z\alpha$ is

$$E^{(6)} = \left(\frac{\alpha}{\pi}\right)^3 \frac{(Z\alpha)^4}{n^3} F^{(6)}(Z\alpha) m_e c^2, \tag{24}$$

where

$$F^{(6)}(x) = C_{40} + C_{50}x + C_{63}x^2\ln^3(x) + C_{62}x^2\ln^2(x) + C_{61}x^2\ln x + C_{60}x^2 + \cdots. \tag{25}$$

The leading term C_{40} is

$$C_{40} = \left[-\frac{568a_4}{9} + \frac{85\zeta(5)}{24} - \frac{121\pi^2\zeta(3)}{72} - \frac{84\,071\zeta(3)}{2304} - \frac{71\ln^4 2}{27} - \frac{239\pi^2\ln^2 2}{135} + \frac{4787\pi^2\ln 2}{108} + \frac{1591\pi^4}{3240} - \frac{252\,251\pi^2}{9720} + \frac{679\,441}{93\,312}\right]\delta_{\ell 0} + \left[-\frac{100a_4}{3} + \frac{215\zeta(5)}{24} - \frac{83\pi^2\zeta(3)}{72} - \frac{139\zeta(3)}{18} - \frac{25\ln^4 2}{18} + \frac{25\pi^2\ln^2 2}{18} + \frac{298\pi^2\ln 2}{9} + \frac{239\pi^4}{2160} - \frac{17\,101\pi^2}{810} - \frac{28\,259}{5\,184}\right]\frac{1-\delta_{\ell 0}}{\kappa(2\ell+1)},$$

where $a_4 = \sum_{n=1}^{\infty} 1/(2^n n^4) = 0.517\,479\,061\ldots$. Partial results for C_{50} have been calculated by Eides and Shelyuto (2004, 2007). We use $C_{50} = 0$ with uncertainty $30\delta_{\ell 0}$ of type u_0.

Karshenboim and Ivanov (2018b) derived that

$$C_{63} = 0$$

and

$$C_{62} = -\frac{2}{3}\left(-\frac{1523}{648} - \frac{10\pi^2}{27} + \frac{3}{2}\pi^2\ln 2 - \frac{9}{4}\zeta(3) - \frac{82}{81}\right)\delta_{\ell 0}.$$

They also presented an expression for the difference $C_{61}(n\mathrm{S}) - C_{61}(1\mathrm{S})$ as well as

$$C_{61}(n\mathrm{P}) = \frac{2}{9}\frac{n^2-1}{n^2}\left(-\frac{1523}{648} - \frac{10\pi^2}{27} + \frac{3}{2}\pi^2\ln 2 - \frac{9}{4}\zeta(3) - \frac{82}{81}\right),$$

and $C_{61}(n\ell) = 0$ for $\ell > 1$. We do not use the expression for the difference. Instead, we assume that $C_{61}(n\mathrm{S}) = 0$ with an uncertainty of 10 of type u_n. Finally, we set $C_{60} = 0$ with uncertainty 1 of type u_n for P and higher ℓ states. For S states we also use $C_{60} = 0$, but do not need to specify an uncertainty as the uncertainty of their three-photon correction is determined by the uncertainties of C_{50} and C_{61}.

The dominant effect of the finite mass of the nucleus is taken into account by multiplying terms proportional to $\delta_{\ell 0}$ by the reduced-mass factor $(m_r/m_e)^3$ and the term proportional to $1/[\kappa(2\ell+1)]$, the magnetic-moment term, by the factor $(m_r/m_e)^2$.

The contribution from four photons is expected to be negligible at the level of uncertainty of current interest.

7. Finite nuclear size and polarizability

Finite-nuclear-size and nuclear-polarizability corrections are ordered by powers in α, following Yerokhin, Pachucki, and Patkóš (2019), rather than by finite size and polarizability. Thus, we write for the total correction

$$E_{\mathrm{nucl}} = \sum_{i=4}^{\infty} E_{\mathrm{nucl}}^{(i)}, \tag{26}$$

where index i indicates the order in α. The first and lowest-order contribution is

$$E_{\mathrm{nucl}}^{(4)} = \frac{2}{3} m_e c^2 \frac{(Z\alpha)^4}{n^3}\left(\frac{m_r}{m_e}\right)^3\left(\frac{r_N}{\lambda\!\!\!^{-}_C}\right)^2\delta_{\ell 0} \tag{27}$$

and is solely due to the finite root-mean-square (rms) charge radius r_N of nucleus N. Here, $\lambda\!\!\!^{-}_C = \hbar/m_e c$ is the reduced Compton wavelength of the electron.

The α^5 correction has both nuclear-size and polarizability contributions and has been computed by Tomalak (2019). For hydrogen, the correction is parametrized as

$$E_{\mathrm{nucl}}^{(5)}(\mathrm{H}) = -\frac{1}{3} m_e c^2 \frac{(Z\alpha)^5}{n^3}\left(\frac{m_r}{m_e}\right)^3\left(\frac{r_{\mathrm{pF}}}{\lambda\!\!\!^{-}_C}\right)^3\delta_{\ell 0} \tag{28}$$

with effective Friar radius for the proton

$$r_{\mathrm{pF}} = 1.947(75)\ \mathrm{fm}. \tag{29}$$

The functional form of Eq. (28) is inspired by the results of Friar (1979) and his definition of the third Zemach moment.

For deuterium, the α^5 correction is parametrized as (Yerokhin, Pachucki, and Patkóš, 2019)

$$E^{(5)}_{\rm nucl}({\rm D}) = -\frac{1}{3} m_{\rm e} c^2 \frac{(Z\alpha)^5}{n^3} \left(\frac{m_{\rm r}}{m_{\rm e}}\right)^3 \times \left[Z\left(\frac{r_{\rm pF}}{\lambda\!\!\!^{-}_{\rm C}}\right)^3 + (A-Z)\left(\frac{r_{\rm nF}}{\lambda\!\!\!^{-}_{\rm C}}\right)^3\right]\delta_{\ell 0} + E^{(5)}_{\rm pol}({\rm D}) \quad (30)$$

with atomic number A, effective Friar radius for the neutron

$$r_{\rm nF} = 1.43(16)\ {\rm fm}, \quad (31)$$

and two-photon polarizability

$$E^{(5)}_{\rm pol}({\rm D})/h = -21.78(22)\frac{\delta_{\ell 0}}{n^3}\ {\rm kHz}. \quad (32)$$

In principle, the effective Friar radius for the proton might be different in hydrogen and deuterium. Similarly, the Friar radius of the neutron extracted from electron-neutron scattering can be different from that in a deuteron. We assume that such changes in the Friar radii are smaller than the quoted uncertainties.

The α^6 correction has finite-nuclear-size, nuclear-polarizability, and radiative finite-nuclear-size contributions and can thus be written as $E^{(6)}_{\rm nucl} = E^{(6)}_{\rm fns} + E^{(6)}_{\rm pol} + E^{(6)}_{\rm rad}$. The finite-nuclear-size and nuclear-polarizability contributions are given by Pachucki, Patkóš, and Yerokhin (2018). The finite-nuclear-size contribution is

$$E^{(6)}_{\rm fns} = m_{\rm e} c^2 \frac{(Z\alpha)^6}{n^3}\left(\frac{m_{\rm r}}{m_{\rm e}}\right)^3\left(\frac{r_N}{\lambda\!\!\!^{-}_{\rm C}}\right)^2\left\{-\frac{2}{3}\left[\frac{9}{4n^2} - 3 - \frac{1}{n} + 2\gamma - \ln(n/2) + \psi(n) + \ln\left(\frac{m_{\rm r}}{m_{\rm e}}\frac{r_{N2}}{\lambda\!\!\!^{-}_{\rm C}} Z\alpha\right)\right]\delta_{\ell 0} + \frac{1}{6}\left(1 - \frac{1}{n^2}\right)\delta_{\kappa 1}\right\}, \quad (33)$$

and the polarization contribution for hydrogen is

$$E^{(6)}_{\rm pol}({\rm H})/h = 0.393\frac{\delta_{\ell 0}}{n^3}\ {\rm kHz} \quad (34)$$

with a 100% uncertainty and for deuterium

$$E^{(6)}_{\rm pol}({\rm D})/h = -0.541\frac{\delta_{\ell 0}}{n^3}\ {\rm kHz} \quad (35)$$

with a 75% uncertainty. The effective radius r_{N2} describes high-energy contributions and is given by

$$r_{N2} = 1.068\,497 r_N. \quad (36)$$

The radiative finite-nuclear-size contribution of order α^6 is (Eides, Grotch, and Shelyuto, 2001)

$$E^{(6)}_{\rm rad} = \frac{2}{3} m_{\rm e} c^2 \frac{\alpha(Z\alpha)^5}{n^3}\left(\frac{m_{\rm r}}{m_{\rm e}}\right)^3\left(\frac{r_N}{\lambda\!\!\!^{-}_{\rm C}}\right)^2 (4\ln 2 - 5)\delta_{\ell 0}. \quad (37)$$

Next-order radiative finite-nuclear-size corrections of order α^7 also have logarithmic dependencies on α; see Yerokhin (2011). In fact, for nS states we have

$$E^{(7)}_{\rm nucl} = \frac{2}{3} m_{\rm e} c^2 \frac{\alpha(Z\alpha)^6}{\pi n^3}\left(\frac{m_{\rm r}}{m_{\rm e}}\right)^3\left(\frac{r_N}{\lambda\!\!\!^{-}_{\rm C}}\right)^2 \times \left[-\frac{2}{3}\ln^2\{(Z\alpha)^{-2}\} + \ln^2\left(\frac{m_{\rm r}}{m_{\rm e}}\frac{r_N}{\lambda\!\!\!^{-}_{\rm C}}\right)\right]. \quad (38)$$

We assume a zero value with uncertainty 1 for the uncomputed coefficient of $\ln(Z\alpha)^{-2}$ inside the square brackets. For $n{\rm P}_j$ states we have

$$E^{(7)}_{\rm nucl} = \frac{1}{6} m_{\rm e} c^2 \frac{\alpha(Z\alpha)^6}{\pi n^3}\left(\frac{m_{\rm r}}{m_{\rm e}}\right)^3\left(\frac{r_N}{\lambda\!\!\!^{-}_{\rm C}}\right)^2\left(1 - \frac{1}{n^2}\right) \times \left[\frac{8}{9}\ln\{(Z\alpha)^{-2}\} - \frac{8}{9}\ln 2 + \frac{11}{27} + \delta_{\kappa 1} + \frac{4n^2}{n^2-1}N(n{\rm P})\right] \quad (39)$$

with a zero value for the uncomputed coefficient of $Z\alpha$ inside the square brackets with an uncertainty of 1. [This equation fixes a typographical error in Eq. (64) of Yerokhin, Pachucki, and Patkóš (2019). See also Eq. (31) of Jentschura (2003).] We assume a zero value for states with $\ell > 1$.

Uncertainties in this subsection are of type u_0. Higher-order corrections are expected to be negligible.

8. Radiative-recoil corrections

Corrections for radiative-recoil effects are

$$E_{\rm RR} = \frac{m_{\rm r}^3}{m_{\rm e}^2 m_N}\frac{\alpha(Z\alpha)^5}{\pi^2 n^3} m_{\rm e} c^2 \delta_{\ell 0}\left[6\zeta(3) - 2\pi^2\ln 2 + \frac{35\pi^2}{36} - \frac{448}{27} + \frac{2}{3}\pi(Z\alpha)\ln^2\{(Z\alpha)^{-2}\} + \cdots\right]. \quad (40)$$

We assume a zero value for the uncomputed coefficient of $(Z\alpha)\ln(Z\alpha)^{-2}$ inside the square brackets with an uncertainty of 10 of type u_0 and 1 for type u_n. Corrections for higher-ℓ states are negligible.

9. Nucleus self-energy

The nucleus self-energy correction is

$$E_{\rm SEN} = \frac{4Z^2\alpha(Z\alpha)^4}{3\pi n^3}\frac{m_{\rm r}^3}{m_N^2} c^2\left[\ln\left(\frac{m_N}{m_{\rm r}(Z\alpha)^2}\right)\delta_{\ell 0} - \ln k_0(n,\ell)\right], \quad (41)$$

with an uncertainty of 0.5 for S states in the constant (α-independent) term in square brackets. This uncertainty is of type u_0 and given by Eq. (41) with the factor in the square brackets replaced by 0.5. For higher-ℓ states, the correction is negligibly small compared to current experimental uncertainties.

B. Total theoretical energies and uncertainties

The theoretical energy of centroid $E_n(L)$ of a relativistic level $L = n\ell_j$ is the sum of the contributions given in Secs. VII.A.1–VII.A.9. Here, atom $X = {\rm H}$ or D. Uncertainties in the adjusted constants that enter the

theoretical expressions are found by the least-squares adjustment. Here, the most important adjusted constants are $R_\infty = \alpha^2 m_e c^2/2hc$, α, r_p, and r_d.

The uncertainty in the theoretical energy is taken into account by introducing additive corrections to the energies. Specifically, we write

$$E_X(L) \to E_X(L) + \delta_{\rm th}(X, L)$$

for relativistic levels $L = n\ell_j$ in atom X. Here, energy $\delta_{\rm th}(X, L)$ is treated as an adjusted constant and we include $\delta_X(L)$ as an input datum with zero value and an uncertainty that is the square root of the sum of the squares of the uncertainties of the individual contributions. That is,

$$u^2[\delta_X(L)] = \sum_i [u_{0i}^2(X, L) + u_{ni}^2(X, L)], \tag{42}$$

where energies $u_{0i}(X, L)$ and $u_{ni}(X, L)$ are type-u_0 and -u_n uncertainties of contribution i. The observational equation $\delta_X(L) \doteq \delta_{\rm th}(X, L)$ is added to χ^2.

Covariances among the corrections $\delta_X(L)$ are accounted for in the adjustment. We assume that nonzero covariances for a given atom X only occur between states with the same ℓ and j. We then have

$$u[\delta_X(n_1\ell_j), \delta_X(n_2\ell_j)] = \sum_i u_{0i}(X, n_2\ell_j) u_{0i}(X, n_1\ell_j),$$

when $n_1 \neq n_2$ and only uncertainties of type u_0 are present. Covariances between the corrections δ for hydrogen and deuterium in the same electronic state L are

$$u[\delta_{\rm H}(L), \delta_{\rm D}(L)] = \sum_{i=\{i_c\}} [u_{0i}({\rm H}, L) u_{0i}({\rm D}, L) + u_{ni}({\rm H}, L) u_{ni}({\rm D}, L)]$$

and for $n_1 \neq n_2$

$$u[\delta_{\rm H}(n_1\ell_j), \delta_{\rm D}(n_2\ell_j)] = \sum_{i=\{i_c\}} u_{0i}({\rm H}, n_1\ell_j) u_{0i}({\rm D}, n_2\ell_j),$$

where the summation over i is only over the uncertainties common to hydrogen and deuterium. This excludes, for example, contributions that depend on the nuclear-charge radii.

Values and standard uncertainties of $\delta_X(n\ell_j)$ are given in Table VIII and the non-negligible covariances of the corrections δ are given as correlation coefficients in Table IX.

C. Experimentally determined transition energies in hydrogen and deuterium

Table X gives the measured transition energies as well as measured weighted differences between transition energies in hydrogen and deuterium used as input data in the 2018 adjustment. All but four data are the same as in the 2014 CODATA report. The new results in hydrogen are reviewed in the next three subsections. The transition energies were measured at the Max-Planck-Institut für Quantenoptik (MPQ), Garching, Germany, the Laboratoire Kastler-Brossel (LKB), Paris, France, and York University (York), Toronto, Canada.

TABLE VIII. Summary of input data for the additive energy corrections to account for missing contributions to the theoretical description of the electronic hydrogen (H) and deuterium (D) energy levels. These correspond to 25 additive corrections $\delta_{\rm H,D}(n\ell_j)$ for the centroids of levels $n\ell_j$. The label in the first column is used in Table IX to list correlation coefficients among these data and in Table XXIII for observational equations. Relative uncertainties are with respect to the binding energy.

	Input datum	Value (kHz)	Rel. stand. uncert. u_r
B1	$\delta_{\rm H}(1{\rm S}_{1/2})/h$	0.0(1.6)	4.9×10^{-13}
B2	$\delta_{\rm H}(2{\rm S}_{1/2})/h$	0.00(20)	2.4×10^{-13}
B3	$\delta_{\rm H}(3{\rm S}_{1/2})/h$	0.000(59)	1.6×10^{-13}
B4	$\delta_{\rm H}(4{\rm S}_{1/2})/h$	0.000(25)	1.2×10^{-13}
B5	$\delta_{\rm H}(6{\rm S}_{1/2})/h$	0.000(12)	1.3×10^{-13}
B6	$\delta_{\rm H}(8{\rm S}_{1/2})/h$	0.0000(51)	9.9×10^{-14}
B7	$\delta_{\rm H}(2{\rm P}_{1/2})/h$	0.0000(39)	4.8×10^{-15}
B8	$\delta_{\rm H}(4{\rm P}_{1/2})/h$	0.0000(16)	7.6×10^{-15}
B9	$\delta_{\rm H}(2{\rm P}_{3/2})/h$	0.0000(39)	4.8×10^{-15}
B10	$\delta_{\rm H}(4{\rm P}_{3/2})/h$	0.0000(16)	7.6×10^{-15}
B11	$\delta_{\rm H}(8{\rm D}_{3/2})/h$	0.000 000(13)	2.6×10^{-16}
B12	$\delta_{\rm H}(12{\rm D}_{3/2})/h$	0.000 0000(40)	1.8×10^{-16}
B13	$\delta_{\rm H}(4{\rm D}_{5/2})/h$	0.000 00(17)	8.2×10^{-16}
B14	$\delta_{\rm H}(6{\rm D}_{5/2})/h$	0.000 000(58)	6.3×10^{-16}
B15	$\delta_{\rm H}(8{\rm D}_{5/2})/h$	0.000 000(22)	4.2×10^{-16}
B16	$\delta_{\rm H}(12{\rm D}_{5/2})/h$	0.000 0000(64)	2.8×10^{-16}
B17	$\delta_{\rm D}(1{\rm S}_{1/2})/h$	0.0(1.5)	4.5×10^{-13}
B18	$\delta_{\rm D}(2{\rm S}_{1/2})/h$	0.00(18)	2.2×10^{-13}
B19	$\delta_{\rm D}(4{\rm S}_{1/2})/h$	0.000(23)	1.1×10^{-13}
B20	$\delta_{\rm D}(8{\rm S}_{1/2})/h$	0.0000(49)	9.6×10^{-14}
B21	$\delta_{\rm D}(8{\rm D}_{3/2})/h$	0.000 0000(95)	1.8×10^{-16}
B22	$\delta_{\rm D}(12{\rm D}_{3/2})/h$	0.000 0000(28)	1.2×10^{-16}
B23	$\delta_{\rm D}(4{\rm D}_{5/2})/h$	0.000 00(15)	7.5×10^{-16}
B24	$\delta_{\rm D}(8{\rm D}_{5/2})/h$	0.000 000(19)	3.8×10^{-16}
B25	$\delta_{\rm D}(12{\rm D}_{5/2})/h$	0.000 0000(58)	2.5×10^{-16}

These researchers considered the $2{\rm S} - 4{\rm P}$, $1{\rm S} - 3{\rm S}$, and $2{\rm S} - 2{\rm P}_{1/2}$ transitions.

Observational equations for the data are given in Table XXIII. Values for additive corrections $\delta_X(n\ell_j)$ and $\delta_{\rm hfs,H}[n\ell_j(f)]$ to account for the uncertainties in the theoretical expressions are given in Table VIII. Some of the data are correlated and their correlation coefficients when greater than 0.0001 are given in Table IX.

The H and D input data are displayed in Fig. 4. The first thing to note is that the data separate into $1{\rm S} - 2{\rm S}$ transition energies measured to approximately $h \times 10$ Hz and those that have been measured to $\sim h \times 10$ kHz. The uncertainties of these input data are shown without the 1.6 expansion factor applied to these data in the least-squares adjustment. Secondly, the figure shows the adjusted, or fitted, transition energies and their standard uncertainties for these input data after the application of the 1.6 expansion factor. The values and standard uncertainties of the fitted $1{\rm S} - 2{\rm S}$ transition energies are in agreement with those of the experimental data. The standard uncertainties of the fitted values for most of the other data are an order of magnitude smaller than the uncertainties of the corresponding input data. The exceptions are three of the four newly added data. They are indicated as MPQ(2017), LKB(2018), and York(2019) in Fig. 4. In

TABLE IX. Correlation coefficients $r(x_i, x_j) > 0.0001$ among the input data for the hydrogen and deuterium energy levels given in Tables X and VIII. Coefficients r are strictly zero between input data An and Bm for positive integers n and m.

$r(\mathrm{A1,A2}) = 0.1049$	$r(\mathrm{A1,A3}) = 0.2095$	$r(\mathrm{A1,A4}) = 0.0404$	$r(\mathrm{A2,A3}) = 0.0271$	$r(\mathrm{A2,A4}) = 0.0467$
$r(\mathrm{A3,A4}) = 0.0110$	$r(\mathrm{A6,A7}) = 0.7069$	$r(\mathrm{A10,A11}) = 0.3478$	$r(\mathrm{A10,A12}) = 0.4532$	$r(\mathrm{A10,A13}) = 0.1225$
$r(\mathrm{A10,A14}) = 0.1335$	$r(\mathrm{A10,A15}) = 0.1419$	$r(\mathrm{A10,A16}) = 0.0899$	$r(\mathrm{A10,A17}) = 0.1206$	$r(\mathrm{A10,A18}) = 0.0980$
$r(\mathrm{A10,A19}) = 0.1235$	$r(\mathrm{A10,A20}) = 0.0225$	$r(\mathrm{A10,A21}) = 0.0448$	$r(\mathrm{A11,A12}) = 0.4696$	$r(\mathrm{A11,A13}) = 0.1273$
$r(\mathrm{A11,A14}) = 0.1387$	$r(\mathrm{A11,A15}) = 0.1475$	$r(\mathrm{A11,A16}) = 0.0934$	$r(\mathrm{A11,A17}) = 0.1253$	$r(\mathrm{A11,A18}) = 0.1019$
$r(\mathrm{A11,A19}) = 0.1284$	$r(\mathrm{A11,A20}) = 0.0234$	$r(\mathrm{A11,A21}) = 0.0466$	$r(\mathrm{A12,A13}) = 0.1648$	$r(\mathrm{A12,A14}) = 0.1795$
$r(\mathrm{A12,A15}) = 0.1908$	$r(\mathrm{A12,A16}) = 0.1209$	$r(\mathrm{A12,A17}) = 0.1622$	$r(\mathrm{A12,A18}) = 0.1319$	$r(\mathrm{A12,A19}) = 0.1662$
$r(\mathrm{A12,A20}) = 0.0303$	$r(\mathrm{A12,A21}) = 0.0602$	$r(\mathrm{A13,A14}) = 0.5699$	$r(\mathrm{A13,A15}) = 0.6117$	$r(\mathrm{A13,A16}) = 0.1127$
$r(\mathrm{A13,A17}) = 0.1512$	$r(\mathrm{A13,A18}) = 0.1229$	$r(\mathrm{A13,A19}) = 0.1548$	$r(\mathrm{A13,A20}) = 0.0282$	$r(\mathrm{A13,A21}) = 0.0561$
$r(\mathrm{A14,A15}) = 0.6667$	$r(\mathrm{A14,A16}) = 0.1228$	$r(\mathrm{A14,A17}) = 0.1647$	$r(\mathrm{A14,A18}) = 0.1339$	$r(\mathrm{A14,A19}) = 0.1687$
$r(\mathrm{A14,A20}) = 0.0307$	$r(\mathrm{A14,A21}) = 0.0612$	$r(\mathrm{A15,A16}) = 0.1305$	$r(\mathrm{A15,A17}) = 0.1750$	$r(\mathrm{A15,A18}) = 0.1423$
$r(\mathrm{A15,A19}) = 0.1793$	$r(\mathrm{A15,A20}) = 0.0327$	$r(\mathrm{A15,A21}) = 0.0650$	$r(\mathrm{A16,A17}) = 0.4750$	$r(\mathrm{A16,A18}) = 0.0901$
$r(\mathrm{A16,A19}) = 0.1136$	$r(\mathrm{A16,A20}) = 0.0207$	$r(\mathrm{A16,A21}) = 0.0412$	$r(\mathrm{A17,A18}) = 0.1209$	$r(\mathrm{A17,A19}) = 0.1524$
$r(\mathrm{A17,A20}) = 0.0278$	$r(\mathrm{A17,A21}) = 0.0553$	$r(\mathrm{A18,A19}) = 0.5224$	$r(\mathrm{A18,A20}) = 0.0226$	$r(\mathrm{A18,A21}) = 0.0449$
$r(\mathrm{A19,A20}) = 0.0284$	$r(\mathrm{A19,A21}) = 0.0566$	$r(\mathrm{A20,A21}) = 0.1412$	$r(\mathrm{A24,A25}) = 0.0834$	
$r(\mathrm{B1,B2}) = 0.9946$	$r(\mathrm{B1,B3}) = 0.9937$	$r(\mathrm{B1,B4}) = 0.9877$	$r(\mathrm{B1,B5}) = 0.6140$	$r(\mathrm{B1,B6}) = 0.6124$
$r(\mathrm{B1,B17}) = 0.9700$	$r(\mathrm{B1,B18}) = 0.9653$	$r(\mathrm{B1,B19}) = 0.9575$	$r(\mathrm{B1,B20}) = 0.5644$	$r(\mathrm{B2,B3}) = 0.9937$
$r(\mathrm{B2,B4}) = 0.9877$	$r(\mathrm{B2,B5}) = 0.6140$	$r(\mathrm{B2,B6}) = 0.6124$	$r(\mathrm{B2,B17}) = 0.9653$	$r(\mathrm{B2,B18}) = 0.9700$
$r(\mathrm{B2,B19}) = 0.9575$	$r(\mathrm{B2,B20}) = 0.5644$	$r(\mathrm{B3,B4}) = 0.9869$	$r(\mathrm{B3,B5}) = 0.6135$	$r(\mathrm{B3,B6}) = 0.6119$
$r(\mathrm{B3,B17}) = 0.9645$	$r(\mathrm{B3,B18}) = 0.9645$	$r(\mathrm{B3,B19}) = 0.9567$	$r(\mathrm{B3,B20}) = 0.5640$	$r(\mathrm{B4,B5}) = 0.6097$
$r(\mathrm{B4,B6}) = 0.6082$	$r(\mathrm{B4,B17}) = 0.9586$	$r(\mathrm{B4,B18}) = 0.9586$	$r(\mathrm{B4,B19}) = 0.9704$	$r(\mathrm{B4,B20}) = 0.5605$
$r(\mathrm{B5,B6}) = 0.3781$	$r(\mathrm{B5,B17}) = 0.5959$	$r(\mathrm{B5,B18}) = 0.5959$	$r(\mathrm{B5,B19}) = 0.5911$	$r(\mathrm{B5,B20}) = 0.3484$
$r(\mathrm{B6,B17}) = 0.5944$	$r(\mathrm{B6,B18}) = 0.5944$	$r(\mathrm{B6,B19}) = 0.5896$	$r(\mathrm{B6,B20}) = 0.9884$	$r(\mathrm{B7,B8}) = 0.0001$
$r(\mathrm{B9,B10}) = 0.0001$	$r(\mathrm{B11,B12}) = 0.6741$	$r(\mathrm{B11,B21}) = 0.9428$	$r(\mathrm{B11,B22}) = 0.4803$	$r(\mathrm{B12,B21}) = 0.4782$
$r(\mathrm{B12,B22}) = 0.9428$	$r(\mathrm{B13,B14}) = 0.2061$	$r(\mathrm{B13,B15}) = 0.2391$	$r(\mathrm{B13,B16}) = 0.2421$	$r(\mathrm{B13,B23}) = 0.9738$
$r(\mathrm{B13,B24}) = 0.1331$	$r(\mathrm{B13,B25}) = 0.1352$	$r(\mathrm{B14,B15}) = 0.2225$	$r(\mathrm{B14,B16}) = 0.2253$	$r(\mathrm{B14,B23}) = 0.1128$
$r(\mathrm{B14,B24}) = 0.1238$	$r(\mathrm{B14,B25}) = 0.1258$	$r(\mathrm{B15,B16}) = 0.2614$	$r(\mathrm{B15,B23}) = 0.1309$	$r(\mathrm{B15,B24}) = 0.9698$
$r(\mathrm{B15,B25}) = 0.1459$	$r(\mathrm{B16,B23}) = 0.1325$	$r(\mathrm{B16,B24}) = 0.1455$	$r(\mathrm{B16,B25}) = 0.9692$	$r(\mathrm{B17,B18}) = 0.9955$
$r(\mathrm{B17,B19}) = 0.9875$	$r(\mathrm{B17,B20}) = 0.5821$	$r(\mathrm{B18,B19}) = 0.9874$	$r(\mathrm{B18,B20}) = 0.5821$	$r(\mathrm{B19,B20}) = 0.5774$
$r(\mathrm{B21,B22}) = 0.3407$	$r(\mathrm{B23,B24}) = 0.0729$	$r(\mathrm{B23,B25}) = 0.0740$	$r(\mathrm{B24,B25}) = 0.0812$	

summary, the $1S - 2S$ transition energies, these three input data, and the muonic-H and muonic-D Lamb-shift measurements to be discussed in Sec. XII determine the values of the Rydberg constant and charge radii.

1. Measurement of the hydrogen 2S – 4P transition

The hydrogen transition energy from the $2S_{1/2}$ hyperfine centroid to the 4P fine-structure centroid was measured by Beyer *et al.* (2017) at the MPQ. This new datum is item A9 in Table X. Here, the fine-structure centroid of a level $n\ell$ is

$$E_X(n\ell) = \frac{1}{\sum_j (2j+1)} \sum_j (2j+1) E_X(n\ell_j), \qquad (43)$$

where the sum over quantum number j runs from $|\ell - 1/2|$ to $\ell + 1/2$ and $E_X(n\ell_j)$ is the hyperfine centroid of level $n\ell_j$.

In the experiment, cold ground-state hydrogen atoms emerge from a copper nozzle held at a temperature of 5.8 K. These atoms are excited to the metastable $2S_{1/2}(f = 0)$ hyperfine level by a Doppler-free two-photon excitation using 243 nm light, chopped on and off at 160 Hz, enabling a thorough study of Doppler shifts. Starting from this metastable state, transition energies for the hyperfine-resolved transitions $2S_{1/2}(f = 0) \rightarrow 4P_{1/2}(f = 1)$ and $2S_{1/2}(f = 0) \rightarrow 4P_{3/2}(f = 1)$ were measured to about 1 part in 10 000 of the linewidth using a stable retroreflected 486 nm laser (Beyer *et al.*, 2016) oriented perpendicular to the propagation direction of the atoms. Here, crucially dipole selection rules forbid excitations to $P_{3/2}(f = 0)$ and $P_{3/2}(f = 2)$ states.

Atomic hydrogen in the 4P state mainly decays to the ground 1S state by emission of a Lyman-γ 97 nm photon. At MPQ, the emission rate of these photons as a function of the 486 nm laser frequency was detected. Lyman-γ radiation ejects electrons from graphite, which, in turn, can be efficiently counted with channel electron multipliers. Two such detectors were used to retain some directional information about the emitted Lyman-γ photons.

Important for the experiments was an analysis of line-shape shifts and distortions of the two measured transitions due to the presence of neighboring resonances. Following Jentschura and Mohr (2002) but also Horbatsch and Hessels (2010, 2011), the MPQ researchers developed a line-shape model that accounted for these so-called quantum interference effects as well as demonstrated its validity based on directional information of the Lyman-γ photons as a function of the direction of the linear polarization of the 486 nm light.

Quantum interference effects in precision spectroscopic measurements have a long history starting with Kramers and Heisenberg (1925) and Low (1952) in the context of QED. For a review of early observations of these effects, see Marrus and Mohr (1979). Jentschura and Mohr (2002) gave an early theoretical analysis of the effect and noted that these interferences are enhanced in differential or angular-dependent measurements.

The line-shape model indicated that the two measured transition energies shifted up to $h \times 40$ kHz by quantum interference, which is much larger than the proton-radius

TABLE X. Summary of measured transition energies $\Delta\mathcal{E}_X(i-i')$ between states i and i' for electronic hydrogen ($X=\mathrm{H}$) and electronic deuterium ($X=\mathrm{D}$) considered as input data for the determination of the Rydberg constant R_∞. The label in the first column is used in Table IX to list correlation coefficients among these data and in Table XXIII for observational equations. Columns two and three give the reference and an abbreviation of the name of the laboratory in which the experiment has been performed. An extensive list of abbreviations is found at the end of this report.

	Reference	Lab.	Energy interval(s)	Reported value $\Delta\mathcal{E}/h$ (kHz)	Rel. stand. uncert. u_r
A1	Weitz *et al.* (1995)	MPQ	$\Delta\mathcal{E}_\mathrm{H}(2\mathrm{S}_{1/2}-4\mathrm{S}_{1/2})-\frac{1}{4}\Delta\mathcal{E}_\mathrm{H}(1\mathrm{S}_{1/2}-2\mathrm{S}_{1/2})$	4 797 338(10)	2.1×10^{-6}
A2			$\Delta\mathcal{E}_\mathrm{H}(2\mathrm{S}_{1/2}-4\mathrm{D}_{5/2})-\frac{1}{4}\Delta\mathcal{E}_\mathrm{H}(1\mathrm{S}_{1/2}-2\mathrm{S}_{1/2})$	6 490 144(24)	3.7×10^{-6}
A3			$\Delta\mathcal{E}_\mathrm{D}(2\mathrm{S}_{1/2}-4\mathrm{S}_{1/2})-\frac{1}{4}\Delta\mathcal{E}_\mathrm{D}(1\mathrm{S}_{1/2}-2\mathrm{S}_{1/2})$	4 801 693(20)	4.2×10^{-6}
A4			$\Delta\mathcal{E}_\mathrm{D}(2\mathrm{S}_{1/2}-4\mathrm{D}_{5/2})-\frac{1}{4}\Delta\mathcal{E}_\mathrm{D}(1\mathrm{S}_{1/2}-2\mathrm{S}_{1/2})$	6 494 841(41)	6.3×10^{-6}
A5	Parthey *et al.* (2010)	MPQ	$\Delta\mathcal{E}_\mathrm{D}(1\mathrm{S}_{1/2}-2\mathrm{S}_{1/2})-\Delta\mathcal{E}_\mathrm{H}(1\mathrm{S}_{1/2}-2\mathrm{S}_{1/2})$	670 994 334.606(15)	2.2×10^{-11}
A6	Parthey *et al.* (2011)	MPQ	$\Delta\mathcal{E}_\mathrm{H}(1\mathrm{S}_{1/2}-2\mathrm{S}_{1/2})$	2 466 061 413 187.035(10)	4.2×10^{-15}
A7	Matveev *et al.* (2013)	MPQ	$\Delta\mathcal{E}_\mathrm{H}(1\mathrm{S}_{1/2}-2\mathrm{S}_{1/2})$	2 466 061 413 187.018(11)	4.4×10^{-15}
A8	Yost *et al.* (2016)	MPQ	$\Delta\mathcal{E}_\mathrm{H}(1\mathrm{S}_{1/2}-3\mathrm{S}_{1/2})$	2 922 743 278 659(17)	5.8×10^{-12}
A9	Beyer *et al.* (2017)	MPQ	$\Delta\mathcal{E}_\mathrm{H}(2\mathrm{S}_{1/2}-4\mathrm{P})$	616 520 931 626.8(2.3)	3.7×10^{-12}
A10	de Beauvoir *et al.* (1997)	LKB/	$\Delta\mathcal{E}_\mathrm{H}(2\mathrm{S}_{1/2}-8\mathrm{S}_{1/2})$	770 649 350 012.0(8.6)	1.1×10^{-11}
A11		SYRTE	$\Delta\mathcal{E}_\mathrm{H}(2\mathrm{S}_{1/2}-8\mathrm{D}_{3/2})$	770 649 504 450.0(8.3)	1.1×10^{-11}
A12			$\Delta\mathcal{E}_\mathrm{H}(2\mathrm{S}_{1/2}-8\mathrm{D}_{5/2})$	770 649 561 584.2(6.4)	8.3×10^{-12}
A13			$\Delta\mathcal{E}_\mathrm{D}(2\mathrm{S}_{1/2}-8\mathrm{S}_{1/2})$	770 859 041 245.7(6.9)	8.9×10^{-12}
A14			$\Delta\mathcal{E}_\mathrm{D}(2\mathrm{S}_{1/2}-8\mathrm{D}_{3/2})$	770 859 195 701.8(6.3)	8.2×10^{-12}
A15			$\Delta\mathcal{E}_\mathrm{D}(2\mathrm{S}_{1/2}-8\mathrm{D}_{5/2})$	770 859 252 849.5(5.9)	7.7×10^{-12}
A16	Schwob *et al.* (1999)	LKB/	$\Delta\mathcal{E}_\mathrm{H}(2\mathrm{S}_{1/2}-12\mathrm{D}_{3/2})$	799 191 710 472.7(9.4)	1.2×10^{-11}
A17		SYRTE	$\Delta\mathcal{E}_\mathrm{H}(2\mathrm{S}_{1/2}-12\mathrm{D}_{5/2})$	799 191 727 403.7(7.0)	8.7×10^{-12}
A18			$\Delta\mathcal{E}_\mathrm{D}(2\mathrm{S}_{1/2}-12\mathrm{D}_{3/2})$	799 409 168 038.0(8.6)	1.1×10^{-11}
A19			$\Delta\mathcal{E}_\mathrm{D}(2\mathrm{S}_{1/2}-12\mathrm{D}_{5/2})$	799 409 184 966.8(6.8)	8.5×10^{-12}
A20	Bourzeix *et al.* (1996)	LKB	$\Delta\mathcal{E}_\mathrm{H}(2\mathrm{S}_{1/2}-6\mathrm{S}_{1/2})-\frac{1}{4}\Delta\mathcal{E}_\mathrm{H}(1\mathrm{S}_{1/2}-3\mathrm{S}_{1/2})$	4 197 604(21)	4.9×10^{-6}
A21			$\Delta\mathcal{E}_\mathrm{H}(2\mathrm{S}_{1/2}-6\mathrm{D}_{5/2})-\frac{1}{4}\Delta\mathcal{E}_\mathrm{H}(1\mathrm{S}_{1/2}-3\mathrm{S}_{1/2})$	4 699 099(10)	2.2×10^{-6}
A22	Arnoult *et al.* (2010)	LKB	$\Delta\mathcal{E}_\mathrm{H}(1\mathrm{S}_{1/2}-3\mathrm{S}_{1/2})$	2 922 743 278 678(13)	4.4×10^{-12}
A23	Fleurbaey *et al.* (2018)	LKB	$\Delta\mathcal{E}_\mathrm{H}(1\mathrm{S}_{1/2}-3\mathrm{S}_{1/2})$	2 922 743 278 671.5(2.6)	8.9×10^{-13}
A24	Berkeland, Hinds, and Boshier (1995)	Yale	$\Delta\mathcal{E}_\mathrm{H}(2\mathrm{S}_{1/2}-4\mathrm{P}_{1/2})-\frac{1}{4}\Delta\mathcal{E}_\mathrm{H}(1\mathrm{S}_{1/2}-2\mathrm{S}_{1/2})$	4 664 269(15)	3.2×10^{-6}
A25			$\Delta\mathcal{E}_\mathrm{H}(2\mathrm{S}_{1/2}-4\mathrm{P}_{3/2})-\frac{1}{4}\Delta\mathcal{E}_\mathrm{H}(1\mathrm{S}_{1/2}-2\mathrm{S}_{1/2})$	6 035 373(10)	1.7×10^{-6}
A26	Hagley and Pipkin (1994)	Harvard	$\Delta\mathcal{E}_\mathrm{H}(2\mathrm{S}_{1/2}-2\mathrm{P}_{3/2})$	9 911 200(12)	1.2×10^{-6}
A27	Newton, Andrews, and Unsworth (1979)	Sussex	$\Delta\mathcal{E}_\mathrm{H}(2\mathrm{P}_{1/2}-2\mathrm{S}_{1/2})$	1 057 862(20)	1.9×10^{-5}
A28	Lundeen and Pipkin (1981)	Harvard	$\Delta\mathcal{E}_\mathrm{H}(2\mathrm{P}_{1/2}-2\mathrm{S}_{1/2})$	1 057 845.0(9.0)	8.5×10^{-6}
A29	Bezginov *et al.* (2019)	York	$\Delta\mathcal{E}_\mathrm{H}(2\mathrm{P}_{1/2}-2\mathrm{S}_{1/2})$	1 057 829.8(3.2)	3.0×10^{-6}

discrepancy of $h\times 9$ kHz. More importantly, the two transitions shift in opposite directions. In fact, by constructing the hyperfine and fine-structure centroid energies from the measurements the shifts cancel to a large extent. This led to the final MPQ result for the $2\mathrm{S}_{1/2}-4\mathrm{P}$ transition energy with $u(\Delta\mathcal{E}/h)=2.3$ kHz and a relative uncertainty of 3.7×10^{-12}. In addition to the quantum interference corrections, Beyer *et al.* (2017) investigated 13 other systematic shifts and corrections. The first-order Doppler shift is negligible, but its $h\times 2.1$ kHz uncertainty is by far the largest contributor to the final uncertainty.

2. Measurement of the hydrogen two-photon 1S – 3S transition

The hydrogen $1\mathrm{S}-3\mathrm{S}$ transition energy was measured by Yost *et al.* (2016) at the MPQ and Fleurbaey *et al.* (2018) at the LKB. These new data are items A8 and A23 in Table X, respectively. The measurement uncertainty of the LKB group is significantly smaller than that obtained at the MPQ and, hence, we only describe details of the LKB experimental setup.

The researchers at the LKB used two-photon spectroscopy. In this technique, the first-order Doppler shift is eliminated by having room-temperature atoms simultaneously absorb photons from counter-propagating laser beams. The measured transition energy has a five times smaller uncertainty than two older measurements of the same transition energy. The latter are listed as items A8 and A22 in Table X. Fleurbaey (2017) and Thomas *et al.* (2019) give more information about the LKB measurement. A history of Doppler-free spectroscopy is given by Biraben (2019).

The development of a continuous-wave laser source at 205 nm for the two-photon excitation by Galtier *et al.* (2015) contributed significantly to the fivefold uncertainty reduction by improving the signal-to-noise ratio compared to previous LKB experiments with a chopped laser source. The frequency of the 205 nm laser was determined with the help of a transfer laser, several Fabry-Perot cavities, and a femtosecond frequency comb whose repetition rate was referenced to a Cs-fountain frequency standard.

The laser frequency was scanned to excite the $1\mathrm{S}_{1/2}(f=1)-3\mathrm{S}_{1/2}(f=1)$ transition and the resonance was detected from the 656 nm radiation emitted by the atoms when they decay from the 3S to the 2P level. The well-known 1S and 3S hyperfine splittings were used to obtain

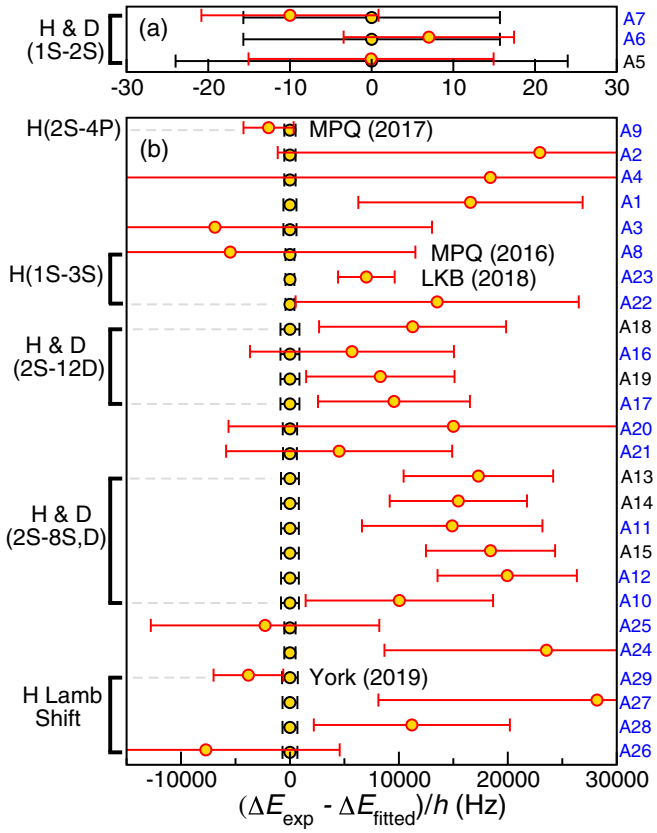


FIG. 4. Experimental hydrogen and deuterium transition energies and differences of transition energies (yellow-filled red circles with red error bars) used as input data in the 2018 least-squares adjustment. For all data, the 2018 adjusted value of the transition energy has been subtracted. Data new to this adjustment have been indicated with the abbreviation of the name of the laboratory and year of publication in parentheses. An extensive list of abbreviations is found at the end of this report. Panel (a) shows data for the $1S-2S$ transition with one-standard-deviation uncertainties on the order of tens of $h \times$ Hz. Panel (b) shows the remaining input data with uncertainties on the scale of tens of $h \times$ kHz. Labels on the left-hand side of the figure group data belonging to the same class of transitions, i.e., $n\ell - n'\ell'$ transitions. Input data without such label correspond to data that depend on (weighted) differences of four energy levels. Finally, the yellow-filled black circles with black error bars are the fitted values and their uncertainties. In the figure, the uncertainties of the input data have not been multiplied by 1.6, the expansion factor in this adjustment to make the H and D spectroscopic and muonic Lamb-shift data consistent. Fitted values are for the data when multiplied by this factor. Blue and black labels A*n* on the right-hand side of the figure correspond to hydrogen and deuterium entries in Table X, respectively.

the final transition energy between the hyperfine centroids with $u(\Delta\mathcal{E}/h) = 2.6$ kHz and $u_r = 8.9 \times 10^{-13}$.

The distribution of velocities of the atoms in the room-temperature hydrogen beam led to a second-order Doppler shift of roughly -140 kHz, or 500 parts in 10^{13}, and was the largest systematic effect in the experiment. To account for this shift, the velocity distribution of the hydrogen atoms was mapped out by applying a small magnetic flux density $\boldsymbol{B}$ perpendicular to the hydrogen beam. In addition to Zeeman shifts, the flux density leads to Stark shifts of 3S hyperfine states by mixing with the nearby $3P_{1/2}$ level via the motional electric field perceived by the atoms. Both this motional Stark shift and the second-order Doppler shift have a quadratic dependence on velocity. Then the LKB researchers fit resonance spectra obtained at different $\boldsymbol{B}$ to a line-shape model averaged over a modified Maxwellian velocity distribution of an effusive beam. The fit gives the temperature of the H beam, distortion parameters from a Maxwellian distribution, and a line position with the second-order Doppler shift removed.

Finally, the observed line position was corrected for light shifts due to the finite 205 nm laser intensity and pressure shifts due to elastic collisions with background hydrogen molecules. Light shifts increase the apparent transition energy by up to $h \times 10$ kHz depending on the laser intensity in the data runs, while pressure shifts decrease this energy by slightly less than $h \times 1$ kHz$/(10^{-5}$ hPa). Pressures up to 20×10^{-5} hPa were used in the experiments. Quantum interference effects, mainly from the 3D state, are small for the $1S - 3S$ transition and led to a correction of $h \times 0.6(2)$ kHz.

3. Measurement of the hydrogen 2S – 2P Lamb shift

The hyperfine-resolved hydrogen $2S_{1/2}(f{=}0) - 2P_{1/2} \times (f{=}1)$ transition energy or Lamb shift was measured by Bezginov *et al.* (2019) at York University to help resolve the proton-radius puzzle. This new datum is item A29 in Table X. The Dirac equation predicts that the $2S_{1/2}$ and $2P_{1/2}$ energy levels in hydrogen are degenerate, but because of vacuum fluctuations and vacuum polarization, the $2S_{1/2}$ level lies $h \times 1058$ MHz above the $2P_{1/2}$ level and $h \times 9911$ MHz below the $2P_{3/2}$ level. In fact, historically the discovery of the Lamb shift led to the development of QED. Previous determinations of the Lamb shift are items A27 and A28 in Table X. A determination of the $2S_{1/2} - 2P_{3/2}$ transition energy is given as item A26.

The York researchers had to overcome the constraints that arise from the 1.6 ns natural lifetime of the $2P_{1/2}$ state and the minimal dimensions of the ≈1 GHz microwave cavities of several centimeters. They solved this by preparing fast monoenergetic beams of $2S_{1/2}(f = 0)$ hydrogen atoms with velocities up to 0.32 cm/ns or 1% of the speed of light in vacuum. This beam was obtained by passing protons with a kinetic energy up to 55 keV through a H_2 molecular gas and by rejecting H atoms in unwanted states, especially those in the three metastable $2S_{1/2}(f = 1)$ Zeeman states.

The York researchers then used a modified version of the separated oscillatory field method to measure the Lamb shift, as described by Vutha and Hessels (2015). In this design, the frequencies of the microwave radiation applied to the two spatially separated field regions have a fixed small frequency difference and only the carrier frequency is scanned. Crucial for the effectiveness of the method is that the researchers could alternate between whether the atoms encounter the lower or higher frequency radiation first. This change occurred every few seconds. Also, part of the apparatus could be physically rotated by 180°, done about once per hour, so that the atoms encounter the separate oscillatory fields in reverse order.

Data from these four cases were used to eliminate shifts due to imperfections in state preparation and microwave cavities. The frequency difference of the radiation in the two field regions leads to a time-dependent signal of $2S_{1/2}$ population that oscillates at the difference frequency with a phase offset that is proportional to the difference of the applied carrier frequency and the frequency equivalent of the Lamb shift. The sign of the slope depends on whether the atoms encounter the lower or higher frequency radiation first. The number of remaining H atoms in the $2S_{1/2}$ state at the end of the beam line was measured by applying an electric field in a detection zone and collecting the 121.6 nm Lyman-α photon emitted by the atoms.

Data were obtained with 18 different combinations of beam velocity, strength of the 910 MHz microwave field, and distance between the separated field regions. No dependence on these parameters was observed.

The final $h \times 3.2$ kHz uncertainty for the $2S_{1/2}(f=0) - 2P_{1/2}(f=1)$ transition energy, which corresponds to $u_r = 3.6 \times 10^{-6}$, arises from an $h \times 1.4$ kHz statistical uncertainty and uncertainties from several systematic effects: $h \times 2.3$ kHz from the AC Stark shift, $h \times 1.5$ kHz from the measurement of phase, and $h \times 1.0$ kHz from the second-order Doppler shift. Quantum interference from hyperfine states with $n \geq 3$ had no discernible effect on the measurement.

Marsman *et al.* (2018) reevaluated the experiment of Lundeen and Pipkin (1981, 1986), input datum A28 in Table X. They suggested that the transition energy should be reduced by $h \times 6$ kHz and the uncertainty increased from $h \times 9$ kHz to $h \times 20$ kHz. For the 2018 CODATA adjustment, the results of Lundeen and Pipkin (1981, 1986) have not been modified.

VIII. ELECTRON MAGNETIC-MOMENT ANOMALY

The interaction of the magnetic moment of a charged lepton ℓ in a magnetic flux density (or magnetic field) $\boldsymbol{B}$ is described by the Hamiltonian $\mathcal{H} = -\boldsymbol{\mu}_\ell \cdot \boldsymbol{B}$, with

$$\boldsymbol{\mu}_\ell = g_\ell \frac{e}{2m_\ell} \boldsymbol{s}, \tag{44}$$

where $\ell = e^\pm, \mu^\pm$, or $\tau^\pm$, g_ℓ is the g-factor, with the convention that it has the same sign as the charge of the particle, e is the positive elementary charge, m_ℓ is the lepton mass, and $\boldsymbol{s}$ is its spin. Since the spin has projection eigenvalues of $s_z = \pm\hbar/2$, the magnitude of a magnetic moment is

TABLE XI. Twenty-five of the 75 adjusted constants in the 2018 CODATA least-squares minimization. These variables account for missing contributions to the theoretical description of the electronic hydrogen (H) and deuterium (D) energy levels. Their input data are given in Table VIII.

Atom		Level $n\ell_j$
H	δ_H	$1S_{1/2}$, $2S_{1/2}$, $3S_{1/2}$, $4S_{1/2}$, $6S_{1/2}$, $8S_{1/2}$, $2P_{1/2}$, $2P_{3/2}$, $4P_{1/2}$, $4P_{3/2}$, $4D_{5/2}$, $6D_{5/2}$, $8D_{3/2}$, $8D_{5/2}$, $12D_{3/2}$, $12D_{5/2}$
D	δ_D	$1S_{1/2}$, $2S_{1/2}$, $4S_{1/2}$, $8S_{1/2}$, $4D_{5/2}$, $8D_{3/2}$, $8D_{5/2}$, $12D_{3/2}$, $12D_{5/2}$

$$\mu_\ell = \frac{g_\ell}{2} \frac{e\hbar}{2m_\ell}. \tag{45}$$

The lepton magnetic-moment anomaly a_ℓ is defined by the relationship

$$|g_\ell| \equiv 2(1 + a_\ell), \tag{46}$$

based on the Dirac g-value of -2 and $+2$ for the negatively and positively charged lepton ℓ, respectively.

The Bohr magneton is defined as

$$\mu_B = \frac{e\hbar}{2m_e}, \tag{47}$$

and the theoretical expression for the anomaly of the electron $a_e(\text{th})$ is

$$a_e(\text{th}) = a_e(\text{QED}) + a_e(\text{weak}) + a_e(\text{had}), \tag{48}$$

where terms denoted by "QED," "weak," and "had" account for the purely quantum electrodynamic, predominantly electroweak, and predominantly hadronic (that is, strong interaction) contributions, respectively.

The QED contribution may be written as

$$a_e(\text{QED}) = \sum_{n=1}^{\infty} C_e^{(2n)} \left(\frac{\alpha}{\pi}\right)^n, \tag{49}$$

where the index n corresponds to contributions with n virtual photons and

$$C_e^{(2n)} = A_1^{(2n)} + A_2^{(2n)}(x_{e\mu}) + A_2^{(2n)}(x_{e\tau}) + \cdots \tag{50}$$

with mass-independent coefficients $A_1^{(2n)}$ and functions $A_2^{(2n)}(x)$ evaluated at mass ratio $x = x_{eX} \equiv m_e/m_X \ll 1$ for lepton $X = \mu$ or τ. For $n = 1$, we have

$$A_1^{(2)} = 1/2, \tag{51}$$

and function $A_2^{(2)}(x) = 0$, while for $n > 1$ coefficients $A_1^{(2n)}$ include vacuum-polarization corrections with virtual electron/positron pairs. In fact,

$$A_1^{(4)} = -0.328\,478\,965\,579\,193\ldots, \tag{52}$$

$$A_1^{(6)} = 1.181\,241\,456\,587\ldots, \tag{53}$$

$$A_1^{(8)} = -1.912\,245\,764\ldots, \tag{54}$$

$$A_1^{(10)} = 6.675(192). \tag{55}$$

The functions $A_2^{(2n)}(x)$ for $n > 1$ are vacuum-polarization corrections due to heavier leptons. For $x \to 0$, we have $A_2^{(4)}(x) = x^2/45 + \mathcal{O}(x^4)$ and $A_2^{(6)}(x) = x^2(b_0 + b_1 \ln x) + \mathcal{O}(x^4)$ with $b_0 = 0.593274\ldots$ and $b_1 = 23/135$ (Laporta,

1993; Laporta and Remiddi, 1993). The $\mathcal{O}(x^4)$ contributions are known and included in the calculations but not reproduced here. The functions $A_2^{(8)}(x)$ and $A_2^{(10)}(x)$ are also $\mathcal{O}(x^2)$ for small x, but not reproduced here (Kurz *et al.*, 2014a; Aoyama *et al.*, 2015). Currently, terms with $n > 5$ and vacuum-polarization corrections that depend on two lepton mass ratios can be neglected.

Table XII summarizes the relevant QED coefficients and summed $C_e^{(2n)}$ with their one-standard-deviation uncertainties where appropriate as used in the 2018 CODATA adjustment. Additional references to the original literature can be found in descriptions of previous CODATA adjustments. It is worth noting that since 2014 the coefficient $A_1^{(8)}$ has been evaluated by Laporta (2017), while the value for $A_2^{(10)}$ has been updated by Aoyama, Kinoshita, and Nio (2018).

Recently, the value for $A_2^{(10)}$ has been refined by Aoyama, Kinoshita, and Nio (2019), although Volkov (2019) found a value for $A_2^{(10)}$, absent lepton loop contributions, that is significantly discrepant with that based on results in Aoyama, Kinoshita, and Nio (2018, 2019). Both Aoyama, Kinoshita, and Nio (2019) and Volkov (2019) were published after our closing date.

The electroweak contribution is

$$a_e(\text{weak}) = 0.030\,53(23) \times 10^{-12} \tag{56}$$

and is calculated as discussed in the 1998 CODATA adjustment, but with the 2018 values of the Fermi coupling constant $G_F/(\hbar c)^3$ and the weak mixing angle θ_W (Tanabashi *et al.*, 2018).

Jegerlehner (2019) has provided updates to hadronic contributions to the electron anomaly. Currently, four such contributions have been considered. They are

$$a_e(\text{had}) = a_e^{\text{LO,VP}}(\text{had}) + a_e^{\text{NLO,VP}}(\text{had}) + a_e^{\text{NNLO,VP}}(\text{had}) + a_e^{\text{LL}}(\text{had}) \tag{57}$$

corresponding to leading-order (LO), next-to-leading-order (NLO), and next-to-next-to-leading-order (NNLO) hadronic vacuum-polarization corrections and a hadronic light-by-light (LL) scattering term, respectively. Contributions are determined from analyzing experimental cross sections for electron-positron annihilation into hadrons and tau-lepton-decay data. The values in the 2018 adjustment are

$$\begin{aligned} a_e^{\text{LO,VP}}(\text{had}) &= 1.849(11) \times 10^{-12}, \\ a_e^{\text{NLO,VP}}(\text{had}) &= -0.2213(12) \times 10^{-12}, \\ a_e^{\text{NNLO,VP}}(\text{had}) &= 0.028\,00(20) \times 10^{-12}, \\ a_e^{\text{LL}}(\text{had}) &= 0.0370(50) \times 10^{-12} \end{aligned} \tag{58}$$

leading to the total hadronic contribution

$$a_e(\text{had}) = 1.693(12) \times 10^{-12}. \tag{59}$$

A first-principle lattice quantum chromodynamics (QCD) evaluation of the leading-order hadronic correction $a_e^{\text{LO,VP}}(\text{had})$ to the electron anomaly was published in 2018 (Borsanyi *et al.*, 2018). The value is

$$a_e^{\text{LO,VP}}(\text{had}) = 1.893(26)(56) \times 10^{-12}, \tag{60}$$

where the first and second numbers in parentheses correspond to the statistical and systematic uncertainty, respectively. The systematic uncertainty is dominated by finite-volume artifacts. The combined uncertainty is six times larger than that obtained by analyzing electron-positron scattering data.

Figure 5 shows a graphical representation of 14 contributions to the electron anomaly. The QED corrections decrease roughly exponentially in size with order n for both mass-independent and -dependent contributions. Contributions from virtual loops containing τ leptons are mostly negligible.

The theoretical uncertainty of the electron anomaly (apart from uncertainty in the fine-structure constant) is dominated by two contributions: the mass-independent $n = 5$ QED correction and the hadronic contribution. In fact, its value is

$$u[a_e(\text{th})] = 0.018 \times 10^{-12} = 1.5 \times 10^{-11} a_e, \tag{61}$$

and is shown in Fig. 5 as well.

This theoretical uncertainty is significantly smaller than the uncertainty $2.4 \times 10^{-10} a_e$ of the best by far experimental value for the electron anomaly from Hanneke, Fogwell, and Gabrielse (2008). Consequently, the relative uncertainty of the fine-structure constant based on only this experimental input datum would be the same as that for this experiment. Atom-recoil experiments, discussed in Sec. X, form a second competitive means to determine α.

For the least-squares adjustment, we use the observational equations

TABLE XII. Coefficients for the QED contributions to the electron anomaly. The coefficients $A_1^{(2n)}$ and functions $A_2^{(2n)}(x)$, evaluated at mass ratios $x_{e\mu} = m_e/m_\mu$ and $x_{e\tau} = m_e/m_\tau$ for the muon and tau lepton, respectively; summed values $C_e^{(2n)}$, based on values for lepton mass ratios from the 2018 CODATA adjustment, are listed as accurately as needed for the tests described in this article. Missing values indicate that their contribution to the electron anomaly is negligible.

n	$A_1^{(2n)}$	$A_2^{(2n)}(x_{e\mu})$	$A_2^{(2n)}(x_{e\tau})$	$C_e^{(2n)}$
1	1/2	0	0	0.5
2	−0.328 478 965 579 193…	5.197 386 74(23) × 10^{-7}	1.837 90(25) × 10^{-9}	−0.328 478 444 00
3	1.181 241 456 587…	−7.373 941 69(24) × 10^{-6}	−6.582 73(79) × 10^{-8}	1.181 234 017
4	−1.912 245 764…	9.161 970 80(33) × 10^{-4}	7.428 93(88) × 10^{-6}	−1.911 322 138 91(88)
5	6.675(192)	−0.003 82(39)		6.67(19)

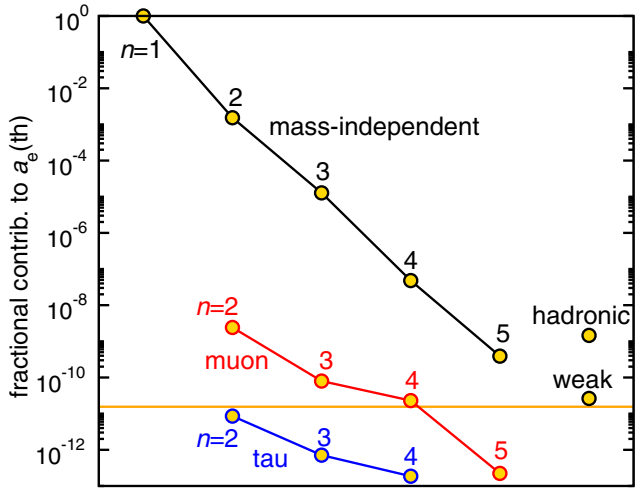


FIG. 5. Fourteen fractional contributions to the theoretical anomaly of the electron $|\delta a_e|/a_e(\mathrm{th})$. QED contributions are due to the mass-independent $A_1^{(2n)}$ (yellow-filled black circles), to the muon-dependent $A_2^{(2n)}(x_{e\mu})$ (yellow-filled red circles), and to the tau-dependent $A_2^{(2n)}(x_{e\tau})$ (yellow-filled blue circles) corrections, respectively. Weak and hadronic corrections are also shown. The horizontal orange line shows the theoretical relative uncertainty of $a_e(\mathrm{th})$. The 2018 CODATA values for the fine-structure constant and lepton mass ratios are used here.

$$a_e(\mathrm{exp}) \doteq a_e(\mathrm{th}) + \delta_{\mathrm{th}}(\mathrm{e}) \tag{62}$$

and

$$\delta_e \doteq \delta_{\mathrm{th}}(\mathrm{e}) \tag{63}$$

with additive adjusted constant $\delta_{\mathrm{th}}(\mathrm{e})$. Input datum $a_e(\mathrm{exp})$ is from Hanneke, Fogwell, and Gabrielse (2008), while input datum $\delta_e = 0$ with $u[\delta_e] = 0.018 \times 10^{-12}$ accounts for the uncertainty of the theoretical expression. The input data are entries D1 and D2 in Table XXI. Relevant observational equations are found in Table XXVI.

IX. RELATIVE ATOMIC MASSES

In this section, we discuss the input data that determine the relative atomic masses of various nuclei and atoms relevant to the adjustment. Specifically, we focus on light nuclei, i.e., neutron n, proton p, deuteron d, triton t, helion h, and the alpha particle α. These are the nuclei of hydrogen ^{1}H, deuterium ^{2}H, tritium ^{3}H, helium-3 ^{3}He, and helium-4 ^{4}He, respectively. This section also summarizes corresponding input data for the atoms ^{12}C, ^{28}Si, ^{87}Rb, and ^{133}Cs as they are relevant for the determination of the mass of the electron and the fine-structure constant discussed in Sec. VI. The input data for the mass of the muon are discussed in Sec. XVII.

Table XIII gives the relative atomic masses of the neutron and six neutral atoms that are used as input data in the 2018 CODATA adjustment. The carbon-12 relative atomic mass is by definition simply the number 12. The remaining values have been taken from the 2016 Atomic Mass Evaluation (Huang *et al.*, 2017; Wang *et al.*, 2017). Task Group and Atomic-Mass-Data-Center (AMDC) member M. Wang supplied extra digits to reduce rounding errors. Correlation coefficients with $r(X_i, X_j) > 0.0001$ among these relative atomic masses are given in Table XIV. These input data are also given as items D5, D6, D11, and D18–D20 in Table XXI.

The relative atomic masses of n, ^{87}Rb, and ^{133}Cs are adjusted constants and their observational equations are simply $A_r(X) \doteq A_r(X)$. On the other hand, we find it more convenient to use the relative atomic masses of the proton p, the alpha particle α, and the hydrogenic ^{28}Si^{13+} as adjusted constants, rather than those of neutral ^{1}H, ^{4}He, and ^{28}Si. Since the mass of an atom or atomic ion is the sum of the nuclear mass and the masses of its electrons minus the mass equivalent of the binding energy of the electrons, the observational equation for the relative atomic mass of a neutral atom X in terms of that of ion X^{n+} in charge state $n = 1, 2, \ldots$ is

$$A_r(X) \doteq A_r(X^{n+}) + nA_r(\mathrm{e}) - \frac{\Delta E_B(X^{n+})}{m_u c^2}, \tag{64}$$

where $A_r(\mathrm{e})$ is the relative atomic mass of the electron and $\Delta E_B(X^{n+}) > 0$ is the binding or removal energy needed to remove n electrons from the neutral atom. This binding energy is the sum of the electron ionization energies $E_I(X^{i+})$ of ion X^{i+}. That is,

$$\Delta E_B(X^{n+}) = \sum_{i=0}^{n-1} E_I(X^{i+}). \tag{65}$$

For a bare nucleus $n = Z$, while for a neutral atom $n = 0$ and $\Delta E_B(X^{0+}) = 0$. With our definition of observational equations, the quantities $A_r(\mathrm{e})$ and $\Delta E_B(X^{n+})$ are adjusted constants.

TABLE XIII. Relative atomic masses used as input data in the 2018 CODATA adjustment and taken from the 2016 Atomic-Mass-Data-Center (AMDC) mass evaluation (Huang *et al.*, 2017; Wang *et al.*, 2017). Correlations among these data are given in Table XIV.

Atom	Relative atomic mass[a] $A_r(X)$	Relative standard uncertainty u_r
n	1.008 664 915 82(49)	4.9×10^{-10}
^{1}H	1.007 825 032 241(94)	9.3×10^{-11}
^{4}He	4.002 603 254 130(63)	1.6×10^{-11}
^{12}C	12	exact
^{28}Si	27.976 926 534 99(52)	1.9×10^{-11}
^{87}Rb	86.909 180 5312(65)	7.4×10^{-11}
^{133}Cs	132.905 451 9610(86)	6.5×10^{-11}

[a]The relative atomic mass $A_r(X)$ of particle X with mass $m(X)$ is defined by $A_r(X) = m(X)/m_u$, where $m_u = m(^{12}\mathrm{C})/12$ is the atomic mass constant.

TABLE XIV. Correlation coefficients $r(X_i, X_j) > 0.0001$ among the input data for the relative atomic masses $A_r(X)$ given in Table XIII based on covariances from the 2016 AMDC mass evaluation available in Supplementary files at http://amdc.impcas.ac.cn/web/masseval.html or at https://www-nds.iaea.org/amdc.

$r(\mathrm{n}, {}^1\mathrm{H}) = -0.1340$	$r(\mathrm{n}, {}^{28}\mathrm{Si}) = -0.0198$
$r(\mathrm{n}, {}^{87}\mathrm{Rb}) = -0.0070$	$r(\mathrm{n}, {}^{133}\mathrm{Cs}) = -0.0070$
$r({}^1\mathrm{H}, {}^{28}\mathrm{Si}) = 0.1934$	$r({}^1\mathrm{H}, {}^{87}\mathrm{Rb}) = 0.0657$
$r({}^1\mathrm{H}, {}^{133}\mathrm{Cs}) = 0.0602$	$r({}^{28}\mathrm{Si}, {}^{87}\mathrm{Rb}) = 0.0495$
$r({}^{28}\mathrm{Si}, {}^{133}\mathrm{Cs}) = 0.0402$	$r({}^{87}\mathrm{Rb}, {}^{133}\mathrm{Cs}) = 0.1004$

In addition to the input data in Table XIII, we also use measurements of four cyclotron frequency ratios as input data to further constrain the relative atomic mass of the proton and determine those of the remaining three light nuclei: the deuteron, triton, and helion. These measurements rely on the fact that ions X^{n+} with charge ne in a homogeneous flux density or magnetic field of strength B undergo circular motion with a cyclotron frequency $\omega_c(X^{n+}) = ne\hbar B/m(X^{n+})$ that can be accurately measured. With the right experimental design, ratios of cyclotron frequencies for ions X^{n+} and Y^{p+} in the same magnetic-field environment then satisfy

$$\frac{\omega_c(X^{n+})}{\omega_c(Y^{p+})} = \frac{nA_r(Y^{p+})}{pA_r(X^{n+})} \tag{66}$$

independent of field strength. For ease of reference, the four cyclotron frequency ratios are summarized in Table XXI as items D14–D17. Observational equations are given in Table XXVI.

The first of these measurements is relevant for the determination of the relative atomic mass of the proton. In 2017, the ratio of cyclotron frequencies of the proton and the $^{12}C^{6+}$ ion, $\omega_c(^{12}C^{6+})/\omega_c(p)$, was measured at a Max-Planck Institute in Heidelberg, Germany (MPIK) (Heiße *et al.*, 2017). Their ratio has a relative uncertainty of 3.3×10^{-11}, mostly limited by residual magnetic-field inhomogeneities in the multi-zone cryogenic Penning trap. Optimized for measuring the cyclotron frequencies of light ions, the trap has three separate but connected areas that are coaxial with an applied magnetic field. A single $^{12}C^{6+}$ ion and a proton are then shuttled in and out of the central measurement trap.

Heiße *et al.* (2017) recognized that their value of $A_r(p)$ does not agree with that implied by $A_r(^1H)$ in Table XIII. As a check on their experiment, they carried out measurements on other ions but found results consistent with literature values. Figure 6 gives a graphical representation of the two discrepant input data as well as our fitted values for these data. Our predicted value for $A_r(^1H)$ is significantly smaller than that from the 2016 Atomic Mass Evaluation. For our 2018 CODATA adjustment, we have applied an expansion factor of 1.7 to the uncertainties of these two input data, also shown in the figure, in order to obtain a consistent least-squares adjustment.

The 2014 cyclotron-frequency-ratio measurement for the deuteron d and $^{12}C^{6+}$ essentially determines $A_r(d)$. Reported by Zafonte and Van Dyck (2015) and identified with UWash-15, the result was already discussed in the 2014 CODATA adjustment. The measurement has a relative uncertainty of 2.0×10^{-11} and agrees with a preliminary value (Van Dyck *et al.*, 2006) based on only 30% of the data. The 2016 AMDC evaluation of $A_r(^2H)$ is not included in our CODATA adjustment, as it was based on this preliminary determination.

The final two cyclotron-frequency-ratio measurements determine the triton and helion relative atomic masses, $A_r(t)$ and $A_r(h)$, respectively. These masses are primarily determined by the ratios $\omega_c(t)/\omega_c(^3He^+)$ and $\omega_c(HD^+)/\omega_c(^3He^+)$, both of which were measured at Florida State University, Florida, USA. The ratios have been reported by Myers *et al.* (2015) and Hamzeloui *et al.* (2017), respectively. The former was already

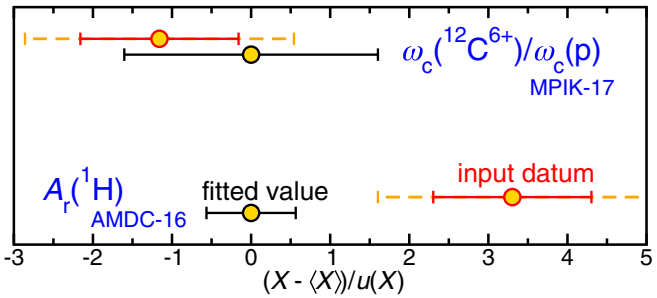


FIG. 6. Input data for the determination of the relative atomic mass of the proton p. The input data (yellow-filled red circles with red error bars) and fitted values (yellow-filled black circles with black error bars) of the cyclotron frequency ratio of $^{12}C^{6+}$ and p and the relative atomic mass of the hydrogen atom $A_r(^1H)$ are shown. Error bars correspond to one-standard-deviation uncertainties. Datum X is shifted by the fitted value $\langle X \rangle$ and normalized by the standard uncertainty of the input datum. Thus, fitted values shift to zero and input data become normalized residuals. Dashed orange lines are the standard uncertainties of the input data multiplied by the 1.7 expansion factor that ensures a consistent fit.

discussed in the 2014 CODATA adjustment. See also the recent review by Myers (2019).

The quantity $\omega_c(t)/\omega_c(^3He^+)$ is not directly measured by Myers *et al.* (2015), but determined from the quotient of ratios $\omega_c(HD^+)/\omega_c(^3He^+)$ and $\omega_c(HD^+)/\omega_c(t)$. While $u_r = 4.8 \times 10^{-11}$ for each of these directly measured ratios, $u_r = 2.4 \times 10^{-11}$ for their quotient because of a cancellation of several uncertainty components from systematic effects common to both.

The 2016 AMDC evaluations of $A_r(^3H)$ and $A_r(^3He)$ are not included in this CODATA adjustment. They were primarily determined by $\omega_c(HD^+)/\omega_c(^3He^+)$ and $\omega_c(HD^+)/\omega_c(t)$ from Myers *et al.* (2015). The former ratio is now superseded by the twice as accurate corresponding value from Hamzeloui *et al.* (2017).

Binding energies are most accurately tabulated in terms of wave number equivalents $\Delta E_B(X^{n+})/hc$ but are needed as their relative atomic mass unit equivalents $\Delta E_B(X^{n+})/m_u c^2$. Given that the Rydberg energy $hcR_\infty = \alpha^2 m_e c^2/2$, the last term in Eq. (64) is then rewritten as

$$\frac{\Delta E_B(X^{n+})}{m_u c^2} = \frac{\alpha^2 A_r(e)}{2R_\infty}\frac{\Delta E_B(X^{n+})}{hc}. \tag{67}$$

Binding energies for $^1H^+$, $^3He^+$, $^4He^{2+}$, $^{12}C^{5+}$, $^{12}C^{6+}$, and $^{28}Si^{13+}$ are used in this CODATA adjustment. Their values are determined or constructed from ionization energies in Table XV taken from the 2018 NIST Atomic Spectra Database (ASD) at https://doi.org/10.18434/T4W30F. The relevant binding energies are listed in Table XXI as items D8, D12, and D21-24. Corresponding observational equations are given in Table XXVI.

The uncertainties of the ionization data are sufficiently small that correlations among them or with any other data used in the 2018 adjustment are inconsequential. Nevertheless, the binding or removal energies of $^{12}C^{5+}$ and $^{12}C^{6+}$ are highly

TABLE XV. Ionization energies for ^{1}H, ^{3}H, ^{3}He, ^{4}He, ^{12}C, and ^{28}Si. The full description of unit m^{-1} is cycles or periods per meter. Covariances among the data in this table have not been included in the adjustment. See text for explanation.

	E_I/hc (10^7 m^{-1})		E_I/hc (10^7 m^{-1})
^{1}H	1.096 787 717 4307(10)		
^{3}H	1.097 185 4390(13)		
^{3}He^{+}	4.388 891 936(3)		
^{4}He	1.983 106 6637(20)	^{4}He^{+}	4.389 088 785(2)
^{12}C	0.908 203 480(90)	^{12}C^{+}	1.966 634(1)
^{12}C^{2+}	3.862 410(20)	^{12}C^{3+}	5.201 753(15)
^{12}C^{4+}	31.624 233(2)	^{12}C^{5+}	39.520 616 7(5)
^{28}Si	0.657 4776(25)	^{28}Si^{+}	1.318 381(3)
^{28}Si^{2+}	2.701 393(7)	^{28}Si^{3+}	3.640 931(6)
^{28}Si^{4+}	13.450 7(3)	^{28}Si^{5+}	16.556 90(40)
^{28}Si^{6+}	19.887(4)	^{28}Si^{7+}	24.4864(42)
^{28}Si^{8+}	28.333(5)	^{28}Si^{9+}	32.374(3)
^{28}Si^{10+}	38.414(2)	^{28}Si^{11+}	42.216 3(6)
^{28}Si^{12+}	196.610 389(16)	^{28}Si^{13+}	215.606 31(2)

correlated with a correlation coefficient of 0.999 98, due to the uncertainties in the common ionization energies at lower stages of ionization. The observational equations for binding energies are simply

$$\Delta E_B(X^{n+})/hc \doteq \Delta E_B(X^{n+})/hc, \tag{68}$$

thereby allowing all binding-energy uncertainties and covariances to be properly taken into account.

A word on the relative atomic mass of the molecular ion HD^+ is in order. Its value helps determine the relative atomic mass of the ^{3}He nucleus. We take

$$A_r(HD^+) = A_r(p) + A_r(d) + A_r(e) - \frac{\Delta E_I(HD^+)}{m_u c^2}, \tag{69}$$

and have used the wave number equivalent of the ionization energy of the HD^+ ion, $\Delta E_I(HD^+)/hc$, as an adjusted constant whose value is constrained by the measurement or input datum

$$\Delta E_I(HD^+)/hc = 13\,122\,468.415(6)\ m^{-1} \tag{70}$$

from Liu *et al.* (2010) and Sprecher *et al.* (2010). This input datum is item D25 in Table XXI.

X. ATOM-RECOIL MEASUREMENTS

Atom-recoil measurements with rubidium and cesium atoms from the stimulated absorption and emission of photons are relevant for the CODATA adjustment as they determine the electron mass, the atomic mass constant, and the fine-structure constant (Peters *et al.*, 1997; Young, Kasevich, and Chu, 1997; Mohr and Taylor, 2000). This can be understood as follows. First and foremost, recoil measurements determine the mass $m(X)$ of a neutral atom X in kg using interferometers with atoms in superpositions of momentum states and taking advantage of the fact that photon energies can be precisely measured. Equally precise photon momenta p follow from their dispersion or energy-momentum relation $E = pc$. In practice, Bloch oscillations are used to transfer a large number of photon momenta to the atoms in order to improve the sensitivity of the measurement (Cladé, 2015; Estey *et al.*, 2015). Before the adoption of the revised SI on 20 May 2019, these experiments only measured the ratio $h/m(X)$, since the Planck constant h was not an exactly defined constant.

Second, atom-recoil measurements are a means to determine the atomic mass constant, $m_u = m(^{12}C)/12$, and the mass of the electron, m_e, in kg. This follows, as many relative atomic masses $A_r(X) = m(X)/m_u$ of atoms X are well known. For ^{87}Rb and ^{133}Cs, the relative atomic masses have a relative uncertainty smaller than 1×10^{-10} from the 2016 recommended values of the AMDC (see Table XIII). The relative atomic mass of the electron can be determined even more precisely with spin-precession and cyclotron-frequency-ratio measurements on hydrogenic $^{12}C^{5+}$ and $^{28}Si^{13+}$ as discussed in Sec. XI. We thus have

$$m_u = m(X)/A_r(X) \tag{71}$$

and

$$m_e = \frac{A_r(e)}{A_r(X)} m(X) \tag{72}$$

from a measurement of the mass of atom X.

Finally, the fine-structure constant follows from the observation that the Rydberg constant $R_\infty = \alpha^2 m_e c/2h$ has a relative standard uncertainty of 1.9×10^{-12} based on spectroscopy of atomic hydrogen discussed in Sec. VII. The expression for R_∞ can be rewritten as

$$\alpha = \sqrt{\frac{2hcR_\infty}{m(X)c^2}\frac{A_r(X)}{A_r(e)}} \tag{73}$$

and a value of α with a competitive uncertainty can be obtained from a measurement of $m(X)$.

Two $m(X)$ measurements, represented by values for $h/m(X)$, are input data in the current least-squares adjustment: A mass for ^{87}Rb measured at the LKB, France by Bouchendira *et al.* (2011) and a mass for ^{133}Cs measured at the University of California at Berkeley, USA by Parker *et al.* (2018). The rubidium mass was already available for previous adjustments, while this value for the cesium mass is a new input datum. The results are items D3 and D4 in Table XXI and satisfy the relevant observational equations in Table XXVI.

The values of α inferred from the two atom-recoil measurements are shown in Fig. 2, together with that inferred from an electron magnetic-moment anomaly a_e measurement. Their comparison provides a useful test of the QED-based determination of a_e and is discussed in Sec. IV.D.

The new University-of-California-at-Berkeley value of $m(^{133}Cs)$ has $u_r = 4.0 \times 10^{-10}$ and currently provides a value of α with the smallest uncertainty. Thirteen systematic effects were investigated and included in the uncertainty budget. In parts in 10^{10}, the net correction from systematic effects is $-91.6(2.4)$. The two largest systematic corrections by far are

−35.8(4) in parts in 10^{10} from acceleration gradients and −52.0(6) in parts in 10^{10} from wave front curvature and the Gouy phase of their Gaussian laser beams. The relative statistical uncertainty is 3.2×10^{-10}. See also the review by Yu *et al.* (2019).

Generalizations of the Gouy phase are of particular interest in atom-recoil experiments. In efforts to improve their rubidium apparatus, the researchers at LKB realized that small-scale intensity fluctuations in laser beams at the atomic positions lead to additional contributions to the Gouy phase (Bade *et al.*, 2018; Cladé *et al.*, 2019). In fact, in the new apparatus they expect to study this systematic effect in detail. Cladé *et al.* (2019) also concluded that the 2011 evaluation remains the most accurate determination of $m(^{87}\mathrm{Rb})$, unaffected by generalizations of the Gouy phase. Acknowledging the insights of Bade *et al.* (2018), Parker *et al.* (2018) at Berkeley realized that their relevant laser propagates a considerable distance before reaching the cesium atoms and small-scale intensity fluctuations smooth out, thereby significantly reducing the size of the effect.

XI. ATOMIC *g*-FACTORS IN HYDROGENIC ^{12}C AND ^{28}Si IONS

The most accurate value for the relative atomic mass of the electron is obtained from measurements of the ratio of spin-precession and cyclotron frequencies in hydrogenic carbon and silicon and theoretical expressions for the g-factors of their bound electron. See, for example, the recent analysis by Zatorski *et al.* (2017). These measurements also play an important role in determining the fine-structure constant using atom-recoil experiments discussed in Sec. X.

For a hydrogenic ion X in its electronic ground state $1S_{1/2}$ and with a spinless nucleus, the Hamiltonian in an applied magnetic flux density $\boldsymbol{B}$ is

$$\mathcal{H} = -g_e(X)\frac{e}{2m_e}\boldsymbol{J}\cdot\boldsymbol{B}, \tag{74}$$

where $\boldsymbol{J}$ is the electron angular momentum and $g_e(X)$ is the bound-state g-factor for the electron. The electron angular momentum projection is $J_z = \pm\hbar/2$ along the direction of $\boldsymbol{B}$, so the energy splitting between the two levels is

$$\Delta E = |g_e(X)|\frac{e\hbar}{2m_e}B, \tag{75}$$

and the spin-flip precession frequency is

$$\omega_s = \frac{\Delta E}{\hbar} = |g(X)|\frac{eB}{2m_e}. \tag{76}$$

In the same flux density, the ion's cyclotron frequency is

$$\omega_c = \frac{q_X B}{m_X}, \tag{77}$$

where $q_X = (Z-1)e$, Z, and m_X are its net charge, atomic number, and mass, respectively. The frequency ratio ω_s/ω_c is then independent of $\boldsymbol{B}$ and satisfies

$$\frac{\omega_s}{\omega_c} = \frac{|g_e(X)|}{2(Z-1)}\frac{m_X}{m_e} = \frac{|g_e(X)|}{2(Z-1)}\frac{A_r(X)}{A_r(e)}, \tag{78}$$

where $A_r(X)$ is the relative atomic mass of the ion.

We summarize the theoretical computations of the g-factor in Sec. XI.A and describe the experimental input data and observational equations in Secs. XI.B and XI.C.

A. Theory of the bound-electron *g*-factor

The bound-electron g-factor is given by

$$g_e(X) = g_D + \Delta g_{rad} + \Delta g_{rec} + \Delta g_{ns} + \cdots, \tag{79}$$

where the individual terms on the right-hand side are the Dirac value, radiative corrections, recoil corrections, and nuclear-size corrections, and the dots represent possible additional corrections not already included.

The Dirac value is (Breit, 1928)

$$\begin{aligned} g_D &= -\frac{2}{3}\left[1 + 2\sqrt{1-(Z\alpha)^2}\right] \\ &= -2\left[1 - \frac{1}{3}(Z\alpha)^2 - \frac{1}{12}(Z\alpha)^4 - \frac{1}{24}(Z\alpha)^6 + \cdots\right], \end{aligned} \tag{80}$$

where the only uncertainty is due to that in α.

The radiative correction is given by the series

$$\Delta g_{rad} = \sum_{n=1}^{\infty} \Delta g^{(2n)}, \tag{81}$$

where

$$\Delta g^{(2n)} = -2C_e^{(2n)}(Z\alpha)\left(\frac{\alpha}{\pi}\right)^n \tag{82}$$

with coefficients $C_e^{(2n)}(x)$ that depend on $x = Z\alpha$.

The first or one-photon coefficient in the series has self-energy (SE) and vacuum-polarization (VP) contributions, i.e., $C_e^{(2)}(x) = C_{e,SE}^{(2)}(x) + C_{e,VP}^{(2)}(x)$. The self-energy coefficient is (Faustov, 1970; Grotch, 1970; Close and Osborn, 1971; Pachucki, Jentschura, and Yerokhin, 2004; Pachucki *et al.*, 2005)

$$\begin{aligned} C_{e,SE}^{(2)}(x) = \frac{1}{2}\Bigg\{1 + \frac{x^2}{6} + x^4\Bigg[\frac{32}{9}\ln(x^{-2}) \\ + \frac{247}{216} - \frac{8}{9}\ln k_0 - \frac{8}{3}\ln k_3\Bigg] + x^5 R_{SE}(x)\Bigg\}, \end{aligned} \tag{83}$$

where

$$\ln k_0 = 2.984\,128\,556, \tag{84}$$

$$\ln k_3 = 3.272\,806\,545, \tag{85}$$

$$R_{SE}(6\alpha) = 22.1660(10), \tag{86}$$

$$R_{SE}(14\alpha) = 21.0005(1). \tag{87}$$

Values for the remainder function $R_{\mathrm{SE}}(x)$ for carbon and silicon have been taken from Yerokhin and Harman (2017) and correspond to an almost tenfold improvement over the values used in the previous adjustment. It is worth noting that Pachucki and Puchalski (2017) have derived that

$$R_{\mathrm{SE}}(0) = \pi\left\{\frac{89}{16} + \frac{8}{3}\ln 2\right\}. \tag{88}$$

Finally, we have

$$\begin{aligned} C^{(2)}_{\mathrm{e,SE}}(6\alpha) &= 0.500\,183\,607\,131(80), \\ C^{(2)}_{\mathrm{e,SE}}(14\alpha) &= 0.501\,312\,638\,14(56). \end{aligned} \tag{89}$$

The lowest-order vacuum-polarization coefficient $C^{(2)}_{\mathrm{e,VP}}(x)$ has a wave-function and a potential contribution, each of which can be separated into a lowest-order Uehling-potential contribution and a higher-order Wichmann-Kroll contribution. The wave-function correction is (Beier, 2000; Beier *et al.*, 2000; Karshenboim, 2000; Karshenboim, Ivanov, and Shabaev, 2001a, 2001b)

$$\begin{aligned} C^{(2)}_{\mathrm{e,VPwf}}(6\alpha) &= -0.000\,001\,840\,3431(43), \\ C^{(2)}_{\mathrm{e,VPwf}}(14\alpha) &= -0.000\,051\,091\,98(22). \end{aligned} \tag{90}$$

For the potential correction, the Uehling contribution vanishes Beier *et al.* (2000), and for the Wichmann-Kroll part we take the value of Lee *et al.* (2005), which has a negligible uncertainty from omitted binding corrections for the present level of uncertainty. This leads to

$$\begin{aligned} C^{(2)}_{\mathrm{e,VPp}}(6\alpha) &= 0.000\,000\,008\,201(11), \\ C^{(2)}_{\mathrm{e,VPp}}(14\alpha) &= 0.000\,000\,5467(11), \end{aligned} \tag{91}$$

and for the total lowest-order vacuum-polarization coefficient

$$\begin{aligned} C^{(2)}_{\mathrm{e,VP}}(6\alpha) &= -0.000\,001\,832\,142(12), \\ C^{(2)}_{\mathrm{e,VP}}(14\alpha) &= -0.000\,050\,5452(11). \end{aligned} \tag{92}$$

Moreover, we have

$$\begin{aligned} C^{(2)}_{\mathrm{e}}(6\alpha) &= C^{(2)}_{\mathrm{e,SE}}(6\alpha) + C^{(2)}_{\mathrm{e,VP}}(6\alpha) \\ &= 0.500\,181\,774\,989(81), \\ C^{(2)}_{\mathrm{e}}(14\alpha) &= C^{(2)}_{\mathrm{e,SE}}(14\alpha) + C^{(2)}_{\mathrm{e,VP}}(14\alpha) \\ &= 0.501\,262\,0929(12). \end{aligned} \tag{93}$$

The two-photon $n = 2$ correction factor for the ground S state is (Pachucki *et al.*, 2005; Jentschura *et al.*, 2006)

$$\begin{aligned} C^{(4)}_{\mathrm{e}}(x) = \left(1 + \frac{x^2}{6}\right) C^{(4)}_{\mathrm{e}} + x^4 \Bigg[& \frac{14}{9}\ln(x^{-2}) + \frac{991\,343}{155\,520} \\ & - \frac{2}{9}\ln k_0 - \frac{4}{3}\ln k_3 + \frac{679\pi^2}{12\,960} \\ & - \frac{1441\pi^2}{720}\ln 2 + \frac{1441}{480}\zeta(3) + \frac{16 - 19\pi^2}{216}\Bigg] \\ & + \frac{1}{2}x^5 R^{(4)}(x), \end{aligned} \tag{94}$$

where $C^{(4)}_{\mathrm{e}} = -0.328\,478\,444\,00\ldots$. The last term in square brackets for the contribution of order x^4, absent in the previous adjustment, is the light-by-light scattering contribution (Czarnecki and Szafron, 2016).

The term $x^5 R^{(4)}(x)$ in Eq. (94) is the contribution of order x^5 and higher from diagrams with zero, one, or two vacuum-polarization loops. Yerokhin and Harman (2013) have performed nonperturbative calculations for many of the vacuum-polarization contributions to this function, denoted here by $R^{(4)}_{\mathrm{VP}}$, with the results

$$R^{(4)}_{\mathrm{VP}}(6\alpha) = 14.28(39), \qquad R^{(4)}_{\mathrm{VP}}(14\alpha) = 12.72(4) \tag{95}$$

for our two ions. These vacuum-polarization values are the sum of three contributions. The first, denoted with subscript SVPE, is from self-energy vertex diagrams with a free-electron vacuum-polarization loop included in the photon line and magnetic interactions on the bound-electron line. This calculation involves severe numerical cancellations when lower-order terms are subtracted for small Z. The results

$$R^{(4)}_{\mathrm{SVPE}}(6\alpha) = 0.00(15), \qquad R^{(4)}_{\mathrm{SVPE}}(14\alpha) = -0.152(43) \tag{96}$$

were extrapolated from results for $Z \geq 20$. The second contribution, denoted with subscript SEVP, is from screening-like diagrams with separate self-energy and vacuum-polarization loops. The vacuum-polarization loop includes the higher-order Wichmann-Kroll terms and magnetic interactions are only included in the bound-electron line. This set gives

$$R^{(4)}_{\mathrm{SEVP}}(6\alpha) = 7.97(36), \qquad R^{(4)}_{\mathrm{SEVP}}(14\alpha) = 7.62(1). \tag{97}$$

The third contribution, denoted with subscript VPVP, comes from twice-iterated vacuum-polarization diagrams and from the Källén-Sabry corrections with free-electron vacuum-polarization loops, all with magnetic interactions on the bound-electron line. This set gives

$$R^{(4)}_{\mathrm{VPVP}}(6\alpha) = 6.31, \qquad R^{(4)}_{\mathrm{VPVP}}(14\alpha) = 5.25. \tag{98}$$

The results for this latter contribution are consistent with a perturbative result at $x = 0$ given by (Jentschura, 2009)

$$\begin{aligned} R^{(4)}_{\mathrm{VPVP}}(0) &= \left(\frac{1\,420\,807}{238\,140} + \frac{832}{189}\ln 2 - \frac{400}{189}\pi\right)\pi \\ &= 7.4415\ldots. \end{aligned} \tag{99}$$

Czarnecki *et al.* (2018) performed perturbative calculations at $x = 0$ for a complementary set of diagrams contributing

to $R^{(4)}(x)$. These calculations include self-energy diagrams without vacuum-polarization loops, with the combined result

$$\Delta R^{(4)}(0) = 4.730\,4(9). \tag{100}$$

This value has three contributions. One is from self-energy diagrams without vacuum-polarization loops given by

$$R^{(4)}_{\mathrm{SE}}(0) = 0.587\,35(9)\pi^2. \tag{101}$$

The second set has light-by-light diagrams with nuclear interactions in a vacuum-polarization loop inserted into the photon line in a self-energy diagram, which gives

$$R^{(4)}_{\mathrm{LBL}}(0) = -0.172\,452\,6(1)\pi^2. \tag{102}$$

The remaining contribution with external magnetic-field coupling to a virtual-electron loop is given by

$$\begin{aligned} R^{(4)}_{\mathrm{ML}}(0) &= \left(-\frac{101\,698\,907}{3\,402\,000} + \frac{92\,368}{2025}\ln 2 - \frac{7843}{16\,200}\pi\right)\pi \\ &= 0.064\,387\ldots\pi^2. \end{aligned} \tag{103}$$

The results by Yerokhin and Harman (2013) and Czarnecki *et al.* (2018) can be combined to give

$$R^{(4)}(x) = R^{(4)}_{\mathrm{VP}}(x) + \Delta R^{(4)}(0), \tag{104}$$

which has uncertainty computed in quadrature from that of $R^{(4)}_{\mathrm{VP}}(x)$ and, following Czarnecki *et al.* (2018),

$$u[\Delta R^{(4)}(0)] = |x\ln^3(1/x^2)| \tag{105}$$

taken to be on the order of the contribution of the next-order term. For $x = 6\alpha$ and 14α, this uncertainty is approximately twice $\Delta R^{(4)}(0)$. Finally, we have for the two-photon coefficients

$$\begin{aligned} C^{(4)}_{\mathrm{e}}(6\alpha) &= -0.328\,579\,22(86), \\ C^{(4)}_{\mathrm{e}}(14\alpha) &= -0.329\,161(54). \end{aligned} \tag{106}$$

For $n > 2$ contributions $\Delta g^{(2n)}$ to the radiative correction, it is sufficient to use the observations of Eides and Grotch (1997) and Czarnecki, Melnikov, and Yelkhovsky (2000), who showed that

$$C^{(2n)}_{\mathrm{e}}(Z\alpha) = \left(1 + \frac{(Z\alpha)^2}{6} + \cdots\right) C^{(2n)}_{\mathrm{e}} \tag{107}$$

for all n. The values for constants $C^{(2n)}_{\mathrm{e}}$ for $n = 1$ through 5 are given in Table XII. This dependence for $n = 1$ and 2 can be recognized in Eqs. (83) and (106), respectively. For $n = 3$ we use

$$\begin{aligned} C^{(6)}_{\mathrm{e}}(Z\alpha) &= 1.181\,611\ldots \quad \text{for } Z = 6, \\ &= 1.183\,289\ldots \quad \text{for } Z = 14, \end{aligned} \tag{108}$$

while for $n = 4$ we have

$$\begin{aligned} C^{(8)}_{\mathrm{e}}(Z\alpha) &= -1.911\,933\ldots \quad \text{for } Z = 6, \\ &= -1.914\,647\ldots \quad \text{for } Z = 14, \end{aligned} \tag{109}$$

and, finally, for $n = 5$

$$\begin{aligned} C^{(10)}_{\mathrm{e}}(Z\alpha) &= 6.67(19)\ldots \quad \text{for } Z = 6 \\ &= 6.68(19)\ldots \quad \text{for } Z = 14. \end{aligned} \tag{110}$$

Recoil of the nucleus gives a correction Δg_{rec} proportional to the electron-nucleus mass ratio and can be written as $\Delta g_{\mathrm{rec}} = \Delta g^{(0)}_{\mathrm{rec}} + \Delta g^{(2)}_{\mathrm{rec}} + \cdots$, where the two terms are zero and first order in α/π, respectively. The first term is (Eides and Grotch, 1997; Shabaev and Yerokhin, 2002)

$$\begin{aligned} \Delta g^{(0)}_{\mathrm{rec}} = &\left\{-(Z\alpha)^2 + \frac{(Z\alpha)^4}{3[1+\sqrt{1-(Z\alpha)^2}]^2} - (Z\alpha)^5 P(Z\alpha)\right\}\frac{m_{\mathrm{e}}}{m_N} \\ &+ (1+Z)(Z\alpha)^2\left(\frac{m_{\mathrm{e}}}{m_N}\right)^2, \end{aligned} \tag{111}$$

where m_N is the mass of the nucleus. Mass ratios, based on the current adjustment values of the constants, are $m_{\mathrm{e}}/m(^{12}\mathrm{C}^{6+}) = 0.000\,045\,727\,5\ldots$ and $m_{\mathrm{e}}/m(^{28}\mathrm{Si}^{14+}) = 0.000\,019\,613\,6\ldots$. For carbon $P(6\alpha) = 10.493\,95(1)$, and for silicon we use the interpolated value $P(14\alpha) = 7.162\,23(1)$.

For $\Delta g^{(2)}_{\mathrm{rec}}$ we have

$$\Delta g^{(2)}_{\mathrm{rec}} = \frac{\alpha}{\pi}\frac{(Z\alpha)^2}{3}\frac{m_{\mathrm{e}}}{m_N} + \cdots. \tag{112}$$

The uncertainty in $\Delta g^{(2)}_{\mathrm{rec}}$ is negligible compared to that of $\Delta g^{(2)}_{\mathrm{rad}}$.

Glazov and Shabaev (2002) have calculated the nuclear-size correction $\Delta g_{\mathrm{ns,LO}}$ within lowest-order perturbation theory based on a homogeneous-sphere nuclear-charge distribution and Dirac wave functions for the electron bound to a point charge. To good approximation, the correction is (Karshenboim, 2000)

$$-\frac{8}{3}(Z\alpha)^4\left(\frac{R_N}{\lambda\!\!\!^{-}_{\mathrm{C}}}\right)^2, \tag{113}$$

where R_N is the root-mean-square nuclear-charge radius and $\lambda\!\!\!^{-}_{\mathrm{C}}$ is the reduced Compton wavelength of the electron. In the CODATA adjustment, we scale the values of Glazov and Shabaev (2002) with the squares of updated values for the nuclear radii $R_N = 2.4702(22)$ fm and $R_N = 3.1224(24)$ fm from the compilation of Angeli and Marinova (2013) for ^{12}C and ^{28}Si, respectively.

Recently, higher-order contributions of the nuclear-size correction have been computed by Karshenboim and Ivanov (2018a). They are

$$\Delta g_{\mathrm{ns,NLO}} = -\left(\frac{2}{3}Z\alpha\frac{R_N}{\lambda\!\!\!^{-}_{\mathrm{C}}}C_{\mathrm{ZF}} + \frac{\alpha}{4\pi}\right)\Delta g_{\mathrm{ns,LO}}, \tag{114}$$

where $C_{ZF} = 3.3$ is the ratio of the Zemach or Friar moment (Friar and Payne, 1997) to R_N^3 for a homogeneous-sphere nuclear-charge distribution. We assume that $\Delta g_{ns,NLO}$ has a 10% uncertainty.

The sum of the scaled nuclear-size correction of Glazov and Shabaev (2002) and Eq. (114) yields

$$\begin{aligned} \Delta g_{ns} &= -0.000\,000\,000\,407(1) \quad \text{for } {}^{12}C^{5+}, \\ \Delta g_{ns} &= -0.000\,000\,020\,48(3) \quad \text{for } {}^{28}Si^{13+} \end{aligned} \tag{115}$$

for the total nuclear-size correction.

Tables XVI and XVII list the contributions discussed above to $g_e(X)$ for $X = {}^{12}C^{5+}$ and ${}^{28}Si^{13+}$, respectively. The final values are

$$\begin{aligned} g_e({}^{12}C^{5+}) &= -2.001\,041\,590\,153(25), \\ g_e({}^{28}Si^{13+}) &= -1.995\,348\,9571(17) \end{aligned} \tag{116}$$

with uncertainties that are dominated by that of the two-photon radiative correction $\Delta g^{(4)}$. This uncertainty is dominated by terms proportional to $(Z\alpha)^6$ multiplying various powers of $\ln[(Z\alpha)^{-2}]$. We shall assume that the uncertainties for this contribution are correlated with a correlation coefficient of

$$r = 0.80 \tag{117}$$

TABLE XVI. Theoretical contributions and total value for the g-factor of hydrogenic ${}^{12}C^{5+}$ based on the 2018 recommended values of the constants.

Contribution	Value	Source
Dirac g_D	−1.998 721 354 3910(4)	Eq. (80)
$\Delta g_{SE}^{(2)}$	−0.002 323 672 4382(5)	Eq. (89)
$\Delta g_{VP}^{(2)}$	0.000 000 008 511	Eq. (92)
$\Delta g^{(4)}$	0.000 003 545 708(25)	Eq. (106)
$\Delta g^{(6)}$	−0.000 000 029 618	Eq. (108)
$\Delta g^{(8)}$	0.000 000 000 111	Eq. (109)
$\Delta g^{(10)}$	−0.000 000 000 001	Eq. (110)
Δg_{rec}	−0.000 000 087 629	Eqs. (111) and (112)
Δg_{ns}	−0.000 000 000 407(1)	Eq. (115)
$g({}^{12}C^{5+})$	−2.001 041 590 153(25)	Eq. (116)

TABLE XVII. Theoretical contributions and total value for the g-factor of hydrogenic ${}^{28}Si^{13+}$ based on the 2018 recommended values of the constants.

Contribution	Value	Source
Dirac g_D	−1.993 023 571 552(2)	Eq. (80)
$\Delta g_{SE}^{(2)}$	−0.002 328 917 509(3)	Eq. (89)
$\Delta g_{VP}^{(2)}$	0.000 000 234 81(1)	Eq. (92)
$\Delta g^{(4)}$	0.000 003 5530(17)	Eq. (106)
$\Delta g^{(6)}$	−0.000 000 029 66	Eq. (108)
$\Delta g^{(8)}$	0.000 000 000 11	Eq. (109)
$\Delta g^{(10)}$	−0.000 000 000 00	Eq. (110)
Δg_{rec}	−0.000 000 205 88	Eqs. (111) and (112)
Δg_{ns}	−0.000 000 020 48(3)	Eq. (115)
$g({}^{28}Si^{13+})$	−1.995 348 9571(17)	Eq. (116)

for our two hydrogenic ions. The derived value for the electron mass depends only weakly on this assumption; the value for the mass changes by only 2 in the last digit and the uncertainty varies by 1 in its last digit.

B. Measurements of precession and cyclotron frequencies of ${}^{12}C^{5+}$ and ${}^{28}Si^{13+}$

The experimentally determined quantities are ratios of the electron spin-precession (or spin-flip) frequency in hydrogenic carbon and silicon ions to the cyclotron frequency of the ions, both in the same magnetic flux density. The input data used in the 2018 adjustment for hydrogenic carbon and silicon are

$$\frac{\omega_s({}^{12}C^{5+})}{\omega_c({}^{12}C^{5+})} = 4376.210\,500\,87(12) \quad [2.8 \times 10^{-11}] \tag{118}$$

and

$$\frac{\omega_s({}^{28}Si^{13+})}{\omega_c({}^{28}Si^{13+})} = 3912.866\,064\,84(19) \quad [4.8 \times 10^{-11}] \tag{119}$$

with correlation coefficient

$$r\left[\frac{\omega_s({}^{12}C^{5+})}{\omega_c({}^{12}C^{5+})}, \frac{\omega_s({}^{28}Si^{13+})}{\omega_c({}^{28}Si^{13+})}\right] = 0.347, \tag{120}$$

both obtained at MPIK using a multi-zone cylindrical Penning trap operating at $B = 3.8$ T and in thermal contact with a liquid helium bath (Sturm *et al.*, 2013, 2014; Köhler *et al.*, 2015; Sturm, 2015). The development of this trap and associated measurement techniques has occurred over a number of years, leading to the current uncertainties below 5 parts in 10^{11}. A detailed discussion of the uncertainty budget and covariance and additional references can be found in the 2014 CODATA adjustment. We identify the results in Eqs. (118) and (119) by MPIK-15.

C. Observational equations for ${}^{12}C^{5+}$ and ${}^{28}Si^{13+}$ experiments

The observational equations that apply to the frequency-ratio experiments on hydrogenic carbon and silicon and theoretical computations of their g-factors follow from Eq. (78) when it is expressed in terms of the adjusted constants. That is,

$$\begin{aligned} \frac{\omega_s({}^{12}C^{5+})}{\omega_c({}^{12}C^{5+})} \doteq -\frac{g_e({}^{12}C^{5+}) + \delta_{th}(C)}{10A_r(e)} \\ \times \left[12 - 5A_r(e) + \frac{\alpha^2 A_r(e)}{2R_\infty}\frac{\Delta E_B({}^{12}C^{5+})}{hc}\right] \end{aligned} \tag{121}$$

for ${}^{12}C^{5+}$ using $A_r({}^{12}C) \equiv 12$, Eq. (64), and Eq. (67). Similarly,

$$\frac{\omega_s({}^{28}Si^{13+})}{\omega_c({}^{28}Si^{13+})} \doteq -\frac{g_e({}^{28}Si^{13+}) + \delta_{th}(Si)}{26A_r(e)} A_r({}^{28}Si^{13+}) \tag{122}$$

for ${}^{28}Si^{13+}$. In these two equations, α, R_∞, the relative atomic masses $A_r(e)$ and $A_r({}^{28}Si^{13+})$, binding energy $\Delta E_B({}^{12}C^{5+})$, and additive corrections $\delta_{th}(C)$ and $\delta_{th}(Si)$ to the theoretical

g-factors of $^{12}C^{5+}$ and $^{28}Si^{13+}$ are adjusted constants. Of course, the observational equation

$$A_r(^{28}\mathrm{Si}) \doteq A_r(^{28}\mathrm{Si}^{13+}) + 13A_r(\mathrm{e}) - \frac{\alpha^2 A_r(\mathrm{e})}{2R_\infty}\frac{\Delta E_B(^{28}\mathrm{Si}^{13+})}{hc} \tag{123}$$

relates the relative atomic mass of the silicon ion to that of the input datum of the neutral atom and $\Delta E_B(^{28}Si^{13+})$ is an adjusted constant.

The theoretical expressions for g-factors $g_e(^{12}C^{5+})$ and $g_e(^{28}Si^{13+})$ are functions of adjusted constant α. The observational equations for the additive corrections $\delta_{th}(C)$ and $\delta_{th}(Si)$ for these g-factors are

$$\delta_X \doteq \delta_{th}(X)$$

for $X = C$ and Si with input data

$$\delta_C = 0.0(2.5) \times 10^{-11},$$
$$\delta_{Si} = 0.0(1.7) \times 10^{-9}, \tag{124}$$

and $u(\delta_C, \delta_{Si}) = 3.4 \times 10^{-20}$ from Eqs. (116) and (117).

The input data are summarized as entries D7 through D13 in Table XXI and observational equations can be found in Table XXVI.

XII. MUONIC HYDROGEN AND DEUTERIUM LAMB SHIFT

Muonic hydrogen and deuterium, μH and μD, respectively, are atoms consisting of a proton or a deuteron and a negatively charged muon. Since the mass of a muon is just over 200 times larger than that of the electron, the muonic Bohr radius is 200 times smaller than the electronic Bohr radius and the muon wave-function overlap with the proton or deuteron is more than a million times larger than in normal H or D. Consequently, the "muonic" Lamb shift, the energy difference $\Delta\mathcal{E}_{LS}(X) = E_{2P_{1/2}}(X) - E_{2S_{1/2}}(X)$ between the $2S_{1/2}$ and $2P_{1/2}$ levels, is much more sensitive to the proton and deuteron charge radii, r_p and r_d.

The energy of the $2S_{1/2}$ level in H and D is higher than that of $2P_{1/2}$. Because of the much larger electron vacuum-polarization contribution, however, the energy of the $2S_{1/2}$ level in μH and μD lies below that of $2P_{1/2}$. In normal H and D, the Lamb shift is about $h \times 1$ GHz or 0.004 meV, while in μH and μD it is about $h \times 50$ THz or 200 meV.

The first successful measurement of the Lamb shift of μH was carried out by the Charge Radius Experiment with Muonic Atoms (CREMA) collaboration at the Paul Scherrer Institute, Switzerland, in 2010 (Pohl *et al.*, 2010). (Strictly speaking, the authors measured the transition energy between the $2S_{1/2}$ and $2P_{3/2}$ levels. The $2P_{1/2}$-$2P_{3/2}$ fine-structure interval is sufficiently well known from theory that the uncertainty budget for the Lamb shift is not affected.) Based on the theory of $\Delta\mathcal{E}_{LS}(\mu H)$ as it existed at the time, the CREMA collaboration derived that $r_p = 0.841\,84(67)$ fm. This value was inconsistent with the 2006 CODATA recommended value based on hydrogen spectroscopic and e-p elastic scattering data and gave rise to the "proton-radius puzzle."

For the CODATA 2010 adjustment, new elastic e-p scattering data from Bernauer *et al.* (2010) also became available. Their derived value for r_p agreed with the CODATA 2006 recommended value. Because of the strong disagreement of r_p derived from μH spectroscopy and the value of r_p derived from hydrogen spectroscopic and e-p scattering data, the Task Group decided not to include μH data in 2010. As a consequence, the disagreement between r_p based on the μH Lamb shift and the CODATA 2010 recommended value increased to seven standard deviations.

In 2013, the CREMA collaboration reported a second experimental value for $\Delta\mathcal{E}_{LS}(\mu H)$ (Antognini *et al.*, 2013; Antognini, Kottmann *et al.*, 2013), as well as advances in the theory of μH, which together yielded a value for r_p that was consistent with their 2010 estimate and had an even smaller uncertainty. Thus it did not alter the status of the proton-radius puzzle and the Task Group decided to omit μH data from the 2014 adjustment as well. In simplest terms, the puzzle was that there are two plausible values for r_p: a "low" value of about 0.84 fm and a CODATA recommended "high" value of about 0.88 fm.

Efforts to solve the proton-radius puzzle have continued. For example, a value for the deuteron radius r_d, obtained from a measurement of $\Delta\mathcal{E}_{LS}(\mu D)$, has been reported by the CREMA collaboration (Pohl *et al.*, 2016). Their value for r_d also confirmed the value for r_p based on μH data when it was combined with a measurement of the difference of the Lyman-α transition energy of normal H and D by Parthey *et al.* (2010), item A5 in Table X, and the theory of H and D.

The Task Group believes that the muonic data have been sufficiently verified and has decided to include the μH and μD Lamb-shift data in the 2018 CODATA adjustment. Moreover, three measurements of transition energies in hydrogen have become available since the previous adjustment. Their contributions decrease the value of r_p based solely on hydrogen spectroscopy. See also the discussions in Sec. IV.C and VII.C. Inconsistencies that exist among data that relate to the determination of r_p and r_d are dealt with by applying a multiplicative expansion factor to the uncertainties of the relevant data. We review the μH and μD Lamb-shift data and relevant theory in the next two sections. Input data from the Lamb-shift measurements, theoretical additive constants, and theoretical parameters are summarized in Table XVIII. Observational equations are found in Table XXIII.

A. Muonic hydrogen Lamb shift

The CREMA collaboration measured the μH Lamb shift $\Delta\mathcal{E}_{LS}(\mu H) = 202.3706(23)$ meV with $u_r = 1.1 \times 10^{-5}$ (Antognini *et al.*, 2013). The value was derived from the measured hyperfine-resolved $2S_{1/2}(f = 0) \to 2P_{3/2}(f = 1)$ transition energy, the previously reported CREMA value of the $2S_{1/2}(f = 1) \to 2P_{3/2}(f = 2)$ transition energy (Pohl *et al.*, 2010) updated as described by Antognini *et al.* (2013), and the sufficiently accurate theoretical estimates of the 2P fine-structure and $2P_{3/2}$ hyperfine splittings by

TABLE XVIII. Input data for the experimental determinations of muonic hydrogen and muonic deuterium Lamb shifts $\Delta\mathcal{E}_{\rm LS}(\mu{\rm X})$, theoretical coefficients $\mathcal{D}_{i{\rm X}}$ for these Lamb shifts, additive energy corrections $\delta E_{\rm LS}(\mu{\rm X})$, as well as the proton (p) and deuteron (d) root-mean-square charge radii r_N based on electron-proton and electron-deuteron scattering. The label in the first column is used in Table XXIII for observational equations. Only items C1, C2, and C7–C10 are input data in the adjustment. Columns two and three give the reference and an abbreviation of the name of the laboratory in which the experiment has been performed. An extensive list of abbreviations is found at the end of this report. The role of the expansion coefficients, items C3–C6, and the rationale for the values and uncertainties of the radii, C9 and C10, are discussed in the text. Relative standard uncertainties in square brackets are relative to the value of the theoretical quantity to which the additive correction corresponds. There are no correlations among these data.

	Reference	Lab.	Input datum	Value	Rel. stand. unc. $u_{\rm r}$
C1	Antognini *et al.* (2013)	CREMA	$\Delta\mathcal{E}_{\rm LS}(\mu{\rm H})$	202.3706(23) meV	1.1×10^{-5}
C2	Pohl *et al.* (2016)	CREMA	$\Delta\mathcal{E}_{\rm LS}(\mu{\rm D})$	202.8785(34) meV	1.7×10^{-5}
C3	Peset and Pineda (2015)	UBarc	$\mathcal{D}_{0{\rm H}}$	206.0698(129) meV	6.2×10^{-5}
C4	Peset and Pineda (2015)	UBarc	$\mathcal{D}_{2{\rm H}}$	$-5.2270(7)$ meV fm^{-2}	1.3×10^{-4}
C5	Kalinowski (2019)	WarsU	$\mathcal{D}_{0{\rm D}}$	230.5247(210) meV	9.1×10^{-5}
C6	Krauth *et al.* (2016)	MPQ	$\mathcal{D}_{2{\rm D}}$	$-6.110\,25(28)$ meV fm^{-2}	4.6×10^{-5}
C7		theory	$\delta E_{\rm LS}(\mu{\rm H})$	0.0000(129) meV	$[6.4\times10^{-5}]$
C8		theory	$\delta E_{\rm LS}(\mu{\rm D})$	0.0000(210) meV	$[1.0\times10^{-4}]$
C9			$r_{\rm p}$	0.880(20) fm	2.3×10^{-2}
C10			$r_{\rm d}$	2.111(19) fm	9.0×10^{-3}

Antognini, Kottmann *et al.* (2013). The two experimental transition energies also led to the determination of the magnetic Zemach radius of the proton. Details regarding the CREMA experiment have been described in the 2014 CODATA publication. The measured value is datum C1 in Table XVIII.

We use the theoretical expression for the muonic hydrogen Lamb shift from Peset and Pineda (2015) in order to derive a value for the proton charge radius $r_{\rm p}$. It is based on perturbation theory in a nonrelativistic effective field theory derived from higher-energy QED and QCD descriptions. For example, QED contributions up to $\alpha^5 m_\mu c^2$ and $\alpha^6\ln(\alpha^{-2})m_\mu c^2$ have been included. Unlike for the theoretical description of the H and D energy levels in Sec. VII.A, where we add many contributions to find level energies, we use

$$\mathcal{D}_{0{\rm H}}+\mathcal{D}_{2{\rm H}}r_{\rm p}^2 \tag{125}$$

for the theoretical Lamb shift in the least-squares adjustment. The values and uncertainties for $\mathcal{D}_{0{\rm H}}$ and $\mathcal{D}_{2{\rm H}}$ are taken from Peset and Pineda (2015) and given as items C3 and C4 in Table XVIII. This simpler procedure is justified, as nearly 95% of the muonic Lamb shift is due to the electron vacuum-polarization correction of order $\alpha^3 m_\mu c^2$ in $\mathcal{D}_{0{\rm H}}$ and the uncertainty of $\mathcal{D}_{0{\rm H}}$ is due to uncertainties in proton-structure corrections that are independent of $r_{\rm p}$. The corresponding relative standard uncertainty is orders of magnitude larger than those in α and m_μ. Approximately 5% of the Lamb shift is due to the second term in Eq. (125). An early description of the theory for the muonic Lamb shift was published by Pachucki (1996).

For the CODATA adjustment, the relevant observational equations are

$$\Delta\mathcal{E}_{\rm LS}(\mu{\rm H})\doteq\mathcal{D}_{0{\rm H}}+\mathcal{D}_{2{\rm H}}r_{\rm p}^2+\delta_{\rm th}(\mu{\rm H}) \tag{126}$$

and

$$\delta E_{\rm LS}(\mu{\rm H})\doteq\delta_{\rm th}(\mu{\rm H}). \tag{127}$$

Here, the proton charge radius $r_{\rm p}$ and additive constant $\delta_{\rm th}(\mu{\rm H})$ are adjusted constants and input datum $\delta E_{\rm LS}(\mu{\rm H})=0.0000(129)$ meV accounts for the uncertainty from uncomputed terms in $\mathcal{D}_{0{\rm H}}$ and the uncertainty of $\mathcal{D}_{2{\rm H}}$, although the latter uncertainty is currently inconsequential. Substitution of input data C1, C3, C4, and C7 from Table XVIII into Eq. (126) yields $r_{\rm p}=0.8413(15)$ fm.

In 2013, Antognini *et al.* (2013) used theoretical estimates for $\mathcal{D}_{0{\rm H}}$ and $\mathcal{D}_{2{\rm H}}$ by Antognini, Kottmann *et al.* (2013) to publish a value for $r_{\rm p}$. The value for $\mathcal{D}_{0{\rm H}}$ is consistent with that of Peset and Pineda (2015). The uncertainty from Antognini, Kottmann *et al.* (2013), however, is five times smaller. The theory of Peset and Pineda (2015) is chosen over that of Antognini, Kottmann *et al.* (2013) as their estimate and uncertainty of hadronic corrections provide a more conservative value of $r_{\rm p}$. Similarly, Karshenboim *et al.* (2015) gave smaller uncertainties on the quantities $\mathcal{D}_{0{\rm H}}$ and $\mathcal{D}_{2{\rm H}}$. Because the proton-radius puzzle is only partly resolved, a more conservative approach seems warranted. It, however, does point to the need for future research and possible future improvements in the accuracy of the proton charge radius.

B. Muonic deuterium Lamb shift

The CREMA collaboration measured the μD Lamb shift $\Delta\mathcal{E}_{\rm LS}(\mu{\rm D})=202.8785(34)$ meV with $u_{\rm r}=1.7\times10^{-5}$ (Pohl *et al.*, 2016). In fact, the data were acquired during the same measurement period and using the same general method as for the muonic hydrogen data described in the previous section. The result is based on the measurement of the three hyperfine-resolved transition energies $2{\rm S}_{1/2}(f=3/2)\to2{\rm P}_{3/2}(f=5/2)$, $2{\rm S}_{1/2}(f=1/2)\to2{\rm P}_{3/2}(f=3/2)$, and $2{\rm S}_{1/2}(f=1/2)\to2{\rm P}_{3/2}(f=1/2)$. As with the μH data,

Pohl *et al.* (2016) made use of the sufficiently well-known 2P fine-structure splitting and the $2P_{3/2}$ hyperfine splitting, both due to Krauth *et al.* (2016), to derive the Lamb shift. The 0.0034 meV total uncertainty is the root-sum-square of a 0.0031 meV statistical component and a 0.0014 meV component from systematic effects. The measured value is datum C2 in Table XVIII.

The observational equations for $\Delta\mathcal{E}_{\rm LS}(\mu{\rm D})$ are based on the recent theoretical treatment of the $n = 2$ energy levels of μD by Krauth *et al.* (2016) and Kalinowski (2019). That is,

$$\Delta\mathcal{E}_{\rm LS}(\mu{\rm D}) \doteq \mathcal{D}_{0{\rm D}} + \mathcal{D}_{2{\rm D}} r_{\rm d}^2 + \delta_{\rm th}(\mu{\rm D}) \tag{128}$$

and

$$\delta E_{\rm LS}(\mu{\rm D}) \doteq \delta_{\rm th}(\mu{\rm D}), \tag{129}$$

where the deuteron charge radius $r_{\rm d}$ and additive constant $\delta_{\rm th}(\mu{\rm D})$ are adjusted constants. Values and uncertainties for $\mathcal{D}_{0{\rm D}}$ and $\mathcal{D}_{2{\rm D}}$ are given as items C5 and C6 in Table XVIII. The coefficient $\mathcal{D}_{2{\rm D}}$ is due to Krauth *et al.* (2016). The coefficient $\mathcal{D}_{0{\rm D}}$ is the sum of two terms. The first is 228.776 66(96) meV also due to Krauth *et al.* (2016) and accounts for all contributions that do not explicitly depend on $r_{\rm d}$. The second is 1.748(21) meV from Kalinowski (2019), which we use for the nuclear-polarizability contribution instead of the corresponding value by Krauth *et al.* (2016). Input datum $\delta E_{\rm LS}(\mu{\rm D}) = 0.0000(210)$ meV incorporates the uncertainty from uncomputed terms in the theoretical energy $\mathcal{D}_{0{\rm D}}$ and the uncertainty of the coefficient $\mathcal{D}_{2{\rm D}}$, although the latter uncertainty has currently no influence on the adjustment. Substitution of input data C2, C5, C6, and C8 from Table XVIII into Eq. (128) yields $r_{\rm d} = 2.127\,10(81)$ fm.

C. Deuteron-proton charge radius difference

The deuteron-proton radius difference $r_{\rm d}^2 - r_{\rm p}^2$ is constrained by the μH and μD Lamb-shift measurements, but also by the measurement of the isotope shift of the 1S-2S transition in H and D by Parthey *et al.* (2010), item A5 in Table X. From the 2018 CODATA adjustment its recommended value is

$$r_{\rm d}^2 - r_{\rm p}^2 = 3.820\,36(41)\ {\rm fm}^2, \tag{130}$$

mainly constrained by the H to D isotope shift measurement.

XIII. ELECTRON-PROTON AND ELECTRON-DEUTERON SCATTERING

In electron-proton and electron-deuteron elastic scattering experiments, the differential scattering cross section for the electron is measured as a function of the incident energy of the electrons, $E_{\rm inc}$, and the electron scattering angle θ. From these data, the electric form factor of the proton $G_E(Q^2)$ as a function of the negative of the squared four-momentum transfer Q^2 can be extracted. Here, Q^2 is uniquely specified by $E_{\rm inc}$ and θ, as in these experiments the initial momentum of the proton is negligibly small and the incident and final electron energies are much larger than the rest energy of the electron [see, for example, Bernauer *et al.* (2014)]. A typical upper bound for the incident electron energy is the rest energy of the proton or deuteron.

A function is then fit to the data for the form factor $G_E(Q^2)$ and the root-mean-square charge radius r_N is calculated from the slope of $G_E(Q^2)$ at $Q^2 = 0$. Because cross-section measurements are not possible at $Q^2 = 0$, the function chosen to

TABLE XIX. Fifty of the 75 adjusted constants in the 2018 CODATA least-squares minimization. Other variables in the adjustment are given in Table XI.

Adjusted constant	Symbol
fine-structure constant	α
Rydberg constant	R_∞
proton rms charge radius	$r_{\rm p}$
deuteron rms charge radius	$r_{\rm d}$
Newtonian constant of gravitation	G
electron relative atomic mass	$A_{\rm r}({\rm e})$
proton relative atomic mass	$A_{\rm r}({\rm p})$
neutron relative atomic mass	$A_{\rm r}({\rm n})$
deuteron relative atomic mass	$A_{\rm r}({\rm d})$
triton relative atomic mass	$A_{\rm r}({\rm t})$
helion relative atomic mass	$A_{\rm r}({\rm h})$
alpha particle relative atomic mass	$A_{\rm r}(\alpha)$
$^{28}Si^{13+}$ relative atomic mass	$A_{\rm r}(^{28}{\rm Si}^{13+})$
^{87}Rb relative atomic mass	$A_{\rm r}(^{87}{\rm Rb})$
^{133}Cs relative atomic mass	$A_{\rm r}(^{133}{\rm Cs})$
$^1H^+$ electron removal energy	$\Delta E_{\rm B}(^1{\rm H}^+)$
HD^+ electron ionization energy	$\Delta E_{\rm I}({\rm HD}^+)$
$^3He^+$ electron ionization energy	$\Delta E_{\rm I}(^3{\rm He}^+)$
$^4He^{2+}$ electron removal energy	$\Delta E_{\rm B}(^4{\rm He}^{2+})$
$^{12}C^{5+}$ electron removal energy	$\Delta E_{\rm B}(^{12}{\rm C}^{5+})$
$^{12}C^{6+}$ electron removal energy	$\Delta E_{\rm B}(^{12}{\rm C}^{6+})$
$^{28}Si^{13+}$ electron removal energy	$\Delta E_{\rm B}(^{28}{\rm Si}^{13+})$
additive correction to $a_{\rm e}$(th)	$\delta_{\rm th}({\rm e})$
muon magnetic-moment anomaly	a_μ
additive correction to $g_{\rm C}$(th)	$\delta_{\rm th}({\rm C})$
additive correction to $g_{\rm Si}$(th)	$\delta_{\rm th}({\rm Si})$
additive correction to $\Delta\nu_{\rm Mu}$(th)	$\delta_{\rm th}({\rm Mu})$
electron-muon mass ratio	$m_{\rm e}/m_\mu$
additive correction to μ-H Lamb shift	$\delta_{\rm th}(\mu{\rm H})$
additive correction to μ-D Lamb shift	$\delta_{\rm th}(\mu{\rm D})$
deuteron-electron magnetic-moment ratio	$\mu_{\rm d}/\mu_{\rm e^-}$
electron-proton magnetic-moment ratio	$\mu_{\rm e^-}/\mu_{\rm p}$
electron to shielded proton magnetic moment ratio	$\mu_{\rm e^-}/\mu'_{\rm p}$
shielded helion to shielded proton magnetic moment ratio	$\mu'_{\rm h}/\mu'_{\rm p}$
neutron to shielded proton magnetic-moment ratio	$\mu_{\rm n}/\mu'_{\rm p}$
triton to proton magnetic-moment ratio	$\mu_{\rm t}/\mu_{\rm p}$
shielding difference of d and p in HD	$\sigma_{\rm dp}$
shielding difference of t and p in HT	$\sigma_{\rm tp}$
d_{220} of an ideal natural Si crystal	d_{220}
d_{220} of Si crystal ILL	$d_{220}({\rm ILL})$
d_{220} of Si crystal MO*	$d_{220}({\rm MO}^*)$
d_{220} of Si crystal N	$d_{220}({\rm N})$
d_{220} of Si crystal NR3	$d_{220}({\rm NR3})$
d_{220} of Si crystal NR4	$d_{220}({\rm NR4})$
d_{220} of Si crystal WASO 04	$d_{220}({\rm W04})$
d_{220} of Si crystal WASO 17	$d_{220}({\rm W17})$
d_{220} of Si crystal WASO 4.2a	$d_{220}({\rm W4.2a})$
Copper $K\alpha_1$ x unit	$xu(CuK\alpha_1)$
Ångstrom star	Å*
Molybdenum $K\alpha_1$ x unit	$xu(MoK\alpha_1)$

extrapolate to this limit and the largest Q^2 value in the data set are critical for the determination of the uncertainty budget for r_N. In addition, various systematic effects must be accounted for in the procedure to extract the form factor from the cross section.

We review r_p and r_d obtained from scattering data in the next two sections. Input data and observation equations are summarized in Tables XVIII and XXIII, respectively.

A. Proton radius from e-p scattering

Currently, the most extensive e-p scattering data are those obtained by the A1 Collaboration at Mainz University, Germany, with the Mainz linear accelerator (MAMI). Their data have been published by Bernauer *et al.* (2010, 2014). About 1400 cross sections were measured at six electron beam energies ranging from 180 MeV to 855 MeV with Q^2 from $0.003(\mathrm{GeV}/c)^2$ to $1(\mathrm{GeV}/c)^2$. The 2010 value $r_p = 0.8791(79)$ fm from these authors was used in the CODATA 2010 adjustment, as was the value $r_p = 0.895(18)$ fm due to Sick (2003, 2007, 2008). The only scattering value of the proton radius used as an input datum in the 2014 adjustment was $r_p = 0.879(11)$ fm, a weighted mean of the values by Arrington and Sick (2015) and Bernauer and Distler (2015). The uncertainty was the simple average of the individual uncertainties because each value was based on essentially the same data.

Before the closing date for new data for the 2018 adjustment, various authors reanalyzed the e-p scattering data with a variety of methods. Four such values are $r_p = 0.840(16)$ fm given by Griffioen, Carlson, and Maddox (2016), obtained from the Mainz data with values of Q^2 below $0.02(\mathrm{GeV}/c)^2$; $r_p = 0.844(7)$ fm obtained by Alarcón *et al.* (2019) using chiral effective field theory; $r_p = 0.845(1)$ fm from Zhou *et al.* (2019) employing constrained Gaussian processes; and $r_p = 0.855(11)$ fm due to Horbatsch, Hessels, and Pineda (2017) using chiral perturbation theory. Larger values, for example, $r_p = 0.916(24)$ fm obtained by Lee, Arrington, and Hill (2015), were found by only analyzing the e-p scattering data of Bernauer *et al.* (2010). Most recently, Hayward and Griffioen (2020) found $r_p = 0.841(4)$ fm from characterizing the effects of bias when omitting large-Q^2 data.

Based on these new analyses and the input data used for the 2010 and 2014 adjustments, the Task Group has decided to adopt as the only e-p scattering input datum $r_p = 0.880(20)$ fm. This value and uncertainty are chosen so that all evaluations of r_p lie within two standard deviations from this mean value. The value is essentially the same value as used in the 2014 adjustment but with an uncertainty that is approximately twice as large.

For completeness, we note that results for r_p from two new e-p scattering experiments have become available after the 31 December 2018 closing date of the 2018 adjustment. Xiong *et al.* (2019) report $r_p = 0.831(24)$ fm determined by the PRad Collaboration at the Thomas Jefferson National Accelerator Laboratory, USA; and Mihovilovič *et al.* (2019) report $r_p = 0.870(28)$ fm from a recent experiment performed at MAMI.

B. Deuteron radius from e-d scattering

Since 1998, the input datum for the charge radius of the deuteron obtained from elastic e-d scattering data in the CODATA adjustments is $r_d = 2.130(10)$ fm as determined by Sick and Trautmann (1998) and Sick (2001). This value is based on some 340 cross-section data points for momentum transfers less than $2\ \mathrm{GeV}/c$.

Recently, Hayward and Griffioen (2020) determined with a novel algorithm the structure function $A(Q^2)$, a combination of electric, magnetic, and quadrupole form factors, from elastic e-d scattering data and extrapolated to $Q^2 = 0$. The radius r_d is then determined from the slope of $A(Q^2)$ at $Q^2 = 0$. Only the data set of Simon, Schmitt, and Walther (1981), however, could be usefully analyzed with their algorithm. This yielded $r_d = 2.092(19)$ fm.

In view of this result and the many questions raised concerning the extraction of reliable values of r_p and r_d from scattering data, the value $r_d = 2.111(19)$ fm is adopted as the e-d scattering input datum for the 2018 adjustment. It is the average of $r_d = 2.092(19)$ fm and the long-used historical value $r_d = 2.130(10)$ fm with an uncertainty of one-half their difference. Coincidentally, this uncertainty is the same as that of Hayward and Griffioen (2020).

XIV. MAGNETIC-MOMENT RATIOS OF LIGHT ATOMS AND MOLECULES

The CODATA Task Group recommends values for the free-particle magnetic moments of leptons, the neutron, and light nuclei. The most precise means to determine the free magnetic moments of the electron, muon, and proton are discussed in Secs. VIII, XVI, and XV, respectively. In this section, we describe the determination of the neutron, deuteron, triton, and helion magnetic moments. The magnetic moment of the ^{4}He nucleus or α particle is zero.

Nuclear magnetic moments are determined from hydrogen and deuterium maser experiments and nuclear-magnetic-resonance (NMR) experiments on atoms and molecules. Both types of experiments measure ratios of magnetic moments to remove the need to know the strength of the applied magnetic field. We rely on NMR measurements for ratios of nuclear magnetic moments in the HD and HT molecules as well as the ratio of the magnetic moment of the neutron and the helion in ^{3}He with respect to that of the proton in H_2O. For these molecules, the electronic ground state is an electron spin singlet.

The magnetic moment of a nucleus or electron in an atom or molecule, however, differs from that of a free nucleus or electron and theoretical binding corrections are used to relate bound moments to free moments. In the remainder of this section, we give the relevant theoretical binding corrections to magnetic-moment ratios and describe experimental input data. We also describe the binding corrections for magnetic-moment ratios of an antimuon and electron bound in muonium (Mu). These will be relevant in the determination of the electron-to-muon mass ratio in Sec. XVII.

A. Definitions of bound-state and free *g*-factors

We recall that the Hamiltonian for a magnetic moment $\boldsymbol{\mu}$ in a magnetic flux density $\boldsymbol{B}$ is $\mathcal{H} = -\boldsymbol{\mu} \cdot \boldsymbol{B}$. For lepton ℓ, the

magnetic moment $\boldsymbol{\mu}_\ell = g_\ell(e/2m_\ell)\boldsymbol{s}$, where g_ℓ, m_ℓ, and $\boldsymbol{s}$ are its g-factor, mass, and spin, respectively. By convention, the magnetic moment of a neutron or nucleus with spin $\boldsymbol{I}$ is denoted by

$$\boldsymbol{\mu} = g\frac{e}{2m_\mathrm{p}}\boldsymbol{I}, \tag{131}$$

where g is the g-factor of the neutron or nucleus. The charge and mass of the proton m_p appear in the definition, regardless whether or not the particle in question is a proton. The magnitude of the magnetic moment of a charged lepton is

$$\mu_\ell = \frac{1}{2}g_\ell\frac{e\hbar}{2m_\ell}, \tag{132}$$

while that for the neutron or a nucleus is defined as

$$\mu = g\mu_\mathrm{N} i, \tag{133}$$

where $\mu_\mathrm{N} = e\hbar/2m_\mathrm{p}$ is the nuclear magneton and integer or half-integer i is the maximum positive spin projection of $\boldsymbol{I}$ given by $i\hbar$.

When electrons bind with nuclei to form ground-state atoms or molecules, the effective g-factors change. For atomic H and D in their electronic ground state, the Hamiltonian is

$$\mathcal{H} = \frac{\Delta\omega_X}{\hbar}\boldsymbol{s}\cdot\boldsymbol{I} - g_\mathrm{e}(X)\frac{e}{2m_\mathrm{e}}\boldsymbol{s}\cdot\boldsymbol{B} - g_N(X)\frac{e}{2m_\mathrm{p}}\boldsymbol{I}\cdot\boldsymbol{B}, \tag{134}$$

where $(X, N) = (\mathrm{H}, \mathrm{p})$ or (D, d) and the coefficients $g_\mathrm{e}(X)$ and $g_N(X)$ are bound-state g-factors. For muonium, an atom where an electron is bound to an antimuon, the corresponding Hamiltonian is

$$\begin{aligned}\mathcal{H}_\mathrm{Mu} = {}& \frac{\Delta\omega_\mathrm{Mu}}{\hbar}\boldsymbol{s}_\mathrm{e}\cdot\boldsymbol{s}_\mu - g_\mathrm{e}(\mathrm{Mu})\frac{e}{2m_\mathrm{e}}\boldsymbol{s}_\mathrm{e}\cdot\boldsymbol{B} \\ & - g_\mu(\mathrm{Mu})\frac{e}{2m_\mu}\boldsymbol{s}_\mu\cdot\boldsymbol{B}.\end{aligned} \tag{135}$$

B. Theoretical ratios of g-factors in H, D, ^{3}He, and muonium

Theoretical binding corrections to g-factors in the relevant atoms and muonium have already been discussed in previous CODATA reports. Relevant references can be found there as well. Here, we only give the final results. For atomic hydrogen, we have

$$\begin{aligned}\frac{g_\mathrm{e}(\mathrm{H})}{g_\mathrm{e}} = {}& 1 - \frac{1}{3}(Z\alpha)^2 - \frac{1}{12}(Z\alpha)^4 + \frac{1}{4}(Z\alpha)^2\frac{\alpha}{\pi} \\ & + \frac{1}{2}(Z\alpha)^2\frac{m_\mathrm{e}}{m_\mathrm{p}} + \frac{1}{2}\left(A_1^{(4)} - \frac{1}{4}\right)(Z\alpha)^2\left(\frac{\alpha}{\pi}\right)^2 \\ & - \frac{5}{12}(Z\alpha)^2\frac{\alpha}{\pi}\frac{m_\mathrm{e}}{m_\mathrm{p}} + \cdots\end{aligned} \tag{136}$$

and

$$\begin{aligned}\frac{g_\mathrm{p}(\mathrm{H})}{g_\mathrm{p}} = {}& 1 - \frac{1}{3}\alpha(Z\alpha) - \frac{97}{108}\alpha(Z\alpha)^3 + \frac{1}{6}\alpha(Z\alpha)\frac{m_\mathrm{e}}{m_\mathrm{p}}\frac{3+4a_\mathrm{p}}{1+a_\mathrm{p}} \\ & + \cdots,\end{aligned} \tag{137}$$

where $A_1^{(4)}$ is given in Eq. (52) and the proton magnetic-moment anomaly is $a_\mathrm{p} = \mu_\mathrm{p}/(e\hbar/2m_\mathrm{p}) - 1 \approx 1.793$. For deuterium, we have

$$\begin{aligned}\frac{g_\mathrm{e}(\mathrm{D})}{g_\mathrm{e}} = {}& 1 - \frac{1}{3}(Z\alpha)^2 - \frac{1}{12}(Z\alpha)^4 + \frac{1}{4}(Z\alpha)^2\frac{\alpha}{\pi} + \frac{1}{2}(Z\alpha)^2\frac{m_\mathrm{e}}{m_\mathrm{d}} \\ & + \frac{1}{2}\left(A_1^{(4)} - \frac{1}{4}\right)(Z\alpha)^2\left(\frac{\alpha}{\pi}\right)^2 - \frac{5}{12}(Z\alpha)^2\frac{\alpha}{\pi}\frac{m_\mathrm{e}}{m_\mathrm{d}} + \cdots\end{aligned} \tag{138}$$

and

$$\begin{aligned}\frac{g_\mathrm{d}(\mathrm{D})}{g_\mathrm{d}} = {}& 1 - \frac{1}{3}\alpha(Z\alpha) - \frac{97}{108}\alpha(Z\alpha)^3 + \frac{1}{6}\alpha(Z\alpha)\frac{m_\mathrm{e}}{m_\mathrm{d}}\frac{3+4a_\mathrm{d}}{1+a_\mathrm{d}} \\ & + \cdots,\end{aligned} \tag{139}$$

where the deuteron magnetic-moment anomaly is $a_\mathrm{d} = \mu_\mathrm{d}/(e\hbar/m_\mathrm{d}) - 1 \approx -0.143$. For helium-3, we have

$$\frac{\mu_\mathrm{h}(^3\mathrm{He})}{\mu_\mathrm{h}} = 1 - 59.967\,43(10)\times 10^{-6} \tag{140}$$

for the magnitude of the magnetic moments (Rudziński, Puchalski, and Pachucki, 2009). This ratio, however, is not used as an input datum. It is not coupled to any other data, but allows the Task Group to provide a recommended value for the unshielded helion magnetic moment along with other related quantities.

Finally, for muonium we have

$$\begin{aligned}\frac{g_\mathrm{e}(\mathrm{Mu})}{g_\mathrm{e}} = {}& 1 - \frac{1}{3}(Z\alpha)^2 - \frac{1}{12}(Z\alpha)^4 + \frac{1}{4}(Z\alpha)^2\frac{\alpha}{\pi} \\ & + \frac{1}{2}(Z\alpha)^2\frac{m_\mathrm{e}}{m_\mu} + \frac{1}{2}\left(A_1^{(4)} - \frac{1}{4}\right)(Z\alpha)^2\left(\frac{\alpha}{\pi}\right)^2 \\ & - \frac{5}{12}(Z\alpha)^2\frac{\alpha}{\pi}\frac{m_\mathrm{e}}{m_\mu} - \frac{1}{2}(1+Z)(Z\alpha)^2\left(\frac{m_\mathrm{e}}{m_\mu}\right)^2 + \cdots\end{aligned} \tag{141}$$

and

$$\begin{aligned}\frac{g_\mu(\mathrm{Mu})}{g_\mu} = {}& 1 - \frac{1}{3}\alpha(Z\alpha) - \frac{97}{108}\alpha(Z\alpha)^3 + \frac{1}{2}\alpha(Z\alpha)\frac{m_\mathrm{e}}{m_\mu} \\ & + \frac{1}{12}\alpha(Z\alpha)\frac{\alpha}{\pi}\frac{m_\mathrm{e}}{m_\mu} - \frac{1}{2}(1+Z)\alpha(Z\alpha)\left(\frac{m_\mathrm{e}}{m_\mu}\right)^2 + \cdots.\end{aligned} \tag{142}$$

Numerical values for the corrections in Eqs. (136) to (142) based on 2018 recommended values for α, mass ratios, etc. are listed in Table XX; uncertainties are negligible. See Ivanov, Karshenboim, and Lee (2009) for a negligible additional term.

TABLE XX. Theoretical values for various bound-particle to free-particle g-factor ratios based on the 2018 recommended values of the constants.

Ratio	Value
$g_e(\mathrm{H})/g_e$	$1 - 17.7054 \times 10^{-6}$
$g_p(\mathrm{H})/g_p$	$1 - 17.7354 \times 10^{-6}$
$g_e(\mathrm{D})/g_e$	$1 - 17.7126 \times 10^{-6}$
$g_d(\mathrm{D})/g_d$	$1 - 17.7461 \times 10^{-6}$
$g_e(\mathrm{Mu})/g_e$	$1 - 17.5926 \times 10^{-6}$
$g_\mu(\mathrm{Mu})/g_\mu$	$1 - 17.6254 \times 10^{-6}$

C. Theoretical ratios of nuclear g-factors in HD and HT

Bound-state corrections to the magnitudes of nuclear magnetic moments in the diatomic molecules HD and HT are expressed as

$$\mu_N(X) = [1 - \sigma_N(X)]\mu_N, \tag{143}$$

for nucleus N in molecule X. Here, μ_N is the magnitude of the magnetic moment of the free nucleus and $\sigma_N(X)$ is the nuclear magnetic shielding correction. In fact, $|\sigma_N(X)| \ll 1$.

NMR experiments for these molecules measure the ratio

$$\frac{\mu_N(X)}{\mu_{N'}(X)} = [1 + \sigma_{N'N} + \mathcal{O}(\sigma^2)]\frac{\mu_N}{\mu_{N'}} \tag{144}$$

for nuclei N and N' in molecule $X = \mathrm{HD}$ or HT and $\sigma_{N'N} = \sigma_{N'}(X) - \sigma_N(X)$ is the shielding difference of molecule X. In the adjustment, corrections of $\mathcal{O}(\sigma^2)$, quadratic in $\sigma_N(X)$, are much smaller than the uncertainties in the experiments and are omitted.

The theoretical values for shielding differences in HD and HT are $\sigma_{dp} = 20.20(2) \times 10^{-9}$ and $\sigma_{tp} = 24.14(2) \times 10^{-9}$, respectively, as reported by Puchalski, Komasa, and Pachucki (2015). The values are approximately 100 times more accurate than those used in the 2014 CODATA adjustment and are also listed as items D42 and D43 in Table XXI. The two shielding differences are taken as adjusted constants with observational equations $\sigma_{dp} \doteq \sigma_{dp}$ and $\sigma_{tp} \doteq \sigma_{tp}$, respectively.

D. Ratio measurements in atoms and molecules

Nine atomic and molecular magnetic-moment ratios obtained with H and D masers and NMR experiments are used as input data in the 2018 adjustment, and determine the magnetic moments of the neutron, deuteron, triton, and helion. For ease of reference, these experimental frequency ratios are summarized in Table XXI and given labels D33 through D41. There are no correlation coefficients among these data greater than 0.0001. Observational equations are summarized in Table XXVI.

We note that the primed magnetic moment μ_p' appearing in three input data in Table XXI indicates that the proton is bound in a H_2O molecule in a spherical sample of liquid water at 25 °C surrounded by vacuum. The shielding factor for the proton in water is not known theoretically and, thus, these measurements cannot be used to determine the free-proton magnetic moment. The relationships among these three input data, however, help determine other magnetic moments as well as the shielding factor of the proton in water. Finally, the primed quantity μ_h' in item D36 is the magnetic moment of the helion bound in a ^{3}He atom in a 25 °C spherical gaseous sample of helium-3. In principle, its value can differ from that of a helion in an isolated ^{3}He atom, that is, $\mu_h(^3\mathrm{He})$ as found in Eq. (140). We assume that environmental effects from distant helium-3 atoms are negligible and equate the two quantities, i.e., $\mu_h' = \mu_h(^3\mathrm{He})$, to determine the magnetic moment of the free helion.

Our adjusted constants for the determination of the relevant magnetic moments are μ_d/μ_e, μ_e/μ_p, μ_e/μ_p', μ_h'/μ_p', μ_n/μ_p', μ_t/μ_p, σ_{dp}, and σ_{tp}.

The ratio $\mu_p(\mathrm{HD})/\mu_d(\mathrm{HD})$ obtained by Neronov and Seregin (2012), item D40 in Table XXI, is a relatively old result that was not included in the 2014 adjustment, but is included in the current adjustment. We rely on three determinations of $\mu_p(\mathrm{HD})/\mu_d(\mathrm{HD})$ in the 2018 CODATA adjustment. The values are from Garbacz *et al.* (2012), researchers at the University of Warsaw, Poland; and from Neronov and Karshenboim (2003) and Neronov and Seregin (2012), researchers in Saint Petersburg, Russia, who have a long history of NMR measurements in atoms and molecules. (The remaining experimental input data have been reviewed in previous CODATA reports and are not discussed further.)

Neronov and Seregin (2012) describe a complex set of experiments to determine the free-helion to free-proton magnetic-moment ratio. We had previously overlooked their frequency-ratio measurements on HD, which satisfy

$$\frac{\omega_p(\mathrm{HD})}{\omega_d(\mathrm{HD})} = 2\frac{\mu_p(\mathrm{HD})}{\mu_d(\mathrm{HD})}, \tag{145}$$

where the factor two appears because the spins of the proton and deuteron are 1/2 and 1, respectively. The statistical relative uncertainty of the frequency ratio is given as 7.7 parts in 10^{10}. The line-shape fits by Neronov and Seregin (2012), however, visibly disagree with the experimental data and, thus, systematic effects are present. We account for these effects by increasing the uncertainty by a factor of 4.0 consistent with determining the NMR frequency of d in HD to approximately one-tenth of the full-width-half-maximum of the Lorentzian line.

XV. PROTON MAGNETIC MOMENT IN NUCLEAR MAGNETONS

The 2017 measurement of the proton magnetic moment in nuclear magnetons, μ_p/μ_N, has been newly added to the CODATA adjustment. It was obtained using a single proton in a double Penning trap at the University of Mainz, Germany (Schneider *et al.*, 2017). The ratio was determined by measuring its spin-flip transition frequency $\omega_s = 2\mu_p B/\hbar$ and its cyclotron frequency $\omega_c = eB/m_p$ in a magnetic flux density $\boldsymbol{B}$. As $\boldsymbol{B}$ is the same in both measurements,

$$\frac{\omega_s}{\omega_c} = \frac{\mu_p}{\mu_N} \tag{146}$$

independent of $\boldsymbol{B}$ and where $\mu_N = e\hbar/2m_p$ is the nuclear magneton.

TABLE XXI. Input data for the 2018 CODATA adjustment to determine the fine-structure constant, muon mass, masses of nuclei with $Z \leq 2$, and magnetic-moment ratios among these nuclei as well as those of leptons. Relative standard uncertainties in square brackets are relative to the value of the theoretical quantity to which the additive correction corresponds. The label in the first column is used to specify correlation coefficients among these data and in Table XXVI observational equations. Columns five and six give the reference, an abbreviation of the name of the laboratory in which the experiment has been performed, and the year of publication. An extensive list of abbreviations is found at the end of this report. Correlations among these data are given in Table XXII.

Input datum	Value	Rel. stand. unc. u_r	Lab.	Reference(s)	Sec.
Input data relevant for the fine-structure constant and the electron mass					
D1 a_e(exp)	$1.159\,652\,180\,73(28) \times 10^{-3}$	2.4×10^{-10}	HarvU-08	Hanneke, Fogwell, and Gabrielse (2008)	VIII
D2 δ_e	$0.000(18) \times 10^{-12}$	$[1.5 \times 10^{-11}]$	theory		VIII
D3 $h/m(^{87}\mathrm{Rb})$	$4.591\,359\,2729(57) \times 10^{-9}$ m^2 s^{-1}	1.2×10^{-9}	LKB-11	Bouchendira *et al.* (2011)	X
D4 $h/m(^{133}\mathrm{Cs})$	$3.002\,369\,4721(12) \times 10^{-9}$ m^2 s^{-1}	4.0×10^{-10}	UCB-18	Parker *et al.* (2018)	X
D5 $A_r(^{87}\mathrm{Rb})$	86.909 180 5312(65)	7.4×10^{-11}	AMDC-16	Huang *et al.* (2017)	IX
D6 $A_r(^{133}\mathrm{Cs})$	132.905 451 9610(86)	6.5×10^{-11}	AMDC-16	Huang *et al.* (2017)	IX
D7 ω_s/ω_c for $^{12}\mathrm{C}^{5+}$	4376.210 500 87(12)	2.8×10^{-11}	MPIK-15	Köhler *et al.* (2015)	XI.B
D8 $\Delta E_B(^{12}\mathrm{C}^{5+})/hc$	$43.563\,233(25) \times 10^7$ m^{-1}	5.8×10^{-7}	ASD-18		IX
D9 δ_C	$0.0(2.5) \times 10^{-11}$	$[1.3 \times 10^{-11}]$	theory		XI.C
D10 ω_s/ω_c for $^{28}\mathrm{Si}^{13+}$	3912.866 064 84(19)	4.8×10^{-11}	MPIK-15	Sturm *et al.* (2013) and Sturm (2015)	XI.B
D11 $A_r(^{28}\mathrm{Si})$	27.976 926 534 99(52)	1.9×10^{-11}	AMDC-16	Huang *et al.* (2017)	IX
D12 $\Delta E_B(^{28}\mathrm{Si}^{13+})/hc$	$420.6467(85) \times 10^7$ m^{-1}	2.0×10^{-5}	ASD-18		IX
D13 δ_{Si}	$0.0(1.7) \times 10^{-9}$	$[8.3 \times 10^{-10}]$	theory		XI.C
Input data relevant for masses of light nuclei					
D14 $\omega_c(\mathrm{d})/\omega_c(^{12}\mathrm{C}^{6+})$	0.992 996 654 743(20)	2.0×10^{-11}	UWash-15	Zafonte and Van Dyck (2015)	IX
D15 $\omega_c(^{12}\mathrm{C}^{6+})/\omega_c(\mathrm{p})$	0.503 776 367 662(17)	3.3×10^{-11}	MPIK-17	Heiße *et al.* (2017)	IX
D16 $\omega_c(\mathrm{t})/\omega_c(^3\mathrm{He}^+)$	0.999 993 384 997(24)	2.4×10^{-11}	FSU-15	Myers *et al.* (2015)	IX
D17 $\omega_c(\mathrm{HD}^+)/\omega_c(^3\mathrm{He}^+)$	0.998 048 085 122(23)	2.3×10^{-11}	FSU-17	Hamzeloui *et al.* (2017)	IX
D18 A_r(n)	1.008 664 915 82(49)	4.9×10^{-10}	AMDC-16	Huang *et al.* (2017)	IX
D19 $A_r(^1\mathrm{H})$	1.007 825 032 241(94)	9.3×10^{-11}	AMDC-16	Huang *et al.* (2017)	IX
D20 $A_r(^4\mathrm{He})$	4.002 603 254 130(63)	1.6×10^{-11}	AMDC-16	Huang *et al.* (2017)	IX
D21 $\Delta E_B(^1\mathrm{H}^+)/hc$	$1.096\,787\,717\,4307(10) \times 10^7$ m^{-1}	9.1×10^{-13}	ASD-18		IX
D22 $\Delta E_B(^4\mathrm{He}^{2+})/hc$	$6.372\,195\,4487(28) \times 10^7$ m^{-1}	4.4×10^{-10}	ASD-18		IX
D23 $\Delta E_B(^{12}\mathrm{C}^{6+})/hc$	$83.083\,850(25) \times 10^7$ m^{-1}	3.0×10^{-7}	ASD-18		IX
D24 $\Delta E_I(^3\mathrm{He}^+)/hc$	43 888 919.36(3) m^{-1}	6.8×10^{-10}	ASD-18		IX
D25 $\Delta E_I(\mathrm{HD}^+)/hc$	13 122 468.415(6) m^{-1}	4.6×10^{-10}		Liu *et al.* (2010) and Sprecher *et al.* (2010)	IX
Input datum relevant for the muon anomaly					
D26 $\bar{R}$	0.003 707 2063(20)	5.4×10^{-7}	BNL-06	Bennett *et al.* (2006)	XVI.A
Input data relevant for the muon mass and muon magnetic moment					
D27 $E(58\ \mathrm{MHz})/h$	627 994.77(14) kHz	2.2×10^{-7}	LAMPF-82	Mariam (1981) and Mariam *et al.* (1982)	XVII.B
D28 $E(72\ \mathrm{MHz})/h$	668 223 166(57) Hz	8.6×10^{-8}	LAMPF-99	Liu *et al.* (1999)	XVII.B
D29 $\Delta E_{Mu}/h$	4 463 302.88(16) kHz	3.6×10^{-8}	LAMPF-82	Mariam (1981) and Mariam *et al.* (1982)	XVII.B
D30 $\Delta E_{Mu}/h$	4 463 302 765(53) Hz	1.2×10^{-8}	LAMPF-99	Liu *et al.* (1999)	XVII.B
D31 δ_{Mu}/h	0(85) Hz	$[1.9 \times 10^{-8}]$	theory		XVII.A
Input data relevant for the magnetic moments of light nuclei					
D32 μ_p/μ_N	2.792 847 344 62(82)	2.9×10^{-10}	UMZ-17	Schneider *et al.* (2017)	XV
D33 $\mu_e(\mathrm{H})/\mu_p(\mathrm{H})$	−658.210 7058(66)	1.0×10^{-8}	MIT-72	Sec. III.C.3 of Mohr and Taylor (2000)	XIV.D
D34 $\mu_d(\mathrm{D})/\mu_e(\mathrm{D})$	$-4.664\,345\,392(50) \times 10^{-4}$	1.1×10^{-8}	MIT-84	Sec. III.C.4 of Mohr and Taylor (2000)	XIV.D
D35 $\mu_e(\mathrm{H})/\mu'_p$	−658.215 9430(72)	1.1×10^{-8}	MIT-77	Sec. III.C.6 of Mohr and Taylor (2000)	XIV.D
D36 μ'_h/μ'_p	−0.761 786 1313(33)	4.3×10^{-9}	NPL-93	Flowers, Petley, and Richards (1993)	XIV.D
D37 μ_n/μ'_p	−0.684 996 94(16)	2.4×10^{-7}	ILL-79	Sec. III.C.8 of Mohr and Taylor (2000)	XIV.D
D38 $\mu_p(\mathrm{HD})/\mu_d(\mathrm{HD})$	3.257 199 531(29)	8.9×10^{-9}	StPtrsb-03	Neronov and Karshenboim (2003)	XIV.D
D39 $\mu_p(\mathrm{HD})/\mu_d(\mathrm{HD})$	3.257 199 514(21)	6.6×10^{-9}	WarsU-12	Garbacz *et al.* (2012)	XIV.D
D40 $\mu_p(\mathrm{HD})/\mu_d(\mathrm{HD})$	3.257 199 516(10)	3.1×10^{-9}	StPtrsb-12	Neronov and Seregin (2012)	XIV.D
D41 $\mu_t(\mathrm{HT})/\mu_p(\mathrm{HT})$	1.066 639 8933(21)	2.0×10^{-9}	StPtrsb-11	Neronov and Aleksandrov (2011)	XIV.D
D42 σ_{dp}	$20.20(2) \times 10^{-9}$			Puchalski, Komasa, and Pachucki (2015)	XIV.C
D43 σ_{tp}	$24.14(2) \times 10^{-9}$			Puchalski, Komasa, and Pachucki (2015)	XIV.C

The Mainz value

$$\frac{\omega_s}{\omega_c} = 2.792\,847\,344\,62(82) \quad [2.9 \times 10^{-10}] \qquad (147)$$

is consistent with but supersedes the 2014 result by the same research group (Mooser *et al.*, 2014). Improvements in the apparatus led to a relative uncertainty that is more than an order of magnitude smaller than in 2014. The

TABLE XXII. Correlation coefficients $r(x_i, x_j) > 0.0001$ among the input data in Table XXI.

$r(\mathrm{D5}, \mathrm{D6}) = 0.1004$	$r(\mathrm{D5}, \mathrm{D11}) = 0.0495$
$r(\mathrm{D5}, \mathrm{D18}) = -0.0070$	$r(\mathrm{D5}, \mathrm{D19}) = 0.0657$
$r(\mathrm{D6}, \mathrm{D11}) = 0.0402$	$r(\mathrm{D6}, \mathrm{D18}) = -0.0070$
$r(\mathrm{D6}, \mathrm{D19}) = 0.0602$	$r(\mathrm{D7}, \mathrm{D10}) = 0.3473$
$r(\mathrm{D8}, \mathrm{D23}) = 0.9998$	$r(\mathrm{D9}, \mathrm{D13}) = 0.7994$
$r(\mathrm{D11}, \mathrm{D18}) = -0.0198$	$r(\mathrm{D11}, \mathrm{D19}) = 0.1934$
$r(\mathrm{D18}, \mathrm{D19}) = -0.1340$	$r(\mathrm{D27}, \mathrm{D29}) = 0.2267$
$r(\mathrm{D28}, \mathrm{D30}) = 0.1946$	

linewidth of the resonant Lorentzian signal was narrowed by reducing magnetic-field inhomogeneity, and an improved detector for the cyclotron frequency doubled the data acquisition rate. The relative uncertainty of the new result comprises 2.7 and 1.2 parts in 10^{10} from statistical and systematic effects, respectively. The two largest components contributing to the systematic uncertainty are due to limits on line-shape fitting and on the characterization of a relativistic shift and have been added linearly to account for correlations. The total correction from systematic effects is -1.3 parts in 10^{10}.

The observational equation for ω_s/ω_c and thus μ_p/μ_N is

$$\frac{\mu_p}{\mu_N} \doteq -[1 + a_e(\mathrm{th}) + \delta_{\mathrm{th}}(\mathrm{e})]\frac{A_r(\mathrm{p})}{A_r(\mathrm{e})}\frac{\mu_p}{\mu_e} \tag{148}$$

using the definition of μ_e in Eq. (45). The quantities $\delta_{\mathrm{th}}(\mathrm{e})$, $A_r(\mathrm{e})$, $A_r(\mathrm{p})$, and μ_e/μ_p are adjusted constants. The theoretical expression for the electron anomaly $a_e(\mathrm{th})$ is mainly a function of adjusted constant α.

The input datum has identifier UMZ-17 and is item D32 in Table XXI. Its observational equation can be found in Table XXVI.

XVI. MUON MAGNETIC-MOMENT ANOMALY

The muon magnetic-moment anomaly a_μ and thus muon g-factor $g_\mu = -2(1 + a_\mu)$ were measured in 2006. A theoretical expression for a_μ is also available and has steadily been improved since this measurement. Only the measured value of the muon anomaly, however, is included in the 2018 adjustment of the constants due to the disagreement between theory and experiment. The measurement of a_μ and the theory are summarized in the following sections.

A. Measurement of the muon anomaly

The 2006 determination of a_μ at Brookhaven National Laboratory (BNL), USA has been discussed in the past five CODATA reports. The quantity measured is the anomaly difference frequency $\omega_a = \omega_s - \omega_c$, where $\omega_s = |g_\mu|(e/2m_\mu)B$ is the muon spin-flip (or precession) frequency in the applied magnetic flux density B and $\omega_c = (e/m_\mu)B$ is the muon cyclotron frequency. The flux density is eliminated from these expressions by determining its value from a measurement of the precession frequency of the proton in water in the same apparatus combined with the proton shielding correction in water. This leads to a measurement of proton precession frequency $\omega_p = 2\mu_p B/\hbar$, where the magnitude of the proton magnetic moment, μ_p, and the g-factor of the muon are defined in Sec. XIV.A.

The value of $\bar{R} = \omega_a/\omega_p$ is reported by the BNL experimentalists. From Table XV of Bennett *et al.* (2006), we have

$$\bar{R} = 0.003\,707\,2063(20) \quad [5.4 \times 10^{-7}]. \tag{149}$$

It is input datum D26 in Table XXI with identification BNL-06. The corresponding observational equation is

$$\bar{R} \doteq a_\mu \frac{e\hbar/(2m_\mu)}{\mu_p} \doteq \frac{a_\mu}{1 + a_e(\mathrm{th}) + \delta_{\mathrm{th}}(\mathrm{e})}\frac{m_e}{m_\mu}\frac{\mu_e}{\mu_p}, \tag{150}$$

where the right-hand side of the equation is explicitly expressed in terms of adjusted constants a_μ, m_e/m_μ, μ_e/μ_p, and additive correction $\delta_{\mathrm{th}}(\mathrm{e})$ for the theoretical electron anomaly $a_e(\mathrm{th})$. The anomaly $a_e(\mathrm{th})$ is mainly a function of the adjusted constant α.

In practice, the muon anomaly can also be calculated from

$$a_\mu = \frac{\bar{R}}{|\mu_\mu/\mu_p| - \bar{R}}, \tag{151}$$

as the uncertainty of the magnetic-moment ratio μ_μ/μ_p is much smaller than that of $\bar{R}$. The 2018 CODATA recommended value of the muon anomaly is

$$a_\mu = 1.165\,920\,89(63) \times 10^{-3}. \tag{152}$$

B. Theory of the muon anomaly

The muon magnetic-moment anomaly can be expressed as

$$a_\mu(\mathrm{th}) = a_\mu(\mathrm{QED}) + a_\mu(\mathrm{weak}) + a_\mu(\mathrm{had}), \tag{153}$$

where terms denoted by "QED," "weak," and "had" account for the purely quantum electrodynamic, predominantly electroweak, and predominantly hadronic (that is, with hadrons in intermediate states) contributions, respectively. The QED contribution may be written as

$$a_\mu(\mathrm{QED}) = \sum_{n=1}^{\infty} C_\mu^{(2n)}\left(\frac{\alpha}{\pi}\right)^n, \tag{154}$$

where

$$C_\mu^{(2n)} = A_1^{(2n)} + A_2^{(2n)}(x_{\mu e}) + A_2^{(2n)}(x_{\mu\tau}) + A_3^{(2n)}(x_{\mu e}, x_{\mu\tau}) \tag{155}$$

with mass-independent coefficients $A_1^{(2n)}$ given by Eqs. (51)–(55) and functions $A_2^{(2n)}(x)$ and $A_3^{(2n)}(x, y)$ evaluated at mass ratios m_μ/m_X for lepton $X = \mathrm{e}$ or τ. The expression for the QED contribution has the same functional form as that for the electron anomaly described in Sec. VIII, except that the mass-dependent terms $A_2^{(2n)}(x)$ are evaluated at different mass ratios, while contributions due to $A_3^{(2n)}(x, y)$ are negligibly small for the electron anomaly. Contributions from the mass-dependent terms are generally more important for the muon anomaly.

TABLE XXIII. Observational equations for input data on H/D spectroscopy, muonic-H and -D Lamb shifts, and electron-proton or deuteron scattering given in Tables X, VIII, and XVIII as functions of adjusted constants. Labels in the first column correspond to those defined in the tables with input data. Subscript X is H or D for hydrogen or deuterium, respectively. The symbol $\doteq$ is defined in Sec. III. Energy levels of hydrogenic atoms, $E_X(n\ell_j;\Gamma_X)$, are discussed in Sec. VII.A. Here, the symbol Γ_X represents the six adjusted constants $R_\infty, \alpha, A_r(e), m_e/m_\mu, A_r(N)$, and r_N such that when $X = \mathrm{H}$ nucleus $N = \mathrm{p}$, the proton, and when $X = \mathrm{D}$ nucleus $N = \mathrm{d}$, the deuteron. The Lamb shift for muonic atoms, $\Delta\mathcal{E}_{\mathrm{LS}}(\mu X)$, is discussed in Sec. XII. The last two entries are observational equations for nuclear-charge radii as obtained from electron-proton and electron-deuteron scattering data discussed in Sec. XIII.

Input data	Observational equation
A6–A8, A10–A19, A22, A23, A26–A29	$\nu_X(n_1\ell_{1j_1} - n_2\ell_{2j_2}) \doteq \Big[E_X(n_2\ell_{2j_2};\Gamma_X) + \delta_X(n_2\ell_{2j_2}) - E_X(n_1\ell_{1j_1};\Gamma_X) - \delta_X(n_1\ell_{1j_1})\Big]/h$
A1–A4, A20, A21, A24, A25	$\nu_X(n_1\ell_{1j_1} - n_2\ell_{2j_2}) - \frac{1}{4}\nu_X(n_3\ell_{3j_3} - n_4\ell_{4j_4}) \doteq \Big\{E_X(n_2\ell_{2j_2};\Gamma_X) + \delta_X(n_2\ell_{2j_2}) - E_X(n_1\ell_{1j_1};\Gamma_X) - \delta_X(n_1\ell_{1j_1}) - \frac{1}{4}\Big[E_X(n_4\ell_{4j_4};\Gamma_X) + \delta_X(n_4\ell_{4j_4}) - E_X(n_3\ell_{3j_3};\Gamma_X) - \delta_X(n_3\ell_{3j_3})\Big]\Big\}/h$
A5	$\nu_{\mathrm{D}}(1\mathrm{S}_{1/2} - 2\mathrm{S}_{1/2}) - \nu_{\mathrm{H}}(1\mathrm{S}_{1/2} - 2\mathrm{S}_{1/2}) \doteq \Big\{E_{\mathrm{D}}(2\mathrm{S}_{1/2};\Gamma_{\mathrm{D}}) + \delta_{\mathrm{D}}(2\mathrm{S}_{1/2}) - E_{\mathrm{D}}(1\mathrm{S}_{1/2};\Gamma_{\mathrm{D}}) - \delta_{\mathrm{D}}(1\mathrm{S}_{1/2}) - \Big[E_{\mathrm{H}}(2\mathrm{S}_{1/2};\Gamma_{\mathrm{H}}) + \delta_{\mathrm{H}}(2\mathrm{S}_{1/2}) - E_{\mathrm{H}}(1\mathrm{S}_{1/2};\Gamma_{\mathrm{H}}) - \delta_{\mathrm{H}}(1\mathrm{S}_{1/2})\Big]\Big\}/h$
A9	$\nu_{\mathrm{H}}(2\mathrm{S}_{1/2} - 4\mathrm{P}, \mathrm{centroid}) \doteq \Big\{(E_{\mathrm{H}}(4\mathrm{P}_{1/2};\Gamma_{\mathrm{H}}) + \delta_{\mathrm{H}}(4\mathrm{P}_{1/2}))/3 + 2(E_{\mathrm{H}}(4\mathrm{P}_{3/2};\Gamma_{\mathrm{H}}) + \delta_{\mathrm{H}}(4\mathrm{P}_{3/2}))/3 - E_{\mathrm{H}}(2\mathrm{S}_{1/2};\Gamma_{\mathrm{H}}) - \delta_{\mathrm{H}}(2\mathrm{S}_{1/2})\Big\}/h$
B1–B25	$\delta_X(n\ell_j) \doteq \delta_X(n\ell_j)$
C1–C6	$\Delta\mathcal{E}_{\mathrm{LS}}(\mu X) \doteq \mathcal{E}_{0X} + \mathcal{E}_{2X} r_N^2 + \delta_{\mathrm{th}}(\mu X)$
C7, C8	$\delta E_{\mathrm{LS}}(\mu X) \doteq \delta_{\mathrm{th}}(\mu X)$
C9	$r_{\mathrm{p}} \doteq r_{\mathrm{p}}$
C10	$r_{\mathrm{d}} \doteq r_{\mathrm{d}}$

The mass-dependent functions $A_2^{(2)}(x)$, $A_3^{(2)}(x)$, and $A_3^{(4)}(x,y)$ are zero. The remaining nonzero mass-dependent coefficients computed at the relevant mass ratios are given in Table XXIV. Their fractional contributions to the muon anomaly are given in Table XXV. Only four of the mass-dependent QED corrections contribute significantly to the theoretical value for the muon anomaly. Finally, $a_\mu(\mathrm{QED})$ based on the 2018 recommended value of α and lepton mass ratios is

$$a_\mu(\mathrm{QED}) = 0.001\,165\,847\,188\,97(84) \quad [7.2 \times 10^{-10}]. \tag{156}$$

The primarily electroweak contribution is (Czarnecki, Marciano, and Vainshtein, 2003; Gnendiger, Stöckinger, and Stöckinger-Kim, 2013)

$$a_\mu(\mathrm{weak}) = 154(1) \times 10^{-11} \tag{157}$$

and contains both the leading term and also some higher-order corrections.

Five terms of the hadronic correction of the muon anomaly have been computed. They are

$$a_\mu(\mathrm{had}) = a_\mu^{\mathrm{LO,VP}}(\mathrm{had}) + a_\mu^{\mathrm{NLO,VP}}(\mathrm{had}) + a_\mu^{\mathrm{NNLO,VP}}(\mathrm{had}) + a_\mu^{\mathrm{LL}}(\mathrm{had}) + a_\mu^{\mathrm{NLO,LL}}(\mathrm{had}) + \cdots, \tag{158}$$

corresponding to leading-order (LO), next-to-leading-order (NLO), and next-to-next-to-leading-order (NNLO) vacuum-polarization corrections and hadronic light-by-light (LL), and higher-order light-by-light (NLO,LL) scattering terms, respectively. Their values are

TABLE XXIV. Mass-dependent functions $A_2^{(2n)}(x)$, $A_3^{(2n)}(x,y)$, and summed $C_\mu^{(2n)}$ coefficients for the QED contributions to the muon anomaly based on the 2018 recommended values of lepton mass ratios. The functions are evaluated at mass ratios $x_{\mu e} \equiv m_\mu/m_e$ and/or $x_{\mu\tau} \equiv m_\mu/m_\tau$.

n	$A_2^{(2n)}(x_{\mu e})$	$A_2^{(2n)}(x_{\mu\tau})$	$A_3^{(2n)}(x_{\mu e}, x_{\mu\tau})$	$C_\mu^{(2n)}$
1	0	0	0	0.5
2	1.094 258 3098(72)	0.000 078 076(10)	0	0.765 857 420(10)
3	22.868 379 99(17)	0.000 360 599(86)	0.000 527 738(71)	24.050 509 78(16)
4	132.6852(60)	0.042 4928(40)	0.062 72(4)	130.8782(60)
5	742.18(87)	−0.068(5)	2.011(10)	750.80(89)

TABLE XXV. Fractional contribution of mass-dependent functions $A_2^{(2n)}(x)$ and $A_3^{(2n)}(x,y)$ for the QED contributions to the muon anomaly based on the 2018 recommended values for α and lepton mass ratios. Fractional contributions are defined as $A_j^{(2n)} \times (\alpha/\pi)^n/a_\mu(\mathrm{th})$ for $j = 2$ or 3 and the relative standard uncertainty of $a_\mu(\mathrm{th})$ is 3.3×10^{-7}. The functions are evaluated at mass ratios $x_{\mu e} \equiv m_\mu/m_e$ and/or $x_{\mu\tau} \equiv m_\mu/m_\tau$.

n	$A_2^{(2n)}(x_{\mu e})$	$A_2^{(2n)}(x_{\mu\tau})$	$A_3^{(2n)}(x_{\mu e}, x_{\mu\tau})$
2	5.06×10^{-3}	3.61×10^{-7}	
3	2.46×10^{-4}	3.88×10^{-9}	5.67×10^{-9}
4	3.31×10^{-6}	1.06×10^{-9}	1.57×10^{-9}
5	4.30×10^{-8}	-3.94×10^{-12}	1.17×10^{-10}

$$a_\mu^{\mathrm{LO,VP}}(\mathrm{had}) = 6932.6(24.6) \times 10^{-11}, \tag{159}$$

$$a_\mu^{\mathrm{NLO,VP}}(\mathrm{had}) = -98.2(4) \times 10^{-11} \tag{160}$$

from Keshavarzi, Nomura, and Teubner (2018) based on e^+–e^- annihilation data. Davier *et al.* (2017) and Jegerlehner (2018) gave results that are consistent but slightly less accurate. Of these three publications, only Jegerlehner (2018) has included tau-lepton-decay data. The next-to-next-to-leading-order correction is

$$a_\mu^{\mathrm{NNLO,VP}}(\mathrm{had}) = 12.4(1) \times 10^{-11} \tag{161}$$

from Kurz *et al.* (2014b). Light-by-light corrections are

$$a_\mu^{\mathrm{LL}}(\mathrm{had}) = 103(29) \times 10^{-11} \tag{162}$$

from Jegerlehner (2018) and

$$a_\mu^{\mathrm{NLO,LL}}(\mathrm{had}) = 3.0(2.0) \times 10^{-11} \tag{163}$$

from Colangelo *et al.* (2014). The combined hadronic contribution is then

$$a_\mu(\mathrm{had}) = 6967(59) \times 10^{-11}. \tag{164}$$

Based on the 2018 recommended value of α and lepton mass ratios,

$$a_\mu(\mathrm{th}) = 1.165\,918\,13(38) \times 10^{-3} \tag{165}$$

for the theoretically predicted value of a_μ with standard uncertainty

$$u[a_\mu(\mathrm{th})] = 38 \times 10^{-11} = 3.3 \times 10^{-7} a_\mu. \tag{166}$$

The largest and equally important contributions to the uncertainty of $a_\mu(\mathrm{th})$ are from $a_\mu^{\mathrm{LO,VP}}(\mathrm{had})$ and $a_\mu^{\mathrm{LL}}(\mathrm{had})$. By comparison, the uncertainty of $a_\mu(\mathrm{QED})$ is negligible.

C. Analysis of experiment and theory for the muon anomaly

Figure 7(a) compares three recent determinations of $a_\mu^{\mathrm{LO,VP}}(\mathrm{had})$ based on electron-positron annihilation data with that mentioned in the 2014 CODATA report, i.e., the value from Hagiwara *et al.* (2011). Although the four values are consistent, the spread in values is rather large given that they are based on the same input data. This suggests that uncertainties remain underestimated. Nevertheless, for this discussion we have chosen the value given by Keshavarzi, Nomura, and Teubner (2018), because it has the smallest uncertainty.

In addition, Fig. 7 shows the results of two independent first-principle lattice-QCD evaluations of $a_\mu^{\mathrm{LO,VP}}(\mathrm{had})$, both published in 2018. We have

$$a_\mu^{\mathrm{LO,VP}}(\mathrm{had}) = 7111(75)(174) \times 10^{-11} \tag{167}$$

from Borsanyi *et al.* (2018) and

$$a_\mu^{\mathrm{LO,VP}}(\mathrm{had}) = 7154(163)(92) \times 10^{-11} \tag{168}$$

from Blum *et al.* (2018). The first and second numbers in parentheses correspond to the statistical and systematic uncertainties, respectively. The systematic uncertainty is dominated by finite-volume artifacts. In Fig. 7, the two uncertainties are added in quadrature. Blum *et al.* (2018) also describe a model that merges data from electron-positron annihilation data with their lattice-QCD evaluation. This leads to a more accurate determination of $a_\mu^{\mathrm{LO,VP}}(\mathrm{had})$ with the value

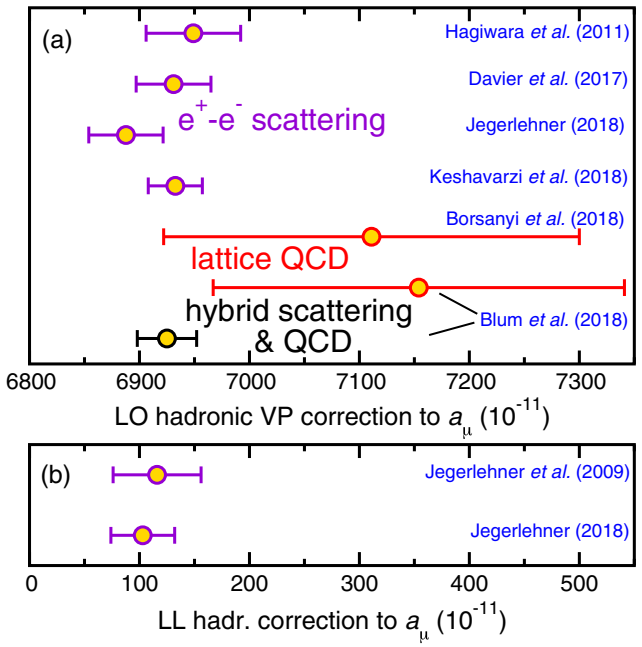


FIG. 7. Comparison of recent determinations of the leading-order hadronic (LO) vacuum-polarization [panel (a)] and light-by-light (LL) [panel (b)] contributions to the muon anomaly. Error bars are one-standard-deviation uncertainties. The LO,VP, and LL contributions limit the uncertainty of $a_\mu(\mathrm{th})$. The horizontal interval of the two panels is the same so that uncertainties can be compared. From top to bottom, data are from Hagiwara *et al.* (2011), Davier *et al.* (2017), Jegerlehner (2018), Keshavarzi, Nomura, and Teubner (2018), Borsanyi *et al.* (2018), and Blum *et al.* (2018) in panel (a) and from Jegerlehner and Nyffeler (2009) and Jegerlehner (2018) in panel (b).

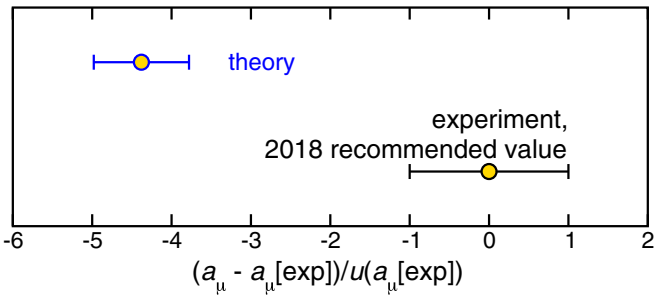


FIG. 8. Comparison of the experimental and theoretical value for the muon anomaly. Values have been scaled by the uncertainty of the 2018 recommended value.

$$a_\mu^{\mathrm{LO,VP}}(\mathrm{had})|_{\mathrm{hybrid}} = 6925(27) \times 10^{-11} \tag{169}$$

consistent in both value and uncertainty with data solely based on electron-positron annihilation data.

Figure 7(b) compares two evaluations of the leading-order light-by-light correction. Separated by almost ten years in publication date, the value has only slightly improved. The newest is considered here. As in the 2014 CODATA report, based on the analyses of Dorokhov, Radzhabov, and Zhevlakov (2014a, 2014b), Nyffeler (2014), and Adikaram *et al.* (2015), not shown in the figure, we note that $a_\mu^{\mathrm{LL}}(\mathrm{had})$ is model dependent and that a reliable estimate might still be missing.

The experimental and theoretical values for the muon magnetic-moment anomaly, i.e., Eqs. (152) and (165), respectively, are compared in Fig. 8. The difference between experiment and theory is just under four times the uncertainty of the difference. This is larger than in the 2014 CODATA report, as both $a_\mu^{\mathrm{LO,VP}}(\mathrm{had})$ and $a_\mu^{\mathrm{LL}}(\mathrm{had})$ have become smaller.

An expansion of only the uncertainty of $a_\mu(\mathrm{th})$ to attempt to account for the spread in the values of $a_\mu^{\mathrm{LO,VP}}(\mathrm{had})$ and $a_\mu^{\mathrm{LL}}(\mathrm{had})$ would significantly reduce its contribution in a least-squares adjustment that includes both input data $\bar{R}$ and $a_\mu(\mathrm{th})$. Expanding the uncertainties of $a_\mu(\mathrm{th})$ and $a_\mu(\mathrm{exp})$ to reduce the residual for both input data to less than two leads to a recommended value that ceases to be a useful reference value for future comparisons of theory and experiment. For all these reasons, the Task Group chose not to include $a_\mu(\mathrm{th})$ in the 2018 adjustment and to base the 2018 recommended value on experiment only.

XVII. ELECTRON-TO-MUON MASS RATIO AND MUON-TO-PROTON MAGNETIC-MOMENT RATIO

Muonium (Mu) is an atom consisting of a (positively charged) antimuon and a (negatively charged) electron. Measurements of two muonium ground-state hyperfine transition energies in a strong magnetic flux density combined with theoretical expressions for these energies provide information on the electron-to-muon mass ratio, m_e/m_μ, as well as the antimuon-to-proton magnetic-moment ratio, μ_{μ^+}/μ_p. Here, the proton magnetic moment only appears because the applied magnetic field or flux density is found by "replacing" the muonium with a proton in the experimental apparatus and measuring the transition frequency ω_p of its precessing spin. (More precisely, replacing muonium with a liquid-water sample, measuring the proton spin-precession frequency in water, and accounting for a shielding correction.)

In the remainder of this section, we summarize the theoretical determination of the zero-flux-density muonium hyperfine splitting (HFS) and the experimental measurements at field fluxes between one and two tesla. Results of relevant calculations and measurements are given along with references to new work; references to the original literature used in earlier CODATA adjustments are not repeated. We finish with an analysis of the data.

A. Theory of the muonium ground-state hyperfine splitting

The theoretical expression for the muonium hyperfine energy splitting absent a magnetic field may be factored into

$$\Delta E_{\mathrm{Mu}}(\mathrm{th}) = \Delta E_{\mathrm{F}} \mathcal{F} \tag{170}$$

with the Fermi energy formula

$$\Delta E_{\mathrm{F}} = \frac{16}{3} hcR_\infty Z^3 \alpha^2 \frac{m_e}{m_\mu} \left(1 + \frac{m_e}{m_\mu}\right)^{-3}, \tag{171}$$

which contains the main dependence on fundamental constants, and a function $\mathcal{F} = 1 + \alpha/\pi + \cdots$ that only depends weakly on them. (Recall $E_h = 2R_\infty hc = \alpha^2 m_e c^2$.) The charge of the antimuon is specified by Ze rather than e in order to identify the source of terms contributing to $\Delta E_{\mathrm{Mu}}(\mathrm{th})$.

The Fermi formula in Eq. (171) is expressed in terms of our adjusted constants R_∞, α, and m_e/m_μ. The relative uncertainties of R_∞ and α are much smaller than those for the measured ΔE_{Mu}. Hence, a measurement of ΔE_{Mu} determines the electron-to-muon mass ratio.

The general expression for the hyperfine splitting and thus also $\mathcal{F}$ is

$$\Delta E_{\mathrm{Mu}}(\mathrm{th}) = \Delta E_{\mathrm{D}} + \Delta E_{\mathrm{rad}} + \Delta E_{\mathrm{rec}} + \Delta E_{\mathrm{r\text{-}r}} + \Delta E_{\mathrm{weak}} + \Delta E_{\mathrm{had}}, \tag{172}$$

where subscripts D, rad, rec, r-r, weak, and had denote the Dirac, radiative, recoil, radiative-recoil, electroweak, and hadronic contributions to the hyperfine splitting, respectively.

The Dirac equation yields

$$\Delta E_{\mathrm{D}} = \Delta E_{\mathrm{F}}(1 + a_\mu)\left[1 + \frac{3}{2}(Z\alpha)^2 + \frac{17}{8}(Z\alpha)^4 + \cdots\right], \tag{173}$$

where a_μ is the muon magnetic-moment anomaly. Radiative corrections are

$$\Delta E_{\mathrm{rad}} = \Delta E_{\mathrm{F}}(1 + a_\mu) \sum_{n=1}^{\infty} D^{(2n)}(Z\alpha) \left(\frac{\alpha}{\pi}\right)^n, \tag{174}$$

where functions $D^{(2n)}(x)$ are contributions from n virtual photons. The leading term is

TABLE XXVI. Observational equations for input data in Tables XXI and XXVII as functions of the adjusted constants. The data determine the fine-structure constant, electron and muon masses and anomalies, masses and magnetic moments of light nuclei, as well as the lattice spacing of an ideal natural Si crystal and x-ray units. The labels in the first column correspond to those in the first column of Tables XXI and XXVII. For simplicity, the lengthier functions are not explicitly given. See Sec. III for an explanation of the symbol $\doteq$.

Input data	Observational equation	Sec.
D1	$a_e(\text{exp}) \doteq a_e(\text{th}) + \delta_{\text{th}}(\text{e})$	VIII
D2	$\delta_e \doteq \delta_{\text{th}}(\text{e})$	VIII
D3, D4	$\frac{h}{m(X)} \doteq \frac{A_r(\text{e})}{A_r(X)} \frac{c\alpha^2}{2R_\infty}$	X
D5, D6, D18	$A_r(X) \doteq A_r(X)$	IX
D7	$\frac{\omega_s(^{12}\text{C}^{5+})}{\omega_c(^{12}\text{C}^{5+})} \doteq -\frac{g_e(^{12}\text{C}^{5+}) + \delta_{\text{th}}(\text{C})}{10A_r(\text{e})}[12 - 5A_r(\text{e}) + \Delta E_B(^{12}\text{C}^{5+})\alpha^2 A_r(\text{e})/2R_\infty hc]$	XI.C
D8, D12, D21–D23	$\Delta E_B(X^{n+}) \doteq \Delta E_B(X^{n+})$	IX
D9	$\delta_C \doteq \delta_{\text{th}}(\text{C})$	XI.C
D10	$\frac{\omega_s(^{28}\text{Si}^{13+})}{\omega_c(^{28}\text{Si}^{13+})} \doteq -\frac{g_e(^{28}\text{Si}^{13+}) + \delta_{\text{th}}(\text{Si})}{26A_r(\text{e})} A_r(^{28}\text{Si}^{13+})$	XI.C
D11	$A_r(^{28}\text{Si}) \doteq A_r(^{28}\text{Si}^{13+}) + 13A_r(\text{e}) - \Delta E_B(^{28}\text{Si}^{13+})\alpha^2 A_r(\text{e})/2R_\infty hc$	IX
D13	$\delta_{\text{Si}} \doteq \delta_{\text{th}}(\text{Si})$	XI.C
D14	$\frac{\omega_c(\text{d})}{\omega_c(^{12}\text{C}^{6+})} \doteq \frac{12 - 6A_r(\text{e}) + \Delta E_B(^{12}\text{C}^{6+})\alpha^2 A_r(\text{e})/2R_\infty hc}{6A_r(\text{d})}$	IX
D15	$\frac{\omega_c(^{12}\text{C}^{6+})}{\omega_c(\text{p})} \doteq \frac{6A_r(\text{p})}{12 - 6A_r(\text{e}) + \Delta E_B(^{12}\text{C}^{6+})\alpha^2 A_r(\text{e})/2R_\infty hc}$	IX
D16	$\frac{\omega_c(\text{t})}{\omega_c(^3\text{He}^+)} \doteq \frac{A_r(\text{h}) + A_r(\text{e}) - \Delta E_I(^3\text{He}^+)\alpha^2 A_r(\text{e})/2R_\infty hc}{A_r(\text{t})}$	IX
D17	$\frac{\omega_c(\text{HD}^+)}{\omega_c(^3\text{He}^+)} \doteq \frac{A_r(\text{h}) + A_r(\text{e}) - E_I(^3\text{He}^+)\alpha^2 A_r(\text{e})/2R_\infty hc}{A_r(\text{p}) + A_r(\text{d}) + A_r(\text{e}) - \Delta E_I(\text{HD}^+)\alpha^2 A_r(\text{e})/2R_\infty hc}$	IX
D19	$A_r(^1\text{H}) \doteq A_r(\text{p}) + A_r(\text{e}) - \Delta E_B(^1\text{H}^+)\alpha^2 A_r(\text{e})/2R_\infty hc$	IX
D20	$A_r(^4\text{He}) \doteq A_r(\alpha) + 2A_r(\text{e}) - \Delta E_B(^4\text{He}^{2+})\alpha^2 A_r(\text{e})/2R_\infty hc$	IX
D24, D25	$\Delta E_I(X^+) \doteq \Delta E_I(X^+)$	IX
D26	$\bar{R} \doteq -\frac{a_\mu}{1 + a_e(\text{th}) + \delta_{\text{th}}(\text{e})} \frac{m_e}{m_\mu} \frac{\mu_e}{\mu_p}$	XVI.A
D27, D28	$E(\omega_p) \doteq E(\omega_p; R_\infty, \alpha, \frac{m_e}{m_\mu}, a_\mu, \frac{\mu_e}{\mu_p}, \delta_{\text{th}}(\text{e}), \delta_{\text{th}}(\text{Mu}))$	XVII.B
D29, D30	$\Delta E_{\text{Mu}} \doteq \Delta E_{\text{Mu}}(\text{th}; R_\infty, \alpha, \frac{m_e}{m_\mu}, a_\mu) + \delta_{\text{th}}(\text{Mu})$	XVII.A
D31	$\delta_{\text{Mu}} \doteq \delta_{\text{th}}(\text{Mu})$	XVII.A
D32	$\frac{\mu_p}{\mu_N} \doteq -(1 + a_e(\text{th}) + \delta_{\text{th}}(\text{e})) \frac{A_r(\text{p})}{A_r(\text{e})} \frac{\mu_p}{\mu_e}$	XV
D33	$\frac{\mu_e(\text{H})}{\mu_p(\text{H})} \doteq \frac{g_e(\text{H})}{g_e} \left(\frac{g_p(\text{H})}{g_p}\right)^{-1} \frac{\mu_e}{\mu_p}$	XIV.D
D34	$\frac{\mu_d(\text{D})}{\mu_e(\text{D})} \doteq \frac{g_d(\text{D})}{g_d} \left(\frac{g_e(\text{D})}{g_e}\right)^{-1} \frac{\mu_d}{\mu_e}$	XIV.D
D35	$\frac{\mu_e(\text{H})}{\mu'_p} \doteq \frac{g_e(\text{H})}{g_e} \frac{\mu_e}{\mu'_p}$	XIV.D
D36	$\frac{\mu'_h}{\mu'_p} \doteq \frac{\mu'_h}{\mu'_p}$	XIV.D
D37	$\frac{\mu_n}{\mu'_p} \doteq \frac{\mu_n}{\mu'_p}$	XIV.D
D38–D40	$\frac{\mu_p(\text{HD})}{\mu_d(\text{HD})} \doteq [1 + \sigma_{\text{dp}}] \frac{\mu_p}{\mu_e} \frac{\mu_e}{\mu_d}$	XIV.D
D41	$\frac{\mu_t(\text{HT})}{\mu_p(\text{HT})} \doteq \frac{1}{1 + \sigma_{\text{tp}}} \frac{\mu_t}{\mu_p}$	XIV.D
D42, D43	$\sigma_{NN'} \doteq \sigma_{NN'}$	XIV.C
E1–E4	$1 - \frac{d_{220}(Y)}{d_{220}(X)} \doteq 1 - \frac{d_{220}(Y)}{d_{220}(X)}$	XVIII

(Table continued)

TABLE XXVI. *(Continued)*

Input data	Observational equation	Sec.
E5–E13	$\frac{d_{220}(X)}{d_{220}(Y)} - 1 \doteq \frac{d_{220}(X)}{d_{220}(Y)} - 1$	XVIII
E14–E17	$d_{220}(X) \doteq d_{220}(X)$	XVIII
E18, E19	$\frac{\lambda(\mathrm{CuK}\alpha_1)}{d_{220}(X)} \doteq \frac{1537.400\ \mathrm{xu}(\mathrm{CuK}\alpha_1)}{d_{220}(X)}$	XVIII
E20	$\frac{\lambda(\mathrm{WK}\alpha_1)}{d_{220}(\mathrm{N})} \doteq \frac{0.209\,010\,0\ \text{Å}^*}{d_{220}(\mathrm{N})}$	XVIII
E21	$\frac{\lambda(\mathrm{MoK}\alpha_1)}{d_{220}(\mathrm{N})} \doteq \frac{707.831\ \mathrm{xu}(\mathrm{MoK}\alpha_1)}{d_{220}(\mathrm{N})}$	XVIII

$$D^{(2)}(x) = A_1^{(2)} + \left(\ln 2 - \frac{5}{2}\right)\pi x + \left[-\frac{2}{3}\ln^2(x^{-2}) + \left(\frac{281}{360} - \frac{8}{3}\ln 2\right)\ln(x^{-2}) + 16.9037\ldots\right]x^2 + \left[\left(\frac{5}{2}\ln 2 - \frac{547}{96}\right)\ln(x^{-2})\right]\pi x^3 + G(x)x^3, \quad (175)$$

where $A_1^{(2)} = 1/2$, as in Eq. (51). The function $G(x)$ accounts for all higher-order contributions in powers of x; it can be divided into self-energy (SE) and vacuum-polarization (VP) contributions, $G(x) = G_{\mathrm{SE}}(x) + G_{\mathrm{VP}}(x)$. Yerokhin and Jentschura (2008, 2010) and Karshenboim, Ivanov, and Shabaev (1999, 2000) have calculated the one-loop self-energy and vacuum-polarization contributions for the muonium HFS with $x = \alpha$. Their results are

$$G_{\mathrm{SE}}(\alpha) = -13.8308(43) \quad (176)$$

and

$$G_{\mathrm{VP}}(\alpha) = 7.227(9), \quad (177)$$

where the latter uncertainty is meant to account for neglected higher-order Uehling-potential terms; it corresponds to energy uncertainties less than $h \times 0.1$ Hz, and is thus entirely negligible.

For $D^{(4)}(x)$, we have

$$D^{(4)}(x) = A_1^{(4)} + 0.770\,99(2)\pi x + \left[-\frac{1}{3}\ln^2(x^{-2}) - 0.6390\ldots \times \ln(x^{-2}) + 10(2.5)\right]x^2 + \cdots, \quad (178)$$

where $A_1^{(4)}$ is given in Eq. (52). The next term is

$$D^{(6)}(x) = A_1^{(6)} + \cdots, \quad (179)$$

where the leading contribution $A_1^{(6)}$ is given in Eq. (53), but only partial results of relative order $Z\alpha$ have been calculated (Eides and Shelyuto, 2007). Higher-order functions $D^{(2n)}(x)$ with $n > 3$ are expected to be negligible.

The recoil contribution is

$$\Delta E_{\mathrm{rec}} = \Delta E_{\mathrm{F}}\frac{m_e}{m_\mu}\left(-\frac{3}{1-(m_e/m_\mu)^2}\ln\left(\frac{m_\mu}{m_e}\right)\frac{Z\alpha}{\pi} + \frac{1}{(1+m_e/m_\mu)^2}\left\{\ln(Z\alpha)^{-2} - 8\ln 2 + \frac{65}{18} + \left[\frac{9}{2\pi^2}\ln^2\left(\frac{m_\mu}{m_e}\right) + \left(\frac{27}{2\pi^2} - 1\right)\ln\left(\frac{m_\mu}{m_e}\right) + \frac{93}{4\pi^2} + \frac{33\zeta(3)}{\pi^2} - \frac{13}{12} - 12\ln 2\right]\frac{m_e}{m_\mu}\right\}(Z\alpha)^2 + \left\{-\frac{3}{2}\ln\left(\frac{m_\mu}{m_e}\right)\ln(Z\alpha)^{-2} - \frac{1}{6}\ln^2(Z\alpha)^{-2} + \left(\frac{101}{18} - 10\ln 2\right)\ln(Z\alpha)^{-2} + 40(10)\right\}\frac{(Z\alpha)^3}{\pi}\right) + \cdots. \quad (180)$$

The leading-order $\mathcal{O}(\Delta E_{\mathrm{F}}\alpha^2)$ radiative-recoil contribution is

$$\Delta E_{\mathrm{r\text{-}r}} = \Delta E_{\mathrm{F}}\left(\frac{\alpha}{\pi}\right)^2\frac{m_e}{m_\mu}\left\{\left[-2\ln^2\left(\frac{m_\mu}{m_e}\right) + \frac{13}{12}\ln\left(\frac{m_\mu}{m_e}\right) + \frac{21}{2}\zeta(3) + \frac{\pi^2}{6} + \frac{35}{9}\right] + \left[\frac{4}{3}\ln^2\alpha^{-2} + \left(\frac{16}{3}\ln 2 - \frac{341}{180}\right)\ln\alpha^{-2} - 40(10)\right]\pi\alpha + \left[-\frac{4}{3}\ln^3\left(\frac{m_\mu}{m_e}\right) + \frac{4}{3}\ln^2\left(\frac{m_\mu}{m_e}\right)\right]\frac{\alpha}{\pi}\right\} - \Delta E_{\mathrm{F}}\alpha^2\left(\frac{m_e}{m_\mu}\right)^2\left(6\ln 2 + \frac{13}{6}\right) + \cdots, \quad (181)$$

where, for simplicity, the explicit dependence on Z is not shown. Single-logarithmic and nonlogarithmic three-loop radiative-recoil corrections of $\mathcal{O}(\Delta E_{\mathrm{F}}\alpha^3)$ are (Eides and Shelyuto, 2014)

$$\Delta E_{\mathrm{F}}\left(\frac{\alpha}{\pi}\right)^3\frac{m_e}{m_\mu}\left\{\left[-6\pi^2\ln 2 + \frac{\pi^2}{3} + \frac{27}{8}\right]\ln\frac{m_\mu}{m_e} + 68.507(2)\right\} = h \times -30.99\ \mathrm{Hz}. \quad (182)$$

Uncalculated remaining terms of the same order as those included in Eq. (182) have been estimated by Eides and Shelyuto (2014) to be about $h \times 10$ Hz to $h \times 15$ Hz. Additional radiative-recoil corrections have been calculated, but are negligibly small, less than $h \times 0.5$ Hz.

The electroweak contribution due to the exchange of a Z^0 boson is (Eides, 1996)

$$\Delta E_{\rm weak}/h = -65 \text{ Hz}, \tag{183}$$

while for the hadronic vacuum-polarization contribution we have

$$\Delta E_{\rm had}/h = 237.7(1.5) \text{ Hz}. \tag{184}$$

This hadronic contribution combines the result of Nomura and Teubner (2013) with a newly computed $h \times 4.97(19)$ Hz contribution from Shelyuto, Karshenboim, and Eidelman (2018). A negligible contribution ($\approx h \times 0.0065$ Hz) from the hadronic light-by-light correction has been given by Karshenboim, Shelyuto, and Vainshtein (2008).

The uncertainty of $\Delta E_{\rm Mu}({\rm th})$ in Eq. (172) is determined, from the largest to smallest component, by those in $\Delta E_{\rm rec}$, $\Delta E_{\rm r\text{-}r}$, $\Delta E_{\rm rad}$, and $\Delta E_{\rm had}$. The $h \times 1.5$ Hz uncertainty in the latter is only of marginal interest.

For $\Delta E_{\rm rec}$, the total uncertainty is $h \times 64$ Hz and has three components. They are $h \times 53$ Hz from twice the uncertainty 10 of the number 40 in Eq. (180) as discussed in the 2002 CODATA adjustment, $h \times 34$ Hz due to a possible recoil correction of order $\Delta E_{\rm F}(m_{\rm e}/m_\mu) \times (Z\alpha)^3 \ln(m_{\rm e}/m_\mu)$, and, finally, $h \times 6$ Hz to reflect a possible recoil term of order $\Delta E_{\rm F}(m_{\rm e}/m_\mu) \times (Z\alpha)^4 \ln^2(Z\alpha)^{-2}$.

The uncertainty in $\Delta E_{\rm r\text{-}r}$ is $h \times 55$ Hz, with $h \times 53$ Hz due to twice the uncertainty 10 of the number -40 in Eq. (181) as above, and $h \times 15$ Hz as discussed in connection with Eq. (182). The uncertainty in $\Delta E_{\rm rad}$ is $h \times 5$ Hz and consists of two components: $h \times 4$ Hz from an uncertainty of 1 in $G_{\rm VP}(\alpha)$ due to the uncalculated contribution of order $\alpha(Z\alpha)^3$, and $h \times 3$ Hz from the uncertainty 2.5 of the number 10 in the function $D^{(4)}(x)$.

The final uncertainty in $\Delta E_{\rm Mu}({\rm th})$ is then

$$u[\Delta E_{\rm Mu}({\rm th})]/h = 85 \text{ Hz}. \tag{185}$$

For the least-squares calculations, we use the observational equations

$$\Delta E_{\rm Mu} \doteq \Delta E_{\rm Mu}({\rm th}) + \delta_{\rm th}({\rm Mu}) \tag{186}$$

and

$$\delta_{\rm Mu} \doteq \delta_{\rm th}({\rm Mu}), \tag{187}$$

where $\delta_{\rm th}({\rm Mu})$ accounts for the uncertainty of the theoretical expression and is taken to be an adjusted constant. Based on Eq. (185), its corresponding input datum in the 2018 adjustment is $\delta_{\rm Mu} = 0(85)$ Hz. The input data $\Delta E_{\rm Mu}$ are discussed later. The theoretical hyperfine splitting $\Delta E_{\rm Mu}({\rm th})$ is mainly a function of the adjusted constants R_∞, α, and $m_{\rm e}/m_\mu$. Finally, the covariance between $\Delta E_{\rm Mu}$ and $\delta_{\rm Mu}$ is zero.

B. Measurements of muonium transition energies

The two most precise determinations of muonium hyperfine transition energies were carried out by researchers at the Meson Physics Facility at Los Alamos (LAMPF), New Mexico, USA and published in 1982 and 1999, respectively. These transition energies are compared to differences between eigenvalues of the Breit-Rabi Hamiltonian (Breit and Rabi, 1931; Millman, Rabi, and Zacharias, 1938) modified for muonium using a magnetic flux density determined from the free-proton NMR frequency measured in the apparatus. The experiments were reviewed in the 1998 CODATA adjustment.

Data reported in 1982 by Mariam (1981) and Mariam *et al.* (1982) are

$$\Delta E_{\rm Mu}/h = 4\,463\,302.88(16) \text{ kHz} \quad [3.6 \times 10^{-8}] \tag{188}$$

for the hyperfine splitting and

$$E(\omega_{\rm p})/h = 627\,994.77(14) \text{ kHz} \quad [2.2 \times 10^{-7}] \tag{189}$$

for the difference of two transition energies with correlation coefficient

$$r[\Delta E_{\rm Mu}, E(\omega_{\rm p})] = 0.227. \tag{190}$$

In fact, $\Delta E_{\rm Mu}$ and $E(\omega_{\rm p})$ are the sum and difference of two measured transition energies, $\hbar\omega_{\rm p} = 2\mu_{\rm p}B$ is the free-proton NMR transition energy, and only $E(\omega_{\rm p})$ depends on $\omega_{\rm p}$. In this experiment, $\hbar\omega_{\rm p} = h \times 57.972\,993$ MHz at its 1.3616 T magnetic flux density.

The data reported in 1999 by Liu *et al.* (1999) are

$$\Delta E_{\rm Mu}/h = 4\,463\,302\,765(53) \text{ Hz} \quad [1.2 \times 10^{-8}], \tag{191}$$

$$E(\omega_{\rm p})/h = 668\,223\,166(57) \text{ Hz} \quad [8.6 \times 10^{-8}] \tag{192}$$

with correlation coefficient

$$r[\Delta E_{\rm Mu}, E(\omega_{\rm p})] = 0.195 \tag{193}$$

and $\hbar\omega_{\rm p} = h \times 72.320\,000$ MHz for the proton transition energy in a flux density of approximately 1.7 T.

The observational equations are Eq. (186) and

$$E(\omega_{\rm p}) \doteq -(W_{\rm e^-} + W_{\mu^+}) + \sqrt{[\Delta E_{\rm Mu}({\rm th}) + \delta_{\rm th}({\rm Mu})]^2 + (W_{\rm e^-} - W_{\mu^+})^2}, \tag{194}$$

where $W_\ell = -[\mu_\ell({\rm Mu})/\mu_{\rm p}]\hbar\omega_{\rm p}$. Explicitly expressing $W_{\rm e^-}$ and W_{μ^+} in terms of adjusted constants then yields

$$W_{\rm e^-} = -\frac{g_{\rm e}({\rm Mu})}{g_{\rm e}}\frac{\mu_{\rm e^-}}{\mu_{\rm p}}\hbar\omega_{\rm p} \tag{195}$$

and

$$W_{\mu^+} = \frac{g_\mu({\rm Mu})}{g_\mu}\frac{1+a_\mu}{1+a_{\rm e}({\rm th})+\delta_{\rm th}({\rm e})}\frac{m_{\rm e}}{m_\mu}\frac{\mu_{\rm e^-}}{\mu_{\rm p}}\hbar\omega_{\rm p}. \tag{196}$$

Here, we have used the fact that $\mu_\ell(\mathrm{Mu}) = g_\ell(\mathrm{Mu})e\hbar/4m_\ell$ for the magnitude of the magnetic moment of lepton ℓ in muonium (see Secs. VIII and XIV.A), $|g_\ell| = 2(1 + a_\ell)$, and crucially $g_{\mu^+} = -g_{\mu^-}$. The g-factor ratios $g_e(\mathrm{Mu})/g_e$ and $g_\mu(\mathrm{Mu})/g_\mu$ are given in Table XX.

The adjusted constants in Eq. (186) and Eqs. (194)–(196) are the magnetic-moment anomaly a_μ, mass ratio m_e/m_μ, magnetic-moment ratio μ_{e^-}/μ_p, and additive constants $\delta_{th}(\mathrm{Mu})$ and $\delta_{th}(e)$. The latter two constants account for uncomputed theoretical contributions to $\Delta E_{Mu}(\mathrm{th})$ and $a_e(\mathrm{th})$, respectively. Finally, $\Delta E_{Mu}(\mathrm{th})$ is mainly a function of adjusted constants m_e/m_μ, R_∞, and α; $a_e(\mathrm{th})$ is mainly a function of R_∞ and α. The accurately measured or computed $\hbar\omega_p$ and ratios $g_\ell(\mathrm{Mu})/g_\ell$ are treated as exact in our least-squares adjustment.

It is worth noting that in Eq. (194) the energy $W_{e^-} > 0$, and at the flux densities used in the experiments $|W_{e^-}| \sim \Delta E_{Mu}(\mathrm{th})$ and $|W_{\mu^+}| \ll |W_{e^-}|$. Consequently, the right-hand side of Eq. (194) only has a weak dependence on $\Delta E_{Mu}(\mathrm{th})$ and the corresponding input datum does not significantly constrain $\Delta E_{Mu}(\mathrm{th})$ and thus m_e/m_μ in the adjustment.

For ease of reference, the experimental and theoretical input data for muonium hyperfine splittings are summarized in Table XXI and given labels D27 through D31. Observational equations are summarized in Table XXVI.

C. Analysis of the muonium hyperfine splitting and mass ratio m_μ/m_e

The 2018 recommended value for the muonium hyperfine splitting is

$$\Delta E_{Mu}(\mathrm{th}) + \delta_{th}(\mathrm{Mu}) = h \times 4\,463\,302\,776(51)\ \mathrm{Hz} \quad [1.1 \times 10^{-8}], \tag{197}$$

which is consistent in both value and uncertainty with the most accurately measured value of Eq. (191). More importantly, the prediction $\delta_{th}(\mathrm{Mu})/h = -4(83)$ Hz for the additive constant falls well inside the 85 Hz theoretical uncertainty. As $\delta_{th}(\mathrm{Mu})$ is a measure of uncomputed terms in the theory, the value implies that the theory is sufficiently accurate given the current constraints. Eides (2019) gave an alternative prediction for the uncertainty of the recommended muonium hyperfine splitting.

The 2018 recommended value for the muon-to-electron mass ratio is

$$m_\mu/m_e = 206.768\,2830(46) \tag{198}$$

and has a relative standard uncertainty of 2.2×10^{-8} that is nearly twice that of the 1999 measurement of ΔE_{Mu} in Eq. (191). This increase simply reflects the fact that the square of the relative standard uncertainty for m_μ/m_e to good approximation satisfies

$$u_r^2(m_\mu/m_e) = u_r^2(\Delta E_{Mu}(\mathrm{th})) + u_r^2(\Delta E_{Mu}), \tag{199}$$

which follows from error propagation with Eqs. (170) and (186). The relative standard uncertainties in the theory for and measurement of the hyperfine splitting are almost the same.

New data on the muonic hyperfine splitting by the MuSEUM collaboration at the J-PARC Muon Science Facility are expected in the near future (Strasser *et al.*, 2019).

XVIII. LATTICE SPACINGS OF SILICON CRYSTALS

In this section, we summarize efforts to determine the lattice spacing of an ideal (or nearly perfect) natural-silicon single crystal. We also present values for several historical x-ray units in terms of the SI unit meter. Three stable isotopes of silicon exist in nature. They are ^{28}Si, ^{29}Si, and ^{30}Si with amount-of-substance fractions $x(^A\mathrm{Si})$ of approximately 0.92, 0.05, and 0.03, respectively. Highly enriched silicon single crystals have $x(^{28}\mathrm{Si}) \approx 0.999\,96$.

The quantities of interest are the {220} crystal lattice spacing $d_{220}(X)$ in meters of a number of different crystals X using a combined x-ray and optical interferometer (XROI) as well as the fractional differences

$$\frac{d_{220}(X) - d_{220}(Y)}{d_{220}(Y)} \tag{200}$$

for single crystals X and Y, determined using a lattice comparator based on x-ray double-crystal nondispersive diffractometry.

Data on eight natural Si crystals, in the literature denoted by WASO 4.2a, WASO 04, WASO 17, NRLM3, NRLM4, MO*, ILL, and N, are relevant for the 2018 CODATA adjustment. Their lattice spacings $d_{220}(X)$ are adjusted constants in our least-squares calculations. The simplified notation W4.2a, W04, W17, NR3, and NR4 is used in quantity symbols and tables for the first five crystals. The lattice spacing for the ideal natural-silicon single crystal d_{220} is an adjusted constant.

Lattice-spacing data included in this adjustment are items E1–E17 in Table XXVII and quoted at a temperature of 22.5 °C and in vacuum. All data but one were already included in the 2014 adjustment. The new measurement is from Kessler *et al.* (2017) at the National Institute of Standards and Technology, Gaithersburg, USA and given as item E13 in the table. They measured the fractional difference for natural Si crystals ILL and W04. Consistent with previous adjustments and, in particular, following the discussions by Mohr and Taylor (1999, 2000), we expand their quoted uncertainty by 20×10^{-9} in quadrature to properly account for uncertainties due to carbon and oxygen impurities in the crystal.

The copper $K\alpha_1$ x unit with symbol $\mathrm{xu}(\mathrm{CuK}\alpha_1)$, the molybdenum $K\alpha_1$ x unit with symbol $\mathrm{xu}(\mathrm{MoK}\alpha_1)$, and the ångström star with symbol Å* are historic x-ray units that are still of current interest. They are defined by assigning an exact, conventional value to the wavelength of the $\mathrm{CuK}\alpha_1$, $\mathrm{MoK}\alpha_1$, and $\mathrm{WK}\alpha_1$ x-ray lines. These assigned wavelengths for $\lambda(\mathrm{CuK}\alpha_1)$, $\lambda(\mathrm{MoK}\alpha_1)$, and $\lambda(\mathrm{WK}\alpha_1)$ are 1537.400 $\mathrm{xu}(\mathrm{CuK}\alpha_1)$, 707.400 $\mathrm{xu}(\mathrm{MoK}\alpha_1)$, and 0.209 010 0 Å*, respectively. The four relevant experimental input data are the measured ratios of $\mathrm{CuK}\alpha_1$, $\mathrm{MoK}\alpha_1$, and $\mathrm{WK}\alpha_1$ wavelengths to the {220} lattice spacings of crystals WASO 4.2a and N and are items E18–E21 in Table XXVII. In the least-squares calculations, the units $\mathrm{xu}(\mathrm{CuK}\alpha_1)$, $\mathrm{xu}(\mathrm{MoK}\alpha_1)$, and Å* are adjusted constants.

TABLE XXVII. Input data for the determination of the 2018 recommended values of the lattice spacings of an ideal natural Si crystal and x-ray units. The label in the first column is used in Table XXVIII to list correlation coefficients among the data and in Table XXVI for observational equations. The uncertainties are not those as originally published, but corrected according the considerations in Sec. III.I of Mohr and Taylor (2000). For additional information about the uncertainties of data published after the closing data of the 1998 CODATA adjustment, see also the corresponding text in this and other CODATA publications. Columns four and five give the reference and an abbreviation of the name of the laboratory in which the experiment has been performed, and year of publication. An extensive list of abbreviations is found at the end of this report.

	Input datum	Value	Relat. stand. uncert. u_r	Laboratory	Reference(s)
E1	$1 - d_{220}(\mathrm{W17})/d_{220}(\mathrm{ILL})$	$-8(22) \times 10^{-9}$		NIST-99	Kessler *et al.* (2000)
E2	$1 - d_{220}(\mathrm{MO}^*)/d_{220}(\mathrm{ILL})$	$86(27) \times 10^{-9}$		NIST-99	Kessler *et al.* (2000)
E3	$1 - d_{220}(\mathrm{NR3})/d_{220}(\mathrm{ILL})$	$33(22) \times 10^{-9}$		NIST-99	Kessler *et al.* (2000)
E4	$1 - d_{220}(\mathrm{N})/d_{220}(\mathrm{W17})$	$7(22) \times 10^{-9}$		NIST-97	Kessler, Schweppe, and Deslattes (1997)
E5	$d_{220}(\mathrm{W4.2a})/d_{220}(\mathrm{W04}) - 1$	$-1(21) \times 10^{-9}$		PTB-98	Martin *et al.* (1998)
E6	$d_{220}(\mathrm{W17})/d_{220}(\mathrm{W04}) - 1$	$22(22) \times 10^{-9}$		PTB-98	Martin *et al.* (1998)
E7	$d_{220}(\mathrm{W17})/d_{220}(\mathrm{W04}) - 1$	$11(21) \times 10^{-9}$		NIST-06	Hanke and Kessler (2005)
E8	$d_{220}(\mathrm{MO}^*)/d_{220}(\mathrm{W04}) - 1$	$-103(28) \times 10^{-9}$		PTB-98	Martin *et al.* (1998)
E9	$d_{220}(\mathrm{NR3})/d_{220}(\mathrm{W04}) - 1$	$-23(21) \times 10^{-9}$		PTB-98	Martin *et al.* (1998)
E10	$d_{220}(\mathrm{NR3})/d_{220}(\mathrm{W04}) - 1$	$-11(21) \times 10^{-9}$		NIST-06	Hanke and Kessler (2005)
E11	$d_{220}/d_{220}(\mathrm{W04}) - 1$	$10(11) \times 10^{-9}$		PTB-03	Becker *et al.* (2003)
E12	$d_{220}(\mathrm{NR4})/d_{220}(\mathrm{W04}) - 1$	$25(21) \times 10^{-9}$		NIST-06	Hanke and Kessler (2005)
E13	$d_{220}(\mathrm{ILL})/d_{220}(\mathrm{W04}) - 1$	$-20(22) \times 10^{-9}$		NIST-17	Kessler *et al.* (2017)
E14	$d_{220}(\mathrm{MO}^*)$	192 015.5508(42) fm	2.2×10^{-8}	INRIM-08	Ferroglio, Mana, and Massa (2008)
E15	$d_{220}(\mathrm{W04})$	192 015.5702(29) fm	1.5×10^{-8}	INRIM-09	Massa *et al.* (2009)
E16	$d_{220}(\mathrm{W4.2a})$	192 015.5691(29) fm	1.5×10^{-8}	INRIM-09	Massa, Mana, and Kuetgens (2009)
E17	$d_{220}(\mathrm{W4.2a})$	192 015.563(12) fm	6.2×10^{-8}	PTB-81	Becker *et al.* (1981);
E18	$\lambda(\mathrm{Cu\,K}\alpha_1)/d_{220}(\mathrm{W4.2a})$	0.802 327 11(24)	3.0×10^{-7}	FSUJ/PTB-91	Windisch and Becker (1990); and Härtwig *et al.* (1991)
E19	$\lambda(\mathrm{Cu\,K}\alpha_1)/d_{220}(\mathrm{N})$	0.802 328 04(77)	9.6×10^{-7}	NIST-73	Deslattes and Henins (1973)
E20	$\lambda(\mathrm{W\,K}\alpha_1)/d_{220}(\mathrm{N})$	0.108 852 175(98)	9.0×10^{-7}	NIST-79	Kessler, Deslattes, and Henins (1979)
E21	$\lambda(\mathrm{Mo\,K}\alpha_1)/d_{220}(\mathrm{N})$	0.369 406 04(19)	5.3×10^{-7}	NIST-73	Deslattes and Henins (1973)

TABLE XXVIII. Correlation coefficients $r(x_i, x_j) > 0.0001$ among the input data for the lattice spacing of an ideal natural Si crystal and x-ray units given in Table XXVII.

$r(\mathrm{E1,E2}) = 0.4214$	$r(\mathrm{E1,E3}) = 0.5158$	$r(\mathrm{E1,E4}) = -0.2877$	$r(\mathrm{E1,E7}) = -0.3674$	$r(\mathrm{E1,E10}) = 0.0648$
$r(\mathrm{E1,E12}) = 0.0648$	$r(\mathrm{E2,E3}) = 0.4213$	$r(\mathrm{E2,E4}) = 0.0960$	$r(\mathrm{E2,E7}) = 0.0530$	$r(\mathrm{E2,E10}) = 0.0530$
$r(\mathrm{E2,E12}) = 0.0530$	$r(\mathrm{E3,E4}) = 0.1175$	$r(\mathrm{E3,E7}) = 0.0648$	$r(\mathrm{E3,E10}) = -0.3674$	$r(\mathrm{E3,E12}) = 0.0648$
$r(\mathrm{E4,E7}) = 0.5037$	$r(\mathrm{E4,E10}) = 0.0657$	$r(\mathrm{E4,E12}) = 0.0657$	$r(\mathrm{E5,E6}) = 0.4685$	$r(\mathrm{E5,E8}) = 0.3718$
$r(\mathrm{E5,E9}) = 0.5017$	$r(\mathrm{E6,E8}) = 0.3472$	$r(\mathrm{E6,E9}) = 0.4685$	$r(\mathrm{E7,E10}) = 0.5093$	$r(\mathrm{E7,E12}) = 0.5093$
$r(\mathrm{E8,E9}) = 0.3718$	$r(\mathrm{E10,E12}) = 0.5093$	$r(\mathrm{E14,E15}) = 0.0230$	$r(\mathrm{E14,E16}) = 0.0230$	$r(\mathrm{E15,E16}) = 0.0269$

The correlation coefficients among the data on lattice spacings and x-ray units are given in Table XXVIII. Discussions of these correlations can be found in previous adjustments. The sole new data point has no correlations with previous data. Observational equations may be found in Table XXVI.

XIX. NEWTONIAN CONSTANT OF GRAVITATION

Table XXIX summarizes the 16 measured values of the Newtonian constant of gravitation G considered as input data for the 2018 adjustment. Since the 2014 adjustment, two new values have become available (Li *et al.*, 2018) and corrections have been applied to a previously reported value (Parks and Faller, 2010). Figure 9 illustrates all input data. The measurements are inconsistent and an expansion factor of 3.9 is required to bring all residuals to within a factor of two from the 2018 recommended value of

$$G = 6.674\,30(15) \times 10^{-11}\ \mathrm{m^3\,kg^{-1}\,s^{-2}}\ \ [2.2 \times 10^{-5}]. \qquad (201)$$

The five measurements that contribute most to this value are the UWash-00, UZur-06, UCI-14, and the $\mathrm{HUST_{A,T}}$-18 values. The residuals of the data from BIPM-14 and JILA-18 are the largest and determined our expansion factor.

TABLE XXIX. Input data for the Newtonian constant of gravitation G relevant to the 2018 adjustment. The first two columns give the reference and an abbreviation of the name of the laboratory in which the experiment has been performed, and year of publication. The data are uncorrelated except for three cases with correlation coefficients $r(\text{NIST-82}, \text{LANL-97}) = 0.351$, $r(\text{HUST-05}, \text{HUST-09}) = 0.134$, and $r(\text{HUST-09}, \text{HUST}_\text{T}\text{-18}) = 0.068$.

Source	Identification	Method	$G(10^{-11}\ \text{kg}^{-1} \times \text{m}^3\ \text{s}^{-2})$	Rel. stand. uncert. u_r
Luther and Towler (1982)	NIST-82	Fiber torsion balance, dynamic mode	6.672 48(43)	6.4×10^{-5}
Karagioz and Izmailov (1996)	TR&D-96	Fiber torsion balance, dynamic mode	6.672 9(5)	7.5×10^{-5}
Bagley and Luther (1997)	LANL-97	Fiber torsion balance, dynamic mode	6.673 98(70)	1.0×10^{-4}
Gundlach and Merkowitz (2000, 2002)	UWash-00	Fiber torsion balance, dynamic compensation	6.674 255(92)	1.4×10^{-5}
Quinn *et al.* (2001)	BIPM-01	Strip torsion balance, compensation mode, static deflection	6.675 59(27)	4.0×10^{-5}
Kleinevoß (2002) and Kleinvoß *et al.* (2002)	UWup-02	Suspended body, displacement	6.674 22(98)	1.5×10^{-4}
Armstrong and Fitzgerald (2003)	MSL-03	Strip torsion balance, compensation mode	6.673 87(27)	4.0×10^{-5}
Hu, Guo, and Luo (2005)	HUST-05	Fiber torsion balance, dynamic mode	6.672 22(87)	1.3×10^{-4}
Schlamminger *et al.* (2006)	UZur-06	Stationary body, weight change	6.674 25(12)	1.9×10^{-5}
Luo *et al.* (2009) and Tu *et al.* (2010)	HUST-09	Fiber torsion balance, dynamic mode	6.673 49(18)	2.7×10^{-5}
Quinn *et al.* (2013, 2014)	BIPM-14	Strip torsion balance, compensation mode, static deflection	6.675 54(16)	2.4×10^{-5}
Prevedelli *et al.* (2014) and Rosi *et al.* (2014)	LENS-14	Double atom interferometer, gravity gradiometer	6.671 91(99)	1.5×10^{-4}
Newman *et al.* (2014)	UCI-14	Cryogenic torsion balance, dynamic mode	6.674 35(13)	1.9×10^{-5}
Li *et al.* (2018)	HUST_T-18	Fiber torsion balance, dynamic mode	6.674 184(78)	1.2×10^{-5}
Li *et al.* (2018)	HUST_A-18	Fiber torsion balance, dynamic compensation	6.674 484(77)	1.2×10^{-5}
Parks and Faller (2019)	JILA-18	Suspended body, displacement	6.672 60(25)	3.7×10^{-5}

We note, however, that the inconsistencies are smaller than in our previous 2014 adjustment.

We briefly describe the new measurements in the next two sections. Details regarding older measurements can be found in descriptions of previous CODATA adjustments.

A. Corrected value of the 2010 measurement at JILA

In 2010, Parks and Faller (2010) at JILA, University of Colorado and National Institute of Standards and Technology, Boulder, Colorado, USA used simple pendulums to determine G in an experimental design similar to that of Kleinevoß (2002) and Kleinvoß *et al.* (2002). Two pendulums, each with a cylindrical test mass suspended by four wires, were aligned such that the cylinders were colinear. As surrounding source masses moved, changes in the separation between the test masses were interferometrically monitored.

In 2016, the apparatus was transferred to NIST, Gaithersburg, Maryland, USA with the goal of repeating the experiment. During initial preparations at NIST, two calculational errors were discovered, both associated with the rotation of the test masses when they are horizontally displaced. Rotation occurred because the connection points of the suspension wires to the test masses were located above their center of mass. The first error was in the derivation of the pendulums' effective spring constants used to calculate the gravitational force from a measured horizontal separation between the test masses. The contribution from rotation to the spring constants was overestimated. The initial relative correction to G of $5.8(0.4) \times 10^{-5}$ has been updated to $0.40(30) \times 10^{-5}$. The second error arises from the interferometer axis being displaced by about 0.95(30) mm above the horizontal plane containing the test masses' center of mass, resulting in an Abbe error. The relative correction to G to remove the Abbe error is $9.4(3.0) \times 10^{-5}$.

Applying these two corrections results in a relative increase of their 2010 value for G of 3.9×10^{-5} and an increase of the relative uncertainty from 2.1×10^{-5} to 3.7×10^{-5}. The new JILA value and uncertainty (Parks and Faller, 2019) are labeled JILA-18 in Table XXIX and Fig. 9.

B. Measurements from the Huazhong University of Science and Technology

Two new determinations of G, using independent methods and having the lowest uncertainties to date, were reported in

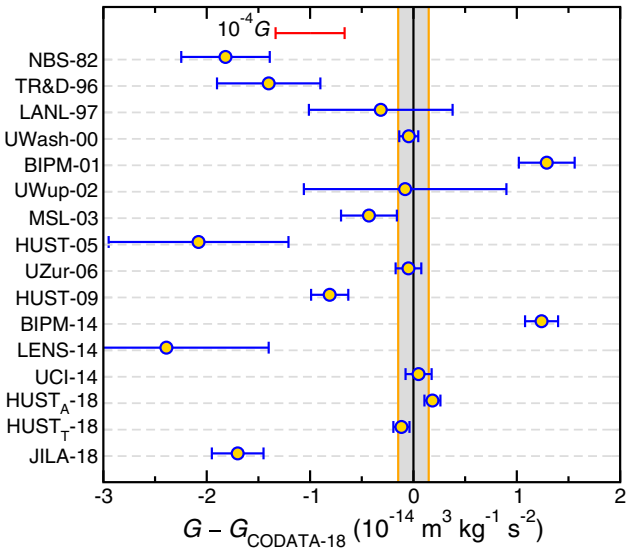


FIG. 9. The 16 input data determining the Newtonian constant of gravitation G ordered by publication year. The 2018 recommended value for G has been subtracted. Error bars correspond to one-standard-deviation uncertainties as reported in Table XXIX. The uncertainties after applying the 3.9 multiplicative expansion factor to determine the 2018 recommended value are not shown. Labels on the left side of the figure denote the laboratories and the last two digits of the year in which the data were reported. See Table XXIX for details. The gray band corresponds to the one-standard-deviation uncertainty of the recommended value.

2018. Both measurements were performed at Huazhong University of Science and Technology (HUST), Wuhan, People's Republic of China (Li *et al.*, 2018). The first determination used the time-of-swing (TOS) method where the change in oscillation frequency of a torsion pendulum for two different positions of source masses is measured. These measurements were performed on two independent apparatuses located in laboratories separated by 150 m. In one apparatus (TOS-I), the researchers used three different silica fibers to check for fiber-induced systematics. In the other apparatus (TOS-II), the same fiber was used for all measurements. The largest uncertainty component for all data sets was statistical, ranging from 10 to 30 parts in 10^6 relative uncertainty. The determination of the horizontal separation between the geometric centers of the spherical source masses had the largest systematic uncertainty; its relative uncertainty ranged from 8.5 to 9.5 parts in 10^6. In the CODATA adjustment, we only use the combined value for G from the two TOS apparatuses. This input datum is labeled $\mathrm{HUST_T}$-18 in Table XXIX and Fig. 9.

Small correlations with the 2009 TOS determination of G at HUST (Luo *et al.*, 2009) exist because the same source masses were used in TOS-II, and the same measurement instrumentation and methods for the determination of various systematic uncertainties were used. A conservative estimate for the correlation coefficient between HUST-09 and $\mathrm{HUST_T}$-18 is 0.068.

TABLE XXX. An abbreviated list of the CODATA recommended values of the fundamental constants of physics and chemistry based on the 2018 adjustment.

Quantity	Symbol	Value	Unit	Relative std. uncert. u_r
speed of light in vacuum	c	299 792 458	$\mathrm{m\,s^{-1}}$	exact
Newtonian constant of gravitation	G	$6.674\,30(15) \times 10^{-11}$	$\mathrm{m^3\,kg^{-1}\,s^{-2}}$	2.2×10^{-5}
Planck constant[a]	h	$6.626\,070\,15 \times 10^{-34}$	$\mathrm{J\,Hz^{-1}}$	exact
	$\hbar$	$1.054\,571\,817\ldots \times 10^{-34}$	J s	exact
elementary charge	e	$1.602\,176\,634 \times 10^{-19}$	C	exact
vacuum magnetic permeability $4\pi\alpha\hbar/e^2c$	μ_0	$1.256\,637\,062\,12(19) \times 10^{-6}$	$\mathrm{N\,A^{-2}}$	1.5×10^{-10}
vacuum electric permittivity $1/\mu_0c^2$	ϵ_0	$8.854\,187\,8128(13) \times 10^{-12}$	$\mathrm{F\,m^{-1}}$	1.5×10^{-10}
Josephson constant $2e/h$	K_J	$483\,597.848\,4\ldots \times 10^9$	$\mathrm{Hz\,V^{-1}}$	exact
von Klitzing constant $\mu_0c/2\alpha = 2\pi\hbar/e^2$	R_K	25 812.807 45…	Ω	exact
magnetic flux quantum $2\pi\hbar/(2e)$	Φ_0	$2.067\,833\,848\ldots \times 10^{-15}$	Wb	exact
conductance quantum $2e^2/2\pi\hbar$	G_0	$7.748\,091\,729\ldots \times 10^{-5}$	S	exact
electron mass	m_e	$9.109\,383\,7015(28) \times 10^{-31}$	kg	3.0×10^{-10}
proton mass	m_p	$1.672\,621\,923\,69(51) \times 10^{-27}$	kg	3.1×10^{-10}
proton-electron mass ratio	m_p/m_e	1836.152 673 43(11)		6.0×10^{-11}
fine-structure constant $e^2/4\pi\epsilon_0\hbar c$	α	$7.297\,352\,5693(11) \times 10^{-3}$		1.5×10^{-10}
inverse fine-structure constant	α^{-1}	137.035 999 084(21)		1.5×10^{-10}
Rydberg frequency $\alpha^2m_ec^2/2h$	cR_∞	$3.289\,841\,960\,2508(64) \times 10^{15}$	Hz	1.9×10^{-12}
Boltzmann constant	k	$1.380\,649 \times 10^{-23}$	$\mathrm{J\,K^{-1}}$	exact
Avogadro constant	N_A	$6.022\,140\,76 \times 10^{23}$	$\mathrm{mol^{-1}}$	exact
molar gas constant N_Ak	R	8.314 462 618…	$\mathrm{J\,mol^{-1}\,K^{-1}}$	exact
Faraday constant N_Ae	F	96 485.332 12…	$\mathrm{C\,mol^{-1}}$	exact
Stefan-Boltzmann constant $(\pi^2/60)k^4/\hbar^3c^2$	σ	$5.670\,374\,419\ldots \times 10^{-8}$	$\mathrm{W\,m^{-2}\,K^{-4}}$	exact
Non-SI units accepted for use with the SI				
electron volt $(e/\mathrm{C})\,\mathrm{J}$	eV	$1.602\,176\,634 \times 10^{-19}$	J	exact
(unified) atomic mass unit $\frac{1}{12}m(^{12}\mathrm{C})$	u	$1.660\,539\,066\,60(50) \times 10^{-27}$	kg	3.0×10^{-10}

[a]The energy of a photon with frequency ν expressed in unit Hz is $E = h\nu$ in unit J. Unitary time evolution of the state of this photon is given by $\exp(-iEt/\hbar)|\varphi\rangle$, where $|\varphi\rangle$ is the photon state at time $t = 0$ and time is expressed in unit s. The ratio $Et/\hbar$ is a phase.

TABLE XXXI. The CODATA recommended values of the fundamental constants of physics and chemistry based on the 2018 adjustment.

Quantity	Symbol	Numerical value	Unit	Relative std. uncert. u_r
		UNIVERSAL		
speed of light in vacuum	c	299 792 458	$\mathrm{m\,s^{-1}}$	exact
vacuum magnetic permeability $4\pi\alpha\hbar/e^2c$	μ_0	$1.256\,637\,062\,12(19)\times10^{-6}$	$\mathrm{N\,A^{-2}}$	1.5×10^{-10}
$\mu_0/(4\pi\times10^{-7})$		1.000 000 000 55(15)	$\mathrm{N\,A^{-2}}$	1.5×10^{-10}
vacuum electric permittivity $1/\mu_0c^2$	ϵ_0	$8.854\,187\,8128(13)\times10^{-12}$	$\mathrm{F\,m^{-1}}$	1.5×10^{-10}
characteristic impedance of vacuum μ_0c	Z_0	376.730 313 668(57)	Ω	1.5×10^{-10}
Newtonian constant of gravitation	G	$6.674\,30(15)\times10^{-11}$	$\mathrm{m^3\,kg^{-1}\,s^{-2}}$	2.2×10^{-5}
	$G/\hbar c$	$6.708\,83(15)\times10^{-39}$	$(\mathrm{GeV}/c^2)^{-2}$	2.2×10^{-5}
Planck constant[a]	h	$6.626\,070\,15\times10^{-34}$	$\mathrm{J\,Hz^{-1}}$	exact
		$4.135\,667\,696\ldots\times10^{-15}$	$\mathrm{eV\,Hz^{-1}}$	exact
	$\hbar$	$1.054\,571\,817\ldots\times10^{-34}$	J s	exact
		$6.582\,119\,569\ldots\times10^{-16}$	eV s	exact
	$\hbar c$	197.326 980 4…	MeV fm	exact
Planck mass $(\hbar c/G)^{1/2}$	m_P	$2.176\,434(24)\times10^{-8}$	kg	1.1×10^{-5}
energy equivalent	m_Pc^2	$1.220\,890(14)\times10^{19}$	GeV	1.1×10^{-5}
Planck temperature $(\hbar c^5/G)^{1/2}/k$	T_P	$1.416\,784(16)\times10^{32}$	K	1.1×10^{-5}
Planck length $\hbar/m_Pc=(\hbar G/c^3)^{1/2}$	l_P	$1.616\,255(18)\times10^{-35}$	m	1.1×10^{-5}
Planck time $l_P/c=(\hbar G/c^5)^{1/2}$	t_P	$5.391\,247(60)\times10^{-44}$	s	1.1×10^{-5}
		ELECTROMAGNETIC		
elementary charge	e	$1.602\,176\,634\times10^{-19}$	C	exact
	$e/\hbar$	$1.519\,267\,447\ldots\times10^{15}$	$\mathrm{A\,J^{-1}}$	exact
magnetic flux quantum $2\pi\hbar/(2e)$	Φ_0	$2.067\,833\,848\ldots\times10^{-15}$	Wb	exact
conductance quantum $2e^2/2\pi\hbar$	G_0	$7.748\,091\,729\ldots\times10^{-5}$	S	exact
inverse of conductance quantum	G_0^{-1}	12 906.403 72…	Ω	exact
Josephson constant $2e/h$	K_J	$483\,597.848\,4\ldots\times10^{9}$	$\mathrm{Hz\,V^{-1}}$	exact
von Klitzing constant $\mu_0c/2\alpha=2\pi\hbar/e^2$	R_K	25 812.807 45…	Ω	exact
Bohr magneton $e\hbar/2m_e$	μ_B	$9.274\,010\,0783(28)\times10^{-24}$	$\mathrm{J\,T^{-1}}$	3.0×10^{-10}
		$5.788\,381\,8060(17)\times10^{-5}$	$\mathrm{eV\,T^{-1}}$	3.0×10^{-10}
	μ_B/h	$1.399\,624\,493\,61(42)\times10^{10}$	$\mathrm{Hz\,T^{-1}}$	3.0×10^{-10}
	μ_B/hc	46.686 447 783(14)	$[\mathrm{m^{-1}T^{-1}}]$[b]	3.0×10^{-10}
	μ_B/k	0.671 713 815 63(20)	$\mathrm{K\,T^{-1}}$	3.0×10^{-10}
nuclear magneton $e\hbar/2m_p$	μ_N	$5.050\,783\,7461(15)\times10^{-27}$	$\mathrm{J\,T^{-1}}$	3.1×10^{-10}
		$3.152\,451\,258\,44(96)\times10^{-8}$	$\mathrm{eV\,T^{-1}}$	3.1×10^{-10}
	μ_N/h	7.622 593 2291(23)	$\mathrm{MHz\,T^{-1}}$	3.1×10^{-10}
	μ_N/hc	$2.542\,623\,413\,53(78)\times10^{-2}$	$[\mathrm{m^{-1}\,T^{-1}}]$[b]	3.1×10^{-10}
	μ_N/k	$3.658\,267\,7756(11)\times10^{-4}$	$\mathrm{K\,T^{-1}}$	3.1×10^{-10}
		ATOMIC AND NUCLEAR		
		General		
fine-structure constant $e^2/4\pi\epsilon_0\hbar c$	α	$7.297\,352\,5693(11)\times10^{-3}$		1.5×10^{-10}
inverse fine-structure constant	α^{-1}	137.035 999 084(21)		1.5×10^{-10}
Rydberg frequency $\alpha^2m_ec^2/2h=E_h/2h$	cR_∞	$3.289\,841\,960\,2508(64)\times10^{15}$	Hz	1.9×10^{-12}
energy equivalent	hcR_∞	$2.179\,872\,361\,1035(42)\times10^{-18}$	J	1.9×10^{-12}
		13.605 693 122 994(26)	eV	1.9×10^{-12}
Rydberg constant	R_∞	10 973 731.568 160(21)	$[\mathrm{m^{-1}}]$[b]	1.9×10^{-12}
Bohr radius $\hbar/\alpha m_ec=4\pi\epsilon_0\hbar^2/m_ee^2$	a_0	$5.291\,772\,109\,03(80)\times10^{-11}$	m	1.5×10^{-10}
Hartree energy $\alpha^2m_ec^2=e^2/4\pi\epsilon_0a_0=2hcR_\infty$	E_h	$4.359\,744\,722\,2071(85)\times10^{-18}$	J	1.9×10^{-12}
		27.211 386 245 988(53)	eV	1.9×10^{-12}
quantum of circulation	$\pi\hbar/m_e$	$3.636\,947\,5516(11)\times10^{-4}$	$\mathrm{m^2\,s^{-1}}$	3.0×10^{-10}
	$2\pi\hbar/m_e$	$7.273\,895\,1032(22)\times10^{-4}$	$\mathrm{m^2\,s^{-1}}$	3.0×10^{-10}
		Electroweak		
Fermi coupling constant[c]	$G_F/(\hbar c)^3$	$1.166\,3787(6)\times10^{-5}$	$\mathrm{GeV^{-2}}$	5.1×10^{-7}
weak mixing angle[d] θ_W (on-shell scheme)				
$\sin^2\theta_W=s_W^2\equiv1-(m_W/m_Z)^2$	$\sin^2\theta_W$	0.222 90(30)		1.3×10^{-3}
		Electron, e^-		
electron mass	m_e	$9.109\,383\,7015(28)\times10^{-31}$	kg	3.0×10^{-10}
		$5.485\,799\,090\,65(16)\times10^{-4}$	u	2.9×10^{-11}
energy equivalent	m_ec^2	$8.187\,105\,7769(25)\times10^{-14}$	J	3.0×10^{-10}
		0.510 998 950 00(15)	MeV	3.0×10^{-10}

(Table continued)

TABLE XXXI. *(Continued)*

Quantity	Symbol	Numerical value	Unit	Relative std. uncert. u_r
electron-muon mass ratio	m_e/m_μ	$4.836\,331\,69(11) \times 10^{-3}$		2.2×10^{-8}
electron-tau mass ratio	m_e/m_τ	$2.875\,85(19) \times 10^{-4}$		6.8×10^{-5}
electron-proton mass ratio	m_e/m_p	$5.446\,170\,214\,87(33) \times 10^{-4}$		6.0×10^{-11}
electron-neutron mass ratio	m_e/m_n	$5.438\,673\,4424(26) \times 10^{-4}$		4.8×10^{-10}
electron-deuteron mass ratio	m_e/m_d	$2.724\,437\,107\,462(96) \times 10^{-4}$		3.5×10^{-11}
electron-triton mass ratio	m_e/m_t	$1.819\,200\,062\,251(90) \times 10^{-4}$		5.0×10^{-11}
electron-helion mass ratio	m_e/m_h	$1.819\,543\,074\,573(79) \times 10^{-4}$		4.3×10^{-11}
electron to alpha particle mass ratio	m_e/m_α	$1.370\,933\,554\,787(45) \times 10^{-4}$		3.3×10^{-11}
electron charge-to-mass quotient	$-e/m_e$	$-1.758\,820\,010\,76(53) \times 10^{11}$	$\mathrm{C\,kg^{-1}}$	3.0×10^{-10}
electron molar mass $N_A m_e$	$M(e), M_e$	$5.485\,799\,0888(17) \times 10^{-7}$	$\mathrm{kg\,mol^{-1}}$	3.0×10^{-10}
reduced Compton wavelength $\hbar/m_e c = \alpha a_0$	$\lambda\!\!\!^{-}_C$	$3.861\,592\,6796(12) \times 10^{-13}$	m	3.0×10^{-10}
Compton wavelength	λ_C	$2.426\,310\,238\,67(73) \times 10^{-12}$	[m][b]	3.0×10^{-10}
classical electron radius $\alpha^2 a_0$	r_e	$2.817\,940\,3262(13) \times 10^{-15}$	m	4.5×10^{-10}
Thomson cross section $(8\pi/3)r_e^2$	σ_e	$6.652\,458\,7321(60) \times 10^{-29}$	$\mathrm{m^2}$	9.1×10^{-10}
electron magnetic moment	μ_e	$-9.284\,764\,7043(28) \times 10^{-24}$	$\mathrm{J\,T^{-1}}$	3.0×10^{-10}
to Bohr magneton ratio	μ_e/μ_B	$-1.001\,159\,652\,181\,28(18)$		1.7×10^{-13}
to nuclear magneton ratio	μ_e/μ_N	$-1838.281\,971\,88(11)$		6.0×10^{-11}
electron magnetic-moment anomaly $\lvert\mu_e\rvert/\mu_B - 1$	a_e	$1.159\,652\,181\,28(18) \times 10^{-3}$		1.5×10^{-10}
electron g-factor $-2(1 + a_e)$	g_e	$-2.002\,319\,304\,362\,56(35)$		1.7×10^{-13}
electron-muon magnetic-moment ratio	μ_e/μ_μ	206.766 9883(46)		2.2×10^{-8}
electron-proton magnetic-moment ratio	μ_e/μ_p	$-658.210\,687\,89(20)$		3.0×10^{-10}
electron to shielded proton magnetic-moment ratio (H_2O, sphere, 25 °C)	μ_e/μ'_p	$-658.227\,5971(72)$		1.1×10^{-8}
electron-neutron magnetic-moment ratio	μ_e/μ_n	960.920 50(23)		2.4×10^{-7}
electron-deuteron magnetic-moment ratio	μ_e/μ_d	$-2143.923\,4915(56)$		2.6×10^{-9}
electron to shielded helion magnetic-moment ratio (gas, sphere, 25 °C)	μ_e/μ'_h	864.058 257(10)		1.2×10^{-8}
electron gyromagnetic ratio $2\lvert\mu_e\rvert/\hbar$	γ_e	$1.760\,859\,630\,23(53) \times 10^{11}$	$\mathrm{s^{-1}\,T^{-1}}$	3.0×10^{-10}
		28 024.951 4242(85)	$\mathrm{MHz\,T^{-1}}$	3.0×10^{-10}
	Muon, μ^-			
muon mass	m_μ	$1.883\,531\,627(42) \times 10^{-28}$	kg	2.2×10^{-8}
		0.113 428 9259(25)	u	2.2×10^{-8}
energy equivalent	$m_\mu c^2$	$1.692\,833\,804(38) \times 10^{-11}$	J	2.2×10^{-8}
		105.658 3755(23)	MeV	2.2×10^{-8}
muon-electron mass ratio	m_μ/m_e	206.768 2830(46)		2.2×10^{-8}
muon-tau mass ratio	m_μ/m_τ	$5.946\,35(40) \times 10^{-2}$		6.8×10^{-5}
muon-proton mass ratio	m_μ/m_p	0.112 609 5264(25)		2.2×10^{-8}
muon-neutron mass ratio	m_μ/m_n	0.112 454 5170(25)		2.2×10^{-8}
muon molar mass $N_A m_\mu$	$M(\mu), M_\mu$	$1.134\,289\,259(25) \times 10^{-4}$	$\mathrm{kg\,mol^{-1}}$	2.2×10^{-8}
reduced muon Compton wavelength $\hbar/m_\mu c$	$\lambda\!\!\!^{-}_{C,\mu}$	$1.867\,594\,306(42) \times 10^{-15}$	m	2.2×10^{-8}
muon Compton wavelength	$\lambda_{C,\mu}$	$1.173\,444\,110(26) \times 10^{-14}$	[m][b]	2.2×10^{-8}
muon magnetic moment	μ_μ	$-4.490\,448\,30(10) \times 10^{-26}$	$\mathrm{J\,T^{-1}}$	2.2×10^{-8}
to Bohr magneton ratio	μ_μ/μ_B	$-4.841\,970\,47(11) \times 10^{-3}$		2.2×10^{-8}
to nuclear magneton ratio	μ_μ/μ_N	$-8.890\,597\,03(20)$		2.2×10^{-8}
muon magnetic-moment anomaly $\lvert\mu_\mu\rvert/(e\hbar/2m_\mu) - 1$	a_μ	$1.165\,920\,89(63) \times 10^{-3}$		5.4×10^{-7}
muon g-factor $-2(1 + a_\mu)$	g_μ	$-2.002\,331\,8418(13)$		6.3×10^{-10}
muon-proton magnetic-moment ratio	μ_μ/μ_p	$-3.183\,345\,142(71)$		2.2×10^{-8}
	Tau, τ^-			
tau mass[e]	m_τ	$3.167\,54(21) \times 10^{-27}$	kg	6.8×10^{-5}
		1.907 54(13)	u	6.8×10^{-5}
energy equivalent	$m_\tau c^2$	$2.846\,84(19) \times 10^{-10}$	J	6.8×10^{-5}
		1776.86(12)	MeV	6.8×10^{-5}
tau-electron mass ratio	m_τ/m_e	3477.23(23)		6.8×10^{-5}
tau-muon mass ratio	m_τ/m_μ	16.8170(11)		6.8×10^{-5}
tau-proton mass ratio	m_τ/m_p	1.893 76(13)		6.8×10^{-5}
tau-neutron mass ratio	m_τ/m_n	1.891 15(13)		6.8×10^{-5}
tau molar mass $N_A m_\tau$	$M(\tau), M_\tau$	$1.907\,54(13) \times 10^{-3}$	$\mathrm{kg\,mol^{-1}}$	6.8×10^{-5}

(Table continued)

TABLE XXXI. *(Continued)*

Quantity	Symbol	Numerical value	Unit	Relative std. uncert. u_r
reduced tau Compton wavelength $\hbar/m_\tau c$	$\lambda\!\!\!^{-}_{C,\tau}$	$1.110\,538(75) \times 10^{-16}$	m	6.8×10^{-5}
tau Compton wavelength	$\lambda_{C,\tau}$	$6.977\,71(47) \times 10^{-16}$	[m][b]	6.8×10^{-5}
	Proton, p			
proton mass	m_p	$1.672\,621\,923\,69(51) \times 10^{-27}$	kg	3.1×10^{-10}
		1.007 276 466 621(53)	u	5.3×10^{-11}
energy equivalent	$m_p c^2$	$1.503\,277\,615\,98(46) \times 10^{-10}$	J	3.1×10^{-10}
		938.272 088 16(29)	MeV	3.1×10^{-10}
proton-electron mass ratio	m_p/m_e	1836.152 673 43(11)		6.0×10^{-11}
proton-muon mass ratio	m_p/m_μ	8.880 243 37(20)		2.2×10^{-8}
proton-tau mass ratio	m_p/m_τ	0.528 051(36)		6.8×10^{-5}
proton-neutron mass ratio	m_p/m_n	0.998 623 478 12(49)		4.9×10^{-10}
proton charge-to-mass quotient	e/m_p	$9.578\,833\,1560(29) \times 10^{7}$	$C\,kg^{-1}$	3.1×10^{-10}
proton molar mass $N_A m_p$	$M(p)$, M_p	$1.007\,276\,466\,27(31) \times 10^{-3}$	$kg\,mol^{-1}$	3.1×10^{-10}
reduced proton Compton wavelength $\hbar/m_p c$	$\lambda\!\!\!^{-}_{C,p}$	$2.103\,089\,103\,36(64) \times 10^{-16}$	m	3.1×10^{-10}
proton Compton wavelength	$\lambda_{C,p}$	$1.321\,409\,855\,39(40) \times 10^{-15}$	[m][b]	3.1×10^{-10}
proton rms charge radius	r_p	$8.414(19) \times 10^{-16}$	m	2.2×10^{-3}
proton magnetic moment	μ_p	$1.410\,606\,797\,36(60) \times 10^{-26}$	$J\,T^{-1}$	4.2×10^{-10}
to Bohr magneton ratio	μ_p/μ_B	$1.521\,032\,202\,30(46) \times 10^{-3}$		3.0×10^{-10}
to nuclear magneton ratio	μ_p/μ_N	2.792 847 344 63(82)		2.9×10^{-10}
proton g-factor $2\mu_p/\mu_N$	g_p	5.585 694 6893(16)		2.9×10^{-10}
proton-neutron magnetic-moment ratio	μ_p/μ_n	−1.459 898 05(34)		2.4×10^{-7}
shielded proton magnetic-moment (H_2O, sphere, 25 °C)	μ'_p	$1.410\,570\,560(15) \times 10^{-26}$	$J\,T^{-1}$	1.1×10^{-8}
to Bohr magneton ratio	μ'_p/μ_B	$1.520\,993\,128(17) \times 10^{-3}$		1.1×10^{-8}
to nuclear magneton ratio	μ'_p/μ_N	2.792 775 599(30)		1.1×10^{-8}
proton magnetic shielding correction $1 - \mu'_p/\mu_p$ (H_2O, sphere, 25 °C)	σ'_p	$2.5689(11) \times 10^{-5}$		4.2×10^{-4}
proton gyromagnetic ratio $2\mu_p/\hbar$	γ_p	$2.675\,221\,8744(11) \times 10^{8}$	$s^{-1}\,T^{-1}$	4.2×10^{-10}
		42.577 478 518(18)	$MHz\,T^{-1}$	4.2×10^{-10}
shielded proton gyromagnetic ratio $2\mu'_p/\hbar$ (H_2O, sphere, 25 °C)	γ'_p	$2.675\,153\,151(29) \times 10^{8}$	$s^{-1}\,T^{-1}$	1.1×10^{-8}
		42.576 384 74(46)	$MHz\,T^{-1}$	1.1×10^{-8}
	Neutron, n			
neutron mass	m_n	$1.674\,927\,498\,04(95) \times 10^{-27}$	kg	5.7×10^{-10}
		1.008 664 915 95(49)	u	4.8×10^{-10}
energy equivalent	$m_n c^2$	$1.505\,349\,762\,87(86) \times 10^{-10}$	J	5.7×10^{-10}
		939.565 420 52(54)	MeV	5.7×10^{-10}
neutron-electron mass ratio	m_n/m_e	1838.683 661 73(89)		4.8×10^{-10}
neutron-muon mass ratio	m_n/m_μ	8.892 484 06(20)		2.2×10^{-8}
neutron-tau mass ratio	m_n/m_τ	0.528 779(36)		6.8×10^{-5}
neutron-proton mass ratio	m_n/m_p	1.001 378 419 31(49)		4.9×10^{-10}
neutron-proton mass difference	$m_n - m_p$	$2.305\,574\,35(82) \times 10^{-30}$	kg	3.5×10^{-7}
		$1.388\,449\,33(49) \times 10^{-3}$	u	3.5×10^{-7}
energy equivalent	$(m_n - m_p)c^2$	$2.072\,146\,89(74) \times 10^{-13}$	J	3.5×10^{-7}
		1.293 332 36(46)	MeV	3.5×10^{-7}
neutron molar mass $N_A m_n$	$M(n)$, M_n	$1.008\,664\,915\,60(57) \times 10^{-3}$	$kg\,mol^{-1}$	5.7×10^{-10}
reduced neutron Compton wavelength $\hbar/m_n c$	$\lambda\!\!\!^{-}_{C,n}$	$2.100\,194\,1552(12) \times 10^{-16}$	m	5.7×10^{-10}
neutron Compton wavelength	$\lambda_{C,n}$	$1.319\,590\,905\,81(75) \times 10^{-15}$	[m][b]	5.7×10^{-10}
neutron magnetic moment	μ_n	$-9.662\,3651(23) \times 10^{-27}$	$J\,T^{-1}$	2.4×10^{-7}
to Bohr magneton ratio	μ_n/μ_B	$-1.041\,875\,63(25) \times 10^{-3}$		2.4×10^{-7}
to nuclear magneton ratio	μ_n/μ_N	−1.913 042 73(45)		2.4×10^{-7}
neutron g-factor $2\mu_n/\mu_N$	g_n	−3.826 085 45(90)		2.4×10^{-7}
neutron-electron magnetic-moment ratio	μ_n/μ_e	$1.040\,668\,82(25) \times 10^{-3}$		2.4×10^{-7}
neutron-proton magnetic-moment ratio	μ_n/μ_p	−0.684 979 34(16)		2.4×10^{-7}
neutron to shielded proton magnetic-moment ratio (H_2O, sphere, 25 °C)	μ_n/μ'_p	−0.684 996 94(16)		2.4×10^{-7}
neutron gyromagnetic ratio $2\lvert\mu_n\rvert/\hbar$	γ_n	$1.832\,471\,71(43) \times 10^{8}$	$s^{-1}\,T^{-1}$	2.4×10^{-7}
		29.164 6931(69)	$MHz\,T^{-1}$	2.4×10^{-7}

(Table continued)

TABLE XXXI. *(Continued)*

Quantity	Symbol	Numerical value	Unit	Relative std. uncert. u_r
		Deuteron, d		
deuteron mass	m_d	$3.343\,583\,7724(10) \times 10^{-27}$	kg	3.0×10^{-10}
		2.013 553 212 745(40)	u	2.0×10^{-11}
energy equivalent	$m_d c^2$	$3.005\,063\,231\,02(91) \times 10^{-10}$	J	3.0×10^{-10}
		1875.612 942 57(57)	MeV	3.0×10^{-10}
deuteron-electron mass ratio	m_d/m_e	3670.482 967 88(13)		3.5×10^{-11}
deuteron-proton mass ratio	m_d/m_p	1.999 007 501 39(11)		5.6×10^{-11}
deuteron molar mass $N_A m_d$	$M(d), M_d$	$2.013\,553\,212\,05(61) \times 10^{-3}$	kg mol^{-1}	3.0×10^{-10}
deuteron rms charge radius	r_d	$2.127\,99(74) \times 10^{-15}$	m	3.5×10^{-4}
deuteron magnetic moment	μ_d	$4.330\,735\,094(11) \times 10^{-27}$	J T^{-1}	2.6×10^{-9}
to Bohr magneton ratio	μ_d/μ_B	$4.669\,754\,570(12) \times 10^{-4}$		2.6×10^{-9}
to nuclear magneton ratio	μ_d/μ_N	0.857 438 2338(22)		2.6×10^{-9}
deuteron g-factor μ_d/μ_N	g_d	0.857 438 2338(22)		2.6×10^{-9}
deuteron-electron magnetic-moment ratio	μ_d/μ_e	$-4.664\,345\,551(12) \times 10^{-4}$		2.6×10^{-9}
deuteron-proton magnetic-moment ratio	μ_d/μ_p	0.307 012 209 39(79)		2.6×10^{-9}
deuteron-neutron magnetic-moment ratio	μ_d/μ_n	−0.448 206 53(11)		2.4×10^{-7}
		Triton, t		
triton mass	m_t	$5.007\,356\,7446(15) \times 10^{-27}$	kg	3.0×10^{-10}
		3.015 500 716 21(12)	u	4.0×10^{-11}
energy equivalent	$m_t c^2$	$4.500\,387\,8060(14) \times 10^{-10}$	J	3.0×10^{-10}
		2808.921 132 98(85)	MeV	3.0×10^{-10}
triton-electron mass ratio	m_t/m_e	5496.921 535 73(27)		5.0×10^{-11}
triton-proton mass ratio	m_t/m_p	2.993 717 034 14(15)		5.0×10^{-11}
triton molar mass $N_A m_t$	$M(t), M_t$	$3.015\,500\,715\,17(92) \times 10^{-3}$	kg mol^{-1}	3.0×10^{-10}
triton magnetic moment	μ_t	$1.504\,609\,5202(30) \times 10^{-26}$	J T^{-1}	2.0×10^{-9}
to Bohr magneton ratio	μ_t/μ_B	$1.622\,393\,6651(32) \times 10^{-3}$		2.0×10^{-9}
to nuclear magneton ratio	μ_t/μ_N	2.978 962 4656(59)		2.0×10^{-9}
triton g-factor $2\mu_t/\mu_N$	g_t	5.957 924 931(12)		2.0×10^{-9}
		Helion, h		
helion mass	m_h	$5.006\,412\,7796(15) \times 10^{-27}$	kg	3.0×10^{-10}
		3.014 932 247 175(97)	u	3.2×10^{-11}
energy equivalent	$m_h c^2$	$4.499\,539\,4125(14) \times 10^{-10}$	J	3.0×10^{-10}
		2808.391 607 43(85)	MeV	3.0×10^{-10}
helion-electron mass ratio	m_h/m_e	5495.885 280 07(24)		4.3×10^{-11}
helion-proton mass ratio	m_h/m_p	2.993 152 671 67(13)		4.4×10^{-11}
helion molar mass $N_A m_h$	$M(h), M_h$	$3.014\,932\,246\,13(91) \times 10^{-3}$	kg mol^{-1}	3.0×10^{-10}
helion magnetic moment	μ_h	$-1.074\,617\,532(13) \times 10^{-26}$	J T^{-1}	1.2×10^{-8}
to Bohr magneton ratio	μ_h/μ_B	$-1.158\,740\,958(14) \times 10^{-3}$		1.2×10^{-8}
to nuclear magneton ratio	μ_h/μ_N	−2.127 625 307(25)		1.2×10^{-8}
helion g-factor $2\mu_h/\mu_N$	g_h	−4.255 250 615(50)		1.2×10^{-8}
shielded helion magnetic moment (gas, sphere, 25 °C)	μ'_h	$-1.074\,553\,090(13) \times 10^{-26}$	J T^{-1}	1.2×10^{-8}
to Bohr magneton ratio	μ'_h/μ_B	$-1.158\,671\,471(14) \times 10^{-3}$		1.2×10^{-8}
to nuclear magneton ratio	μ'_h/μ_N	−2.127 497 719(25)		1.2×10^{-8}
shielded helion to proton magnetic-moment ratio (gas, sphere, 25 °C)	μ'_h/μ_p	−0.761 766 5618(89)		1.2×10^{-8}
shielded helion to shielded proton magnetic-moment ratio (gas/H_2O, spheres, 25 °C)	μ'_h/μ'_p	−0.761 786 1313(33)		4.3×10^{-9}
shielded helion gyromagnetic ratio $2\lvert\mu'_h\rvert/\hbar$ (gas, sphere, 25 °C)	γ'_h	$2.037\,894\,569(24) \times 10^{8}$	s^{-1} T^{-1}	1.2×10^{-8}
		32.434 099 42(38)	MHz T^{-1}	1.2×10^{-8}
		Alpha particle, α		
alpha particle mass	m_α	$6.644\,657\,3357(20) \times 10^{-27}$	kg	3.0×10^{-10}
		4.001 506 179 127(63)	u	1.6×10^{-11}
energy equivalent	$m_\alpha c^2$	$5.971\,920\,1914(18) \times 10^{-10}$	J	3.0×10^{-10}
		3727.379 4066(11)	MeV	3.0×10^{-10}
alpha particle to electron mass ratio	m_α/m_e	7294.299 541 42(24)		3.3×10^{-11}

(Table continued)

TABLE XXXI. *(Continued)*

Quantity	Symbol	Numerical value	Unit	Relative std. uncert. u_r
alpha particle to proton mass ratio	m_α/m_p	3.972 599 690 09(22)		5.5×10^{-11}
alpha particle molar mass $N_A m_\alpha$	$M(\alpha), M_\alpha$	$4.001\,506\,1777(12) \times 10^{-3}$	kg mol^{-1}	3.0×10^{-10}
		PHYSICOCHEMICAL		
Avogadro constant	N_A	$6.022\,140\,76 \times 10^{23}$	mol^{-1}	exact
Boltzmann constant	k	$1.380\,649 \times 10^{-23}$	J K^{-1}	exact
		$8.617\,333\,262\ldots \times 10^{-5}$	eV K^{-1}	exact
	k/h	$2.083\,661\,912\ldots \times 10^{10}$	Hz K^{-1}	exact
	k/hc	69.503 480 04…	[m^{-1} K^{-1}][b]	exact
atomic mass constant[f] $m_u = \frac{1}{12} m(^{12}\mathrm{C}) = 2hcR_\infty/\alpha^2 c^2 A_r(\mathrm{e})$	m_u	$1.660\,539\,066\,60(50) \times 10^{-27}$	kg	3.0×10^{-10}
energy equivalent	$m_u c^2$	$1.492\,418\,085\,60(45) \times 10^{-10}$	J	3.0×10^{-10}
		931.494 102 42(28)	MeV	3.0×10^{-10}
molar mass constant[f]	M_u	$0.999\,999\,999\,65(30) \times 10^{-3}$	kg mol^{-1}	3.0×10^{-10}
molar mass[f] of carbon-12 $A_r(^{12}\mathrm{C})M_u$	$M(^{12}\mathrm{C})$	$11.999\,999\,9958(36) \times 10^{-3}$	kg mol^{-1}	3.0×10^{-10}
molar Planck constant	$N_A h$	$3.990\,312\,712\ldots \times 10^{-10}$	J Hz^{-1} mol^{-1}	exact
molar gas constant $N_A k$	R	8.314 462 618…	J mol^{-1} K^{-1}	exact
Faraday constant $N_A e$	F	96 485.332 12…	C mol^{-1}	exact
standard-state pressure		100 000	Pa	exact
standard atmosphere		101 325	Pa	exact
molar volume of ideal gas RT/p				
$T = 273.15$ K, $p = 100$ kPa	V_m	$22.710\,954\,64\ldots \times 10^{-3}$	m^3 mol^{-1}	exact
or standard-state pressure				
Loschmidt constant N_A/V_m	n_0	$2.651\,645\,804\ldots \times 10^{25}$	m^{-3}	exact
molar volume of ideal gas RT/p				
$T = 273.15$ K, $p = 101.325$ kPa	V_m	$22.413\,969\,54\ldots \times 10^{-3}$	m^{3}mol^{-1}	exact
or standard atmosphere				
Loschmidt constant N_A/V_m	n_0	$2.686\,780\,111\ldots \times 10^{25}$	m^{-3}	exact
Sackur-Tetrode (absolute entropy) constant[g] $\frac{5}{2} + \ln[(m_u k T_1/2\pi\hbar^2)^{3/2} k T_1/p_0]$				
$T_1 = 1$ K, $p_0 = 100$ kPa	S_0/R	−1.151 707 537 06(45)		3.9×10^{-10}
or standard-state pressure				
$T_1 = 1$ K, $p_0 = 101.325$ kPa		−1.164 870 523 58(45)		3.9×10^{-10}
or standard atmosphere				
Stefan-Boltzmann constant $(\pi^2/60)k^4/\hbar^3 c^2$	σ	$5.670\,374\,419\ldots \times 10^{-8}$	W m^{-2} K^{-4}	exact
first radiation constant for spectral radiance $2hc^2$ sr^{-1}	c_{1L}	$1.191\,042\,972\ldots \times 10^{-16}$	[W m^2 sr^{-1}][h]	exact
first radiation constant $2\pi hc^2 = \pi\,\mathrm{sr}\, c_{1L}$	c_1	$3.741\,771\,852\ldots \times 10^{-16}$	[W m^2][h]	exact
second radiation constant hc/k	c_2	$1.438\,776\,877\ldots \times 10^{-2}$	[m K][b]	exact
Wien displacement law constants				
$b = \lambda_{max} T = c_2/4.965\,114\,231\ldots$	b	$2.897\,771\,955\ldots \times 10^{-3}$	[m K][b]	exact
$b' = \nu_{max}/T = 2.821\,439\,372\ldots c/c_2$	b'	$5.878\,925\,757\ldots \times 10^{10}$	Hz K^{-1}	exact

[a]The energy of a photon with frequency ν expressed in unit Hz is $E = h\nu$ in unit J. Unitary time evolution of the state of this photon is given by $\exp(-iEt/\hbar)|\varphi\rangle$, where $|\varphi\rangle$ is the photon state at time $t = 0$ and time is expressed in unit s. The ratio $Et/\hbar$ is a phase.

[b]The full description of m^{-1} is cycles or periods per meter and that of m is meters per cycle (m/cycle). The scientific community is aware of the implied use of these units. It traces back to the conventions for phase and angle and the use of unit Hz versus cycles/s. No solution has been agreed upon.

[c]Value recommended by the Particle Data Group (Tanabashi *et al.*, 2018).

[d]Based on the ratio of the masses of the W and Z bosons m_W/m_Z recommended by the Particle Data Group (Tanabashi *et al.*, 2018). The value for $\sin^2\theta_W$ they recommend, which is based on a variant of the modified minimal subtraction ($\overline{\mathrm{MS}}$) scheme, is $\sin^2\hat{\theta}_W(M_Z) = 0.231\,22(4)$.

[e]This and other constants involving m_τ are based on $m_\tau c^2$ in MeV recommended by the Particle Data Group (Tanabashi *et al.*, 2018).

[f]The relative atomic mass $A_r(X)$ of particle X with mass $m(X)$ is defined by $A_r(X) = m(X)/m_u$, where $m_u = m(^{12}\mathrm{C})/12 = 1$ u is the atomic mass constant and u is the unified atomic mass unit. Moreover, the mass of particle X is $m(X) = A_r(X)$ u and the molar mass of X is $M(X) = A_r(X)M_u$, where $M_u = N_A$ u is the molar mass constant and N_A is the Avogadro constant.

[g]The entropy of an ideal monoatomic gas of relative atomic mass A_r is given by $S = S_0 + \frac{3}{2}R\ln A_r - R\ln(p/p_0) + \frac{5}{2}R\ln(T/\mathrm{K})$.

[h]The full description of m^2 is m^{-2} × (m/cycle)^4. See also the second footnote.

The second 2018 HUST experiment used the angular acceleration feedback (AAF) method where turntables rotate a torsion pendulum and source masses independently at nominally constant but opposite and different rotation rates. Feedback control compensates for gravitational torque acting on the rotating torsion pendulum such that the pendulum does not move with respect to its rotating frame. The difference in rotation rate of the source masses' and pendulum's turntables is held constant by a second feedback controller. For infinite feedback gain, the angular acceleration of the torsion pendulum's turntable is identical to the gravitational angular acceleration generated by the source masses and effects of environmental gravitational forces are minimized.

The final result for G based on AAF, here labeled $\mathrm{HUST_A}$-18, combines values from data sets AAF-I, AAF-II, and AAF-III. Set AAF-I had a different rotation rate from AAF-II and AAF-III. A different research team obtained data set AAF-III. For AAF-III, an improved pre-hanger fiber and additional Mu-metal shielding around the torsion pendulum were used as well. The largest uncertainty components for all data sets were the horizontal and vertical distance determinations between the geometric centers of the spherical source masses, with relative uncertainties of 9.0 and 5.8 parts in 10^6, respectively.

While the two HUST-18 results have the lowest uncertainty of any measurements of G to date and agree with the 2018 recommended value within two standard uncertainties of that value, the difference between the two new HUST values is 2.7 times the standard uncertainty of their difference. Furthermore, the $\mathrm{HUST_T}$-18 and $\mathrm{HUST_A}$-18 values of G exceed the HUST-09 value by about 3.5 and 5.1 times the standard uncertainty of their respective differences. Presently, there are no explanations for the inconsistencies.

XX. ELECTROWEAK QUANTITIES

There are a few cases in the 2018 adjustment, as in previous adjustments, where an inexact constant is used in the analysis of input data but not treated as an adjusted quantity, because the adjustment has a negligible effect on its value. Three such constants, used in the calculation of the theoretical expression for the electron magnetic-moment anomaly a_e, are the mass of the tau lepton m_τ, the Fermi coupling constant G_F, and sine squared of the weak mixing angle $\sin^2\theta_W$. These are electroweak quantities with values obtained from the most recent report of the Particle Data Group (Tanabashi *et al.*, 2018):

$$m_\tau c^2 = 1776.86(12)\ \mathrm{MeV} \quad [6.8\times10^{-5}], \tag{202}$$

$$\frac{G_F}{(\hbar c)^3} = 1.166\,3787(6)\times10^{-5}\ \mathrm{GeV}^{-2} \quad [5.1\times10^{-7}], \tag{203}$$

$$\sin^2\theta_W = 0.222\,90(30) \quad [1.3\times10^{-3}]. \tag{204}$$

We note that $\sin^2\theta_W = 1-(m_W/m_Z)^2$, where m_W and m_Z are the masses of the $W^\pm$ and Z^0 bosons, respectively. The Particle Data Group's value $m_W/m_Z = 0.881\,53(17)$ leads to

TABLE XXXII. The relative uncertainties and correlation coefficients of the values of a selected group of constants based on the 2018 CODATA adjustment. The numbers in bold on the diagonal are the relative uncertainties $u_r(x_i) = u(x_i)/x_i$; the other numbers are the correlation coefficients $r(x_i,x_j) = u(x_i,x_j)/[u(x_i)u(x_j)]$. Here, $u(x_i,x_j)$ is the covariance of x_i and x_j and $u^2(x_i) = u(x_i,x_i)$ is the variance.

	α	R_∞	m_e/m_p	r_p	r_d	m_e/m_μ	m_u
α	$\mathbf{1.5\times10^{-10}}$	0.002 07	−0.031 03	0.003 45	0.003 20	−0.013 45	−0.995 35
R_∞	0.002 07	$\mathbf{1.9\times10^{-12}}$	0.012 06	0.885 92	0.903 66	−0.000 11	0.003 69
m_e/m_p	−0.031 03	0.012 06	$\mathbf{6.0\times10^{-11}}$	−0.005 28	0.011 13	0.000 45	−0.015 54
r_p	0.003 45	0.885 92	−0.005 28	$\mathbf{2.2\times10^{-3}}$	0.991 65	−0.000 12	0.002 38
r_d	0.003 20	0.903 66	0.011 13	0.991 65	$\mathbf{3.5\times10^{-4}}$	−0.000 12	0.002 30
m_e/m_μ	−0.013 45	−0.000 11	0.000 45	−0.000 12	−0.000 12	$\mathbf{2.2\times10^{-8}}$	0.013 38
m_u	−0.995 35	0.003 69	−0.015 54	0.002 38	0.002 30	0.013 38	$\mathbf{3.0\times10^{-10}}$

TABLE XXXIII. Values of some x-ray-related quantities based on the 2018 CODATA adjustment of the constants.

Quantity	Symbol	Value	Unit	Relative std. uncert. u_r
Cu x unit: $\lambda(\mathrm{Cu\,K\alpha_1})/1537.400$	$\mathrm{xu(Cu\,K\alpha_1)}$	$1.002\,076\,97(28)\times10^{-13}$	m	2.8×10^{-7}
Mo x unit: $\lambda(\mathrm{Mo\,K\alpha_1})/707.831$	$\mathrm{xu(Mo\,K\alpha_1)}$	$1.002\,099\,52(53)\times10^{-13}$	m	5.3×10^{-7}
Ångström star: $\lambda(\mathrm{W\,K\alpha_1})/0.209\,010\,0$	Å*	$1.000\,014\,95(90)\times10^{-10}$	m	9.0×10^{-7}
Lattice parameter[a] of Si (in vacuum, 22.5 °C)	a	$5.431\,020\,511(89)\times10^{-10}$	m	1.6×10^{-8}
{220} lattice spacing of Si $a/\sqrt{8}$ (in vacuum, 22.5 °C)	d_{220}	$1.920\,155\,716(32)\times10^{-10}$	m	1.6×10^{-8}
Molar volume of Si $M(\mathrm{Si})/\rho(\mathrm{Si}) = N_A a^3/8$ (in vacuum, 22.5 °C)	$V_m(\mathrm{Si})$	$1.205\,883\,199(60)\times10^{-5}$	$\mathrm{m^3\,mol^{-1}}$	4.9×10^{-8}

[a]This is the lattice parameter (unit cell edge length) of an ideal single crystal of naturally occurring Si with natural isotopic Si abundances, free of impurities and imperfections.

the value of $\sin^2\theta_W$ already given. The uncertainty of this mass ratio has decreased by almost a factor of ten when compared to that in the 2014 adjustment. Finally, the accuracy of the mass of the tau lepton has slightly improved.

XXI. THE 2018 CODATA RECOMMENDED VALUES

The input data and their correlation coefficients considered in the 2018 CODATA adjustment of the values of the constants are given in Tables VIII, X, XVIII, XXI, XXVII, and XXIX. (Here, items C3–C6 in Table XVIII are additional theoretical coefficients and not input data.) The data have been discussed and explained in detail in the previous sections. The 2018 recommended values are calculated from the set of best estimated values, in the least-squares sense, of 75 adjusted constants listed in Tables XI and XIX. A comparison with the values of the adjusted constants in Tables XXV and XXVI of the 2014 CODATA adjustment shows that two prominent quantities among the few that are no longer adjusted constants are the Planck constant h and the molar gas constant R. The reason, of course, is that in the revised SI these constants are exactly known.

The methodology and quality of our least-squares adjustments has been discussed in Sec. III. Briefly, three independent adjustments have been performed. The first concerned the Newtonian constant of gravitation. The corresponding input data are found to be inconsistent and an expansion factor of 3.9 is needed to decrease the residuals to below two. The second independent adjustment concerned the determination of the natural-silicon lattice spacing and values of three historic x-ray units. No expansion factor is needed. Finally, the third adjustment determined the remaining 62 adjusted

TABLE XXXIV. Non-SI units based on the 2018 CODATA adjustment of the constants, although eV and u are accepted for use with the SI.

Quantity	Symbol	Value	Unit	Relative std. uncert. u_r
electron volt: (e/C) J	eV	$1.602\,176\,634 \times 10^{-19}$	J	exact
(unified) atomic mass unit: $\frac{1}{12}m(^{12}\mathrm{C})$	u	$1.660\,539\,066\,60(50) \times 10^{-27}$	kg	3.0×10^{-10}
		Natural units (n.u.)		
n.u. of velocity	c	299 792 458	$\mathrm{m\,s^{-1}}$	exact
n.u. of action	$\hbar$	$1.054\,571\,817\ldots \times 10^{-34}$	J s	exact
		$6.582\,119\,569\ldots \times 10^{-16}$	eV s	exact
	$\hbar c$	197.326 980 4…	MeV fm	exact
n.u. of mass	m_e	$9.109\,383\,7015(28) \times 10^{-31}$	kg	3.0×10^{-10}
n.u. of energy	$m_e c^2$	$8.187\,105\,7769(25) \times 10^{-14}$	J	3.0×10^{-10}
		0.510 998 950 00(15)	MeV	3.0×10^{-10}
n.u. of momentum	$m_e c$	$2.730\,924\,530\,75(82) \times 10^{-22}$	$\mathrm{kg\,m\,s^{-1}}$	3.0×10^{-10}
		0.510 998 950 00(15)	MeV/c	3.0×10^{-10}
n.u. of length: $\hbar/m_e c$	$\lambda\!\!\!^{-}_C$	$3.861\,592\,6796(12) \times 10^{-13}$	m	3.0×10^{-10}
n.u. of time	$\hbar/m_e c^2$	$1.288\,088\,668\,19(39) \times 10^{-21}$	s	3.0×10^{-10}
		Atomic units (a.u.)		
a.u. of charge	e	$1.602\,176\,634 \times 10^{-19}$	C	exact
a.u. of mass	m_e	$9.109\,383\,7015(28) \times 10^{-31}$	kg	3.0×10^{-10}
a.u. of action	$\hbar$	$1.054\,571\,817\ldots \times 10^{-34}$	J s	exact
a.u. of length: Bohr radius (bohr) $\hbar/\alpha m_e c$	a_0	$5.291\,772\,109\,03(80) \times 10^{-11}$	m	1.5×10^{-10}
a.u. of energy: Hartree energy (hartree) $\alpha^2 m_e c^2 = e^2/4\pi\epsilon_0 a_0 = 2hcR_\infty$	E_h	$4.359\,744\,722\,2071(85) \times 10^{-18}$	J	1.9×10^{-12}
a.u. of time	$\hbar/E_h$	$2.418\,884\,326\,5857(47) \times 10^{-17}$	s	1.9×10^{-12}
a.u. of force	E_h/a_0	$8.238\,723\,4983(12) \times 10^{-8}$	N	1.5×10^{-10}
a.u. of velocity: αc	$a_0 E_h/\hbar$	$2.187\,691\,263\,64(33) \times 10^{6}$	$\mathrm{m\,s^{-1}}$	1.5×10^{-10}
a.u. of momentum	$\hbar/a_0$	$1.992\,851\,914\,10(30) \times 10^{-24}$	$\mathrm{kg\,m\,s^{-1}}$	1.5×10^{-10}
a.u. of current	$eE_h/\hbar$	$6.623\,618\,237\,510(13) \times 10^{-3}$	A	1.9×10^{-12}
a.u. of charge density	e/a_0^3	$1.081\,202\,384\,57(49) \times 10^{12}$	$\mathrm{C\,m^{-3}}$	4.5×10^{-10}
a.u. of electric potential	E_h/e	27.211 386 245 988(53)	V	1.9×10^{-12}
a.u. of electric field	E_h/ea_0	$5.142\,206\,747\,63(78) \times 10^{11}$	$\mathrm{V\,m^{-1}}$	1.5×10^{-10}
a.u. of electric field gradient	E_h/ea_0^2	$9.717\,362\,4292(29) \times 10^{21}$	$\mathrm{V\,m^{-2}}$	3.0×10^{-10}
a.u. of electric dipole moment	ea_0	$8.478\,353\,6255(13) \times 10^{-30}$	C m	1.5×10^{-10}
a.u. of electric quadrupole moment	ea_0^2	$4.486\,551\,5246(14) \times 10^{-40}$	$\mathrm{C\,m^2}$	3.0×10^{-10}
a.u. of electric polarizability	$e^2a_0^2/E_h$	$1.648\,777\,274\,36(50) \times 10^{-41}$	$\mathrm{C^2\,m^2\,J^{-1}}$	3.0×10^{-10}
a.u. of 1st hyperpolarizability	$e^3a_0^3/E_h^2$	$3.206\,361\,3061(15) \times 10^{-53}$	$\mathrm{C^3\,m^3\,J^{-2}}$	4.5×10^{-10}
a.u. of 2nd hyperpolarizability	$e^4a_0^4/E_h^3$	$6.235\,379\,9905(38) \times 10^{-65}$	$\mathrm{C^4\,m^4\,J^{-3}}$	6.0×10^{-10}
a.u. of magnetic flux density	$\hbar/ea_0^2$	$2.350\,517\,567\,58(71) \times 10^{5}$	T	3.0×10^{-10}
a.u. of magnetic dipole moment: $2\mu_B$	$\hbar e/m_e$	$1.854\,802\,015\,66(56) \times 10^{-23}$	$\mathrm{J\,T^{-1}}$	3.0×10^{-10}
a.u. of magnetizability	$e^2a_0^2/m_e$	$7.891\,036\,6008(48) \times 10^{-29}$	$\mathrm{J\,T^{-2}}$	6.0×10^{-10}
a.u. of permittivity	e^2/a_0E_h	$1.112\,650\,055\,45(17) \times 10^{-10}$	$\mathrm{F\,m^{-1}}$	1.5×10^{-10}

TABLE XXXV. The values of some energy equivalents derived from the relations $E = mc^2 = hc/\lambda = h\nu = kT$ and based on the 2018 CODATA adjustment of the values of the constants; 1 eV $= (e/\mathrm{C})$ J, 1 u $= m_\mathrm{u} = \frac{1}{12}m(^{12}\mathrm{C})$, and $E_\mathrm{h} = 2hcR_\infty = \alpha^2 m_\mathrm{e} c^2$ is the Hartree energy (hartree).

	Relevant unit			
	J	kg	$[\mathrm{m}^{-1}]$[a]	Hz
1 J	$(1\ \mathrm{J}) =$ 1 J	$(1\ \mathrm{J})/c^2 =$ $1.112\,650\,056\ldots \times 10^{-17}$ kg	$(1\ \mathrm{J})/hc =$ $5.034\,116\,567\ldots \times 10^{24}$ m^{-1}	$(1\ \mathrm{J})/h =$ $1.509\,190\,179\ldots \times 10^{33}$ Hz
1 kg	$(1\ \mathrm{kg})c^2 =$ $8.987\,551\,787\ldots \times 10^{16}$ J	$(1\ \mathrm{kg}) =$ 1 kg	$(1\ \mathrm{kg})c/h =$ $4.524\,438\,335\ldots \times 10^{41}$ m^{-1}	$(1\ \mathrm{kg})c^2/h =$ $1.356\,392\,489\ldots \times 10^{50}$ Hz
1 $[\mathrm{m}^{-1}]$[a]	$(1\ \mathrm{m}^{-1})hc =$ $1.986\,445\,857\ldots \times 10^{-25}$ J	$(1\ \mathrm{m}^{-1})h/c =$ $2.210\,219\,094\ldots \times 10^{-42}$ kg	$(1\ \mathrm{m}^{-1}) =$ 1 m^{-1}	$(1\ \mathrm{m}^{-1})c =$ 299 792 458 Hz
1 Hz	$(1\ \mathrm{Hz})h =$ $6.626\,070\,15 \times 10^{-34}$ J	$(1\ \mathrm{Hz})h/c^2 =$ $7.372\,497\,323\ldots \times 10^{-51}$ kg	$(1\ \mathrm{Hz})/c =$ $3.335\,640\,951\ldots \times 10^{-9}$ m^{-1}	$(1\ \mathrm{Hz}) =$ 1 Hz
1 K	$(1\ \mathrm{K})k =$ $1.380\,649 \times 10^{-23}$ J	$(1\ \mathrm{K})k/c^2 =$ $1.536\,179\,187\ldots \times 10^{-40}$ kg	$(1\ \mathrm{K})k/hc =$ 69.503 480 04...m^{-1}	$(1\ \mathrm{K})k/h =$ $2.083\,661\,912\ldots \times 10^{10}$ Hz
1 eV	$(1\ \mathrm{eV}) =$ $1.602\,176\,634 \times 10^{-19}$ J	$(1\ \mathrm{eV})/c^2 =$ $1.782\,661\,921\ldots \times 10^{-36}$ kg	$(1\ \mathrm{eV})/hc =$ $8.065\,543\,937\ldots \times 10^{5}$ m^{-1}	$(1\ \mathrm{eV})/h =$ $2.417\,989\,242\ldots \times 10^{14}$ Hz
1 u	$(1\ \mathrm{u})c^2 =$ $1.492\,418\,085\,60(45) \times 10^{-10}$ J	$(1\ \mathrm{u}) =$ $1.660\,539\,066\,60(50) \times 10^{-27}$ kg	$(1\ \mathrm{u})c/h =$ $7.513\,006\,6104(23) \times 10^{14}$ m^{-1}	$(1\ \mathrm{u})c^2/h =$ $2.252\,342\,718\,71(68) \times 10^{23}$ Hz
1 E_h	$(1\ E_\mathrm{h}) =$ $4.359\,744\,722\,2071(85) \times 10^{-18}$ J	$(1\ E_\mathrm{h})/c^2 =$ $4.850\,870\,209\,5432(94) \times 10^{-35}$ kg	$(1\ E_\mathrm{h})/hc =$ $2.194\,746\,313\,6320(43) \times 10^{7}$ m^{-1}	$(1\ E_\mathrm{h})/h =$ $6.579\,683\,920\,502(13) \times 10^{15}$ Hz

[a]The full description of m^{-1} is cycles or periods per meter.

TABLE XXXVI. The values of some energy equivalents derived from the relations $E = mc^2 = \hbar c/\lambda = h\nu = kT$ and based on the 2018 CODATA adjustment of the values of the constants; 1 eV $= (e/\mathrm{C})$ J, 1 u $= m_\mathrm{u} = \frac{1}{12}m(^{12}\mathrm{C})$, and $E_\mathrm{h} = 2hcR_\infty = \alpha^2 m_\mathrm{e} c^2$ is the Hartree energy (hartree).

	Relevant unit			
	K	V	u	E_h
1 J	$(1\ \mathrm{J})/k =$ $7.242\,970\,516\ldots \times 10^{22}$ K	$(1\ \mathrm{J}) =$ $6.241\,509\,074\ldots \times 10^{18}$ eV	$(1\ \mathrm{J})/c^2 =$ $6.700\,535\,2565(20) \times 10^{9}$ u	$(1\ \mathrm{J}) =$ $2.293\,712\,278\,3963(45) \times 10^{17}\ E_\mathrm{h}$
1 kg	$(1\ \mathrm{kg})c^2/k =$ $6.509\,657\,260\ldots \times 10^{39}$ K	$(1\ \mathrm{kg})c^2 =$ $5.609\,588\,603\ldots \times 10^{35}$ eV	$(1\ \mathrm{kg}) =$ $6.022\,140\,7621(18) \times 10^{26}$ u	$(1\ \mathrm{kg})c^2 =$ $2.061\,485\,788\,7409(40) \times 10^{34}\ E_\mathrm{h}$
1 $[\mathrm{m}^{-1}]$[a]	$(1\ \mathrm{m}^{-1})hc/k =$ $1.438\,776\,877\ldots \times 10^{-2}$ K	$(1\ \mathrm{m}^{-1})hc =$ $1.239\,841\,984\ldots \times 10^{-6}$ eV	$(1\ \mathrm{m}^{-1})h/c =$ $1.331\,025\,050\,10(40) \times 10^{-15}$ u	$(1\ \mathrm{m}^{-1})hc =$ $4.556\,335\,252\,9120(88) \times 10^{-8}\ E_\mathrm{h}$
1 Hz	$(1\ \mathrm{Hz})h/k =$ $4.799\,243\,073\ldots \times 10^{-11}$ K	$(1\ \mathrm{Hz})h =$ $4.135\,667\,696\ldots \times 10^{-15}$ eV	$(1\ \mathrm{Hz})h/c^2 =$ $4.439\,821\,6652(13) \times 10^{-24}$ u	$(1\ \mathrm{Hz})h =$ $1.519\,829\,846\,0570(29) \times 10^{-16}\ E_\mathrm{h}$
1 K	$(1\ \mathrm{K}) =$ 1 K	$(1\ \mathrm{K})k =$ $8.617\,333\,262\ldots \times 10^{-5}$ eV	$(1\ \mathrm{K})k/c^2 =$ $9.251\,087\,3014(28) \times 10^{-14}$ u	$(1\ \mathrm{K})k =$ $3.166\,811\,563\,4556(61) \times 10^{-6}\ E_\mathrm{h}$
1 eV	$(1\ \mathrm{eV})/k =$ $1.160\,451\,812\ldots \times 10^{4}$ K	$(1\ \mathrm{eV}) =$ 1 eV	$(1\ \mathrm{eV})/c^2 =$ $1.073\,544\,102\,33(32) \times 10^{-9}$ u	$(1\ \mathrm{eV}) =$ $3.674\,932\,217\,5655(71) \times 10^{-2}\ E_\mathrm{h}$
1 u	$(1\ \mathrm{u})c^2/k =$ $1.080\,954\,019\,16(33) \times 10^{13}$ K	$(1\ \mathrm{u})c^2 =$ $9.314\,941\,0242(28) \times 10^{8}$ eV	$(1\ \mathrm{u}) =$ 1 u	$(1\ \mathrm{u})c^2 =$ $3.423\,177\,6874(10) \times 10^{7}\ E_\mathrm{h}$
1 E_h	$(1\ E_\mathrm{h})/k =$ $3.157\,750\,248\,0407(61) \times 10^{5}$ K	$(1\ E_\mathrm{h}) =$ $27.211\,386\,245\,988(53)$ eV	$(1\ E_\mathrm{h})/c^2 =$ $2.921\,262\,322\,05(88) \times 10^{-8}$ u	$(1\ E_\mathrm{h}) =$ 1 E_h

[a]The full description of m^{-1} is cycles or periods per meter.

constants. Two expansion factors are required. A factor of 1.6 is applied to the 60 input data determining the Rydberg constant and proton and deuteron charge radii. A factor of 1.7 is used for the two input data that determine the mass of the proton. As in previous adjustments, we have not excluded input data that individually contribute little to constrain the adjusted constants but taken together do matter. Good examples of such data are transition energies in atomic hydrogen to states with large principal quantum numbers as well as the less-accurate experimental data on the Newtonian constant of gravitation.

A. Tables of values

Tables XXX through XXXVI give the 2018 CODATA recommended values of the basic constants and conversion factors of physics and chemistry and related quantities. Energy conversion factors in Tables XXXV and XXXVI relate energies, masses, photon wavelengths and frequencies, and temperatures of ensembles of particles through the equivalences $E = mc^2 = hc/\lambda = h\nu = kT$. The tables are identical in form and content to their 2010 and 2014 counterparts in that no constants are added or deleted. They also show the profound impact the revised SI has on the values of the fundamental constants. Counting the energy conversion factors in Tables XXXV and XXXVI, 46 constants that had uncertainties in 2014 are now exactly known in the revised SI. Values of the constants and correlation coefficients between any pair of constants can also be found at the website http://physics.nist.gov/constants.

XXII. SUMMARY AND CONCLUSION

In this final section, we discuss (i) the differences between the 2014 and 2018 CODATA recommended values of the constants, (ii) the implications of the 2018 adjustment for metrology and physics, and (iii) future work that could improve our knowledge of the values of the constants.

A. Comparison of 2014 and 2018 CODATA recommended values

A representative group of 2014 and 2018 recommended values are compared in Fig. 10. The first four constants h, e, k, and N_A are exact because of the redefinition of the SI. All other constants were and are inexactly known. Some have become significantly more accurate, some have updated values that fall well outside their 2014 uncertainty, while others have seen no significant change. Changes are a consequence of the revision of the SI and measurements that have become available since the 2014 adjustment. We discuss the changes shown in the figure as well as other notable changes in some detail later.

Not included in Fig. 10 are those few constants that were exactly known before the adoption of the revised SI in 2018. These are the universal constants μ_0, ϵ_0, and Z_0, as well as the physicochemical constants $M(^{12}\mathrm{C})$ and M_u. Their current differences from their previous exact values may be conveniently expressed in the form $\mu_0/(4\pi \times 10^{-7}\ \mathrm{N\,A^{-2}}) = 1 + 55(15) \times 10^{-11}$ and $M(^{12}\mathrm{C})/(0.012\ \mathrm{kg\,mol^{-1}}) = 1 - 35(30) \times 10^{-11}$, where the numbers in parentheses are their 2018 standard uncertainties. [The number $+55(15)$ is the same for $Z_0 = \mu_0 c$ but is $-55(15)$ for $\epsilon_0 = 1/\mu_0 c^2$; the number $-35(30)$ is the same for M_u.] The mass of the international prototype of the kilogram $m(\mathcal{K})$ and the temperature at the triple point of water T_{TPW} were also exactly known before the adoption of the revised SI, but they are not adjusted constants in the 2018 adjustment.

In the revised SI, h, e, k, and N_A are defining constants with exact values and the values of the previously exactly known SI defining constants μ_0, $M(^{12}\mathrm{C})$, $m(\mathcal{K})$, and T_{TPW} must now be determined experimentally. The exact values of h, e, k, and N_A are based on the results of the 2017 CODATA Special Adjustment carried out by the Task Group at the request of the General Conference on Weights and Measures (CGPM) with a closing date for data of 1 July 2017 (Mohr *et al.*, 2018; Newell *et al.*, 2018). Based on the input data available then, the exact values for h, e, k, and N_A had to fall within the one-standard-deviation uncertainty of their then inexact values. The precise criteria can be found in CIPM (2016, 2017). Conversely, the criteria implied that the values and uncertainties of the newly imprecise μ_0 and $M(^{12}\mathrm{C})$ were consistent with their previously exact values.

After the 1 July 2017 closing date of the 2017 CODATA Special Adjustment, a measurement of $h/m(^{133}\mathrm{Cs})$ (item D4 in Table XXI) further constrained the value of the fine-structure constant α. This additional input datum has led to a larger deviation of $\mu_0 = 4\pi\alpha\hbar/e^2c$ and $M(^{12}\mathrm{C})$ from their previous exact values.

The significantly reduced uncertainties of R_∞, r_p, and r_d and shifts of the values compared with their 2014 counterparts are due to improvements in theory, new measurements of hydrogen transition frequencies, and the inclusion of Lamb-shift measurements in muonic hydrogen and deuterium. The latter were not included in the 2014 CODATA adjustment because of inconsistencies between the values of r_p and r_d derived from them and those obtained from hydrogen and deuterium spectroscopic data and e-p and e-d scattering data. Nevertheless, it must be recognized that although including the muonic hydrogen and deuterium data as well as new hydrogen spectroscopic data have led to values of R_∞, r_p, and r_d with significantly smaller uncertainties, the remaining inconsistencies among the 62 data primarily responsible for the determination of these constants required their uncertainties to be increased by the multiplicative factor 1.6 to reduce all normalized residuals to less than 2.

The relative uncertainty $u_r(E_h)$ of the Hartree energy $E_h = 2R_\infty hc$ is now simply that due to the Rydberg constant rather than that of the Planck constant as was the case in the 2014 CODATA adjustment. The uncertainty of the Hartree energy is now 6300 times smaller.

The reduction of the uncertainty of α by a factor of 1.5 to $u_r(\alpha) = 1.5 \times 10^{-10}$ is mainly due to the measurement of $h/m(^{133}\mathrm{Cs})$. The uncertainties of many other constants are directly linked to that of α. Examples are, of course, μ_0, but also the Bohr radius a_0, electron mass m_e, Compton wavelength λ_C, and Thomson cross section σ_e. Their relative uncertainties are 1, 1, 2, 2, and 6 times that of α, respectively. The latter four constants also depend on the Rydberg constant

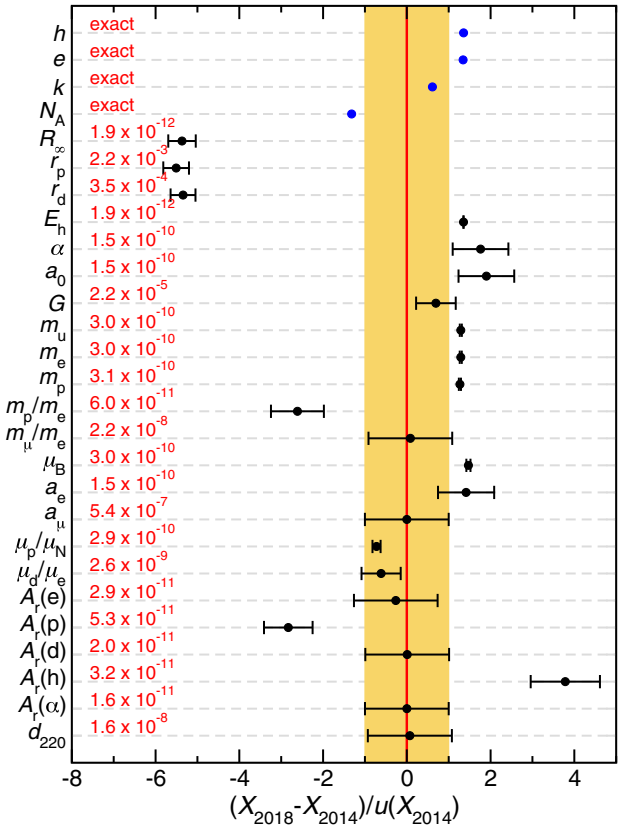


FIG. 10. Comparison of a representative group of fundamental constants from the 2014 and 2018 CODATA adjustments. Symbols of constants are shown along the y axis. Along the x axis the 2018 recommended values and their one-standard-deviation uncertainty, black circles with error bars, are shown as the difference between the 2018 and 2014 values divided by the standard uncertainty of the 2014 value. The vertical solid red line at the origin and yellow/orange band of width 1 represent the 2014 values and standard uncertainties of the indicated constants. The numerical values near the left-hand side of the figure are the relative standard uncertainties from the 2018 adjustment.

R_∞, but its relative uncertainty of 1.9×10^{-12} is much smaller than that of α.

The reduction in the uncertainty of G is due to two new and independent results from HUST in the People's Republic of China, both with $u_r(G) = 1.2 \times 10^{-5}$ ($\mathrm{HUST_T}$-18 and $\mathrm{HUST_A}$-18 in Table XXIX); and a correction of a previously available result (JILA-18 in Table XXIX). This led to a better consistency among the 16 input data for G and a reduction of the applied expansion factor of their uncertainties from 6.3 in 2014 to 3.9 in the current CODATA adjustment.

The relations $1\ \mathrm{u} = m_\mathrm{u} = m(^{12}\mathrm{C})/12$ for the atomic mass unit and $A_r(^{12}\mathrm{C}) = 12$ for the relative atomic mass of $^{12}\mathrm{C}$ remain exact in the revised SI. The mass m_u in kg, however, is now obtained from $m_\mathrm{u} = 2R_\infty h/A_r(\mathrm{e})c\alpha^2$ instead of $m_\mathrm{u} = (10^{-3}\ \mathrm{kg/mol})/N_\mathrm{A}$. Consequently, the relative uncertainty of m_u in the 2018 adjustment is essentially twice that of α or 3.0×10^{-10}, because $u_r(R_\infty)$ and $u_r(A_r(\mathrm{e}))$ are significantly smaller than $u_r(\alpha)$. This relative uncertainty of m_u is 41 times smaller than in the 2014 adjustment, where it was dominated by the relative uncertainty of N_A.

Generally, the mass of a particle X in kg is most reliably determined from $m(X) = A_r(X)m_\mathrm{u}$, where the relative uncertainty of $A_r(X)$ for most particles of interest here is significantly smaller than that of m_u. Hence the u_r of m_e, m_p, m_d, m_t, m_h, and m_α when expressed in kg are now essentially the same as that of m_u.

The significant reductions of the uncertainties of magnetic moments μ_B, μ_N, and μ_e can be understood from their definitions. The Bohr magneton $\mu_\mathrm{B} = e\hbar/2m_\mathrm{e}$ now has the relative uncertainty of that of the electron mass. By comparison, in the 2014 CODATA adjustment u_r of μ_B is 6.3×10^{-9} or 20 times larger. Similarly, the nuclear magneton $\mu_\mathrm{N} = e\hbar/2m_\mathrm{p}$ has the relative uncertainty of that of m_p or m_u. Because the ratio $\mu_\mathrm{e}/\mu_\mathrm{B} = g_\mathrm{e}/2$ and the u_r of the 2018 and 2014 CODATA recommended values of the electron g-factor g_e are 1.7×10^{-13} and 2.6×10^{-13}, respectively, the relative uncertainty of μ_e is essentially the same as that for μ_B.

The value of the magnetic moment of the proton μ_p has been improved due to a new measurement of the ratio $\mu_\mathrm{p}/\mu_\mathrm{N}$. For this measurement, $u_r = 2.9 \times 10^{-10}$. Together with the improved value of μ_N, it provides a value of μ_p with $u_r = 4.2 \times 10^{-10}$. Similarly, the uncertainty $\mu_\mathrm{p}/\mu_\mathrm{B}$ has seen a tenfold improvement, as $\mu_\mathrm{p}/\mu_\mathrm{B} = \mu_\mathrm{p}/\mu_\mathrm{N} \times m_\mathrm{e}/m_\mathrm{p}$ and $m_\mathrm{e}/m_\mathrm{p}$ has a relative uncertainty of 6.0×10^{-11}.

The input data that determine the 2018 CODATA recommended value of $A_r(\mathrm{p})$ are the 2016 AMDC value of $A_r(^1\mathrm{H})$ and the cyclotron frequency ratio $\omega_c(^{12}\mathrm{C}^{6+})/\omega_c(\mathrm{p})$ (item D15 in Table XXI). The two values for $A_r(\mathrm{p})$ from these data disagree, and an expansion factor of 1.7 is applied to their uncertainties to bring them into agreement.

The comparatively large difference between the 2018 and 2014 values of the helion relative atomic mass, $A_r(\mathrm{h})$, is due to the inclusion of a new value of the cyclotron frequency ratio $\omega_c(\mathrm{HD}^+)/\omega_c(^3\mathrm{He}^+)$ (item D17 in Table XXI) and omission of the cyclotron frequency ratio $\omega_c(\mathrm{h})/\omega_c(^{12}\mathrm{C}^{6+})$ used in 2014, because of concerns about its reliability. The relative atomic mass of the triton has changed based on a 2015 measurement (item D16 in Table XXI). No new datum has become available to determine $A_r(\mathrm{e})$, $A_r(\mathrm{d})$, and $A_r(\alpha)$.

The magnetic moment of the neutron μ_n and ratios $\mu_\mathrm{n}/\mu_\mathrm{N}$ and $\mu_\mathrm{n}/\mu_\mathrm{p}$ are determined from the same input datum, namely, $\mu_\mathrm{n}/\mu'_\mathrm{p}$ with $u_r = 2.4 \times 10^{-7}$ obtained in 1979 (item D37 in Table XXI). The 2018 values and uncertainties of these three quantities are essentially the same as in the 2014 adjustment. The magnetic moment of the deuteron μ_d and ratios $\mu_\mathrm{d}/\mu_\mathrm{N}$ and $\mu_\mathrm{d}/\mu_\mathrm{e}$ have a u_r of 2.6×10^{-9}, which is about one-half that of their 2014 u_r. The reason is the presence of an additional input datum for the ratio $\mu_\mathrm{p}(\mathrm{HD})/\mu_\mathrm{d}(\mathrm{HD})$ with $u_r = 3.1 \times 10^{-9}$.

One of the consequences of the revised SI is that the conversion factors among the energy units J, kg, m^{-1}, Hz, K, and eV are now exact based on $E = mc^2 = \hbar c/\lambda = h\nu = kT$. The conversion factor between these six units and the unified atomic mass unit, $1\ \mathrm{u} = m_\mathrm{u}$, is determined by m_u and exact constants. Hence, the relative uncertainties of the six corresponding conversion factors are now that of m_u or 3.0×10^{-10}. This corresponds to a significant improvement compared to the 2014 recommended conversion factor. For example, the

uncertainty of the eV-to-u conversion factor is reduced by a factor of 20.

The situation is similar for the conversion factors from the six energy units to the Hartree energy $E_h = 2R_\infty hc$, but in this case the relevant constant is R_∞ with $u_r = 1.9 \times 10^{-12}$ rather than m_u. As another example, the uncertainty of the K-to-E_h conversion factor is reduced from 5.7×10^{-7} in 2014 to 1.9×10^{-12} in 2018, or by a factor of 3×10^5.

B. Implications of the 2018 adjustment for metrology and physics

1. Electrical metrology

The most significant practical impact of the revised SI is undoubtedly the elimination of the conventional 1990 electrical units that went into effect on 1 January 1990 to ensure the international consistency of electrical measurements. (See https://www.bipm.org/en/publications/si-brochure.) After thirty years, electrical measurements are once more consistent with measurements made in the other units of the SI.

Electrical units have become part of the SI again, simply because the Josephson and von Klitzing constants are now exact in SI units. Between 1990 and the adoption of the revised SI in 2019, the units of voltage and resistance, V_{90} and Ω_{90}, were based on the conventional values $K_{J-90} = 483\,597.9$ GHz/V and $R_{K-90} = 25\,812.807\ \Omega$ for the Josephson and von Klitzing constants, respectively. From 2019 onward, the ratios between $K_J = 2e/h$ and K_{J-90} and between $R_K = h/e^2$ and R_{K-90} are exact. Thus, $1\ V_{90} = (K_{J-90}/K_J)$ V and $1\ \Omega_{90} = (R_K/R_{K-90})\ \Omega$ exactly. Consequently, the conventional electric units for voltage, resistance, current, charge, power, capacitance, inductance, electrical conductance, magnetic flux, and magnetic flux density in terms of the corresponding SI units are

$$1\ V_{90} = \frac{K_{J-90}}{K_J}\mathrm{V} = [1 + 10.666\ldots \times 10^{-8}]\ \mathrm{V},$$

$$1\ \Omega_{90} = \frac{R_K}{R_{K-90}}\Omega = [1 + 1.7793\ldots \times 10^{-8}]\ \Omega,$$

$$1\ A_{90} = \frac{K_{J-90}R_{K-90}}{K_J R_K}\mathrm{A} = [1 + 8.8871\ldots \times 10^{-8}]\ \mathrm{A},$$

$$1\ C_{90} = \frac{K_{J-90}R_{K-90}}{K_J R_K}\mathrm{C} = [1 + 8.8871\ldots \times 10^{-8}]\ \mathrm{C},$$

$$1\ W_{90} = \frac{K_{J-90}^2 R_{K-90}}{K_J^2 R_K}\mathrm{W} = [1 + 19.553\ldots \times 10^{-8}]\ \mathrm{W},$$

$$1\ F_{90} = \frac{R_{K-90}}{R_K}\mathrm{F} = [1 - 1.7793\ldots \times 10^{-8}]\ \mathrm{F},$$

$$1\ H_{90} = \frac{R_K}{R_{K-90}}\mathrm{H} = [1 + 1.7793\ldots \times 10^{-8}]\ \mathrm{H},$$

$$1\ S_{90} = \frac{R_{K-90}}{R_K}\mathrm{S} = [1 - 1.7793\ldots \times 10^{-8}]\ \mathrm{S},$$

$$1\ Wb_{90} = \frac{K_{J-90}}{K_J}\mathrm{Wb} = [1 + 10.666\ldots \times 10^{-8}]\ \mathrm{Wb},$$

$$1\ T_{90} = \frac{K_{J-90}}{K_J}\mathrm{T} = [1 + 10.666\ldots \times 10^{-8}]\ \mathrm{T}.$$

Thus, for example, the 1990 conventional unit of voltage V_{90} exceeds the SI unit of voltage V by the fractional amount $10.666\ldots \times 10^{-8}$. This implies that a voltage measured in the unit V_{90} will have a numerical value that is smaller by this fractional amount than the numerical value of the same voltage measured in the SI volt V. (The 1990 conventional units are viewed as physical quantities and, hence, their symbols are written in italic type.)

2. Electron magnetic-moment anomaly, fine-structure constant, and QED theory

The electron magnetic-moment anomaly a_e has for many years provided fertile ground for testing QED and obtaining an accurate value of α. Within QED, a_e is a function of α with weak and strong interaction contributions that are comparatively small and readily calculated, totaling at present a fractional contribution of $14.86(10) \times 10^{-10}$ to a_e. By comparison, the relative uncertainty of the measured a_e is 2.4×10^{-10}, based on a determination of the ratio of the cyclotron and precession frequencies of a single electron in an applied magnetic flux density.

A convenient way of verifying QED theory is to calculate α that results from equating the theoretical expression for a_e with the experimental value and then comparing it with values obtained from experiments that only weakly depend on QED theory. Two such values are available from interferometric measurements with laser-cooled ^{87}Rb and ^{133}Cs atoms.

The result of the comparison is that α^{-1} from the single-electron experiment exceeds the value from the ^{87}Rb and ^{133}Cs interferometric experiments by 1.7σ and 2.4σ, respectively. Here, σ is the square root of the sum of the squares of the corresponding pair of uncertainties in α^{-1}. The 2.4σ disagreement is mild, but discomforting.

The two leading experimental groups that determined α^{-1} from atom interferometry are carrying out new experiments that should yield values with significantly reduced uncertainties (Cladé *et al.*, 2019; Yu *et al.*, 2019). In addition, G. Gabrielse is constructing a significantly improved version of his single-electron experiment (Gabrielse *et al.*, 2019). The group that has calculated the $A_1^{(10)}$ coefficient in the theoretical expression of a_e is continuing its work and has recently reported $A_1^{(10)} = 6.737(159)$ (Aoyama, Kinoshita, and Nio, 2019). The results of all efforts are anxiously awaited.

3. Proton radius and Rydberg constant

The "proton-radius puzzle" has been with us ever since the 2010 publication of the charge radius of the proton r_p obtained from the measurement of the Lamb shift in muonic hydrogen μH (an atom comprised of a proton and a muon). The severe discrepancy between the μH value of r_p and the values of r_p obtained from hydrogen transition frequency data and e-p elastic scattering data led to the omission of the μH result from 2010 and 2014 CODATA adjustments

A Lamb-shift measurement in muonic deuterium μD (an atom comprised of a deuteron and a muon) provided a charge radius of the deuteron r_d that, like the μH value of r_p, was smaller than the deuterium spectroscopic and e-d scattering value and inconsistent with it. This disagreement was also deemed too significant, and the μD data were not included in the CODATA adjustments.

The situation has improved markedly over the past four years, and the μH as well as recent μD data are now included in the 2018 CODATA adjustment. New hydrogen spectroscopic data and advances in theoretical estimates of transition frequencies contributed to this decision. As a result, the 2018 recommended values of r_p, r_d, and R_∞ and their uncertainties are significantly smaller than in the 2014 CODATA adjustment. The value of r_p is reduced by 3.8% and its uncertainty is reduced from 0.70% to 0.22%; r_d is reduced by 0.62% and its uncertainty from 0.12% to 0.035%; and for R_∞ the reduction in value is fractionally 32×10^{-12} and u_r is reduced from 5.9×10^{-12} to 1.9×10^{-12}.

We can conclude that the proton-radius puzzle has largely been resolved. Nevertheless, the uncertainties of the many input data that contribute to the determination of the charge radii and Rydberg constant had to be increased by a expansion factor of 1.6 in order to ensure that the residuals of these input data are less than two.

New data will be required to obtain further insight into the origin of the remaining discrepancies. In fact, after the closing date for the 2018 CODATA adjustment, new values for r_p based on an improved e-p scattering experiment have become available. A value of $r_p = 0.831(14)$ fm was recently reported by Xiong *et al.* (2019) from the Jefferson Laboratory, Virginia, USA. The result is smaller than, but consistent with, the 2018 CODATA recommended value and the work is expected to continue.

Electron-proton scattering experiments are also being carried out at the Mainz Microtron (MAMI) particle accelerator in Germany. In 2019, it already led to the reported value $r_p = 0.870(28)$ fm (Mihovilovič *et al.*, 2017, 2019). This value is larger than but consistent with, the 2018 CODATA recommended value. A second MAMI experiment is under construction and planned to begin operation in 2020 (Vorobyev, 2019). Finally, we mention an experiment underway at the Paul Scherrer Institut, Switzerland, in which r_p will be determined from simultaneous measurements of muon-proton and electron-proton scattering (Roy *et al.*, 2020).

4. Muon mass and magnetic moment

The values for the mass m_μ and magnetic-moment anomaly a_μ of the muon are essentially unchanged from the 2010 and 2014 adjustments. Their values are determined by experimental measurements published in 1999 and 2006 and have a relative uncertainty of 2.2×10^{-8} and 5.4×10^{-7}, respectively. The muon mass is derived from measurements and accurate theoretical calculations of the hyperfine splitting of the ground state of muonium μ^+e^-. New data on this hyperfine splitting are expected in the near future (Strasser *et al.*, 2019).

The theoretical estimate of the muon magnetic-moment anomaly $a_\mu(\text{th})$ has been discrepant with the experimental value ever since the 2006 measurement; see Fig. 8. The experimental value $a_\mu(\text{exp})$ currently exceeds the theoretical value by about 3.5σ, and models using physics beyond the standard model (SM) have been put forward to explain the discrepancy. Since m_μ/m_e is about 207, $a_\mu(\text{th})$ is more sensitive to possible non-SM contributions than the electron magnetic-moment anomaly a_e. Because of the significant inconsistency, the theoretical expression for the muon anomaly as in previous adjustments is not used in the 2018 CODATA adjustment.

Two separate experiments (Abe *et al.*, 2019; Keshavarzi, 2019) are underway to determine a_μ, promising one-fourth the uncertainty of the current value. Work also continues to improve the theoretical SM expression for a_μ (Keshavarzi, Nomura, and Teubner, 2018). The hope is that the discrepancy will be resolved by the closing date for the next adjustment.

5. Newtonian constant of gravitation

The Newtonian constant of gravitation G, with its 2.2×10^{-5} relative uncertainty, is among the most poorly known constants in our 2018 adjustment. See the discussion of Fig. 9. The large scatter among the 16 measurements of G on which the recommended value is based required an expansion factor of 3.9 to reduce all residuals to less than two.

The need for an expansion factor demonstrates the technological difficulty of determining G. Improving our knowledge of G may ultimately require the development of a new approach that can achieve an uncertainty no greater than one part in 10^6, smaller than the uncertainty of previously reported values by more than an order of magnitude (Rothleitner and Schlamminger, 2017). In addition, such technology could shed light on the reasons for the scatter among the existing data, such as the discovery of previously unknown systematic effects in the measurement methods, and would likely find other useful applications.

Rothleitner and Schlamminger (2017) also suggested that moving an apparatus from a laboratory where it was used to determine G to another laboratory could help uncover unrecognized systematic effects. To this end, the BIPM apparatus that led to the publication in 2014 of a value of G with $u_r = 2.4 \times 10^{-5}$ is now operational at the NIST Gaithersburg laboratory.

6. Proton mass

The relative atomic mass of hydrogen, $A_r(^1\text{H})$, from the Atomic Mass Data Center and a measurement of the cyclotron frequency ratio, $\omega_c(^{12}C^{6+})/\omega_c(p)$, determine $A_r(p)$. In the 2018 adjustment, the uncertainties of these input data are expanded by the factor 1.7 to reduce their normalized residuals to less than two. The value of $A_r(^1\text{H})$ is based on relatively old data and constrains the value of the proton mass less than that determined by the cyclotron frequency ratio. See also Fig. 6. An independent determination of $A_r(p)$ with u_r of a few parts in 10^{11} would help resolve the discrepancy.

7. Physics in general

The 2017 redefinition of the SI has arguably been a milestone in physics and chemistry. As a consequence, many constants in our tables that previously had uncertainties are now exactly known in SI units. Many more have significantly reduced uncertainties. The physicochemical constants that are now exact in addition to N_A and k are, for example, F, R, V_m, and σ. The 30 conversion factors among the six energy units J, kg, m^{-1}, Hz, K, and eV are now exact and the relative

uncertainties of their conversion factors with u and E_h are currently only 3.0×10^{-10} and 1.9×10^{-12}, respectively. Further, u_r of α and R_∞ are now 1.5×10^{-10} and 1.9×10^{-12}, respectively.

A perusal of the input data in Table XXI shows there is only one input datum for some quantities, and some are decades old. Measurements of the same quantity by different methods in different laboratories help to identify unknown systematic effects, thereby improving the reliability of the input data. The six magnetic-moment ratios, items D32 to D37 in the table, are obvious examples of old data. The muon mass is currently only determined by essentially one measurement. It would be useful if researchers kept in mind the limited robustness of the data set on which CODATA adjustments are based in planning research.

LIST OF SYMBOLS AND ABBREVIATIONS

ASD	NIST Atomic Spectra Database (online)
AMDC	Atomic Mass Data Center, Institute of Modern Physics, Chinese Academy of Sciences, Lanzhou, People's Republic of China. AMDC-16 is the atomic mass evaluation completed in 2016, the most recent available.
$A_r(X)$	Relative atomic mass of X: $A_r(X) = m(X)/m_u$
a_0	Bohr radius: $a_0 = \hbar/\alpha m_e c$
a_e	Electron magnetic-moment anomaly: $a_e = (\lvert g_e \rvert - 2)/2$
a_μ	Muon magnetic-moment anomaly: $a_\mu = (\lvert g_\mu \rvert - 2)/2$
Berkeley	University of California at Berkeley, Berkeley, California, USA
BIPM	International Bureau of Weights and Measures, Sèvres, France
BNL	Brookhaven National Laboratory, Upton, New York, USA
CGPM	General Conference on Weights and Measures
CIPM	International Committee for Weights and Measures
CODATA	Committee on Data of the International Science Council
CREMA	The international collaboration *Charge Radius Experiment with Muonic Atoms* at the Paul Scherrer Institute, Villigen, Switzerland
c	Speed of light in vacuum and one of the seven defining constants of the SI
d	Deuteron (nucleus of deuterium D, or ^{2}H)
d_{220}	{220} lattice spacing of an ideal silicon crystal with natural isotopic Si abundances
$d_{220}(X)$	{220} lattice spacing of crystal X of silicon with natural isotopic Si abundances
E_h	Hartree energy: $E_h = 2R_\infty hc = \alpha^2 m_e c^2$
e	Symbol for either member of the electron-positron pair; when necessary, e^- or e^+ is used to indicate the electron or positron
e	Elementary charge: absolute value of the charge of the electron and one of the seven defining constants of the SI
FSU	Florida State University, Tallahassee, Florida, USA
FSUJ	Friedrich-Schiller University, Jena, Germany
G	Newtonian constant of gravitation
G_F	Fermi coupling constant
g_d	Deuteron g-factor: $g_d = \mu_d/\mu_N$
g_e	Electron g-factor: $g_e = 2\mu_e/\mu_B$
g_p	Proton g-factor: $g_p = 2\mu_p/\mu_N$
g'_p	Shielded proton g-factor: $g'_p = 2\mu'_p/\mu_N$
g_t	Triton g-factor: $g_t = 2\mu_t/\mu_N$
$g_X(Y)$	g-factor of particle X in the ground (1S) state of hydrogenic atom Y
g_μ	Muon g-factor: $g_\mu = 2\mu_\mu/(e\hbar/2m_\mu)$
Harvard	HarvU also. Harvard University, Cambridge, Massachusetts, USA
HD	A hydrogen-deuterium molecule
HT	A hydrogen-tritium molecule
HUST	Huazhong University of Science and Technology, Wuhan, People's Republic of China
h	Helion (nucleus of ^{3}He)
h	Planck constant and one of the seven defining constants of the SI
$\hbar$	Reduced Planck constant
ILL	Institut Max von Laue-Paul Langevin, Grenoble, France
INRIM	Istituto Nazionale di Ricerca Metrologica, Torino, Italy
JILA	JILA, University of Colorado and NIST, Boulder, Colorado, USA
J-PARC	Japan Proton Accelerator Research Complex
k	Boltzmann constant and one of the seven defining constants of the SI
KEK	High Energy Accelerator Research Organization, Tsukuba, Japan
LAMPF	Clinton P. Anderson Meson Physics Facility at Los Alamos National Laboratory, Los Alamos, New Mexico, USA
LANL	Los Alamos National Laboratory, Los Alamos, New Mexico, USA

LENS	European Laboratory for Non-Linear Spectroscopy, University of Florence, Italy
LKB	Laboratoire Kastler-Brossel, Paris, France
MIT	Massachusetts Institute of Technology, Cambridge, Massachusetts, USA
MPIK	Max-Planck-Institut für Kernphysik, Heidelberg, Germany
MPQ	Max-Planck-Institut für Quantenoptik, Garching, Germany
MSL	Measurement Standards Laboratory, Lower Hutt, New Zealand
$M(X)$	Molar mass of X: $M(X) = A_r(X)M_u$
$M(^{12}\mathrm{C})$	Molar mass of carbon-12. $M(^{12}\mathrm{C}) = 12M_u = 12N_A m_u \approx 0.012$ kg/mol
M_u	Molar mass constant: $M_u = N_A m_u$
Mu	Muonium (μ^+e^- atom)
m_u	Unified atomic mass constant: $m_u = m(^{12}\mathrm{C})/12 = 2hcR_\infty/\alpha^2c^2A_r(\mathrm{e})$
$m(\mathcal{K})$	Mass of the international prototype of the kilogram: $m(\mathcal{K}) \approx 1$ kg
m_X, $m(X)$	Mass of X (for the electron e, proton p, and other elementary particles, the first symbol is used, i.e., m_e, m_p, etc.)
N_A	Avogadro constant and one of the seven defining constants of the SI
NIST	National Institute of Standards and Technology, Gaithersburg, Maryland and Boulder, Colorado, USA
NPL	National Physical Laboratory, Teddington, UK
n	Neutron
$p(\chi^2\|\nu)$	Probability that an observed value of chi square for ν degrees of freedom would exceed χ^2
p	Proton
PTB	Physikalisch-Technische Bundesanstalt, Braunschweig and Berlin, Germany
QCD	Quantum chromodynamics
QED	Quantum electrodynamics
R	Molar gas constant; $R = N_A k$
R_B	Birge ratio: $R_B = (\chi^2/\nu)^{\frac{1}{2}}$
R_∞	Rydberg constant: $R_\infty = m_e c\alpha^2/2h$
r_i	Normalized residual of an input datum X_i in a least-squares calculation: $r_i = (X_i - \langle X_i \rangle)/u(X_i)$
r_d	Bound-state rms charge radius of the deuteron
r_p	Bound-state rms charge radius of the proton
$r(X, Y)$	Correlation coefficient of quantity or constant X and Y: $r(X, Y) = u(X, Y)/[u(X)u(Y)]$
SI	Système international d'unités (International System of Units)
StPtrsb	D. I. Mendeleyev All-Russian Research Institute for Metrology (VNIIM), St. Petersburg, Russian Federation
Sussex	University of Sussex, Brighton, UK
SYRTE	Systèmes de référence Temps Espace, Paris, France
T_{TPW}	Thermodynamic temperature T of the triple point of water: $T_{TPW} \approx 273.16$ K
TGFC	Task Group on Fundamental Constants of the Committee on Data of the International Science Council (CODATA)
TR&D	Tribotech Research and Development Company, Moscow, Russian Federation
t	Triton (nucleus of tritium T, or ^{3}H)
UBarc	Universitat Autònoma de Barcelona, Barcelona, Spain
UCB	University of California at Berkeley, Berkeley, California, USA
UCI	University of California at Irvine, Irvine, California, USA
UMZ	Institut für Physik, Johannes Gutenberg-Universität Mainz, Mainz, Germany
UWash	University of Washington, Seattle, Washington, USA
UWup	University of Wuppertal, Wuppertal, Germany
UZur	University of Zurich, Zurich, Switzerland
u	Unified atomic mass unit (also called the dalton, Da): $1\,\mathrm{u} = m_u = m(^{12}\mathrm{C})/12$
$u(X)$	Standard uncertainty (i.e., estimated standard deviation) of quantity or constant X
$u_r(X)$	Relative standard uncertainty of a quantity or constant X: $u_r(X) = u(X)/\|X\|$, $X \neq 0$ (also simply u_r)
$u(X, Y)$	Covariance of quantities or constants X and Y
$u_r(X, Y)$	Relative covariance of quantities or constants X and Y: $u_r(X, Y) = u(X, Y)/(XY)$
u_0	Type of uncertainty in the theory of the energy levels of hydrogen and deuterium: The contribution to the energy

has correlated uncertainties for states with the same ℓ and j. See also entry u_n.

u_n Type of uncertainty in the theory of the energy levels of hydrogen and deuterium: The contribution has uncorrelated uncertainties. See also entry u_0.

WarsU University of Warsaw, Warszawa, Poland

Yale Yale University, New Haven, Connecticut, USA

York York University, Toronto, Canada

α Fine-structure constant: $\alpha = e^2/4\pi\epsilon_0\hbar c \approx 1/137$

α Alpha particle (nucleus of ^{4}He)

$\Delta E_B(^A X^{n+})$ Energy required to remove n electrons from a neutral atom

$\Delta E_I(^A X^{i+})$ Electron ionization energies, $i = 0$ to $n-1$

ΔE_{Mu} Ground-state muonium hyperfine splitting energy

$\Delta\mathcal{E}_{LS}(\mu H, \mu D)$ Transition energy of Lamb shift in muonic hydrogen or muonic deuterium

$\delta_{H,D}(X)$ Additive correction to the theoretical expression for the energy of a specified level in hydrogen or deuterium

$\delta_{th}(X)$ Additive correction to a specified theoretical expression

$\doteq$ Symbol used to relate an input datum to its observational equation

θ_W Weak mixing angle

$\lambda\!\!\!^{-}_C$ Reduced Compton wavelength: $\lambda\!\!\!^{-}_C = \hbar/m_e c$

μ Symbol for either member of the muon-antimuon pair; when necessary, μ^- or μ^+ is used to indicate the negative muon or positive antimuon

μD Muonic deuterium (an atom comprising a deuteron and a muon)

μH Muonic hydrogen (an atom comprising a proton and a muon)

μ_B Bohr magneton: $\mu_B = e\hbar/2m_e$

μ_N Nuclear magneton: $\mu_N = e\hbar/2m_p$

$\mu_X(Y)$ Magnetic moment of particle X in atom or molecule Y

μ_X, μ'_X Magnetic moment, or shielded magnetic moment, of particle X

μ_0 Vacuum magnetic permeability: $\mu_0 = 4\pi\alpha\hbar/e^2c \approx 4\pi \times 10^{-7}$ N/A^2

ν Degrees of freedom of a particular least-squares calculation: $\nu = N - M$, N number of input data, M number of variables, or adjusted constants

σ Stefan-Boltzmann constant: $\sigma = (\pi^2/60)k^4/\hbar^3c^2$

τ Symbol for either member of the tau-antitau pair; when necessary, τ^- or τ^+ is used to indicate the negative or positive tau lepton

χ^2 The statistic "chi square"

ACKNOWLEDGMENTS

As always, we gratefully acknowledge the help of our many colleagues throughout the world who provided the CODATA Task Group on Fundamental Constants with results prior to formal publication and for promptly answering our many questions about their work. We wish to thank our fellow Task Group members for their invaluable guidance and suggestions during the course of the 2018 adjustment effort.

REFERENCES

Abe, M., S. Bae, G. Beer, G. Bunce, H. Choi, S. Choi, M. Chung, W. d. Silva, S. Eidelman, and M. Finger, 2019, Prog. Theor. Exp. Phys. **2019**, 053C02.

Abe, M., Y. Murata, H. Iinuma, T. Ogitsu, N. Saito, K. Sasaki, T. Mibe, and H. Nakayama, 2018, Nucl. Instrum. Methods Phys. Res., Sect. A **890**, 51.

Adikaram, D., *et al.*, 2015, Phys. Rev. Lett. **114**, 062003.

Alarcón, J. M., D. W. Higinbotham, C. Weiss, and Z. Ye, 2019, Phys. Rev. C **99**, 044303.

Angeli, I., and K. Marinova, 2013, At. Data Nucl. Data Tables **99**, 69.

Antognini, A., F. Kottmann, F. Biraben, P. Indelicato, F. Nez, and R. Pohl, 2013, Ann. Phys. (Amsterdam) **331**, 127.

Antognini, A., *et al.*, 2013, Science **339**, 417.

Aoyama, T., M. Hayakawa, T. Kinoshita, and M. Nio, 2015, Phys. Rev. D **91**, 033006.

Aoyama, T., T. Kinoshita, and M. Nio, 2018, Phys. Rev. D **97**, 036001.

Aoyama, T., T. Kinoshita, and M. Nio, 2019, Atoms **7**, 28.

Armstrong, T. R., and M. P. Fitzgerald, 2003, Phys. Rev. Lett. **91**, 201101.

Arnoult, O., F. Nez, L. Julien, and F. Biraben, 2010, Eur. Phys. J. D **60**, 243.

Arrington, J., and I. Sick, 2015, J. Phys. Chem. Ref. Data **44**, 031204.

Bade, S., L. Djadaojee, M. Andia, P. Cladé, and S. Guellati-Khelifa, 2018, Phys. Rev. Lett. **121**, 073603.

Bagley, C. H., and G. G. Luther, 1997, Phys. Rev. Lett. **78**, 3047.

Becker, P., H. Bettin, H.-U. Danzebrink, M. Gläser, U. Kuetgens, A. Nicolaus, D. Schiel, P. De Bièvre, S. Valkiers, and P. Taylor, 2003, Metrologia **40**, 271.

Becker, P., K. Dorenwendt, G. Ebeling, R. Lauer, W. Lucas, R. Probst, H.-J. Rademacher, G. Reim, P. Seyfried, and H. Siegert, 1981, Phys. Rev. Lett. **46**, 1540.

Beier, T., 2000, Phys. Rep. **339**, 79.

Beier, T., I. Lindgren, H. Persson, S. Salomonson, P. Sunnergren, H. Häffner, and N. Hermanspahn, 2000, Phys. Rev. A **62**, 032510.

Bennett, G. W., *et al.*, 2006, Phys. Rev. D **73**, 072003.

Berkeland, D. J., E. A. Hinds, and M. G. Boshier, 1995, Phys. Rev. Lett. **75**, 2470.

Bernauer, J. C., and M. O. Distler, 2015 (private communication).

Bernauer, J. C., *et al.*, 2010, Phys. Rev. Lett. **105**, 242001.
Bernauer, J. C., *et al.*, 2014, Phys. Rev. C **90**, 015206.
Beyer, A., *et al.*, 2016, Opt. Express **24**, 17470.
Beyer, A., *et al.*, 2017, Science **358**, 79.
Bezginov, N., T. Valdez, M. Horbatsch, A. Marsman, A. C. Vutha, and E. A. Hessels, 2019, Science **365**, 1007.
Biraben, F., 2019, C.R. Phys. **20**, 671.
Birge, R. T., 1929, Rev. Mod. Phys. **1**, 1.
Blum, T., P. A. Boyle, V. Gülpers, T. Izubuchi, L. Jin, C. Jung, A. Jüttner, C. Lehner, A. Portelli, and J. T. Tsang, 2018, Phys. Rev. Lett. **121**, 022003.
Borsanyi, S., *et al.*, 2018, Phys. Rev. Lett. **121**, 022002.
Bouchendira, R., P. Cladé, S. Guellati-Khélifa, F. Nez, and F. Biraben, 2011, Phys. Rev. Lett. **106**, 080801.
Bourzeix, S., B. de Beauvoir, F. Nez, M. D. Plimmer, F. de Tomasi, L. Julien, F. Biraben, and D. N. Stacey, 1996, Phys. Rev. Lett. **76**, 384.
Breit, G., 1928, Nature (London) **122**, 649.
Breit, G., and I. I. Rabi, 1931, Phys. Rev. **38**, 2082.
CIPM, 2016, Decision CIPM/105-15 of the 105th Meeting of the International Committee for Weights and Measures (CIPM). Available at https://www.bipm.org/en/committees/cipm/meeting/105.html.
CIPM, 2017, Decision CIPM/106-10, -11, -12 of the 106th Meeting of the International Committee for Weights and Measures (CIPM). Available at https://www.bipm.org/en/committees/cipm/meeting/106.html.
Cladé, P., 2015, Riv. Nuovo Cimento **38**, 173.
Cladé, P., F. Nez, F. Biraben, and S. Guellati-Khelifa, 2019, C.R. Phys. **20**, 77.
Close, F. E., and H. Osborn, 1971, Phys. Lett. **34B**, 400.
Colangelo, G., M. Hoferichter, A. Nyffeler, and M. Passera, 2014, Phys. Lett. B **735**, 90.
Czarnecki, A., M. Dowling, J. Piclum, and R. Szafron, 2018, Phys. Rev. Lett. **120**, 043203.
Czarnecki, A., W. J. Marciano, and A. Vainshtein, 2003, Phys. Rev. D **67**, 073006.
Czarnecki, A., K. Melnikov, and A. Yelkhovsky, 2000, Phys. Rev. A **63**, 012509.
Czarnecki, A., and R. Szafron, 2016, Phys. Rev. A **94**, 060501.
Davier, M., A. Hoecker, B. Malaescu, and Z. Zhang, 2017, Eur. Phys. J. C **77**, 827.
de Beauvoir, B., F. Nez, L. Julien, B. Cagnac, F. Biraben, D. Touahri, L. Hilico, O. Acef, A. Clairon, and J. J. Zondy, 1997, Phys. Rev. Lett. **78**, 440.
Deslattes, R. D., and A. Henins, 1973, Phys. Rev. Lett. **31**, 972.
Dorokhov, A. E., A. E. Radzhabov, and A. S. Zhevlakov, 2014a, JETP Lett. **100**, 133.
Dorokhov, A. E., A. E. Radzhabov, and A. S. Zhevlokov, 2014b, Int. J. Mod. Phys. Conf. Ser. **35**, 1460401.
Eides, M. I., 1996, Phys. Rev. A **53**, 2953.
Eides, M. I., 2019, Phys. Lett. B **795**, 113.
Eides, M. I., and H. Grotch, 1997, Ann. Phys. (N.Y.) **260**, 191.
Eides, M. I., H. Grotch, and V. A. Shelyuto, 2001, Phys. Rep. **342**, 63.
Eides, M. I., H. Grotch, and V. A. Shelyuto, 2007, *Theory of Light Hydrogenic Bound States*, Springer Tracts in Modern Physics Vol. 222 (Springer, Berlin, Heidelberg, New York).
Eides, M. I., and V. A. Shelyuto, 2004, Phys. Rev. A **70**, 022506.
Eides, M. I., and V. A. Shelyuto, 2007, Can. J. Phys. **85**, 509.
Eides, M. I., and V. A. Shelyuto, 2014, Phys. Rev. D **90**, 113002.
Erickson, G. W., 1977, J. Phys. Chem. Ref. Data **6**, 831.
Estey, B., C. Yu, H. Müller, P.-C. Kuan, and S.-Y. Lan, 2015, Phys. Rev. Lett. **115**, 083002.
Faustov, R., 1970, Phys. Lett. **33B**, 422.
Ferroglio, L., G. Mana, and E. Massa, 2008, Opt. Express **16**, 16877.
Fleurbaey, H., 2017, "Frequency metrology of the 1*S*-3*S* transition of hydrogen: Contribution to the proton charge radius puzzle," Ph.D. thesis (Université Pierre et Marie Curie).
Fleurbaey, H., S. Galtier, S. Thomas, M. Bonnaud, L. Julien, F. Biraben, F. Nez, M. Abgrall, and J. Guéna, 2018, Phys. Rev. Lett. **120**, 183001.
Flowers, J. L., B. W. Petley, and M. G. Richards, 1993, Metrologia **30**, 75.
Friar, J. L., 1979, Ann. Phys. (N.Y.) **122**, 151.
Friar, J. L., and G. L. Payne, 1997, Phys. Rev. A **56**, 5173.
Gabrielse, G., S. E. Fayer, T. G. Myers, and X. Fan, 2019, Atoms **7**, 45.
Galtier, S., H. Fleurbaey, S. Thomas, L. Julien, F. Biraben, and F. Nez, 2015, J. Phys. Chem. Ref. Data **44**, 031201.
Garbacz, P., K. Jackowski, W. Makulski, and R. E. Wasylishen, 2012, J. Phys. Chem. A **116**, 11896.
Glazov, D. A., and V. M. Shabaev, 2002, Phys. Lett. A **297**, 408.
Gnendiger, C., D. Stöckinger, and H. Stöckinger-Kim, 2013, Phys. Rev. D **88**, 053005.
Griffioen, K., C. Carlson, and S. Maddox, 2016, Phys. Rev. C **93**, 065207.
Grotch, H., 1970, Phys. Rev. Lett. **24**, 39.
Gundlach, J. H., and S. M. Merkowitz, 2000, Phys. Rev. Lett. **85**, 2869.
Gundlach, J. H., and S. M. Merkowitz, 2002 (private communication).
Hagiwara, K., R. Liao, A. D. Martin, D. Nomura, and T. Teubner, 2011, J. Phys. G **38**, 085003.
Hagley, E. W., and F. M. Pipkin, 1994, Phys. Rev. Lett. **72**, 1172.
Hamzeloui, S., J. A. Smith, D. J. Fink, and E. G. Myers, 2017, Phys. Rev. A **96**, 060501.
Hanke, M., and E. G. Kessler, 2005, J. Phys. D **38**, A117.
Hanneke, D., S. Fogwell, and G. Gabrielse, 2008, Phys. Rev. Lett. **100**, 120801.
Härtwig, J., S. Grosswig, P. Becker, and D. Windisch, 1991, Phys. Status Solidi A **125**, 79.
Hayward, T. B., and K. A. Griffioen, 2020, Nucl. Phys. **A999**, 121767.
Heiße, F., *et al.*, 2017, Phys. Rev. Lett. **119**, 033001.
Horbatsch, M., and E. A. Hessels, 2010, Phys. Rev. A **82**, 052519.
Horbatsch, M., and E. A. Hessels, 2011, Phys. Rev. A **84**, 032508.
Horbatsch, M., E. A. Hessels, and A. Pineda, 2017, Phys. Rev. C **95**, 035203.
Hu, Z.-K., J.-Q. Guo, and J. Luo, 2005, Phys. Rev. D **71**, 127505.
Huang, W. J., G. Audi, M. Wang, F. G. Kondev, S. Naimi, and X. Xu, 2017, Chin. Phys. C **41**, 030002.
Ivanov, V. G., S. G. Karshenboim, and R. N. Lee, 2009, Phys. Rev. A **79**, 012512.
Jegerlehner, F., 2018, EPJ Web Conf. **166**, 00022.
Jegerlehner, F., 2019, EPJ Web Conf. **218**, 01003.
Jegerlehner, F., and A. Nyffeler, 2009, Phys. Rep. **477**, 1.
Jentschura, U. D., 2003, J. Phys. A **36**, L229.
Jentschura, U. D., 2006, Phys. Rev. A **74**, 062517.
Jentschura, U. D., 2009, Phys. Rev. A **79**, 044501.
Jentschura, U. D., A. Czarnecki, and K. Pachucki, 2005, Phys. Rev. A **72**, 062102.
Jentschura, U. D., A. Czarnecki, K. Pachucki, and V. A. Yerokhin, 2006, Int. J. Mass Spectrom. **251**, 102.
Jentschura, U. D., and P. J. Mohr, 2002, Can. J. Phys. **80**, 633.
Kalinowski, M., 2019, Phys. Rev. A **99**, 030501.
Karagioz, O. V., and V. P. Izmailov, 1996, Izmer. Tekh. **39**, 3.
Karshenboim, S. G., 2000, Phys. Lett. A **266**, 380.

Karshenboim, S. G., and V. G. Ivanov, 2018a, Phys. Rev. A **97**, 022506.
Karshenboim, S. G., and V. G. Ivanov, 2018b, Phys. Rev. A **98**, 022522.
Karshenboim, S. G., V. G. Ivanov, and V. M. Shabaev, 1999, Phys. Scr. **T80**, 491.
Karshenboim, S. G., V. G. Ivanov, and V. M. Shabaev, 2000, Zh. Eksp. Teor. Fiz. **117**, 67 [J. Exp. Theor. Phys. **90**, 59 (2000)].
Karshenboim, S. G., V. G. Ivanov, and V. M. Shabaev, 2001a, Can. J. Phys. **79**, 81.
Karshenboim, S. G., V. G. Ivanov, and V. M. Shabaev, 2001b, Zh. Eksp. Teor. Fiz. **120**, 546 [J. Exp. Theor. Phys. **93**, 477 (2001)].
Karshenboim, S. G., E. Y. Korzinin, V. A. Shelyuto, and V. G. Ivanov, 2015, J. Phys. Chem. Ref. Data **44**, 031202.
Karshenboim, S. G., V. A. Shelyuto, and A. I. Vainshtein, 2008, Phys. Rev. D **78**, 065036.
Keshavarzi, A., 2019, EPJ Web Conf. **212**, 05003.
Keshavarzi, A., D. Nomura, and T. Teubner, 2018, Phys. Rev. D **97**, 114025.
Kessler, E. G., C. I. Szabo, J. P. Cline, A. Henins, L. T. Hudson, M. H. Mendenhall, and M. D. Vaudin, 2017, J. Res. Natl. Inst. Stand. Technol. **122**, 24.
Kessler, Jr., E. G., R. D. Deslattes, and A. Henins, 1979, Phys. Rev. A **19**, 215.
Kessler, Jr., E. G., M. S. Dewey, R. D. Deslattes, A. Henins, H. G. Börner, M. Jentschel, and H. Lehmann, 2000, in *Capture Gamma-Ray Spectroscopy and Related Topics*, edited by Wender, S. (American Institute of Physics, Melville, NY), pp. 400–407.
Kessler, Jr., E. G., J. E. Schweppe, and R. D. Deslattes, 1997, IEEE Trans. Instrum. Meas. **46**, 551.
Kleinevoß, U., 2002, "Bestimmung der Newtonschen Gravitationskonstanten G," Ph.D. thesis (University of Wuppertal).
Kleinvoß, U., H. Meyer, H. Piel, and S. Hartmann, 2002 (private communication).
Köhler, F., S. Sturm, A. Kracke, G. Werth, W. Quint, and K. Blaum, 2015, J. Phys. B **48**, 144032.
Kramers, H. A., and W. Heisenberg, 1925, Z. Phys. **31**, 681.
Krauth, J. J., M. Diepold, B. Franke, A. Antognini, F. Kottmann, and R. Pohl, 2016, Ann. Phys. (Amsterdam) **366**, 168.
Kurz, A., T. Liu, P. Marquard, and M. Steinhauser, 2014a, Nucl. Phys. **B879**, 1.
Kurz, A., T. Liu, P. Marquard, and M. Steinhauser, 2014b, Phys. Lett. B **734**, 144.
Laporta, S., 1993, Nuovo Cimento Soc. Ital. Fis. **106A**, 675.
Laporta, S., 2017, Phys. Lett. B **772**, 232.
Laporta, S., and E. Remiddi, 1993, Phys. Lett. B **301**, 440.
Lee, G., J. R. Arrington, and R. J. Hill, 2015, Phys. Rev. D **92**, 013013.
Lee, R. N., A. I. Milstein, I. S. Terekhov, and S. G. Karshenboim, 2005, Phys. Rev. A **71**, 052501.
Li, Q., *et al.*, 2018, Nature (London) **560**, 582.
Liu, J., D. Sprecher, C. Jungen, W. Ubachs, and F. Merkt, 2010, J. Chem. Phys. **132**, 154301.
Liu, W., *et al.*, 1999, Phys. Rev. Lett. **82**, 711.
Low, F., 1952, Phys. Rev. **88**, 53.
Lundeen, S., and F. Pipkin, 1981, Phys. Rev. Lett. **46**, 232.
Lundeen, S. R., and F. M. Pipkin, 1986, Metrologia **22**, 9.
Luo, J., Q. Liu, L.-C. Tu, C.-G. Shao, L.-X. Liu, S.-Q. Yang, Q. Li, and Y.-T. Zhang, 2009, Phys. Rev. Lett. **102**, 240801.
Luther, G. G., and W. R. Towler, 1982, Phys. Rev. Lett. **48**, 121.
Mariam, F. G., 1981, "High precision measurement of the muonium ground state hyperfine interval and the muon magnetic moment," Ph.D. thesis (Yale University).
Mariam, F. G., *et al.*, 1982, Phys. Rev. Lett. **49**, 993.
Marrus, R., and P. J. Mohr, 1979, Adv. At. Mol. Phys. **14**, 181.
Marsman, A., M. Horbatsch, Z. A. Corriveau, and E. A. Hessels, 2018, Phys. Rev. A **98**, 012509.
Martin, J., U. Kuetgens, J. Stümpel, and P. Becker, 1998, Metrologia **35**, 811.
Massa, E., G. Mana, and U. Kuetgens, 2009, Metrologia **46**, 249.
Massa, E., G. Mana, U. Kuetgens, and L. Ferroglio, 2009, New J. Phys. **11**, 053013.
Matveev, A., *et al.*, 2013, Phys. Rev. Lett. **110**, 230801.
Mihovilovič, M., *et al.*, 2017, Phys. Lett. B **771**, 194.
Mihovilovič, M., *et al.*, 2019, arXiv:1905.11182.
Millman, S., I. I. Rabi, and J. R. Zacharias, 1938, Phys. Rev. **53**, 384.
Mills, I. M., P. J. Mohr, T. J. Quinn, B. N. Taylor, and E. R. Williams, 2011, Phil. Trans. R. Soc. A **369**, 3907.
Mohr, P. J., D. B. Newell, and B. N. Taylor, 2016a, Rev. Mod. Phys. **88**, 035009.
Mohr, P. J., D. B. Newell, and B. N. Taylor, 2016b, J. Phys. Chem. Ref. Data **45**, 043102.
Mohr, P. J., D. B. Newell, B. N. Taylor, and E. Tiesinga, 2018, Metrologia **55**, 125.
Mohr, P. J., and B. N. Taylor, 1999, J. Phys. Chem. Ref. Data **28**, 1713.
Mohr, P. J., and B. N. Taylor, 2000, Rev. Mod. Phys. **72**, 351.
Mohr, P. J., and B. N. Taylor, 2005, Rev. Mod. Phys. **77**, 1.
Mohr, P. J., B. N. Taylor, and D. B. Newell, 2008a, Rev. Mod. Phys. **80**, 633.
Mohr, P. J., B. N. Taylor, and D. B. Newell, 2008b, J. Phys. Chem. Ref. Data **37**, 1187.
Mohr, P. J., B. N. Taylor, and D. B. Newell, 2012a, Rev. Mod. Phys. **84**, 1527.
Mohr, P. J., B. N. Taylor, and D. B. Newell, 2012b, J. Phys. Chem. Ref. Data **41**, 043109.
Mooser, A., S. Ulmer, K. Blaum, K. Franke, H. Kracke, C. Leiteritz, W. Quint, C. C. Rodegheri, C. Smorra, and J. Walz, 2014, Nature (London) **509**, 596.
Myers, E. G., 2019, Atoms **7**, 37.
Myers, E. G., A. Wagner, H. Kracke, and B. A. Wesson, 2015, Phys. Rev. Lett. **114**, 013003.
Neronov, Y. I., and V. S. Aleksandrov, 2011, Pis'ma Zh. Eksp. Teor. Fiz. **94**, 452 [JETP Lett. **94**, 418 (2011)].
Neronov, Y. I., and S. G. Karshenboim, 2003, Phys. Lett. A **318**, 126.
Neronov, Y. I., and N. N. Seregin, 2012, Zh. Eksp. Teor. Fiz. **115**, 777 [J. Exp. Theor. Phys. **115**, 777 (2012)].
Newell, D. B., *et al.*, 2018, Metrologia **55**, L13.
Newman, R., M. Bantel, E. Berg, and W. Cross, 2014, Phil. Trans. R. Soc. A **372**, 20140025.
Newton, G., D. A. Andrews, and P. J. Unsworth, 1979, Phil. Trans. R. Soc. A **290**, 373.
Nomura, D., and T. Teubner, 2013, Nucl. Phys. **B867**, 236.
Nyffeler, A., 2014, Int. J. Mod. Phys. Conf. Ser. **35**, 1460456.
Pachucki, K., 1996, Phys. Rev. A **53**, 2092.
Pachucki, K., A. Czarnecki, U. D. Jentschura, and V. A. Yerokhin, 2005, Phys. Rev. A **72**, 022108.
Pachucki, K., U. D. Jentschura, and V. A. Yerokhin, 2004, Phys. Rev. Lett. **93**, 150401; **94**, 229902(E) (2005).
Pachucki, K., V. Patkóš, and V. A. Yerokhin, 2018, Phys. Rev. A **97**, 062511.
Pachucki, K., and M. Puchalski, 2017, Phys. Rev. A **96**, 032503.
Parker, R. H., C. Yu, W. Zhong, B. Estey, and H. Müller, 2018, Science **360**, 191.
Parks, H. V., and J. E. Faller, 2010, Phys. Rev. Lett. **105**, 110801.
Parks, H. V., and J. E. Faller, 2019, Phys. Rev. Lett. **122**, 199901.

Parthey, C. G., A. Matveev, J. Alnis, R. Pohl, T. Udem, U. D. Jentschura, N. Kolachevsky, and T. W. Hänsch, 2010, Phys. Rev. Lett. **104**, 233001.
Parthey, C. G., *et al.*, 2011, Phys. Rev. Lett. **107**, 203001.
Peset, C., and A. Pineda, 2015, Eur. Phys. J. A **51**, 156.
Peters, A., K. Y. Chung, B. Young, J. Hensley, and S. Chu, 1997, Phil. Trans. R. Soc. A **355**, 2223.
Pohl, R., *et al.*, 2010, Nature (London) **466**, 213.
Pohl, R., *et al.*, 2016, Science **353**, 669.
Prevedelli, M., L. Cacciapuoti, G. Rosi, F. Sorrentino, and G. M. Tino, 2014, Phil. Trans. R. Soc. A **372**, 20140030.
Puchalski, M., J. Komasa, and K. Pachucki, 2015, Phys. Rev. A **92**, 020501.
Quinn, T., H. Parks, C. Speake, and R. Davis, 2013, Phys. Rev. Lett. **111**, 101102; **113**, 039901(E) (2014).
Quinn, T., C. Speake, H. Parks, and R. Davis, 2014, Phil. Trans. R. Soc. A **372**, 20140032.
Quinn, T. J., 1989, Metrologia **26**, 69.
Quinn, T. J., C. C. Speake, S. J. Richman, R. S. Davis, and A. Picard, 2001, Phys. Rev. Lett. **87**, 111101.
Rosi, G., F. Sorrentino, L. Cacciapuoti, M. Prevedelli, and G. M. Tino, 2014, Nature (London) **510**, 518.
Rothleitner, C., and S. Schlamminger, 2017, Rev. Sci. Instrum. **88**, 111101.
Roy, P., *et al.*, 2020, Nucl. Instrum. Methods Phys. Res., Sect. A **949**, 162874.
Rudziński, A., M. Puchalski, and K. Pachucki, 2009, J. Chem. Phys. **130**, 244102.
Safronova, M. S., D. Budker, D. DeMille, D. F. J. Kimball, A. Derevianko, and C. W. Clark, 2018, Rev. Mod. Phys. **90**, 025008.
Sapirstein, J. R., and D. R. Yennie, 1990, in *Quantum Electrodynamics*, edited by Kinoshita, T. (World Scientific, Singapore), Chap. 12, pp. 560–672.
Schlamminger, S., E. Holzschuh, W. Kündig, F. Nolting, R. E. Pixley, J. Schurr, and U. Straumann, 2006, Phys. Rev. D **74**, 082001.
Schneider, G., *et al.*, 2017, Science **358**, 1081.
Schwob, C., L. Jozefowski, B. de Beauvoir, L. Hilico, F. Nez, L. Julien, F. Biraben, O. Acef, and A. Clairon, 1999, Phys. Rev. Lett. **82**, 4960; **86**, 4193(E) (2001).
Shabaev, V. M., and V. A. Yerokhin, 2002, Phys. Rev. Lett. **88**, 091801.
Shelyuto, V. A., S. G. Karshenboim, and S. I. Eidelman, 2018, Phys. Rev. D **97**, 053001.
Sick, I., 2001, Prog. Part. Nucl. Phys. **47**, 245.
Sick, I., 2003, Phys. Lett. B **576**, 62.
Sick, I., 2007, Can. J. Phys. **85**, 409.
Sick, I., 2008, in *Precision Physics of Simple Atoms and Molecules*, edited by Karshenboim, S. G., Lecture Notes in Physics Vol. 745 (Springer, Berlin, Heidelberg), pp. 57–77.
Sick, I., and D. Trautmann, 1998, Nucl. Phys. **A637**, 559.
Simon, G. G., C. Schmitt, and V. H. Walther, 1981, Nucl. Phys. **A364**, 285.
Sommerfeld, A., 1916, Ann. Phys. (Berlin) **356**, 1.
Sprecher, D., J. Liu, C. Jungen, W. Ubachs, and F. Merkt, 2010, J. Chem. Phys. **133**, 111102.
Strasser, P., *et al.*, 2019, EPJ Web Conf. **198**, 00003.
Sturm, S., 2015 (private communication).
Sturm, S., F. Köhler, J. Zatorski, A. Wagner, Z. Harman, G. Werth, W. Quint, C. H. Keitel, and K. Blaum, 2014, Nature (London) **506**, 467.
Sturm, S., A. Wagner, M. Kretzschmar, W. Quint, G. Werth, and K. Blaum, 2013, Phys. Rev. A **87**, 030501.
Tanabashi, M., *et al.*, 2018, Phys. Rev. D **98**, 030001.
Taylor, B. N., and T. J. Witt, 1989, Metrologia **26**, 47.
Thomas, S., H. Fleurbaey, S. Galtier, L. Julien, F. Biraben, and F. Nez, 2019, Ann. Phys. (Berlin) **531**, 1800363.
Tomalak, O., 2019, Eur. Phys. J. A **55**, 64.
Tu, L.-C., Q. Li, Q.-L. Wang, C.-G. Shao, S.-Q. Yang, L.-X. Liu, Q. Liu, and J. Luo, 2010, Phys. Rev. D **82**, 022001.
Van Dyck, Jr., R. S., D. B. Pinegar, S. V. Liew, and S. L. Zafonte, 2006, Int. J. Mass Spectrom. **251**, 231.
Volkov, S., 2019, Phys. Rev. D **100**, 096004.
Vorobyev, A. A., 2019, Phys. Part. Nucl. Lett. **16**, 524.
Vutha, A. C., and E. A. Hessels, 2015, Phys. Rev. A **92**, 052504.
Wang, M., G. Audi, F. G. Kondev, W. J. Huang, S. Naimi, and X. Xu, 2017, Chin. Phys. C **41**, 030003.
Weitz, M., A. Huber, F. Schmidt-Kaler, D. Leibfried, W. Vassen, C. Zimmermann, K. Pachucki, T. W. Hänsch, L. Julien, and F. Biraben, 1995, Phys. Rev. A **52**, 2664.
Windisch, D., and P. Becker, 1990, Phys. Status Solidi A **118**, 379.
Xiong, W., *et al.*, 2019, Nature (London) **575**, 147.
Yerokhin, V. A., 2009, Phys. Rev. A **80**, 040501.
Yerokhin, V. A., 2011, Phys. Rev. A **83**, 012507.
Yerokhin, V. A., 2018, Phys. Rev. A **97**, 052509.
Yerokhin, V. A., and Z. Harman, 2013, Phys. Rev. A **88**, 042502.
Yerokhin, V. A., and Z. Harman, 2017, Phys. Rev. A **95**, 060501.
Yerokhin, V. A., P. Indelicato, and V. M. Shabaev, 2008, Phys. Rev. A **77**, 062510.
Yerokhin, V. A., and U. D. Jentschura, 2008, Phys. Rev. Lett. **100**, 163001.
Yerokhin, V. A., and U. D. Jentschura, 2010, Phys. Rev. A **81**, 012502.
Yerokhin, V. A., K. Pachucki, and V. Patkóš, 2019, Ann. Phys. (Berlin) **531**, 1800324.
Yerokhin, V. A., and V. M. Shabaev, 2015, Phys. Rev. Lett. **115**, 233002.
Yerokhin, V. A., and V. M. Shabaev, 2016, Phys. Rev. A **93**, 062514.
Yost, D. C., A. Matveev, A. Grinin, E. Peters, L. Maisenbacher, A. Beyer, R. Pohl, N. Kolachevsky, T. W. Hänsch, and T. Udem, 2016, Phys. Rev. A **93**, 042509.
Young, B., M. Kasevich, and S. Chu, 1997, in *Atom Interferometry*, edited by Berman, P. R. (Academic Press, New York), pp. 363–406.
Yu, C., W. Zhong, B. Estey, J. Kwan, R. H. Parker, and H. Müller, 2019, Ann. Phys. (Berlin) **531**, 1800346.
Zafonte, S. L., and R. S. Van Dyck, Jr., 2015, Metrologia **52**, 280.
Zatorski, J., B. Sikora, S. G. Karshenboim, S. Sturm, F. Köhler-Langes, K. Blaum, C. H. Keitel, and Z. Harman, 2017, Phys. Rev. A **96**, 012502.
Zhou, S., P. Giulani, J. Piekarewicz, A. Bhattacharya, and D. Pati, 2019, Phys. Rev. C **99**, 055202.